

**HYDROGEN RICH SYNGAS FROM THE PYROLYSIS
AND GASIFICATION OF SOLID WASTE AND BIOMASS**

By

Emmanuel Chidi Efika

**Submitted in accordance with the requirements for the degree
of Doctor of Philosophy**

The University of Leeds

School of Process, Environmental and Materials Engineering

Energy Research Institute

May 2013

The candidate confirms that the thesis submitted is his own, except where work which has formed part of jointly-authored publication has been included. The contribution of the candidate and the other authors to this work has been indicated clearly below. The candidate confirms that appropriate credit has been given within the thesis where reference has been made to the work of others.

This copy has been supplied on the understanding that it is copyright material and that no quotation from the thesis may be published without proper acknowledgement.

The details of chapter 5 of the thesis are based on the published paper below:

Journal paper

[1] EFIKA, C., WU, C. & WILLIAMS, P. T. (2012). Syngas production from pyrolysis-catalytic steam reforming of waste biomass in a continuous screw kiln reactor. *Journal of Analytical and Applied pyrolysis*, 95: p. 87-94.

The candidate (E. C. Efika) performed the experiments and analytical work, wrote the initial drafts of the paper along with graphical and tabular presentation, calculation and summarisation of the results and discussion.

The co-author (Dr C. Wu) proof read the drafts and made suggestions.

The co-author (Prof P. T. Williams) supervised the research work, proof read the drafts and made suggestions and corrections to the draft papers.

© <2013> The University of Leeds and <Emmanuel Chidi Efika>

ACKNOWLEDGEMENTS

My greatest praise and gratitude goes to GOD for his mercies and grace.

I am grateful to the Niger Delta Development Commission (NDDC) for their financial support during my study.

I am deeply grateful and thankful to my supervisor, Prof Paul T. Williams, for his continuous patience, sincere care, support, motivation, encouragement, kindness, mentoring and sound advice throughout the duration of my research.

I gratefully acknowledge and appreciate the contributions and support from the research, technical and support staff of the School of Process, Environmental and Materials Engineering. I am thankful to Dr Jude Onwudili, Dr Chunfei Wu, Dr Surjit Singh, Mr Ed Woodhouse, Dr Mohamad Nahil and Dr Adrian Cunliffe for their tutoring, assistance and constructive criticism. I am also grateful to Ibrahim, Alfred, Paula, Qari, Eyup, Ramzi, Juniza, Rattana, Ruzinah, Safari, Chika, George, Bala, Akinola, Francis, Kelechi, Jo and PhD students in the Low Carbon Technologies Doctoral Training Centre for their genuine friendship and support.

I am deeply indebted to my family: my brother Ikenna Bruce Efika, My sisters Dr Chigozie Dera Efika and Barrister Olachi Jenifer Efika, my lovely fiancé Uchechi Vivian Nwadike for their patience, love and encouragement. Most importantly I am indebted to my parents Chief, Sir Emmanuel Ifeanyi Efika and Chief, Barrister Mrs Veronica Charity Efika for their financial support, love, encouragement, and emotional support constantly throughout this phase of my life.

Finally, I am grateful to everyone who was instrumental during my study and would like to express my sincere apologies to those I could not personally mention.

ABSTRACT

Biomass and wastes are potential resources for the production of renewable hydrogen, synthetic fuels, chemicals and energy via pyrolysis and gasification. Waste biomass and refuse derived fuel (RDF), and their single components were investigated for pyrolysis to produce a hydrogen rich syngas with a bench scale fixed bed reactor. The samples were pyrolysed at different temperatures, heating rates and particle sizes to recover syngas, oil and char products. The waste biomass was investigated for steam pyrolysis-gasification in a continuous screw kiln reactor to produce hydrogen. The samples were gasified at different temperatures, steam/biomass ratios, and in the presence of nickel catalysts. The effects of nickel loading on the catalyst, the catalyst/waste biomass ratio, the effects of different metal additives and the effect of in-situ CO₂ capture were also investigated for hydrogen production and resistance to catalyst deactivation by coking. A commercial scale pyrolysis reactor was studied for the pyrolysis of real world wastes.

FTIR and GC/MS analysis of the oils from the pyrolysis of waste biomass, RDF and their single components indicated that the oil product from high heating rate pyrolysis contained mostly aromatics and alkenes, while that from slow heating rate contained mostly oxygenates, alkanes and alkenes. Gaseous products from the waste biomass, RDF and their single components contained mostly CO, CO₂, H₂, CH₄ and C₂ – C₄ gases. Increasing the pyrolysis temperature and heating rate both resulted in an increase in gas and hydrogen production while reducing the oil and solid char yields.

The gas yield and hydrogen yield were increased with increasing nickel loading and catalyst to waste biomass ratio during steam pyrolysis-gasification. The lowest tar yield of 0.01g of tar per m³ of gas and highest hydrogen yield of 55 vol% were achieved at catalyst/waste biomass ratio of 2. Ce and La promoted catalysts showed improved catalyst resistance to coking and increased hydrogen yield. CaO resulted in in-situ capture of CO₂ however the H₂ yield was not increased due to the deactivation of CaO by tar in.

The commercial scale system resulted in conversion of wastes to syngas, oil and char however results were not comparable to laboratory scale results due to limitations in the commercial scale process.

TABLE OF CONTENTS

ACKNOWLEDGEMENTS	iii
ABSTRACT.....	iii
CHAPTER 1 INTRODUCTION	1
1.1 Solid waste and biomass resources.....	1
1.2 Routes to Energy from solid wastes and waste biomass.....	5
1.2.1 Pyrolysis and Gasification.....	6
1.2.1.1 Limitations to pyrolysis and gasification of solid wastes.....	7
1.3 Hydrogen potential from pyrolysis and gasification of solid wastes.....	9
1.4 Research objectives.....	10
References	11
CHAPTER 2. LITERATURE REVIEW	14
2.1 Pyrolysis	14
2.1.1 High temperature pyrolysis for hydrogen and syngas	14
2.1.2 Pyrolysis reactors.....	15
2.1.2.1 The fluidized bed reactor	15
2.1.2.2 Free fall reactor	18
2.1.2.3 Rotary kiln & screw kiln reactors.....	19
2.1.2.4 Other Reactors	21
2.1.3 The pyrolysis of solid wastes and biomass	22
2.1.3.1 Products from the pyrolysis of solid wastes and biomass	22
2.1.3.2 Effects of material characteristics	23
2.1.3.3 Effects of temperature and heating rate	24
2.1.3.4 Effects of other process conditions.....	26
2.1.3.5 Effects of catalyst	28
2.2 Gasification.....	30
2.2.1 Gasification for hydrogen yield.....	30
2.2.2 Gasification reactors	31
2.2.2.1 Fluidized bed reactors	31
2.2.2.2 Fixed bed reactors.....	33

2.2.2.3	Entrained flow reactors.....	35
2.2.2.4	Rotary kiln and screw kiln reactor.....	36
2.2.3	The gasification of solid wastes and biomass	38
2.2.3.1	Products from the gasification of solid wastes and biomass	38
2.2.3.2	Effects of reaction atmosphere	39
2.2.3.3	Effects of material characteristics	40
2.2.3.4	Effects of temperature and heating rate	41
2.2.3.5	Effects of other process conditions.....	41
2.2.4	Catalytic gasification of solid waste and biomass	42
2.2.4.1	Nickel based catalysts for gasification	44
2.2.4.2	Mechanisms of nickel catalyst deactivation	48
2.2.4.3	Other available catalysts	51
2.2.5	Novel concepts.....	55
2.2.5.1	In-situ hydrogen removal	55
2.2.5.2	In-situ CO ₂ removal	55
	References	55
CHAPTER 3.	MATERIALS AND METHODS	72
3.1	Materials	72
3.1.1	Solid waste (RDF)	72
3.1.2	Simulated single components of RDF	73
3.1.3	Waste wood	74
3.1.4	Simulated single components of waste wood	75
3.1.5	Researched catalysts and CO ₂ sorbents	76
3.2	Fixed bed reactor.....	77
3.2.1	Fixed bed reactor setup	77
3.2.2	Fixed bed experimental procedure.....	79
3.2.3	Validation of the fixed bed reactor.....	80
3.3	Continuous screw kiln reactor.....	82
3.3.1	Screw kiln reactor setup.....	82
3.3.2	Development and modification of the screw kiln reactor	84
3.3.3	Screw kiln experimental procedure	87
3.3.4	Validation of the modified screw kiln reactor	89
3.4	Gas Analysis.....	91

3.4.1	GC/TCD and GC/FID	91
3.4.2	Determination of sampled gas concentration	92
3.5	Oil analysis	95
3.5.1	Fourier transforms infra-red (FTIR) spectrometry.....	95
3.5.2	Gas chromatography/mass spectrometry (GC/MS)	96
3.6	Solids analysis	98
3.6.1	Thermogravimetric analysis of solids	98
3.6.2	Elemental (CHNSO) analysis	99
3.6.3	Bomb calorimetric analysis	100
3.7	Catalyst analysis	101
3.7.1	Brunauer, Emmett and Teller (BET) surface area analysis.....	101
3.7.2	Temperature programmed oxidation (TPO-FTIR)	103
3.7.3	X-ray diffraction (XRD)	105
3.7.4	Scanning electron microscopy (SEM)	107
3.7.5	Transmission electron microscopy (TEM) and energy dispersive X-ray spectroscopy (EDXS)	108
	References	109
CHAPTER 4.	Pyrolysis of Refuse Derived Fuel (RDF) and waste wood	109
4.1	RDF and waste wood characteristics.....	109
4.1.1	RDF characteristics.....	109
4.1.2	Waste wood characteristics	110
4.2	The influence of slow and fast heating on the pyrolysis of RDF and its single components	111
4.2.1	Product yields	111
4.2.2	Gas composition and hydrogen yield	117
4.2.3	Composition of oil products.....	121
4.2.4	Solid product characteristics	131
4.2.5	Influence of other process conditions.....	131
4.2.5.1	Effects of final pyrolysis temperature.....	131
4.2.5.2	Effects of particle size.....	134
4.2.6	Conclusions	135
4.3	Influence of slow and fast heating on the pyrolysis of waste wood and its single components.....	136
4.3.1	Product yields	137

4.3.2	Gas composition and hydrogen yield	140
4.3.3	Composition of the oil products	144
4.3.4	Solid product characteristics	154
4.3.5	Influence of other process conditions.....	154
4.3.5.1	Effects of final pyrolysis temperature.....	154
4.3.5.2	Effects of particle size.....	156
4.3.6	Conclusions	157
4.4	Mechanisms for the pyrolysis of solid wastes	159
4.4.1	Degradation of cellulose, hemicellulose lignin and polyethylene.....	161
	References	166
CHAPTER 5. PYROLYSIS AND GASIFICATION OF WASTE		
WOOD IN A SCREW KILN REACTOR.....		
5.1	Influence of process conditions on the two stage pyrolysis and steam only gasification of waste wood.....	172
5.1.1	Effects of temperature during two stage pyrolysis of waste wood.....	172
5.1.1.1	Product yields	172
5.1.1.2	Gas composition and hydrogen yield.....	176
5.1.2	Effects of temperature and steam to waste wood ratio on the steam only pyrolysis-gasification of waste wood.....	176
5.1.2.1	Product yields	177
5.1.2.2	Gas composition and hydrogen yield.....	179
5.1.3	Conclusions	179
5.2	Nickel based catalytic pyrolysis-gasification of waste wood.....	180
5.2.1	Effects of nickel loading and catalyst to waste wood ratio	181
5.2.1.1	Product yields	181
5.2.1.2	Gas composition and hydrogen yield.....	186
5.2.1.3	Effect of nickel loading and catalyst to waste wood ratio on tar yields.....	188
5.2.1.4	Catalyst characterization	192
5.2.2	Influence of different metal additives on the catalytic activity and coke resistance of Ni Al ₂ O ₃	196
5.2.2.1	Product yields	198
5.2.2.2	Gas composition and hydrogen yield.....	201

5.2.2.3	Effect of metal additives on tar yield	205
5.2.2.4	Catalyst life, regeneration and re-use of the Ni Al ₂ O ₃ and Ni CeO ₂ Al ₂ O ₃ catalysts.....	207
5.2.2.5	Catalyst characterization	211
5.2.3	Conclusions	222
5.3	Nickel based steam pyrolysis-gasification of waste wood with CaO as a CO ₂ sorbent.....	225
5.3.1	Product yields	226
5.3.2	Gas composition	229
5.3.3	Catalyst-Sorbent characterization	231
5.3.4	Conclusions	234
	References	235
CHAPTER 6. PYROLYSIS AND PARTIAL OXIDATION OF DIFFERENT REAL WORLD WASTES IN AN INDUSTRIAL SCALE SCREW KILN REACTOR		
6.1	Materials and methods.....	239
6.1.1	Materials Characterization	240
6.1.2	Reactor System.....	240
6.2	Results and discussion	245
6.2.1	Materials characteristics.....	245
6.2.2	Product yields	246
6.2.3	Gas product and composition	247
6.2.4	Oil products and composition.....	254
6.2.5	Solid product characteristics	261
6.3	Conclusions	262
	References	263
CHAPTER 7. CONCLUSIONS AND FUTURE WORK		
7.1	Conclusions	265
7.1.1	The pyrolysis of RDF and its single components in the fixed bed reactor	265
7.1.2	The pyrolysis of waste wood and its single components in the fixed bed reactor	266
7.1.3	Two stage pyrolysis and steam pyrolysis-gasification of waste wood in the continuous screw kiln reactor	267
7.1.4	Steam pyrolysis-gasification of waste wood with nickel based catalysts	267

7.1.5 Steam pyrolysis-gasification of waste wood with nickel based catalyst and CaO as a CO ₂ sorbent	269
7.1.6 Pyrolysis and partial oxidation of different real world wastes in an industrial scale screw kiln reactor	270
7.2 Future work.....	271
Appendix.....	275

Figures

Figure 1-1. Municipal waste composition in the European union [5]	4
Figure 1-2. 2009 UK municipal waste composition [4]	4
Figure 2-1 Fluidized bed Reactor [15].....	17
Figure 2-2 Free fall/Entrained flow reactor [45].....	19
Figure 2-3 Schematic of a rotary Kiln reactor [52]	20
Figure 2-4 Schematic of a screw kiln reactor.....	20
Figure 2-5 Dual fluidized bed reactor [121].....	32
Figure 2-6 Cross flow fixed bed reactor.....	34
Figure 2-7 Fixed bed reactors (amended from [15])	34
Figure 2-8 Entrained flow gasifier (amended from [136]).....	36
Figure 2-9 Screw kiln reactor [139].....	37
Figure 2-10 Schematic of the rotary kiln gasifier [140].	38
Figure 3-1 Schematic of the fixed bed reactor	78
Figure 3-2 Photograph of the horizontal fixed bed reactor	79
Figure 3-3 Temperature profile of the fixed bed reactor.....	80
Figure 3-4 Schematic of the continuous screw kiln reactor.....	82
Figure 3-5 Photograph and schematic of continuous screw kiln after modifications.....	86
Figure 3-6 Photograph of a Varian GC with TCD and FID.....	90
Figure 3-7 Example output GC chromatogram showing CO ₂	92
Figure 3-8 Example GC output chromatogram showing H ₂ , O ₂ , N ₂ and CO	92
Figure 3-9 Example GC output chromatogram showing the alkane gases	93
Figure 3-10 Example GC output chromatogram showing the alkene gases	93
Figure 3-11 Photograph of the Thermoscientific Nicolet iS10 spectrometer.....	94
Figure 3-12 Photograph of the Varian 3800-GC/MS	95
Figure 3-13 Photograph of the Stanton-Redcroft TGA.....	97
Figure 3-14 Thermogram for RDF.....	98
Figure 3-15 Photograph of the Parr Isoperibol calorimeter	99

Figure 3-16 Photograph of the Quantachrome BET equipment.....	100
Figure 3-17 Example BET plot for the Ni Al ₂ O ₃ catalyst.....	101
Figure 3-18 TPO-FTIR of spent Ni Al ₂ O ₃ catalyst: (a) TPO (b) FTIR	103
Figure 3-19 CO ₂ spectra from the FTIR and library match.....	103
Figure 3-20 Photograph of the Bruker D8	105
Figure 3-21 XRD spectra for Ni Al ₂ O ₃ : (a) Fresh (b) Reacted	105
Figure 3-22 Photograph of the LEO 1530 SEM instrument.....	106
Figure 3-23 Photograph of the Philips CM200 TEM-EDXS equipment.....	107
Figure 4-1 The thermal degradation of RDF in the TGA	109
Figure 4-2 The thermal degradation of waste wood in the TGA.....	111
Figure 4-3 Effect of heating rate on product gas CV	119
Figure 4-4 FTIR spectrogram of oil from the pyrolysis of RDF at 5 and 350 °C min ⁻¹	121
Figure 4-5 Effects of heating rate on oil compounds from RDF pyrolysis ..	123
Figure 4-6. GC/MS chromatography of liquid from pyrolysis of RDF at 5 °C/min ⁻¹ ; (a) GC/MS Chromatography of aliphatics (b) GC/MS Chromatography of oxygenates and aromatics.	125
Figure 4-7. GC/MS chromatography of liquid from pyrolysis of RDF at ≈ 350 °C/min ⁻¹ ; (a) GC/MS Chromatography of aliphatics (b) GC/MS Chromatography of oxygenates and aromatics.	125
Figure 4-8. GC/MS chromatography of liquid from pyrolysis of paper at 5 °C/min ⁻¹ ; (a) GC/MS Chromatography of aliphatics (b) GC/MS Chromatography of oxygenates and aromatics.	126
Figure 4-9. GC/MS chromatography of liquid from pyrolysis of paper at ≈ 350 °C/min ⁻¹ ; (a) GC/MS Chromatography of aliphatics (b) GC/MS Chromatography of oxygenates and aromatics.	127
Figure 4-10. GC/MS chromatography of liquid from pyrolysis of paper at 5 °C/min ⁻¹ ; (a) GC/MS Chromatography of aliphatics (b) GC/MS Chromatography of oxygenates and aromatics.	128
Figure 4-11. GC/MS chromatography of liquid from pyrolysis of mixed waste plastics at ≈ 350 °C/min ⁻¹ ; (a) GC/MS Chromatography of aliphatics (b) GC/MS Chromatography of oxygenates and aromatics.	128
Figure 4-12 Effect of heating rate on the CV of product gases	143
Figure 4-13 FTIR spectrogram for oil from the pyrolysis of wood at 5 and 360 °C min ⁻¹	145
Figure 4-14 Effects of heating rate on oil compounds from wood pyrolysis.....	147

Figure 4-15. GC/MS chromatography of liquid from pyrolysis of waste wood at 5 °C/min ⁻¹ ; (a) GC/MS Chromatography of aliphatics (b) GC/MS Chromatography of oxygenates and aromatics.....	148
Figure 4-16. GC/MS chromatography of liquid from pyrolysis of waste wood at ≈ 350 °C/min ⁻¹ ; (a) GC/MS Chromatography of aliphatics (b) GC/MS Chromatography of oxygenates and aromatics.	148
Figure 4-17. GC/MS chromatography of liquid from pyrolysis of cellulose at 5 °C/min ⁻¹ ; (a) GC/MS Chromatography of aliphatics (b) GC/MS Chromatography of oxygenates and aromatics.	149
Figure 4-18. GC/MS chromatography of liquid from pyrolysis of cellulose at ≈ 350 °C/min ⁻¹ ; (a) GC/MS Chromatography of aliphatics (b) GC/MS Chromatography of oxygenates and aromatics.....	150
Figure 4-19. GC/MS chromatography of liquid from pyrolysis of cellulose at 5 °C/min ⁻¹ ; (a) GC/MS Chromatography of aliphatics (b) GC/MS Chromatography of oxygenates and aromatics.	151
Figure 4-20. GC/MS chromatography of liquid from pyrolysis of xylan at ≈ 350 °C/min ⁻¹ ; (a) GC/MS Chromatography of aliphatics (b) GC/MS Chromatography of oxygenates and aromatics.....	151
Figure 4-21. GC/MS chromatography of liquid from pyrolysis of lignin at 5 °C/min ⁻¹ ; (a) GC/MS Chromatography of aliphatics (b) GC/MS Chromatography of oxygenates and aromatics.	152
Figure 4-22. GC/MS chromatography of liquid from pyrolysis of lignin at ≈ 350 °C/min ⁻¹ ; (a) GC/MS Chromatography of aliphatics (b) GC/MS Chromatography of oxygenates and aromatics.....	153
Figure 4-23 Proposed pathway for aromatic formation from olefins via Diels-Alder type reactions, from [35].....	161
Figure 4-24 Proposed pathway for cellulose pyrolytic degradation, from [60].....	161
Figure 4-25 Proposed pathway for xylan pyrolytic degradation, from [68] .	162
Figure 4-26 Proposed pathway for lignin degradation, from [73].....	163
Figure 4-27 Proposed degradation pathway for polyethylene from [94].....	164
Figure 5-1 TGA analysis of solid product from first stage reactor temperature of 500 °C.	175
Figure 5-2 TGA analysis of solid product from pyrolysis at first stage temperature of 700 °C.	175
Figure 5-3 Effect of nickel loading on gas yield.....	183
Figure 5-4 Effect of catalyst to waste wood ratio on gas yield	183
Figure 5-5 Effect of catalyst to waste wood ratio on hydrogen yield	187
Figure 5-6 Effect of catalyst to waste wood ratio on hydrogen yield.	187

Figure 5-7 Effects of nickel catalysts on tar from waste wood steam pyrolysis-gasification.....	189
Figure 5-8 SEM of Fresh alumina	191
Figure 5-9 SEM of Fresh Ni(5) Al ₂ O ₃	191
Figure 5-10 SEM of Fresh Ni(20) Al ₂ O ₃	191
Figure 5-11 SEM of Reacted Ni(5) Al ₂ O ₃	192
Figure 5-12 SEM of Reacted Ni(20) Al ₂ O ₃	192
Figure 5-13 SEM of Reacted Ni(20) Al ₂ O ₃ a	192
Figure 5-14 SEM of Reacted Ni(20) Al ₂ O ₃ b	193
Figure 5-15 Micrograph of the Fresh Ni(10) Al ₂ O ₃	193
Figure 5-16 Micrograph of the Reacted Ni(10) Al ₂ O ₃	193
Figure 5-17 Effect of different metal additives on gas yield.....	199
Figure 5-18 Hydrogen production (mol per g waste wood) for the catalysts.....	203
Figure 5-19 Effects of different metal promoters on tar compounds from steam pyrolysis-gasification of waste wood	205
Figure 5-20 Catalyst life, regeneration and re-use test for Ni Al ₂ O ₃	206
Figure 5-21 Catalyst life, regeneration and re-use test for Ni CeO ₂ Al ₂ O ₃	207
Figure 5-22 Comparison of the hydrogen yield for Ni Al ₂ O ₃ and Ni CeO ₂ Al ₂ O ₃ during the catalyst life and re-use tests.....	207
Figure 5-23 SEM of regenerated Ni Al ₂ O ₃	209
Figure 5-24 SEM of regenerated Ni CeO ₂ Al ₂ O ₃	209
Figure 5-25 Micrographs of regenerated Ni Al ₂ O ₃	209
Figure 5-26 Micrographs of regenerated Ni CeO ₂ Al ₂ O ₃	210
Figure 5-27 XRD pattern and Reitvelt model for the fresh Ni CeO ₂ Al ₂ O ₃ catalyst.....	211
Figure 5-28 XRD patterns of the Ni Al ₂ O ₃ catalyst: (a) fresh, (b) reacted...	211
Figure 5-29 TEM-EDXS for Ni Al ₂ O ₃	212
Figure 5-30 TEM-EDXS for Ni CeO ₂ Al ₂ O ₃	212
Figure 5-31 SEM Fresh Ni Al ₂ O ₃	213
Figure 5-32 SEM Reacted Ni Al ₂ O ₃	213
Figure 5-33 SEM Fresh Ni CeO ₂ Al ₂ O ₃	213
Figure 5-34 SEM Reacted Ni CeO ₂ Al ₂ O ₃	213
Figure 5-35 TEM image of the fresh Ni Al ₂ O ₃	214
Figure 5-36 TEM image of the reacted Ni Al ₂ O ₃	214

Figure 5-37 TEM image of the fresh Ni CeO ₂ Al ₂ O ₃	215
Figure 5-38 TEM image of the reacted Ni CeO ₂ Al ₂ O ₃	215
Figure 5-39 TEM-EDXS mapping for the reacted Ni Al ₂ O ₃ catalyst showing its elemental make up and their position. (a) TEM image (b) Al spectra (c) C spectra (d) Ni spectra (e) O spectra.....	217
Figure 5-40 TEM-EDXS mapping for the reacted Ni CeO ₂ Al ₂ O ₃ catalyst showing its elemental make up and their position. (a) TEM image (b) Al spectra (c) C spectra (d) Ce spectra (e) Ni spectra (f) O spectra.....	218
Figure 5-41 CO ₂ evolution during TPO-FTIR of reacted catalysts	220
Figure 5-42 XRD patters for Ni CaO Al ₂ O ₃ : (a) fresh (b) reacted	229
Figure 5-43 XRD patterns for Ni Al ₂ O ₃ and CaO catalyst-sorbent: (a) fresh CaO (b) reacted Ni Al ₂ O ₃ at 700 °C (c) reacted Ni Al ₂ O ₃ +CaO(10g) at 700 °C (d) reacted Ni Al ₂ O ₃ +CaO(10g) at 800 °C.....	230
Figure 5-44 TEM image of the fresh Ni CaO Al ₂ O ₃	230
Figure 5-45 TEM image of the reacted Ni CaO Al ₂ O ₃	231
Figure 5-46 TEM image of the Ni Al ₂ O ₃ +CaO(10g) reacted at 800 °C.....	231
Figure 6-1 Schematic diagram of the pyrolysis/partial oxidation reactor	242
Figure 6-2 Photograph of the pyrolysis/partial oxidation reactor	242
Figure 6-3 3D model of the pyrolysis/partial oxidation reactor	243
Figure 6-4 Carbon conversion for the wastes	248
Figure 6-5 GCMS chromatograph of the oil from the processing of MSW + WSF; (a) Showing oxygenates and aromatics (b) Showing aliphatics.....	257
Figure 6-6GCMS chromatograph of the oil from the processing of MSW + plastic; (a) Showing oxygenates and aromatics (b) Showing aliphatics.....	258
Figure 6-7 GCMS chromatograph of the oil from the processing of Clinical waste; (a) Showing oxygenates and aromatics (b) Showing aliphatics.....	258
Figure 6-8 GCMS chromatograph of the oil from the processing of Offensive clinical waste; (a) Showing oxygenates and aromatics (b) Showing aliphatics.	259
Figure 6-9 GCMS chromatograph of the oil from the processing of SAW; (a) Showing oxygenates and aromatics (b) Showing aliphatics.	259
Figure 6-10 GCMS chromatograph of the oil from the processing of Wood; (a) Showing oxygenates and aromatics (b) Showing aliphatics.....	260

Figure 7-1 Schematic of fixed bed with suggested CaO and catalyst layer274

Appendix

Appendix A- 1 XRD patterns of the Ni CeO ₂ Al ₂ O ₃ catalyst: (a) fresh, (b) reacted.....	275
Appendix A- 2 XRD patterns of the Ni CoO Al ₂ O ₃ catalyst: (a) fresh, (b) reacted.....	275
Appendix A- 3 XRD patterns of the Ni CuO Al ₂ O ₃ catalyst: (a) fresh, (b) reacted.....	276
Appendix A- 4 XRD patterns of the Ni La ₂ O ₃ Al ₂ O ₃ catalyst: (a) fresh, (b) reacted.....	276
Appendix A- 5 XRD patterns of the Ni MgO Al ₂ O ₃ catalyst: (a) fresh, (b) reacted.....	277
Appendix A- 6 XRD patterns of the Ni MnO Al ₂ O ₃ catalyst: (a) fresh, (b) reacted.....	277
Appendix B- 1 TEM-EDXS spectra for Ni CoO Al ₂ O ₃	278
Appendix B- 2 TEM-EDXS spectra for Ni La ₂ O ₃ Al ₂ O ₃	278
Appendix B- 3 TEM-EDXS spectra for Ni MgO Al ₂ O ₃	278
Appendix C- 1 SEM images of the fresh Ni CoO Al ₂ O ₃	279
Appendix C- 2 SEM images of the reacted Ni CoO Al ₂ O ₃	279
Appendix C- 3 SEM images of the fresh Ni CuO Al ₂ O ₃	279
Appendix C- 4 SEM images of the reacted Ni CuO Al ₂ O ₃	279
Appendix C- 5 SEM images of the fresh Ni La ₂ O ₃ Al ₂ O ₃	280
Appendix C- 6 SEM images of the reacted Ni La ₂ O ₃ Al ₂ O ₃	280
Appendix C- 7 SEM images of the fresh Ni MgO Al ₂ O ₃	280
Appendix C- 8 SEM images of the reacted Ni MgO Al ₂ O ₃	280
Appendix C- 9 SEM images of the Fresh Ni MnO Al ₂ O ₃	281
Appendix C- 10 SEM images of the reacted Ni MnO Al ₂ O ₃	281
Appendix D- 1 TEM image of the fresh Ni La ₂ O ₃ Al ₂ O ₃	281
Appendix D- 2 TEM image of the reacted Ni La ₂ O ₃ Al ₂ O ₃	282
Appendix D- 3 TEM image of the fresh Ni CoO Al ₂ O ₃	282
Appendix D- 4 TEM image of the reacted Ni CoO Al ₂ O ₃	282
Appendix D- 5 TEM image of the fresh Ni MgO Al ₂ O ₃	283
Appendix D- 6 TEM image of the reacted Ni MgO Al ₂ O ₃	283
Appendix E-1 TEM-EDXS mapping of the reacted Ni CoO Al ₂ O ₃	284
Appendix E-2 TEM-EDXS mapping of the reacted Ni La ₂ O ₃ Al ₂ O ₃	285

Appendix E-3 TEM-EDXS mapping of the reacted Ni MgO Al₂O₃.....286

Tables

Table 3-1 Ultimate and proximate analysis of RDF	72
Table 3-2 Ultimate and proximate analysis of RDF simulated single components	73
Table 3-3 Ultimate and proximate analysis of wood	74
Table 3-4 Ultimate and proximate analysis of wood simulated single components	75
Table 3-5 Validation of the fixed bed reactor for RDF pyrolysis	81
Table 3-6 Results from pyrolysis and gasification during reactor initial tests	84
Table 3-7 Effects of varying steam to biomass ratio during gasification	85
Table 3-8 Calibration of the feed hopper and kiln screw for waste wood	88
Table 3-9 Validation of the continuous screw kiln reactor for waste wood	89
Table 4-1 Products from the slow and fast heating of RDF and its components at 800 °C	113
Table 4-2 Hydrogen and total gas production per gram of the samples	118
Table 4-3 Detected oil compounds from RDF, paper and plastics pyrolysis at different heating rates	121
Table 4-4 Products from the slow and fast heating of RDF at different temperatures	131
Table 4-5 Effect of particle size on RDF pyrolysis at 800 °C	132
Table 4-6 Products from the slow and fast heating of waste wood and its components at 800 °C	139
Table 4-7 Hydrogen and total gas production per gram of samples	142
Table 4-8 Detected oil compounds from wood, cellulose, xylan and lignin pyrolysis at different heating rates	145
Table 4-9 Products from the slow and fast heating of wood at different temperatures	155
Table 4-10 Effect of particle size on wood pyrolysis at 800 °C	156
Table 5-1 Effects of varying first and second stage temperatures during pyrolysis	173
Table 5-2 Effects of varying the steam to waste wood ratio and second stage temperatures	178
Table 5-3 Effects of varying the nickel loading and the catalyst to waste wood ratio	184

Table 5-4 Tar/oil compounds from steam pyrolysis-gasification of waste wood with Ni Al ₂ O ₃ catalysts with different nickel loading and catalyst to waste wood ratios	188
Table 5-5 Effects of different metal additives on nickel catalytic activity	198
Table 5-6 Tar compounds from steam pyrolysis-gasification of waste wood with different catalysts	204
Table 5-7 Effects of CaO on in-situ CO ₂ capture activity	225
Table 6-1 Properties of fresh waste material	246
Table 6-2 Gas products from the thermal processing of different wastes ..	253
Table 6-3 Oil/tar compounds from the pyrolysis/partial oxidation of different wastes	254
Table 6-4 Characteristics of the solid char products	261

CHAPTER 1 INTRODUCTION

Continuous efforts are being made worldwide in order to shift from an energy culture which is reliant on the carbon economy to an alternatively cleaner hydrogen economy, due to the increasing pressures from the proponents of global warming. A publication by the International Energy Agency (IEA) in 2006 [1] indicated that combustion of fossil fuels for power generation alone contributed to a large amount (about 29%) of the current overall world CO₂ emissions.

De-carbonising the economy however has not been made any easier by the ever increasing world demand for energy and fuels due to increasing populations and the emergence of quickly developing economies in the third world. These in turn multiply the strain on our ever depleting energy resources thereby prompting a need for alternative sources of fuels and energy. Realizations such as these have prompted researches towards harnessing energy sources which are less polluting to the environment, in terms of the generation of greenhouse gases, and energy sources which are widely available and can therefore be sustainably harnessed. Some of the alternative energy options currently being researched and implemented include biomass (including solid wastes), wind, solar, geothermal, tidal etc.

A report published in 2008 by the IEA states that biomass is expected to remain the single most important primary source of renewable energy for decades to come. Extracting energy and fuels from biomass and solid wastes represents an effective solution to two problems faced globally today (especially for solid waste), these are: the increasing demand for efficient energy and a need for sustainable waste management practices, if achieved efficiently.

1.1

Solid waste and biomass resources

Biomass mostly applies to vegetative matter or plant matter but generally includes all living organisms. In this case biomass includes plants grown specifically as energy crops, agricultural wastes, wood wastes, food wastes, forestry residue, algae etc. The nearly universally available nature of biomass makes it a very promising energy resource as countries will be able to use native species of biomass available to them for their energy needs. This provides an energy resource which is less influenced by geopolitical limitations and is therefore more secure.

Biomass like wood are extensively utilized for heating purposes and already represent a large portion of the energy resource for countries like Brazil, Finland etc. However significant challenges including: utilization technology, scale, density, uncertainty of contribution to greenhouse gas reduction and sustainability of production, will need to be overcome if biomass is to meet a significant portion of our energy demand. Some of the sustainability issues associated with biomass utilization include and are not limited to the following:

1. The cultivation of energy crops creates competition between food crops for land and water. It is therefore important to ensure that the production of energy crops will have little or no impact on food crop production by adopting strategies such as growing energy crops on non-arable land.
2. The indiscriminate harvesting of trees to supply wood for energy will lead to deforestation. To minimize this, the use of waste wood such as forestry thinning and the harvesting of short rotation forestry trees only, can be adopted.
3. The utilization of staple food crops for energy production impacts on the price of such crops e.g. the use of corn for the production of ethanol has resulted in the price of corn being impacted directly by the increasing price of ethanol.

Notwithstanding the many challenges, biomass still presents significant potential: Continents like Africa, Latin America and Europe can potentially produce 21.4, 19.9 and 8.9×10^{18} Joules (Ej), corresponding to energy content equivalents of 3.5, 3.2 and 3.4×10^9 barrels of crude oil per year, respectively [2].

In light of the sustainability concerns raised earlier, more focus has been generated for the harnessing of waste biomass, biomass residues (including agricultural and commercial), algae and solid wastes.

The term solid waste used here applies to a large portion of materials in a solid or semi-solid state within the waste stream which excludes hazardous industrial substances (such as toxic wastes) but mostly includes municipal wastes, non-hazardous commercial wastes, sewage sludge and even yard and park wastes and biomass wastes. In the EU in 2008 the total municipal wastes generated was about 251 million tonnes, of which about 38% was landfilled [3]. The general compositions of the municipal wastes in the EU are shown in figure 1.1. While in 2009 the total municipal wastes collected by local authorities in the UK was 32.5 mt (million tonnes) of which 49 % was landfilled [4]. Figure 1.2 below shows the % composition of the municipal wastes collected in the UK in 2009.

The materials sent to landfills contain a large portion of organic compounds such as paper, vegetation and food wastes etc and plastics and these have a potential energy value. Organic substances which are deposited in a landfill, decompose aerobically and anaerobically within the landfills to expose the environment to greenhouse gases in the form of landfill gas (containing mostly CO_2 and CH_4), and also results in ground water pollution from leachate. There is also the risk of disease spread and littering where un-controlled landfills and open dumps are used, like in many developing countries.

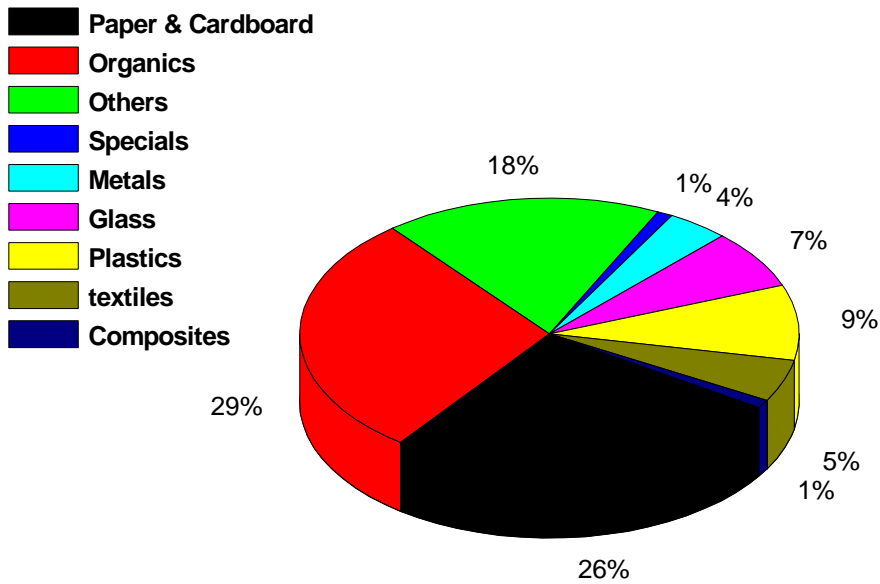


Figure 1-1. Municipal waste composition in the European union [5]

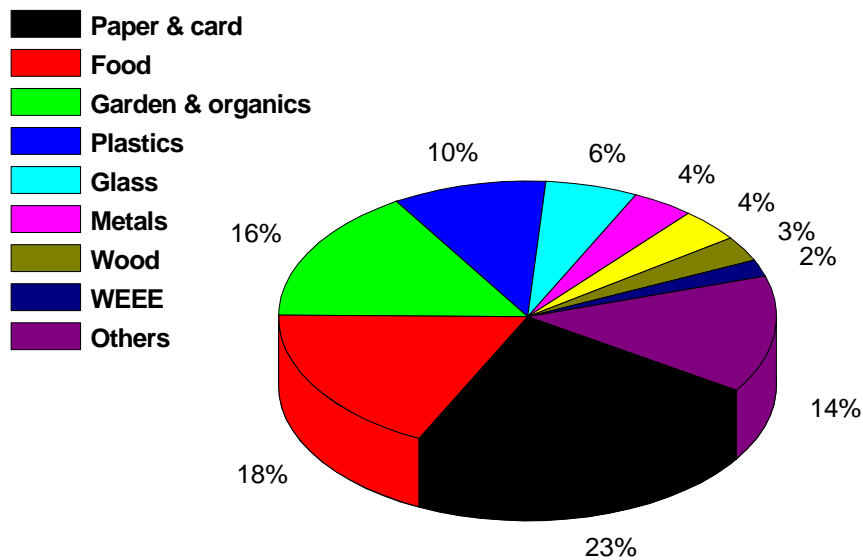


Figure 1-2. 2009 UK municipal waste composition [4]

The potential and existing risks to the environment of standard waste management practices have led to the proposal and adoptions of certain policies and strategies by countries (mostly the developed countries) to limit these risks. These measures are intended to discourage the disposal of solid waste in landfills as the dominant disposal route by making landfilling a more expensive option, and to encourage other means of solid waste disposal. Examples of such policies include in the UK: landfill taxes, Landfill Allowance

Trading Schemes (LATS), and EU wide landfill Directives and the Groundwater directives. These policies and others have all together encouraged operators of the waste industry to investigate and adopt other options which were previously less attractive than landfills, like composting, anaerobic digestion; and where the sole purpose is to extract energy or fuels from the waste, then the options include incineration and pyrolysis/gasification.

A combination of tighter waste management policies and a demand for more energy have promoted more research and development of energy from waste options. Thereby slowly but surely increasing the relevance of these options as well as shifting the view of wastes from 'waste' to 'resource'. The UK government through an energy review in 2006 expressed concerns over the future security and diversity of the energy resources used for power generation, declaring that it would be more sensible and sustainable to utilize the energy value of residual waste before final disposal [6].

1.2 Routes to Energy from solid wastes and waste biomass

Over the years various alternative technologies have been developed and are in operation for the processing of both biomass and solid wastes to extract their energy content for direct utilization or for the production of secondary fuels. The available technologies can be classed into: Biological routes e.g. fermentation and anaerobic digestion, and Thermo-chemical routes e.g. combustion and pyrolysis. Solid wastes are still predominantly handled by disposal in landfills where energy generation can then be integrated by collecting and combusting the produced landfill gas. Some of the other available energy recovery technologies are discussed below.

Anaerobic digestion: Anaerobic digesters convert the bio-degradable matter contained in the MSW and biomass into a product gas comprising mainly of methane and carbon dioxide which can be combusted for energy, and a

residue which is applicable as a soil conditioner [7] and a variety of inorganic salts from the conversion of calcium, magnesium and sodium compounds [8]. The residue from this process (leachate and solids) may require further treatment in order to be utilized or disposed off.

Fermentation: A number of technologies are currently being researched and developed for the fermentation of food wastes and biomass wastes which are rich in lignocellulosic content, to produce ethanol. These technologies differ and could include any combination of the following steam explosion, acid digestion [9], enzymatic digestion [10] followed by fermentation.

Incineration / Combustion: These terms are interchangeable and involve burning the feed to generate heat which can then be utilized. Application of this technology especially to municipal solid waste (MSW) is unpopular due to concerns about the release of pollutant emissions such as dioxins, nitrogen oxides, sulphur dioxide and furans etc [11].

Co-combustion with coal: A mixture of coal and biomass and or MSW can be combusted as an alternative to the combustion of the individual fractions. The Electric Power Research Institute (EPRI), USA have suggested that the highest efficiency, lowest cost lowest risk technology for energy generation from biomass and waste in the near future is co-combustion of waste with coal [12].

Co-gasification with coal: A blend of coal and biomass and or solid waste can also be gasified, with the product gas utilized for energy generation. Gasification of such blends have been reported to increase the net calorific value of the product gases [13].

Thermal plasma treatment: This technology involves exposing MSW or biomass to a plasma arc, created by energy application to a gas, resistivity across the system creates heat which strips away the gas molecule electrons thereby generating a high temperature plasma [14]. This plasma decomposes the feed into synthesis gas, fly ash and vitrified slag.

1.2.1 Pyrolysis and Gasification

Pyrolysis, gasification and a combination of both, are generating increased interest as viable and alternative environmental and economic options for solid waste and biomass processing. Reasons being that depending on the technology applied, the feed can be processed to produce; energy, an oil or gas products for use as petrochemical feedstock and/or a carbonaceous char for use in applications such as effluent treatment or as a gasification feedstock [15-16]. Also there is the added advantage that the derived products can easily be handled stored and transported if need be, therefore eliminating the need to be used at or close to the processing plant [17]. Both pyrolysis and gasification are thermal processing technologies, however process conditions such as reaction atmosphere and temperature, and major end-product stream are the major differences between the two processes [16, 18].

Pyrolysis refers to the thermal decomposition of carbonaceous substances (with reference to solid waste and biomass) at temperature ranges between 400 – 800 °C and in the absence of oxygen to produce mostly combustible gases, char and oil. The quantity of each of these three main products is influenced most importantly by the process temperature and heating rate. According to Williams 2005 [15], at high heating rates, long residence time and high temperatures, the volatile products of waste pyrolysis quickly breakdown to form a mainly gas product (comprising mainly of CO₂, CO, H₂ and CH₄). This type of pyrolysis can be referred to as flash-gas pyrolysis and will be of interest for this research.

Gasification involves the thermal decomposition of organic substances, but unlike pyrolysis, oxygen is introduced during the process in a careful and controlled manner, so as not to allow complete combustion, at high reaction temperatures of between 800 – 1400 °C. Oxygen can be introduced in the form of air, steam, pure oxygen or a mixture of both air and steam. This reaction produces ash, a tar product and a gas product [15], commonly referred to as syngas (comprising mainly of CO₂, CO, H₂ and CH₄). The

gasification process involves a pyrolytic step followed by the reaction of the pyrolysis products with the oxidizing agent [16, 18-19].

The gaseous products from both pyrolysis and gasification can be reformed catalytically in order to improve the H₂ to CO ratio (around 2:1) which can then be used in synthetic fuel production processes, such as methanol and Fischer Tropsch (FT) synthesis. In addition to this, apart from direct combustion of the gaseous feed stock in a boiler setup to generate electricity, there is also the possibility of feeding the gaseous products to gas engines or gas turbines for direct combustion to generate electricity.

1.2.1.1 Limitations to pyrolysis and gasification of solid wastes

Although increased interests and efforts have been put into the development of pyrolysis and gasification technologies for the processing of solid wastes and biomass wastes, there are still socio-economic and technological uncertainties regarding these technologies which have limited their full scale adoption.

The cost of processing wastes via pyrolysis and gasification, compared to the processing of fossil fuels has a major impact on the adoption of these technologies [16]. The much cheaper costs of energy from fossil fuels dictates that the commercial pyrolysis and gasification of wastes for energy has to be subsidized for now. For example incentives from the UK government such as the renewable heat incentive (RHI) and renewable obligation certificates (ROCs) have encouraged investments. The increasing landfill tax is also an added advantage in the UK, because energy from waste operators can charge a substantial gate fee as well, making extra revenue available to offset some of the costs of generating energy from waste pyrolysis and gasification. Significant effort still needs to be put into lowering the costs of waste pyrolysis and gasification technology.

Economies of scale, plays a very significant role in the commercial deployment of any technology due to the ability to reduce costs by building larger processes. However for pyrolysis and gasification of biomass and wastes for energy there are practical upper limitations on the process size due to the diverse location of feedstock resources and the need to transport them. Maximum suggested sizes range from 80MWe for Europe and 150MWe for North America [19].

The heterogeneous, less energy dense and high moisture characteristics of solid wastes introduces a practical challenge in using them directly for pyrolysis and gasification. This means that for most pyrolysis and gasification processes wastes would need to be processed further to change their physical properties by techniques such as shredding, drying, pelletizing and torrefaction. These obviously introduce extra costs to their processing for energy.

Secondary equipment and processes such as gas engines, gas turbines, methanol and FT synthesis processes have limited tolerances on the quality of the gas products both in terms of the tar content [20-21] and the product distribution [18, 22] (for methanol and FT synthesis). These requirements dictate further conditioning of the gaseous products via higher temperature reforming, catalytic cracking and other tar removal technologies, adding to the costs of the process. Furthermore higher temperature reforming/cracking has energy penalties while catalysts suffer from deactivation by coking among others.

In light of the above challenges further effort is required in terms of process improvement and economic incentivising by governments, in order to fully harness the potential of commercial scale energy from pyrolysis and gasification of solid wastes.

1.3 Hydrogen potential from pyrolysis and gasification of solid wastes

The hydrogen economy has become a topic of many debates and numerous research efforts are being put towards developing commercial scale hydrogen production in the future for utilization as a transport fuel to replace fossil fuels. This is because hydrogen presents some important advantages: like electricity, hydrogen is an energy carrier and it can be produced from a variety of very common materials i.e. natural gas, any other carbonaceous material like coal, wastes and water. It can be combusted in internal combustion (IC) engines to yield energy and water vapour without producing any CO₂, hence potentially decarbonising our energy use, and it can be used in fuel cells to generate electricity, and this is viewed by some experts to be paramount to the future of automobiles [23-24]. Other advantages of hydrogen include high octane number, rapid burning speed, wider flammability limits than air and methane and no known ozone toxicity potential. There are however issues with the storage of hydrogen on vehicles, due to its very low density larger storage tanks would be required to provide reasonable vehicle range [24].

The global hydrogen market is worth more than \$40 billion annually and growing [24]. Presently the commercial production of hydrogen for applications in fuel refining, ammonia and methanol synthesis, is done predominantly by reforming fossil fuels (natural gas, oil coal), which releases CO₂ to the environment. A very small portion is generated via electrolysis. However the fossil fuel options still provide the most cost effective means of producing commercial quantity hydrogen. Waste biomass and solid wastes also present an option for the production of renewable hydrogen [23-25] via pyrolysis and gasification [24-27], possibly integrated with CO₂ capture. Materials such as waste plastics contained within solid waste will increase the hydrogen production potential from solid waste [28]. There are currently no commercial scale processes for the production of H₂ from solid wastes due to economic unattractiveness and the need for process efficiency improvements [29].

1.4 Research objectives

The pyrolysis and gasification of solid wastes will play an important role in the future both as alternative waste management options, as alternative energy options and hydrogen production options. It is therefore important to research and develop these technologies in order to address their current limitations, thereby making them commercially ready.

The objective of this research was to carry out the pyrolysis and gasification of solid wastes in order to investigate the following:

- The influence of process conditions on high temperature pyrolysis of solid wastes in order to study its effects product yields and composition.
- The influence of waste components on high temperature pyrolysis of solid wastes in order to study the contributions of the different components to product yields and composition.
- The influence of process conditions on non-catalytic pyrolysis-gasification of solid waste using a continuous feed screw kiln reactor in order to study their effects on gas yield.
- The preparation and testing of high activity (H_2 yield) and high stability (coke resistance) catalysts in order to study their effects on H_2 yield and coke resistance.
- The influence of process conditions such as temperature, steam ratio, catalysis ratio and type on H_2 production from catalytic pyrolysis-gasification of wastes in order to study the effects of the process conditions on gas and H_2 yield.
- The influence of CO_2 capture additives on H_2 production in order to study the effects of CaO for CO_2 capture as well as its impacts on gas and H_2 yield.

- The commercial scale pyrolysis-partial oxidation of different real wastes in a screw kiln reactor in order to study the effects process scale-up on product yield and composition.

References

1. IEA, *IEA bioenergy annual report*. 2006, IEA (International Energy Agency). p. 1/124.
2. Huber, G.W., Iborra, S. and Corma, A., *Synthesis of Transportation Fuels from Biomass: Chemistry, Catalysts, and Engineering*. Chemical Reviews, 2006. **106**(9): p. 4044-4098.
3. Eurostat, *Generation and treatment of municipal waste*. 2011, Eurostat, Bech Building, Luxembourg. Report No. ISSN 1977-0316.
4. DEFRA, *Waste data overview*. 2011.
5. ACRA. *Europe and wastes*. 2003 5-2-2013]; Available from: http://resourcities.acrplus.org/waste_resources/europe_waste.htm.
6. CIWEM. *Energy recovery from waste*. 2006 October 2006 [cited 2009 11-11-2009]; Available from: http://www.ciwem.org/policy/policies/energy_recovery_from_waste.asp.
7. FOE, *Briefing: Anaerobic Digestion*. 2007, Friends of the Earth.
8. Dennis, A. and Burke, P.E., *Diary waste anaerobic digestion handbook: Options for recovering beneficial products from diary manure*. 2001, Environmental Energy Company.
9. Schmitt, E., Bura, R., Gustafson, R., Cooper, J. and Vajzovic, A., *Converting lignocellulosic solid waste into ethanol for the State of Washington: An investigation of treatment technologies and environmental impacts*. Bioresource Technology, 2012. **104**(0): p. 400-409.
10. Park, I., Kim, I., Kang, K., Sohn, H., Rhee, I., Jin, I. and Jang, H., *Cellulose ethanol production from waste newsprint by simultaneous saccharification and fermentation using *Saccharomyces cerevisiae* KNU5377*. Process Biochemistry, 2010. **45**(4): p. 487-492.
11. Giusti, L., *A review of waste management practices and their impact on human health*. Waste Management, 2009. **29**(8): p. 2227-2239.
12. Cliffe, K.R. and Patumsawad, S., *Co-combustion of waste from olive oil production with coal in a fluidised bed*. Waste Management, 2001. **21**(1): p. 49-53.
13. Straka, P. and Bucko, Z., *Co-gasification of a lignite/waste-tyre mixture in a moving bed*. Fuel Processing Technology, 2009. **90**(10): p. 1202-1206.
14. Gomez, E., Rani, D.A., Cheeseman, C.R., Deegan, D., Wise, M. and Boccaccini, A.R., *Thermal plasma technology for the treatment of wastes: A critical review*. Journal of Hazardous Materials, 2009. **161**(2-3): p. 614-626.
15. Williams, P.T., *Waste Treatment and Disposal*. 2nd Edition ed. 2005: John Wiley & Sons, Ltd. 380.
16. Demirbas, A., *Biomass resource facilities and biomass conversion processing for fuels and chemicals*. Energy Conversion and Management, 2001. **42**(11): p. 1357-1378.

17. Williams, P.T., Besler, S. and Taylor, D.T., *The pyrolysis of scrap automotive tyres: The influence of temperature and heating rate on product composition*. Fuel, 1990. **69**(12): p. 1474-1482.
18. Bridgwater, A.V., *Renewable fuels and chemicals by thermal processing of biomass*. Chemical Engineering Journal, 2003. **91**(2-3): p. 87-102.
19. Kaygusuz, K., *Biomass as a Renewable Energy Source for Sustainable Fuels*. 2009, Taylor & Francis. p. 535 - 545.
20. Milne, T.A. and Evans, R.J., *Biomass gasification "tars": their nature, formation and conversion*. 1998, NREL, Golden, CO, USA, Report no. NREL/TP-570-25357.
21. Bui, T., Loof, R. and Bhattacharya, S.C., *Multi-stage reactor for thermal gasification of wood*. Energy, 1994. **19**(4): p. 397-404.
22. Reichling, J.P. and Kulacki, F.A., *Comparative analysis of Fischer–Tropsch and integrated gasification combined cycle biomass utilization*. Energy, 2011. **36**(11): p. 6529-6535.
23. Daniel, S. and S., C.J., *The hydrogen energy transition: moving toward the port petroleum age in transportation*. The hydrogen energy transition: moving toward the port petroleum age in transportation, ed. Daniel, S. and S., C.J. 2004, Oxford: Elsevier academic press. 266.
24. Balat, M., *Potential importance of hydrogen as a future solution to environmental and transportation problems*. International Journal of Hydrogen Energy, 2008. **33**(15): p. 4013-4029.
25. Holladay, J.D., Hu, J., King, D.L. and Wang, Y., *An overview of hydrogen production technologies*. Catalysis Today, 2009. **139**(4): p. 244-260.
26. Demirbas, M.F., *Hydrogen from Various Biomass Species via Pyrolysis and Steam Gasification Processes*. 2006, Taylor & Francis. p. 245 - 252.
27. Garcia, L., French, R., Czernik, S. and Chornet, E., *Catalytic steam reforming of bio-oils for the production of hydrogen: effects of catalyst composition*. Applied Catalysis A: General, 2000. **201**(2): p. 225-239.
28. Pinto, F., Franco, C., André, R.N., Miranda, M., Gulyurtlu, I. and Cabrita, I., *Co-gasification study of biomass mixed with plastic wastes*. Fuel, 2002. **81**(3): p. 291-297.
29. Makihiro, A., Barreto, L. and Riahi, K., *Assessment of alternative hydrogen pathways: Naturag gas and biomass*. 2003, International institute for applied systems analysis: Ladenburg Austria. Report No IR-03-037.

CHAPTER 2. LITERATURE REVIEW

2.1 Pyrolysis

2.1.1 High temperature pyrolysis for hydrogen and syngas

Pyrolysis has been used extensively, especially in the energy and oil industry for the thermal cracking of petroleum oil [1]. However its application for waste conversion is still a recent development and is therefore still under-going research and testing. Such scrutiny is required for the application of this technology to waste especially considering the nature of wastes which has a varied composition. For example the general compositions of UK and EU MSW are shown in figures 1-1 and 1-2, and the different components all have their effects on the yield and composition of the end products of the process.

The production of a mainly gaseous product from pyrolysis can be optimized by operating the process at high heating rates and temperatures and long residence time, thereby converting the heavier vapour products into more gases via further decomposition reactions [2-3]. According to Williams (2005), this type of pyrolysis can be sub-divided into two forms: *flash-gas and ultra pyrolysis* take place at temperatures from 700 °C and 1000 °C respectively, and their main product are gas compounds which can be converted to chemicals. Flash-gas or ultra pyrolysis produces a mainly gaseous product due to a combination of decomposition processes: Primary decomposition of the sample first occurs to release the heavier hydrocarbons and then a further decomposition of some of these heavier hydrocarbons, termed secondary and tertiary decomposition or cracking [4].

The extent of these cracking reactions tends to be favoured by high residence time and high temperatures [4-5]. These factors also influence the composition of the gaseous products [4-5] which is made up of mainly CO, H₂, CO₂, CH₄ and other heavier gases. Higher temperatures and residence times result in severe cracking reactions to yield more of the permanent gases and

less hydrocarbon gases. Such conditions are reported to favour the yield of H₂ in the product gas [2, 6]. The high temperature pyrolysis of waste materials which contain high carbon and hydrogen compounds such as plastics and tyres have been shown to produce gases with high concentrations of methane, hydrogen and other hydrocarbons, which are of high calorific value [7-10].

Most works carried out on biomass and waste pyrolysis have been generally geared towards the production of oils and char [11-14], as these require low temperatures do not add the extra energy penalties required by high temperatures. The trend is normally to apply gasification techniques, where the aim is to obtain gaseous products from the solid wastes. This is because the gasification phase proceeds from the pyrolysis phase [15-16] as is demonstrated by techniques such as the PyRos technology for flash pyrolysis [17] and the Multi-staged Enthalpy Extraction Technology (MEET) [18].

2.1.2 Pyrolysis reactors

There are a variety of pyrolysis reactors and designs which exist and have been utilized, and researched mostly for the pyrolysis of biomass but also solid wastes. These include: the fluidized bed reactor (and all its variants), free-fall or entrained flow reactor, the rotary kiln reactor, rotating cone reactor, etc. These are described in the following literature.

2.1.2.1 The fluidized bed reactor

The fluidized bed design of reactors is popular and has been widely used in the fuels processing and combustion industry [19-22]. The fluidized bed reactor has also been extensively applied for the pyrolysis of biomass and solid wastes [7, 23-26]. Some of the characteristics of the fluidized bed reactor which has made it popular for pyrolysis include ease of operation, good scale-up properties, good heat and mass transfer and therefore high heating rates are achievable [5, 15, 26].

Types of the fluidized bed reactor which have been utilized include: Bubbling, circulating, twin fluid bed, pressurized fluidized bed and spout-fluidized bed [15, 23, 26-29]. The fluidized bed reactors listed above, all have certain basic features in common which are generic to fluidized bed reactors. These features are:

- An inert bed material to aid with heat transfer, commonly used for this purpose is sand, which can be quartz sand [25], silica sand [7] or a combination of sand and a catalyst [30].
- A fluidizing medium also functional to allow equilibrium heat transfer to samples. In most cases the fluidizing medium is the chosen reaction atmosphere which can be air (for gasification) [31], an inert gas (for pyrolysis) such as nitrogen [32], steam [33] or recycled product gas [34] this technique is common with the bubbling and circulating fluidized bed.

The differences which exist in the different types of fluidized bed reactors apply to specific features of their design: The *pressurized fluidized beds* are designed to process samples under pressure [27]. The *circulating fluidized bed* design causes mixing and contact between the bed material, the sample and the fluidizing medium through circulating motion [33]. The *bubbling fluidized bed* is designed like the circulating bed, however without the circulating motion of the reactor [34]. *Spout-fluidized bed* reactors allow the fluidizing medium to be injected vertically to the reactor axis usually below the bed material. This penetrates the bed material creating a spout which is responsible for particle recirculation [29]. Two fluidized bed reactors can be connected so as to have char combustion in the second reactor [15] & [28] this is the setup for a *twin fluid bed* reactor.

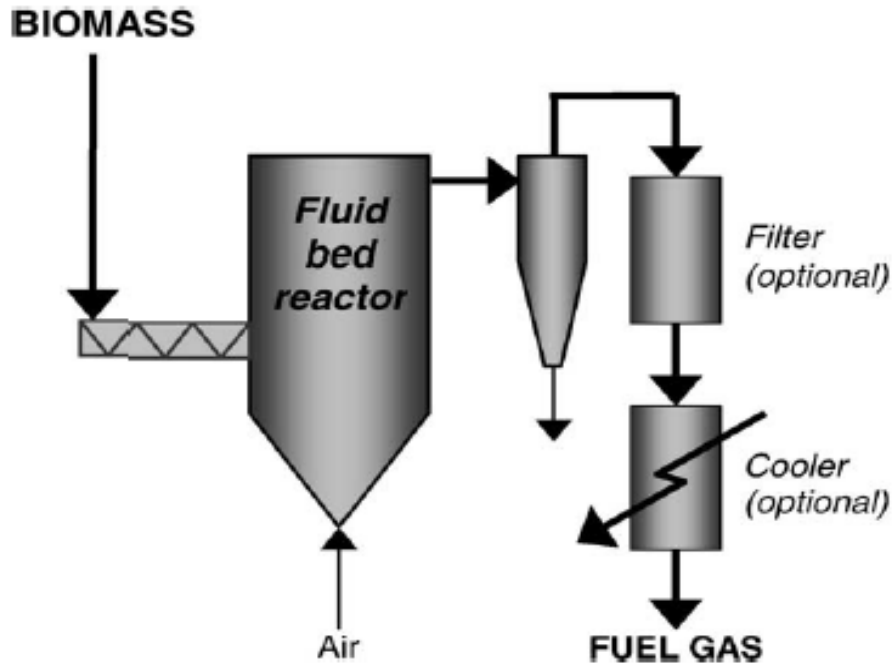


Figure 2-1 Fluidized bed Reactor [15]

In Figure 2-1 above a basic diagram of the fluidized bed reactor setup is shown, this setup can be amended slightly to represent the different types of fluidized beds. In general, materials to be reacted are introduced either in batches or continually into an already hot bed, fluidized by inert gas [31]. Heat transfer from the bed and fluid medium results in the degradation of the material. Generated vapours are pushed out of the reactor by the fluidizing agent through condensers or coolers to capture condensable products, and through filters or a cyclone to trap solid particles and char particles. Product gases are either collected/channelled for analysis or processed for utilization.

Advantages which apply to this reactor design include [15, 24, 34]:

- High reaction rates and good temperature control
- Higher tolerance to a range of particle sizes
- Product gases from this reactor contain moderate tar level and higher particulates

- Enables catalyst to be easily integrated into the bed (excluding circulating fluidized beds).

2.1.2.2 Free fall reactor

The free fall reactor has been investigated for the processing of mostly biomass and biomass waste [35-40]. On a laboratory scale this reactor design has been shown to deliver very high temperatures [41-42], very high heating rates [35, 43] and very short sample and gas residence times from milliseconds to a few seconds [34].

Also called an *Entrained flow* reactor [42, 44], the free fall reactor is technologically quite a simple process design. It is generally made up of a feedstock feeding mechanism which is connected to supply the feed to the reactor's heated zone, consisting of a vertical heated tubular length, normally heated externally [45]. Usually connected at the exit of the tubular reactor (at the bottom) are a char receiver, gas filter, condenser and a gas collection system [40, 46]. The carrier gas which may be pre-heated is channelled through the feeding mechanism into the reactor. The residence time of the feedstock in the reactor hot zone is determined by the length of the heated section [46] usually allowing for only a maximum of a few seconds. Figure 2-2 below shows a general schematic of a free fall/entrained flow reactor.

The design of this reactor is such that heat is supplied to the feedstock by the carrier gas while it drops through the hot zone, as well as the reactor wall, therefore it is important in order to encourage rapid heating that the feedstock size is fairly small (approximately 105 to 250 μm) [47]. Relying on feedstock size and the few seconds contact with the hot gas in order to transfer heat to the feed can generate issues related to heat transfer, also feedstock preparation can be quite cost intensive [34]. This reactor has been reported to be an interesting analytical tool to study pyrolysis at rapid heating rates due to its characteristic high heating rates ($>500 \text{ K s}^{-1}$ & $10^4 \text{ }^\circ\text{C s}^{-1}$) [42, 44].

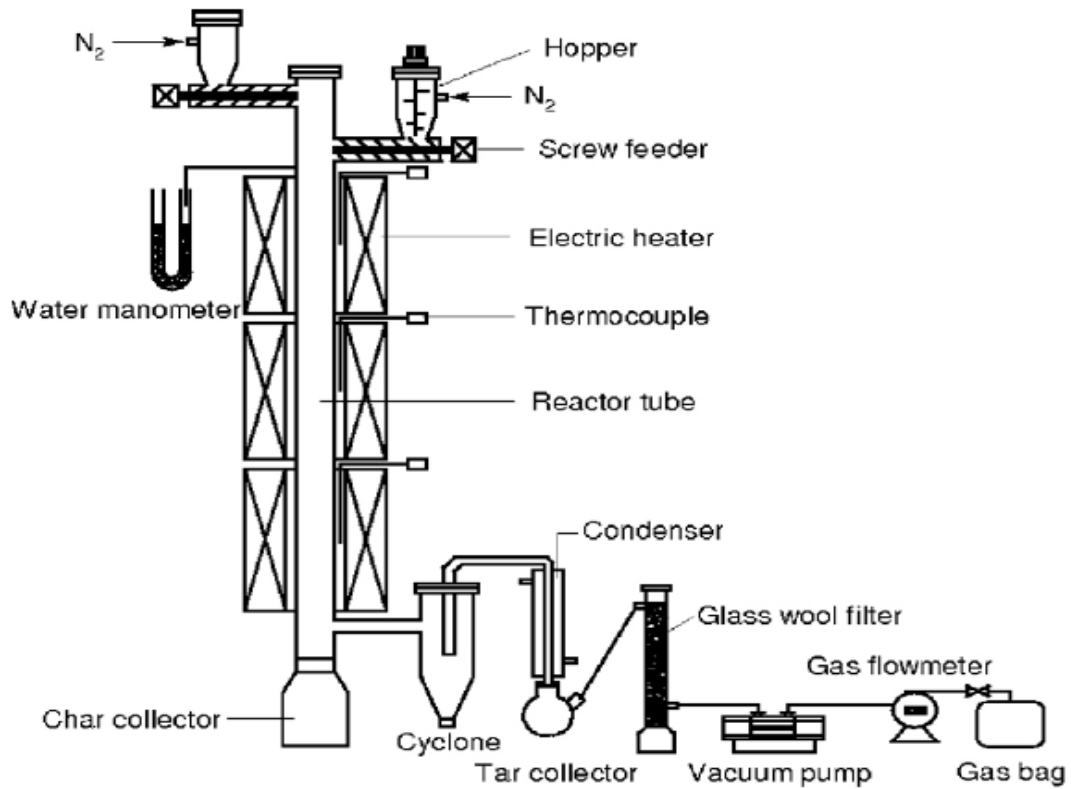


Figure 2-2 Free fall/Entrained flow reactor [45]

2.1.2.3 Rotary kiln & screw kiln reactors

Rotary Kiln and screw kiln reactors have been investigated for the pyrolysis of solid wastes and wood [48-51]. The rotary kiln and screw kiln reactors have similar design features, and are designed for both continuous and batch feed. Figure 2-3 below shows a schematic of the rotary kiln reactor design. While figure 2-4 shows a schematic of the screw kiln reactor design.

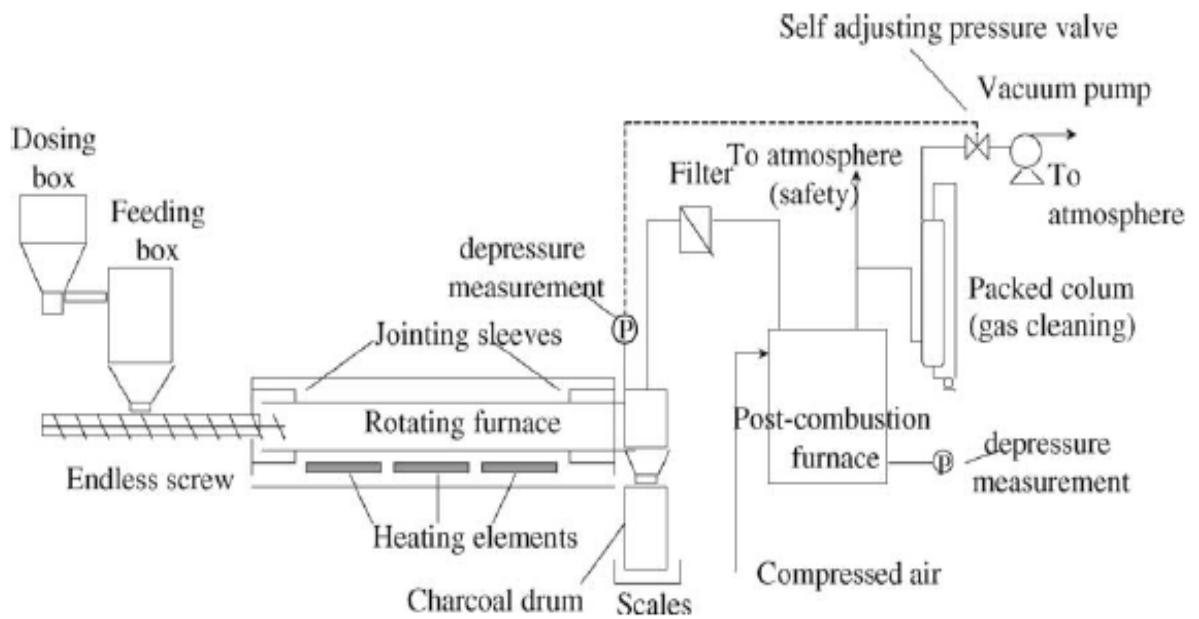


Figure 2-3 Schematic of a rotary Kiln reactor [52]

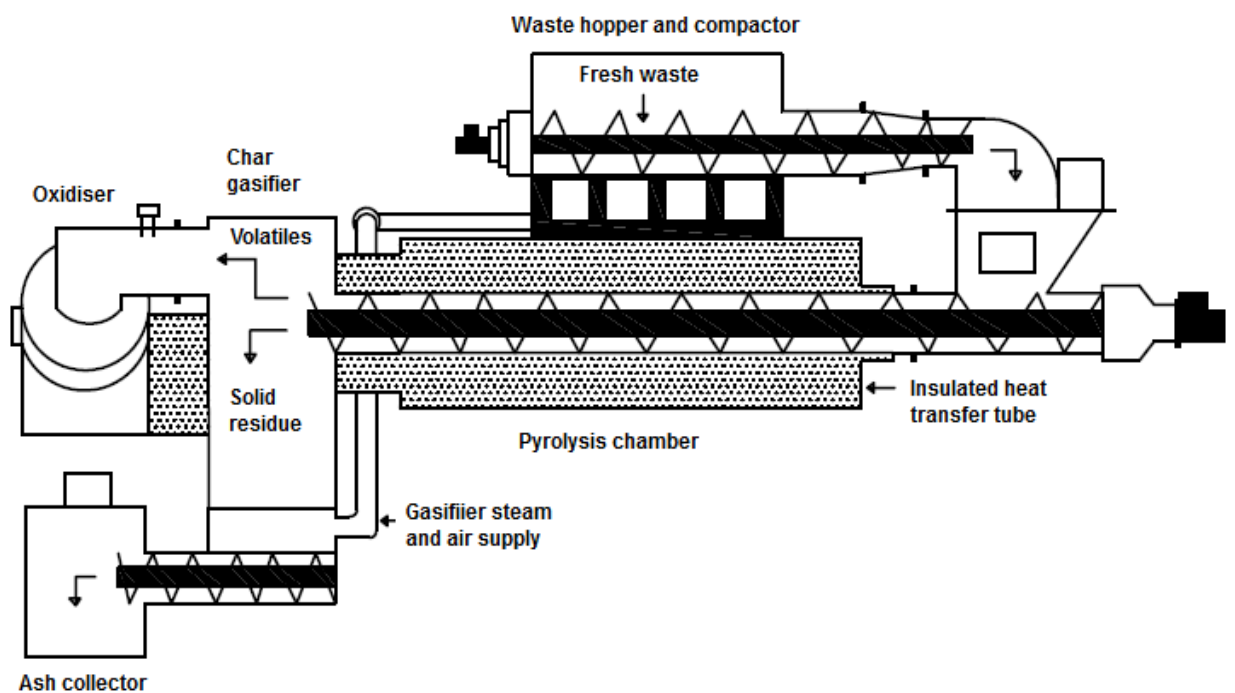


Figure 2-4 Schematic of a screw kiln reactor

The feedstock is initially deposited onto a screw feeder which then feeds the reactor as it extends into the reactor hot-zone. The design difference between the two reactors exists in the way in which the feedstock is transported along the reactor heated zone. For the rotary kiln reactor, feedstock is moved along

the reactor which has a cylindrical shape and is inclined at an angle with a furnace around it. The rotation and incline of the cylindrical reactor causes movement of the feed along the heated zone in the direction of the incline, resulting in its volatilization as it moves along the reactor [53]. For the screw kiln feedstock is moved along the cylindrical reactor by the action of the rotating screw which runs through the heated length of the reactor [48].

Feed residence time in the hot-zone can be altered by alternating the reactor rotation speed in the rotary kiln reactor. While feed residence time in the screw kiln is determined by the speed at which the screw rotates. Residue is collected at the discharge end of the reactor and the product gas is also extracted. Good solid mixing and control makes the rotary kiln reactor popular for waste processing [24]. The screw kiln is characterized by high tolerance to different feedstock types and sizes.

2.1.2.4 Other Reactors

A variety of other reactors both laboratory scale and pilot scale have been investigated for the fast pyrolysis of waste and biomass. Reactors of interest in this section include the: curie point reactors, rotating cone reactors, wire mesh reactors. These reactors are discussed below.

Curie point pyrolyzers are laboratory scale reactors which are capable of delivering high heating rates, high temperatures and short sample residence times [34, 54], just like the pyroprobe, the pyrolyzer is usually connected to a gas analysis unit. Pyrolysis temperature choice for this instrument is limited, as this is determined by the curie point of the ferro-magnetic pyrolysis wire which is responsible for the heating [54].

Rotating cone reactors have been used to investigate the fast pyrolysis of mainly biomass samples [34, 55]. This reactor setup has been reported to deliver rapid heating rates and short residence times [34]. The carrier gas requirement for this reactor is reduced compared to fluidized beds however it is quite an intricate system comprising of: a rotating cone pyrolyzer, a riser for

sand recycling and a bubbling bed char combustor [15, 34]. Feedstock is introduced at the bottom of the system where the centrifugal force created by the rotating cone drives the feed up the walls of the hot rotating cone. Product gases are channelled through filters and condensers while the char and sand is channelled to a combustor where the heat from char combustion reheats the sand for recycling.

Wire mesh reactors have been used for laboratory investigations of pyrolysis biomass and wastes [56-58]. The major design feature of interest regarding this reactor is its ability to apply rapid heating rates to the sample (up to and above $60\text{ }^{\circ}\text{C s}^{-1}$) [59]. The general design comprises a cylindrical externally heated reactor tube with stainless steel rings situated in the heated zone in which a wire mesh basket containing the feed can be inserted on top of the steel rings once the desired temperature has been reached. The volatiles are purged out by the carrier gas while the char residue remains on the mesh.

2.1.3 The pyrolysis of solid wastes and biomass

2.1.3.1 Products from the pyrolysis of solid wastes and biomass

Pyrolysis is thought to be interesting because its process conditions can be manipulated to generate either: oils, char or gases as the main end products by altering mainly the process temperature, the heating rate and residence time [1, 15, 60-61]. Also its end products can all be put to some use as follows [62]:

- The oils derived from pyrolysis of a variety of waste have been shown to be complex in composition, of higher energy density than raw waste, have a potential for direct fuel application, can be upgraded to produce refined fuels and contain a variety of chemicals which may be used as chemical feedstock [4, 11-12, 14, 63].

- The char from the process has a potential to be used as solid fuel, can be used as carbon black, combusted or can be converted into activated carbon [4, 13, 64].
- The product gases have been shown to possess a range of medium to high calorific value, making them useful for combustion to release energy as well as a source of hydrogen [4, 60, 65-67].

This means that energy can be obtained from the solid wastes in a cleaner way than from incineration, since a lesser percentage of sulphur oxides and nitrogen oxides are produced as a result of the inert atmosphere in pyrolysis processes [23]. Pyrolysis at moderate temperatures, fast heating rate and rapid quenching of the volatiles, results in the production of more oil [1, 15, 60]. If the aim of the process is to yield a mostly solid product, a low heating rate and low temperature pyrolysis would be required [1, 15]. For a high gas yield, a high temperature and long volatile residence time is required [15, 60]. Several studies [2, 4-5] have reported the yield of a mainly gaseous product from the pyrolysis of biomass and MSW at temperatures above 700 °C and at extended residence time. The gaseous products detected include H₂, CO, CO₂, CH₄, C₂H₄ and C₂H₆. Others [4, 68-70] have reported the production of maximum oil yields from the pyrolysis of biomass and RDF at temperatures below 700 °C and rapid vapour quenching. The oils were complex and made up of oxygenates, aliphatics and aromatics. In addition it has been reported that maximum char yield is formed at temperatures below 500 °C and at slow heating rates [13-14, 71].

2.1.3.2 Effects of material characteristics

The physical properties of the feedstock intended for pyrolysis is important. Residual solid wastes (after recyclables have been removed) have to be prepared for pyrolysis by pre-treatment processes so as to provide a feed stock with acceptable moisture content and to remove inorganic materials [31, 72]. Some of these pre-treatment processes include size reduction, screening, drying, pelletizing and etc, and are also applicable to other waste biomass.

Significant government and commercial efforts have been put into homogenizing solid wastes in order to make them more suitable for thermal processing for energy. For example energy densified products from MSW processing have been produced which are interchangeably referred to as refuse derived fuel (RDF) or solids recovered fuel (SRF), and are classified based on standards stipulated by the European committee for standardization [73-74]. These pre-treatment options are commercially available and improve both the handling, transportation, storage and processing logistics of wastes, however they also significantly add to the costs of processing [75]. There is also the added economic advantage that the process may qualify to receive ROCs due to the biogenic fraction [73].

Buah et al [4] and Lou et al [76] investigated the pyrolysis of RDF and single components of MSW respectively. They both reported that the products were influenced by the size of the feed. The metal constituents of wastes and biomass are also of influence to their thermal degradation. The volatilization of metals has been reported to occur and is dependent on the process temperature, though most of the metals remain in the residual solids [73, 77]. The metal components have also been reported to possibly catalyze the thermal degradation process [43, 77-78]. The material components of wastes (lignocellulosic and plastics) and biomass (lignin, cellulose and hemicellulose) have impacts on their pyrolysis. The pyrolytic degradation of wastes and biomass have been reported to be a sum of the degradation of its individual components [78-82].

2.1.3.3 Effects of temperature and heating rate

The reaction temperature and heating rate are very important parameters for pyrolysis. Interestingly these two parameters have been shown to be interconnected i.e. higher temperatures result in higher heating rates [40, 43-44], however the heating rate is also influenced by particle size [26, 76] and the nature of the sample. Basically the heating rate affects how long it takes for the sample to get to the intended pyrolysis temperature, i.e. high heating

rates mean shorter time to reach pyrolysis temperature [83]. A comparison of pyrolysis of biomass at 850 °C and at different heating rates indicates that the higher heating rate experiments (up to 1000 °C s⁻¹) resulted in higher feed mass conversion (up to 95%) [84].

Researchers have reported that higher temperatures promote the production of gaseous process products [2, 5, 85-86] and a decrease in char [8, 40, 62] from waste and biomass pyrolysis. Total gas volumes have been recorded to increase with increase in temperature, due to an increases in H₂ [61] and CO [87-88] production at temperatures above 700 °C which encourages cracking of secondary vapours [2]. There are indications that increased temperatures result in increased tar conversion to a more stable compound [2-3] as a result of in-situ steam reforming of hydrocarbons and tar [89]. High reaction temperatures have been reported to increase reaction rates thereby encouraging secondary reactions in the vapour phase as soon as pyrolysis vapours are released from the sample into the hot-zone [43].

The product gas composition has been shown to be affected by high reaction temperatures, which promotes the formation of gas products with increased H₂, CO and CH₄ and reduced CO₂ [40, 43]. In general higher temperature encourages the production of H₂, CO and CO₂ at the expense of high hydrocarbons (C₁-C₄) [3]. Concentrations of H₂ of above 28 mol% and combined H₂ and CO of above 65 mol% [38] and 70 - 80 vol% [44] have been reported for the pyrolysis of biomass at high temperatures (800 °C) without catalysts resulting in an increased H₂/CO ratio.

Process mass conversions of up to 87 wt% are in order for temperatures above 800 °C to 1000 °C [42]. Increased temperatures also promotes an increase in the production of hydrocarbons like CH₄ and C₂H₄, however these tend to decompose into char and H₂ when the temperature is high enough [44]. Gas heating values of above 18 MJ Nm⁻³ have been recorded for temperatures above 750 °C up to 900 °C [56]. High temperature also favours the cracking of tar [40] which is comprised mostly of benzene, xylene, naphthalene and toluene. This is due to the cracking of polycyclic molecules thereby producing a simpler poly-aromatic naphthalene, mono-aromatic

benzene and a decrease in xylene and toluene molecules [3]. Kantarelis et al [3] also reported further cracking of these molecules with further increase in temperature.

As stated earlier the heating rate is influenced by, and works with the pyrolysis temperature to influence the product yields. Increased volatile yield have been reported [90-92] for high heating rate compared to lower heating rate pyrolysis at the same temperature, due to the process severity being impacted by the higher heating rate pyrolysis. The porosity and structure of the produced chars from pyrolysis have also been reported to be affected by heating rate [37, 93].

2.1.3.4 Effects of other process conditions

Feedstock size: The particle size of the feedstock is an important factor for fast pyrolysis because this affects the mass transfer, heat transfer and the level to which secondary reactions occur within the sample particle [43]. The pyrolysis of smaller particle sizes at elevated temperatures results in increased gas yields while simultaneously reducing the char, tar and water products [38, 43, 94] due to increased heating rate [23, 40].

Larger particles create an increased resistance to internal heat transfer conduction, causing a larger temperature gradient from the surface to within the particle thereby limiting complete particle pyrolysis, resulting in higher char content and less volatile products [46, 84]. Larger particles therefore reduce heating rate and encourage carbonization [26]. Wei et al [43] reported char yield decrease from 10.3 wt% to 3.8 wt% when the particle size decreased from 1.2 mm to .3 mm during biomass pyrolysis. There is also a tendency for larger particle sizes to extend the residence time of volatile matter within its structure thereby promoting secondary reactions and gas yield [76], however this tendency is far outweighed by the gas yields from the pyrolysis of smaller particle sizes.

Smaller particle sizes tend to yield gaseous products with higher H₂ content [40] while larger particles tend to yield more CO products [42]. A threefold

increase in H₂ content of the product gas was reported by Dupont et al [42] when the particle size decreased from 1.1 mm to 0.4 mm at temperatures of 800 °C and above, Li et al [38] also reported H₂ increase from 3 to 20 mol% with particle size decrease from 2.00 mm to 0.30 mm. H₂ and CO concentrations [76], H₂/CO ratio increase and CO₂ decrease are also in order as a result of particle size decrease. Lou et al [76] reported a decrease in CO₂ concentration and an increase in H₂, CO, CH₄, C₂H₄ and C₂H₆ when sample size was decreased during the pyrolysis of wood and kitchen garbage samples. Good heat and mass transfer with smaller particles also results in shorter pyrolysis time requirements and higher mass conversions than larger particle.

Volatile residence time: Basically the volatile residence time describes the time taken from when the volatile compounds are generated within or from the sample structure, until they exit the reactor hot-zone. This important pyrolysis factor determines the extent of the pyrolysis reactions by influencing whether or not secondary reactions take place and the extent to which they occur [43]. Long residence time encourages secondary reactions resulting in char reduction and tar cracking thereby increasing the quantities of the gaseous products [26, 42], while short residence time does not encourage secondary reactions and results in increased liquid and char products [8, 61]. The residence time is normally determined by the length of the reactor heated zone and the gas flow rate and can easily be varied by adjusting the gas flow rate within the reactor [95] or adjusting the heated zone.

Long residence time in combination with high temperature encourages increased H₂ production while favouring the olefin (C₁ – C₄) and tar cracking and reforming [3, 44]. At the beginning of the pyrolysis process, the primary reaction releases volatiles comprising mostly of H₂, CO, CO₂, CH₄, olefins, tar in varying quantities and char. Secondary reactions when encouraged by long volatile residence time result in tar and olefin cracking to the advantage of the other gases thereby increasing their quantities [32]. Further reactions as shown in equations 2.1 to 2.3 below will result in a change in the gas composition. [3]:



Yang et al [96] reported increasing total gas yield with increasing residence time to a maximum at 14 sec and after this a decrease in total gas yield was recorded.

Reaction atmosphere: The nature of pyrolysis dictates that it has to be carried out in the absence of oxygen in order to prevent combustion. To ensure this and also provide a constant flow of the product gases from the reactor, reactions are usually carried out in the presence of an inert gas flow [54]. Gases reported to have been widely used for this purpose include nitrogen [2, 10], argon [97] and helium [5, 98]. For the pyrolysis of MSW helium has the advantage over nitrogen, of guaranteeing an inert atmosphere, on the basis that the detection of nitrogen in the product gas will indicate the introduction of air into the reaction atmosphere [5, 99]. In all cases atmosphere or carrier gas is used to:

- Provide an atmosphere void of oxygen or air for the pyrolysis reaction.
- Serve as a means of heat transfer to the sample to be reacted.
- Create a flow out of the product gas from the reactor.

2.1.3.5 Effects of catalyst

Where the aim is to maximize the production of syngas and hydrogen, the syngas quality in regards to tar availability and gas composition is very important because high tar content creates utilization difficulties for the syngas especially in gas engines, turbines and other equipment [100-102], while gas compositions with less H₂ and CO, is less suitable for fuel synthesis. The advantages of catalytic cracking in pyrolysis include the conversion of tar

to useful product gases and the possibility of changing the composition of the product gases [66, 86, 103-104] i.e. to generate more H₂. Compared to other gas cleaning options catalytic cracking can operate at relatively low temperatures (600-800°C) avoiding the necessity of expensive alloys required for reactor design in high temperature (>1000°C) cracking. It also eliminates the need to substantially reduce the thermodynamic efficiency and impair the performance and economics of the processing system by cooling down the syngas (<150°C) before tar removal as required by physical tar removal methods [102].

Tar cracking and improved syngas quality are promoted via a number of processes which are apparently enhanced by the presence of the catalyst thereby increasing the reaction rate within the system. These include: dry reforming, thermal cracking, auto-steam reforming, etc [105]. A simplified description of the catalytic tar cracking is as follows: hydrocarbons are dissociatively adsorbed and catalytically dehydrogenated, water is dissociatively adsorbed and provides hydroxylation, OH radical migration leads to the oxidation of intermediary hydrocarbon fragments and surface carbon to form H₂ and CO [103].

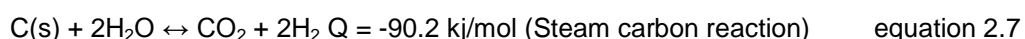
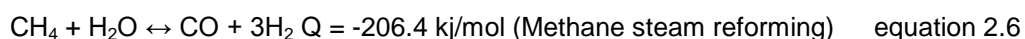
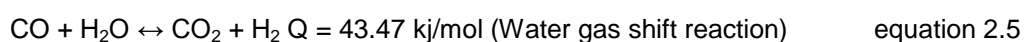
Catalytic cracking can either take place within the pyrolysis reactor (Primary cracking) or can take place in a separate reactor (Secondary cracking). The later obviously adds an extra reactor cost factor, making them not very economical, though quite effective. In the primary cracking method (with reference to catalytic cracking), the catalyst can either be integrated as a mixture with the sample or as a bed material. The primary method has the advantage of producing a syngas with almost similar quality as the secondary cracking method, while eliminating the need for a second reactor [106]. This method therefore promotes tar elimination, positive changes to product gas composition and char gasification, all in one reactor.

Some commonly used catalysts include: Nickel based catalysts [30], zeolites [32], dolomite [66, 104] and char [107].

2.2 Gasification

2.2.1 Gasification for hydrogen yield

Gasification technologies are well established just like pyrolysis for the processing of fuels. This technology is also becoming increasingly popular for the processing of solid fuels e.g. coal, biomass and wastes with the aim of converting them to syngas. The definition of gasification as given above requires that during the thermal conversion process, oxygen (via air, oxygen or steam) needs to be made available in quantities enough to cause partial oxidation without combustion. This is the technical difference between the pyrolysis and gasification processes. In theory the ideal gasification process is designed to produce mostly a syngas and solid product (char), however practically there is also a liquid product formed from condensed vapours (tars) as incomplete products of gasification [62, 108]. It is possible to increase the syngas product while reducing the char and condensed vapour products by altering process conditions such as temperature [109-110], catalyst [111-112], the ratio of oxidizing agent to solid fuel used [113-114] etc. Utilizing steam as the oxidizing agent instead of air, offers the advantage of eliminating the need for nitrogen separation from the process gas. Steam gasification also offers increased hydrogen production [108] via promotion of steam reforming reactions as shown in the equations 2.4 to 2.7 below



The application of gasification technology to waste and biomass processing is also quite recent and still requires further study unlike coal gasification which

is more established. Feedstock preparation for gasification is the same as described for pyrolysis.

2.2.2 Gasification reactors

Most of the reactor designs for pyrolysis are also applicable for gasification. Their major differences exist in the addition of inlet(s) for the oxidizing agent (steam, air or oxygen) for the gasification reactors. These include the fluidized bed reactor (and its variants), the entrained flow reactor, the fixed bed reactor etc. These reactor designs will be reviewed in the following sections. In order to avoid repetitions due to the identical designs features which exist between the gasification reactors and their pyrolysis counter parts, the focus will be on their design differences.

2.2.2.1 Fluidized bed reactors

The fluidized bed designs discussed for pyrolysis: circulating (Li et al 2004), bubbling [115], twin [116], spouted bed [117], pressurized [118] etc., have been investigated and utilized for biomass and waste gasification. In the case of gasification, the fluidizing medium (nitrogen, air, steam, or oxygen) can be bi-functional as follows: as a fluidizing agent for the reaction and as an oxidizing agent (apart from nitrogen) for the partial oxidation reactions.

The reactor design concept is still technically the same for all these reactors and their fast pyrolysis counterparts. However their designs have to accommodate certain criteria which are characteristic of gasification reactions. Firstly designs have to take into consideration the inlet(s) for the oxidizing agent, and this can be plural as gasification can also be carried out with a mixture of either steam, air, CO₂, O₂ and an inert gas [119-120]. Secondly, gasification reactions generally occur at higher temperatures than pyrolysis [62] this is due to the partial oxidation reaction which is generally exothermic. Fluidized bed gasifiers therefore have to be designed to withstand the higher temperatures to be expected. Figure 2-5 below is a schematic of a dual

fluidized bed reactor. Thirdly the type of gasification process to be carried out has to be taken into account i.e. instead of just a one stage gasification system, the gasification can be executed in more than one stage which may include: pyrolysis followed by partial oxidation and then followed by char gasification or combustion.

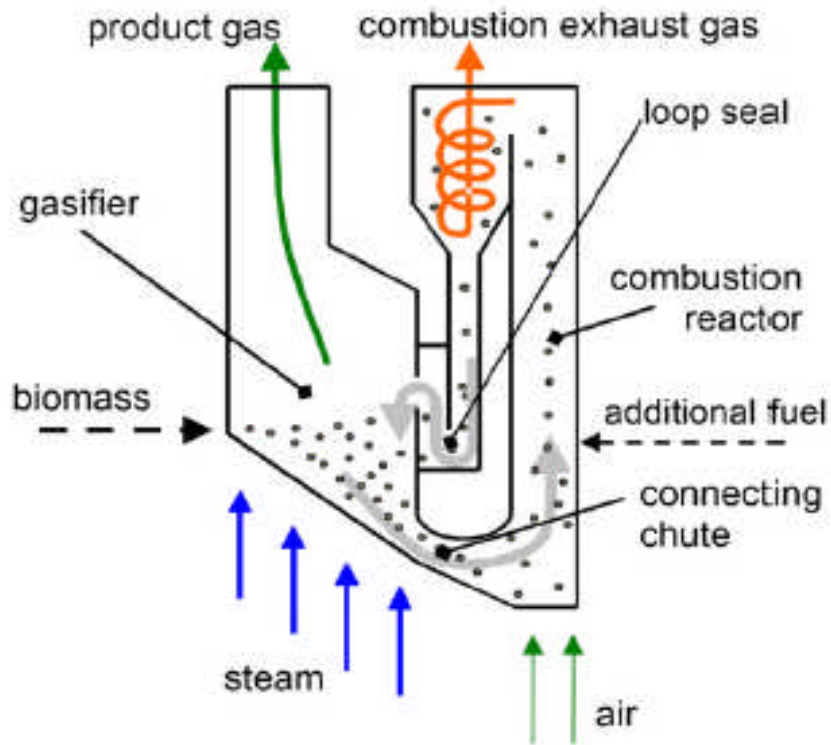


Figure 2-5 Dual fluidized bed reactor [121].

The fluidized bed reactor is advantageous for its thorough particle mixing, promoting exceptional heat and mass transfers [108]. However this thorough mixing can cause even distribution of particles across the bed which can result in converted and also unconverted particles exiting the reactor, increasing the tar content of produced syngas. There are also issues with particle agglomeration and ash leachability. The design of the fluidized bed dictates that feed particles which are of sizes that can be lifted by the fluid medium must be used. This therefore generates issues of very careful and costly feedstock preparation.

2.2.2.2 Fixed bed reactors

Fixed bed gasifiers are quite popular for gasification and have also been actively investigated for waste and biomass gasification [122-126]. Well over a period of 100 years, fixed bed reactors have been used on a commercial scale to process biomass (mostly Sod peat & wood chips) in order to provide district heating [127], initiated as a result of the oil crisis in the 1970's. They are generally the gasifiers of choice for small or medium scale gasification operations.

Different designs of the fixed bed reactor have been developed, mainly including: the vertical updraft and downdraft reactor design [15] and the horizontal reactor design [128-129]. The vertical reactors can either be designed for co-current (mostly for downdraft reactors) or counter-current (mostly for updraft reactors) flow processes [15, 130]. Also the cross flow design [131] and open core design [105] have been developed for gasification. The process type is basically determined by how the reactor is designed to allow for the collection of the product gas i.e. in the counter-current design the product gas is made to exit the reactor in a direction opposite the flow of the incoming sample while in the co-current design the product gas exit is in the same direction as the incoming feed.

The *cross flow* reactor is designed to enable feed stock inlet from the top and solid residue removal from the bottom while gas inlet and syngas outlet is from the same level but at opposite sides of the reactor. The temperature at the gas inlet is usually hottest due to gasification and above this zone a drying and pyrolysis zone occurs. Figure 2-6 is a schematic of the cross flow reactor. The *open core* reactor is an adaptation of any of the other three designs where the feedstock inlet size is increased and a water basin and rotating grates are integrated at the bottom of the reactor. These modifications allow the utilization of bulky feedstock and the effective removal of solid residue from this reactor.

Figure 2-7 below is a diagram generally describing the co-current and counter-current concept for fixed bed reactors. The inert gas together with the hot bed will be responsible for heat transfer to the feed. This gas is also responsible for channelling the product gas out of the reactor.

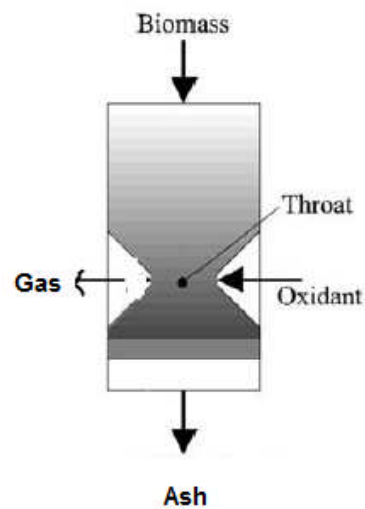


Figure 2-6 Cross flow fixed bed reactor.

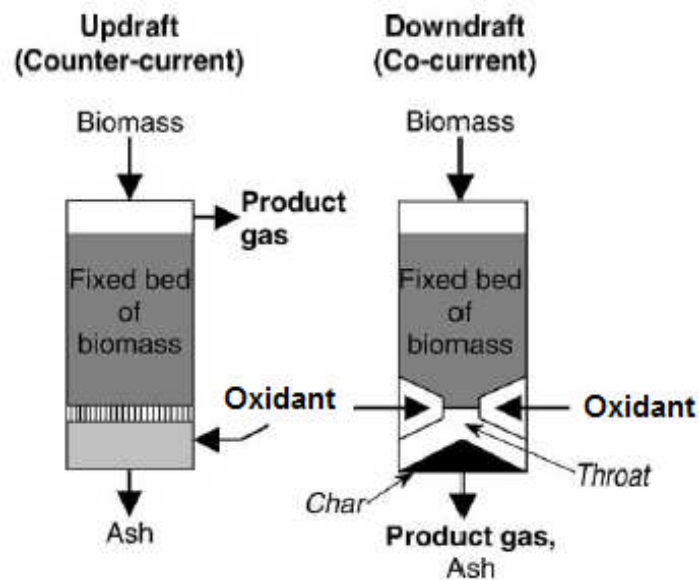


Figure 2-7 Fixed bed reactors (amended from [15])

The co-current or downdraft reactors have been reported to produce gases with much lower tar content and have been most extensively studied for

small-scale application, while the counter-current or updraft reactors have better scale up potential [127]. Other characteristics of both the reactor designs include [15, 127, 130]:

- Technology is simple and reliable for particles of relatively uniform sizes and less fine particles.
- Possibility of hot spots forming within the bed resulting in poor temperature distribution.
- High carbon conversion rate.

The counter-current design is more rugged and can deal with feeds of varied sizes and higher moisture content (up to 50% moisture content).

The simple design of fixed bed gasifiers is advantageous however this design produces a syngas with high tar content and of low calorific value [108]. This means for the syngas to be utilized, steps need to be taken either by separating the drying and pyrolysis stage from the gasification stage in two reactors or by integrating a catalytic process etc. This generally adds to the process operating costs.

2.2.2.3 Entrained flow reactors

Entrained flow gasifiers have been used extensively for coal gasification and are generating a lot of interests for the investigation of biomass gasification [132]. These reactors are commercially available due to experience with coal gasification, and are applicable for large scale uses. Characteristics of this reactor includes: very high temperatures (up to 1500 °C), high heating rate, short feedstock and gas residence times [108]. Another important design feature of this reactor is that feedstock can be injected either as a slurry [133-134] or as dry feed [135]. Figure 2-8 is a schematic of an entrained flow gasifier.

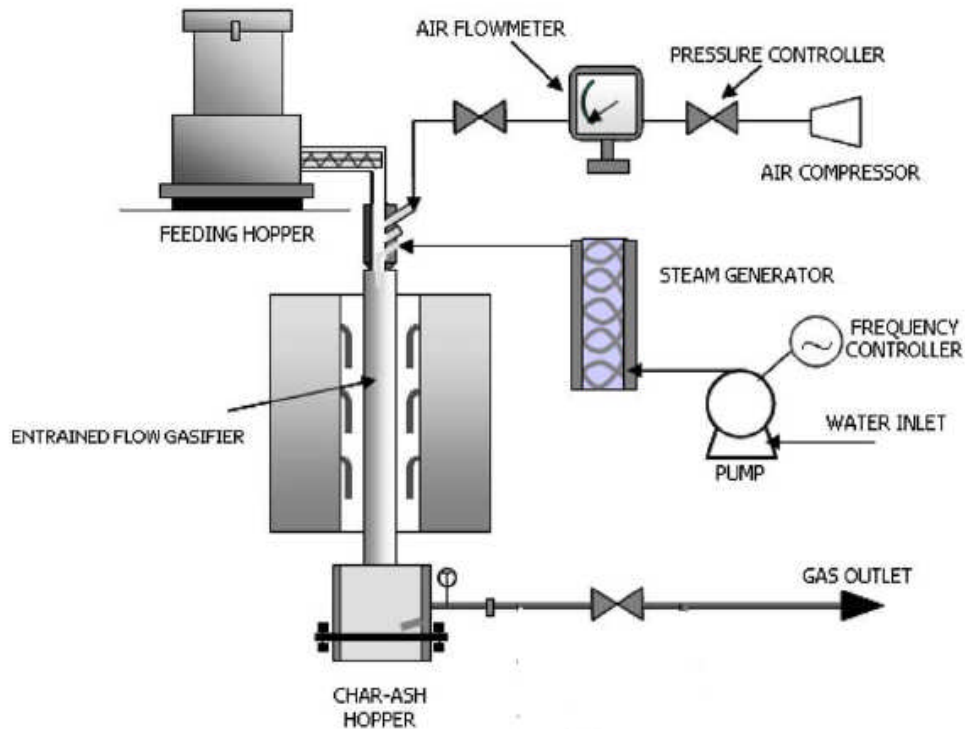


Figure 2-8 Entrained flow gasifier (amended from [136]).

The design and operating principles previously described for entrained flow fast pyrolysis are identical here, with modifications to accommodate the oxidant inlet. The entrained flow reactor is advantageous for its ability to produce a syngas of very low tar content due to the very high operating temperatures. However this requires the hot syngas to be cooled before use, resulting in efficiency losses if the heat of cooling is not utilized [105, 136]. Also this design requires the feedstock to be of very fine particles resulting in additional costs from the expensive feedstock preparation required.

2.2.2.4 Rotary kiln and screw kiln reactor

The rotary kiln and screw kiln reactors are designed to handle feedstock of heterogeneous nature and do not demand specific feed stock size conformity hence its application to processing wastes and biomass [52, 137-139]. The *rotary kiln* design is also very similar to that of a *Screw kiln reactor* [48, 51] as described earlier for pyrolysis. For large scale operations, *rotary and screw*

kiln reactors have been applied mostly for combustion purposes, however their application to pyrolysis and gasification is relatively new and have been largely on laboratory scale. The good mechanical solid mixing and control offered by these reactors design make them of potential for pyrolysis and gasification processes where the feedstock size is not an issue. Figure 2-9 shows a schematic of the screw kiln gasifier while figure 2-10 shows a schematic of the rotary kiln gasifier.

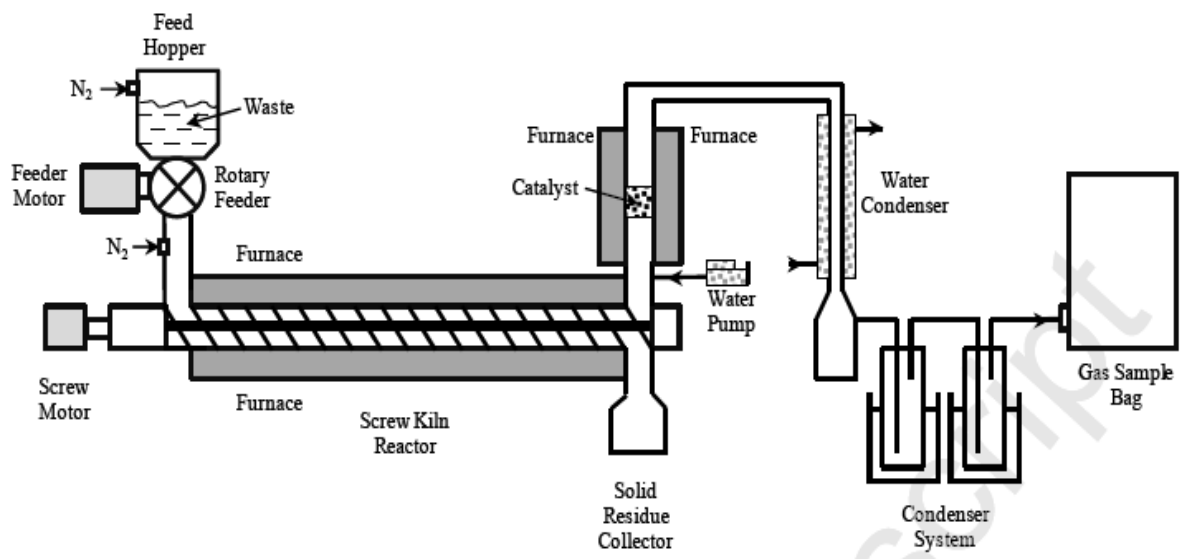


Figure 2-9 Screw kiln reactor [139].

The rotary kiln and screw kiln designs described previously for pyrolysis are applicable for gasification. The only design alterations involve the accommodation of inlets for the oxidizing agent.

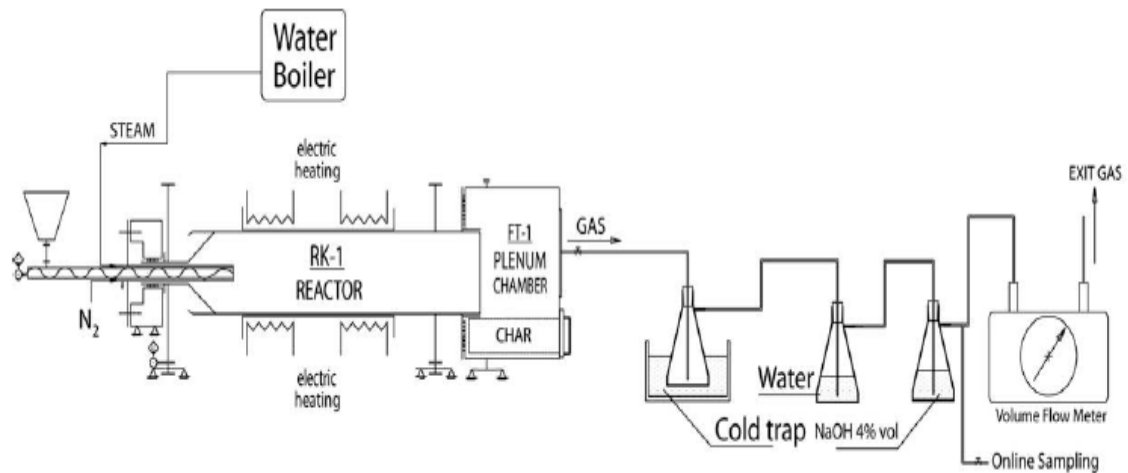


Figure 2-10 Schematic of the rotary kiln gasifier [140].

2.2.3 The gasification of solid wastes and biomass

2.2.3.1 Products from the gasification of solid wastes and biomass

The gasification of solid wastes and biomass results in the production of mainly a gaseous product [131, 141-142] called syngas. Along-side the gaseous products, there are solid products which could be char or ash depending on the process [142-143] and some condensable vapours (tar) [62, 108, 144]. The gaseous products are similar to those from pyrolysis [142] however gasification promotes the increased production of gaseous products and steam gasification especially promoted increased hydrogen production in the syngas [108, 111, 145-146] via various steam reforming reactions. The steam gasification reactions unlike oxygen and air gasification are however endothermic and require temperatures above 800 °C which are practically difficult to achieve [131, 141]. In order to improve the gas and hydrogen production, system efficiency and tar conversion, gasification can be carried out with the aid of a catalyst [131, 141, 147]. Catalytic gasification has been shown to increase gas yield [148-150] increase hydrogen yield [151-154] and increase tar conversion [144, 155-156].

2.2.3.2 Effects of reaction atmosphere

The partial oxidation requirement for gasification dictates that the process has to be carried out in an atmosphere of oxygen, however in a quantity insufficient to cause combustion [62]. This requirement can be met via a number of routes i.e. by carrying out the reactions in the presence of different oxidants or reaction atmosphere. These atmospheres or oxidants include pure O₂, air, CO₂, steam and a combination of any of the former.

Air gasification of biomass has been investigated [134, 157-158]. The use of air as the gasification oxidant is reported to produce a syngas with reduced heating value [159]. This is because of the presence of Nitrogen in the supplied air which dilutes the produced syngas. Also an increased supply of the air results in the combustion of the produced syngas. Air gasification generally produces a syngas of low heating value (4-7 MJ/m³) which is applicable mostly for heating applications [160]. The equivalence ratio, which represents the air–fuel weight ratio used, divided by the air–fuel weight ratio of stoichiometric combustion is an important factor for biomass air gasification as this determines the quantity of air supplied during gasification. This also affects the gasification process because a higher equivalence ratio results in a higher gasification temperature and improves syngas quality, however when the equivalence ratio is too high it will result in conditions close to combustion and therefore reduce syngas quality.

The use of *oxygen* as a gasification medium is a more preferable option than air gasification because O₂ gasification generally produces a higher heating value syngas (10-18 MJ/m³). Such processes require more energy to power the air separation units and there are hazards and complexities associated with this. O₂ gasification of biomass has been investigated [161-162]. Zhou et al [162] reported that O₂ gasification of biomass improved syngas quality up to an optimum level after which the heating value and H₂/CO ratio for the syngas reduced.

Steam gasification produces a syngas with higher H₂ content than air and O₂ gasification [163], because some of the H₂ from the steam is split and forms

part of the syngas resulting in a gas with higher quality. This makes steam gasification more sort after and has been applied to waste [140, 155] and biomass gasification [109, 164]. Umeki et al [109] reported of an increase in the H₂ content and heating value of produced syngas, with increasing steam injection up to an optimum point, after which decreases were recorded due to reverse shift reaction. Other atmospheres which have also been investigated include: O₂ + steam [119], O₂ + CO₂ [165] and air + steam [166-167]. However steam generation also adds an extra energy penalty to the process.

2.2.3.3 Effects of material characteristics

The material characteristics has similar effects on gasification as in pyrolysis as described earlier, since gasification proceeds from pyrolysis. Feedstock preparation is therefore also important for gasification. The moisture content of waste and biomass can promote hydrogen production however this can also lead to a loss of process efficiency [142]. The size of the feedstock impacts on its heat and mass transfer characteristics during gasification [142-143]. Increased hydrogen yield, gas yield, and reduced char and tar yield have been reported for steam gasification with smaller feedstock size [76, 136]. According to Lou et al [168] this may be due to reactions for smaller particles being kinetically driven. Also larger particles tend to possess more heat and mass transfer resistance creating a temperature difference between the surface and the middle of the particle resulting in incomplete reactions during gasification and generating more char [46].

Smaller particle sizes possess a larger external surface area/volume, allowing a close to uniform temperature to be reached through the particle. This allows for reactions to take place throughout the particle resulting generally in better gas quality. The better heat transfer of smaller particle sizes is also responsible for the high ash content in the char, signalling almost complete volatilization. Certain metals which are part of the ash contents within wastes and biomass are also reported to catalyze char gasification reactions [169-170]

2.2.3.4 Effects of temperature and heating rate

The temperature and heating rate play an important role for gasification and are interconnected i.e. an increase in temperature results in a corresponding increase in heating. Increased temperature promotes more conversion to syngas [44, 142-143]. This increase in conversion can be attributed to an increase in the initial pyrolysis reaction, a promotion of steam cracking and tar and hydrocarbon reforming and char gasification [171] all promoted by increased temperature.

An increase in gasification temperature has been reported to also favour the production of H₂ and CO, while resulting in a decrease in CO₂ and CH₄ [162]. It is suggested that temperature promotes more secondary reactions also resulting in more yield [114, 172-173]. In general high temperatures favour reactions of endothermic nature [110, 162]. The char content from higher temperature gasification is reported to decrease significantly while the ash content within the char is increased significantly [111].

2.2.3.5 Effects of other process conditions

Feedstock size: In general gasification of feedstock of smaller sizes result in the production of more gases [168]. This is likely as a result of the improved heat transfer promoted by particles of smaller sizes due to an increase in the effective thermal conductivity and radiation contributions from smaller particles. The particle size also has an effect on the quantity of produced char i.e. smaller particles sizes result in less char production. According to Lou et al [168] this may be due to reactions for smaller particles being kinetically driven. Also larger particles tend to possess more heat and mass transfer resistance creating a temperature difference between the surface and the middle of the particle resulting in incomplete reactions during gasification and generating more char [46]. Gasification reactions with reduced feedstock particle sizes have been reported to produce increased H₂ yields and a corresponding decrease in CO₂ yield [168].

Residence time: The solids residence time represents the time spent by the feedstock in the gasification hot-zone, while the volatile residence time represents the time taken from when the volatile compounds are generated within or from the sample structure, till when they exit the reactor hot-zone. These two factors particularly, the volatile residence time, influences gasification in the same manner as in the pyrolysis process, by influencing the secondary reactions and its extent. Reactors such as the entrained flow gasifiers are influenced especially by these factors [136, 162]. An increase in the volatile residence time is reported to result in improved gas quality due to increased production of H₂, CO and CH₄ [134, 136]. This also resulted in a decrease in the CO₂ gas component, [162].

Pressure: Pressurized gasification is often employed and is reported to enhance the gasification process by promoting secondary reactions [136, 174] and cracking reactions [175]. A pressure increase during gasification has been reported to increase char yield according Ono et al [174], though not significantly. Increased yields of H₂, CO₂ and CH₄ with increasing gasification pressure from 2 to 10 bar has been reported. The opposite trend was noted for CO. The increased CO₂ content may be as a result of the promotion of the water gas shift reaction with increasing pressure. However results of gasification at pressures between 0.5 and 2 MPa where reported to indicate little influence of pressure on the gas products [176-177]. Knight [178] reported the reduction in tar content from the gasification of wood chips at pressures up to 21 bar.

2.2.4 Catalytic gasification of solid waste and biomass

Syngas quality in regards to tar availability and gas composition is very important because high tar content creates utilization difficulties for the syngas especially in gas engines and turbines, while gas compositions of low H₂ to CO ratio (<2) do not meet the requirements for fuel synthesis such as methanol and FT synthesis. The advantages of catalytic gasification include the conversion of tar to useful product gases and the possibility of changing

the composition of the product gases [103]. Compared to other gas cleaning options catalytic cracking can operate at relatively low temperatures (600-800 °C) avoiding the necessity of expensive alloys required for reactor design in high temperature (>1000 °C) cracking. It also eliminates the need to substantially reduce the thermodynamic efficiency and impair the performance and economics of the processing system by cooling down the syngas (<150 °C) before tar removal as required by secondary physical tar removal methods [102, 106].

Tar cracking and improved syngas quality are promoted via a number of processes which are apparently enhanced by the presence of the catalyst thereby increasing the reaction rate within the system. These include: dry reforming, thermal cracking, steam reforming, hydro reforming, hydro-cracking and water-gas reaction [105, 179]. A simplified description of the catalytic tar cracking is as follows: hydrocarbons are dissociatively adsorbed and catalytically dehydrogenated, water is dissociatively adsorbed and provides hydroxylation, OH radical migration leads to the oxidation of intermediary hydrocarbon fragments and surface carbon to form H₂ and CO [103].

Catalytic tar cracking can either take place within the pyrolysis reactor (Primary cracking) or can take place in a separate reactor (Secondary cracking). The later obviously adds an extra reactor cost factor, making them not very economical, though quite effective. In the primary cracking method (with reference to catalytic cracking), the catalyst can either be integrated as a mixture with the sample or as a bed material. The primary method has the possible advantage of producing a syngas with the same quality as the secondary cracking method, while eliminating the need for a second reactor [106]. This method therefore promotes tar elimination, positive changes to product gas composition and char gasification, all in one reactor. It is important however that whatever method chosen has to be incorporated with a catalyst which meets the right criteria including [103]:

- Should be cost effective.
- Should be easily regenerated.

- Must be effective with tar elimination and influence the yield of valuable product gas composition.
- Should be resistant to deactivation.

2.2.4.1 Nickel based catalysts for gasification

A wide range of nickel based catalysts are commercially available, and have been extensively applied in the petrochemical industry especially for methane and naphtha reforming processes [103]. Nickel based catalysts are mostly heterogeneous and may have three major components, which influence the catalyst activity and can be manipulated to optimize catalyst design:

- The active metal or catalytic component which in this case is Ni.
- The promoter component, which is required to increase stability and reactivity e.g. Co and Mg.
- The support component, which is required to disperse the catalytic or metal component e.g. Alumina and silica.

The quantity of these components in a catalyst is responsible for differentiating catalysts, even when produced from the same active metal and support. Ni based catalysts have the added advantage of being quite cheaper than other transition element catalysts such as Ru and Rh. Below are some of the investigated Ni based catalysts.

A review by Devi et al [106] reports on the use of NiO/Al₂O₃ catalysts as a favourable option by many researchers, with H₂/CO ratio close to 2. The steam gasification of toluene as a model compound for tar was investigated using NiO/Al₂O₃ catalysts to investigate different Ni contents [180]. Results showed increased toluene conversion for a Ni content increase up to 15% and no further noticeable increase after Ni content increase to 20%. NiO/Al₂O₃ catalysts have been reported to be deactivated by coking [154, 181]. A sequential cracking process has been suggested to be effective for coke deactivation of NiO/Al₂O₃ catalyst [182]. Alumina (Al₂O₃) has been commonly

used as a support for Ni catalyst, due to its high mechanical resistance because of high Ni dispersion, chemical and physical stability [183]. Biomass derived syngas contains a wide range of impurities within the syngas [184] which can deactivate the catalyst, to this effect, other supports have also been investigated.

The catalytic activity of Nickel aluminium has been studied by different researchers [185-187]. Comparisons between Ni/Al prepared by co-impregnation and NiO/Al₂O₃ prepared by impregnation showed that the Ni/Al had higher catalytic activity due to higher thermal stability and metallic area [186-187]. The use of Ni/Al has also been reported to catalyze the CO₂ gasification of saw dust [188].

Ni/MgO catalysts have been shown to have high catalytic activity for the steam gasification of biomass and model biomass derived tar compounds [189-191]. Freni et al [192] reported reduced coke formation, high tar cracking activity and H₂ production for a Ni/MgO catalyst. Furusawa et al [193] investigated the effects of calcination temperature on the activity of a 10 wt% Ni/MgO. It was reported that the highest gas yield was produced at a calcination temperature of 600 °C while the highest H₂ yield was produced at a calcination temperature of 700 °C.

Ni/CeO₂ has been investigated due to the promoting effect of CeO₂ [194] which can promote the reaction between steam and carbon due to its oxygen storage capacity [183]. Increased H₂ production, carbon conversion and tar conversion were reported for the steam gasification of biomass with a Ni/CeO₂ catalyst at 650 °C [154]. Results from a comparison between Ni/CeO₂ and Ni/SiO₂ catalysts show that no carbon deposits were found on the Ni/CeO₂ catalyst [194]. Miyazawa et al [154] also reported reduced coke formation for the steam reforming of biomass oil with Ni/CeO₂ catalyst.

Other supports investigated include: Ni/ZrO₂, Ni/CeO₂, Ni/MnO, Ni/La₂O₃ and Ni/MnAlO₄ were investigated for the dry reforming of methane [195]. Results indicate that Ni/Al₂O₃ had the highest reactivity but deactivated with time, while this did not occur for Ni/La₂O₃ due to increased stability from La₂O₃

[196]. Ni/SiO₂ was investigated for H₂ production from cellulose [194]. Ni/Mg and Ni/Cu/Mg calcined at different temperatures (450 – 1000 °C) have been investigated for methane decomposition and hydrogen production [197]. Results showed that the Ni/Cu/Mg catalyst showed more resistance to deactivation due to the presence of the Cu, over the periods studied, with hydrogen yields of up to 80 vol% and methane decomposition of up to 67 %.

Ni/Olivine has been investigated for the gasification of biomass [198-200]. High selectivity for H₂ and CO, high tar conversion and high carbon conversion were reported for the steam gasification of toluene with Ni/Olivine [198]. The dry reforming of biomass syngas with Ni/Olivine catalyst resulted in H₂ yield and CH₄ conversions of up to 80% and 95% respectively for calcination temperatures between 900 and 1100 °C [201]. Ni/Olivine catalysts have also been reported to be highly resistant to coking [184]. Ni supported on dolomite has also been researched for gasification [202-203]. The effect of calcination temperature was investigated for steam gasification of tar with Ni/Dolomite [204]. Results showed that the catalyst calcined at 500 °C had the highest activity. Investigations of coke formation on Ni/Dolomite catalyst from gasification at 700 °C by Wang et al [203] proposed that coke was formed on both the nickel and the dolomite surfaces, and the catalyst was easily regenerated at 700 °C in air. Ni based catalyst with either dolomite or Olivine support have been reported to be significantly resistant to coking and H₂S poisoning compared to Ni/SiO₂ and Ni/Al₂O₃ [204].

A Ni/Carbon catalyst was reported to show good catalytic activity and stability for the hydrothermal gasification of organic compounds [205]. Ni supported on Zeolites have been investigated for the reforming and cracking of hydrocarbons due to the properties of zeolite: high surface area, well defined structure and high thermal stability [206-207]. Investigations by Inaba et al [194] showed that a Ni/Zeolite catalyst had more carbon deposits and higher tar cracking activity compared to a Ni/metal oxide catalyst.

Different commercial Ni based catalysts are available and have been used for steam gasification [208-210]. Garcia et al [208] provides a summary of some commercial Ni based catalysts. The contents of the commercial catalysts

included alumina, MgO, CaO, K₂O and SiO₂. The steam gasification of biomass in a small pilot plant using different commercial Ni catalysts was investigated [209]. The commercial catalysts designed for naphtha reforming showed more tar conversion activity than those designed for lighter hydrocarbon reforming. Wang et al [211] investigated some commercial catalysts (G-90C, G-91, G-125S and 46-40 for H₂ production from bio-oil steam gasification. Results showed that H₂ yield was affected by the steam/carbon ratio. The investigation of four commercial Ni based catalysts (46-1, 46-4, C11-NK and G-91) for the steam gasification of bio-oil in a fluidized bed by Garcia et al [208] showed that the C11-NK provided a more efficient gasification at 850 °C.

In order to promote catalytic activity, the addition of other metals to Nickel based catalysts have been investigated [183]. Some of the metals investigated include cerium, cobalt, copper, platinum, rhodium, magnesium and lanthanum [208, 212-215]. Ni/CeO₂/Al₂O₃ promoted by different noble metals was investigated by Profeti et al [216] for the steam reforming of glycerol and ethanol. The promoted catalysts were reported to show high catalytic performance, higher H₂ yield and significantly reduced coke formation. The addition of CeO₂ to Ni/Al₂O₃ catalyst was reported to improve catalytic activity and stability by different researchers [216-218]. During the gasification of biomass the addition of magnesium to a Ni/Al₂O₃ catalyst was reported to increase the catalyst strength however lower gas yield and increased char production were also reported [219]. Choudhary et al [220] also proposed that the introduction of Mg to a commercial Ni catalyst, enhanced its steam adsorption capacity as well as prevented catalyst sintering.

Nickel-based catalysts are very effective for tar conversion and also for NH₃ conversion, they are however also susceptible to deactivation and poisoning mostly due to carbon deposition and sulphur as a result of the presence of H₂S [106, 221].

2.2.4.2 Mechanisms of nickel catalyst deactivation

Deactivation is a term used basically to describe the inevitable (in most cases) condition during a catalyst's lifetime when it is no longer effective towards the pyrolysis and gasification reactions. Though inevitable, this process can be delayed, it is therefore in the interest of a well designed process for the catalyst activity loss to be slow. Deactivation can occur via different means which can be:

- Thermal via thermal degradation and sintering.
- Chemical via vapour transport of catalytic phase and poisoning.
- Mechanical via fouling, attrition and crushing.

Thermal degradation and sintering: The high temperature which is usually present during biomass and syngas processing is significant in causing deactivation. Via this means, deactivation can be caused by catalytic phase transformation to non-catalytic phases, or by sintering. The term sintering describes two major activities: loss of support and catalytic area due to support or pore collapse, and crystallite growth in catalytic phases leading to loss of catalytic surface. This usually takes place above 500 °C and is encouraged by the availability of water vapour. Thermal deactivation is generally difficult to reverse or is irreversible. It is therefore easier to prevent this than to repair after degradation. The re-exposition of catalytic surface due to sintering reversal is referred to as re-dispersion.

Factors affecting sintering include: catalyst texture, porosity, surface area, atmosphere (the presence of oxygen increases sintering), impurities and temperature (sintering rates increase with temperature) [222]. Additives or impurities such as alkali metals, chlorine, steam and dispersed metals in supported metal catalysts e.g. dispersed Ni in Ni/Al₂O₃, have been found to accelerate catalyst support sintering [223]. During temperature reactions such steam reforming, sintering is also possible via direct vaporization. Steps to minimize catalyst sintering and improve process economics can be taken such as correct temperature selection, water vapour minimization and the

addition of thermal stabilizers e.g. noble metals with higher melting point, to the catalyst [224].

Vapour transport of catalytic phase: Catalyst loss via the formation of volatile metal compounds such as: sulphides, carbonyls and oxides, is possible at low temperatures (including room temperature) in the presence of H_2S , CO O_2 and halogen atmospheres, and can be responsible for catalyst deactivation [225]. A basic description of catalyst deactivation via this means is as follows. The metallic content of the catalyst reacts with a volatilization agent such as CO , O_2 and etc to decompose the catalyst and form a volatile metal compound. The formed metal compound becomes vaporized due to its volatile nature and is transported and lost from the system. This finalizes the deactivation process.

Catalyst poisoning: Catalyst poisoning refers to the strong chemisorptions of impurities, reactants or products on catalyst sites which should be available for catalysis [226]. This has the effect of blocking adsorption sites, causing compound formation, inducing changes in the electronic or geometric constitution of the catalyst surface, slowing the surface diffusion of adsorbed reactants or blocking the access of adsorbed reactants to each other. A major element recognized for catalyst poisoning in pyrolysis and gasification reactions is sulphur, however the general term poisoning is reaction specific and therefore a reactant for one reaction can be a poison in another. A good example of this is that oxygen acts as a poison in ammonia synthesis.

Species which readily provide the sulphur poison include H_2S , SO_4^{2-} and SO_2 [227]. Other poison species include amines, ammonia, zinc, halides and compounds of arsenic. In order for the catalyst to enhance catalytic reactions, one or more of the reactants is adsorbed by the catalyst. This action is hindered by poison adsorption, preventing the further adsorption of reactants, leading to the coverage of the catalyst by the poison and a decline in catalytic activity. Poisoning may or may not be reversible. In the case of sulphur poisoning, where reversible the catalyst may be regenerated by steam treatment followed by reduction in H_2 [184]. It is however more economical to prevent poisoning by removing feed impurities where possible, also selective

poisoning of unwanted metals can be used to reduce poisoning by metal impurities [224].

Some inorganic species also present in biomass have been found to contribute to catalyst deactivation via competitive adsorption and poisoning [228]. These contaminants include Al, Ti, Na, Ca, Si, Fe, P and Cl.

Fouling and coking: The deposition of molecules from the fluid phase on the catalyst surface can block pores and sites, preventing reactant adsorption and resulting in catalyst activity loss [229]. Generally coke and carbon deposits on catalysts are responsible for this however it is also possible for other materials like fly ash to cause catalyst activity loss due to plugging or coating. Deactivation from coke and carbon can occur via the following routes [226]:

- Catalyst encapsulation by carbon, causing complete deactivation.
- Catalyst pores plugging, preventing access of reactants into these.
- Chemisorption of carbon to form a monolayer or adsorption of carbon to form a multilayer, thereby preventing reactant access to metal sites.
- Build up of carbon filaments in pores, causing stress and leading to support material fracture, catalyst fracture and plugging of reactor voids.

Increased gasification rate, due to the presence of increased steam or oxygen will result in reduced coking [184]. In the light of reducing fouling by coking it is therefore advantageous to operate the gasification process at conditions which favour gasification over the formation of coke and carbon precursors.

Attrition and crushing: Activity loss can be due to loss of the catalyst itself either by the erosion of the catalyst particles due to fluid velocities and the action of impinging gases and entrained particles flow [230], or by crushing of the catalyst due to stress loading and thermally induced cracks, or by catalyst size reduction to produce fine particles (this is termed attrition) which is common in fluid beds. This can lead to severe catalyst loss because the fine particles are difficult to filter and reuse and can plug filters. Catalysts are generally formed from the processing and finally compaction of smaller

particles to form larger particles of less structural strength than the smaller particles, making them susceptible to failure by crushing, attrition and stress generally.

Stress may be introduced into the catalyst via mechanical, thermal or chemical routes [224]. Thermal stress is encountered from the rapid heating and cooling of catalyst particles. Mechanical stress can be introduced by particle collision, gravitational force for catalysts at the bottom of a catalyst bed or by the turbulences created due to high fluid velocities. While chemical stresses may be encountered due to the different chemical reaction taking place within the catalyst pores. During catalyst preparation, the probability of mechanical failure can be taken into account by improving methods to increase attrition resistance.

2.2.4.3 Other available catalysts

Dolomite and olivine: Dolomite is a naturally occurring calcium magnesium ore ($\text{CaMg}(\text{CO}_3)_2$) generally utilized in industry for the manufacture of magnesium, however when calcined to eliminate two CO_2 molecules to form MgO-CaO , it is effective for tar removal from syngas. It has also been investigated as a support for metal based catalysts like Nickel [184]. Dolomite is relatively cheap and easy to dispose of due to its natural occurrence and is therefore useful both as an in-bed primary or secondary catalyst [231]. These characteristics have prompted a lot investigation into the use of dolomite.

Dolomite has been compared with other catalysts including a Ni based catalyst and was found to be more effective for tar reduction than $\text{NiMo}/\gamma\text{-Al}_2\text{O}_3$ and MgO [103]. Results of in-bed gasification of biomass mixed with calcined dolomite as a catalyst indicate CO production decrease, H_2 increase by a factor of 2 and up to 6 fold decrease in tar content [232]. The effect of dolomite on naphthalene production and tar reduction during biomass pyrolysis were studied to show that the presence of dolomite significantly alters the production of naphthalene and the quantity of tar in the syngas [233]. A comparison was made between in-bed and down-stream catalytic

gasification of biomass with dolomite in a fluidized bed reactor [234]. Results indicate that there is not much difference in the syngas quality obtained from the location of the dolomite. Also for both parameters, there was no variation in hydrocarbon quantities, increase in H₂ production and decrease in CO production.

Dolomite calcined at 900 °C was investigated for the catalytic cracking of syngas from the pyrolysis of olive oil waste in a down-stream reactor [104] to show that it was quite stable. Gas yields of above 54 wt % and hydrogen yields of above 19 mol/kg were obtained resulting a reduced liquid yield. He et al [111] investigated the catalytic pyrolysis of MSW with dolomite calcined at 900°C in a down-stream reactor. Gas yields of above 78 wt%, decrease in liquid product yield, H₂ yield above 36 mol%, CO yield of above 66 mol% and a general decrease in CO₂ and hydrocarbons.

Another naturally occurring catalyst which was found to have similar qualities and better attrition resistance than dolomite, is olivine [103, 106]. Olivine has been investigated extensively also as a catalyst and as a support structure for metal based catalyst [184] and has yielded comparable results to that of dolomite.

Minerals of Iron: Iron ores such as carbonates, sulphides, oxides and silicates of Iron, which are normally used for the production of iron, were found to be catalytically active for the cracking of syngas tar. The cracking of benzene over iron oxide as a catalyst was investigated to show that the presence of the catalyst was effective for benzene conversion [235]. The presence of hydrogen was also found to suppress catalyst deactivation by coking. Simell et al [236] investigated the catalytic activity of iron ore sinter and pellets which contain magnetite (Fe₃O₄) and hematite (Fe₂O₃). They were both found to be effective for tar elimination and H₂ and CO increase, though less active than dolomite. Loss of catalytic activity for minerals of iron is generally through deactivation by coking and this is favoured by the absence of hydrogen.

Char: Char which is also a by product of the pyrolysis process can be used as a catalyst for tar elimination. The catalytic activity of char is probably as a

result of its characteristics such as surface area, pore size and its mineral and ash content. These characteristics are determined both by the char preparation method i.e. pyrolysis temperature and heating rate, and the general source of the char i.e. pyrolysis of coal or biomass etc. Using char as a catalyst is not only cheap but its availability can also be reliable as it is a product of the process.

The catalytic cracking of syngas from the pyrolysis of teak wood was investigated, over charcoal [237] with results indicating almost complete decomposition of the available tar. The decomposition of methane over wood char as a catalyst has been investigated [107]. A methane conversion of up to 70% was achieved to yield more H₂ and CO, while reducing CO₂. Indications are that the catalytic activity of wood char is achieved both by availability of pores and surface, and the chemical nature of the wood char.

While char is attractive for catalytic tar destruction due its availability and effectiveness, it is important to note that char can also get gasified by the steam and CO₂ which is available in the syngas. It may therefore be necessary to integrate a continuous external supply to ensure process balance. Also the properties of char are not fixed as they depend on the char source and the process conditions of preparation [147]. The catalytic activity of this catalyst is normally reduced due to its gasification and deactivation due to coking.

Alkali metal catalysts: These are catalysts of very reactive and mono-valent metals such as rubidium (Rb), francium (Fr), sodium (Na), lithium (Li), potassium (K) and cesium (Cs). Alkali metals can be used in the form of carbonates (Na₂CO₃, K₂CO₃), oxides or hydroxides, or combined with other support materials such as alumina, to be used as primary or secondary catalysts. Potassium and sodium are known to occur naturally in biomass [238] and have generated significant interest for catalytic investigation. These catalysts have the added advantage of being produced naturally in the ashes from the pyrolysis/gasification processes therefore providing a use for the ash and eliminating the need for ash disposal.

Alkali based catalysts have been reported to especially promote equations (2.2) and (2.4) CO_2 and H_2O gasification reactions respectively [239]. Demirbas [86] investigated the pyrolysis of biomass samples impregnated with Na_2CO_3 and K_2CO_3 catalysts. Gaseous yields of up to 62.9 vol% for Na_2CO_3 and 62.6 vol%, compared to a yield of 44.6 vol% without catalyst were reported. Na_2CO_3 , K_2CO_3 , NaHCO_3 and KHCO_3 were investigated for the pyrolysis of dry wood to yield H_2 of up to 41 wt% [240]. A general increase in H_2 and CO_2 and a decrease in CO and hydrocarbons, were reported for the mentioned catalysts mentioned above.

Alkali metal based catalysts are known to undergo deactivation due to agglomeration (especially in fluidized bed reactors) and due to high temperatures of about 900 °C [241]. This may be caused by a variety of activities such as: unfavourable reactions with mineral matter within char, sintering, loss of the alkali metal due to vaporization and loss of contact between the catalyst and char [242]. There are also issues with the In-bed use of these catalysts because the catalyst recovery process can be difficult and costly, and can generate ash disposal problems [147].

Fluid catalytic cracking (FCC) catalysts: FCC catalysts are well known and extensively used for the fuel processing industry in the cracking and conversion of heavier fuel oils into lighter and more valuable product such as Liquefied Petroleum Gas (LPG), gasoline etc. These catalysts in general have high surface acidity unlike other catalysts. They include Zeolites which are a group of crystalline mesoporous aluminosilicates, derived from a frame work of $[\text{SiO}_4]^{4-}$ and $[\text{AlO}_4]^{5-}$ polyhedral [147]. Zeolites have well defined pore structure, high surface area and high acidity, which are influenced strongly by factors such as catalyst preparation method, Si/Al ratio and dehydration temperature. The common Zeolites include: HZSM-5, REY, USY, Rcat-c1 and REUSY. These catalysts have been found to both promote the water gas shift reaction [243] and tar cracking. A study on the steam gasification of sawdust using an FCC catalyst showed a 20% reduction in tar content however rapid deactivation of the catalyst by coking and catalyst entrainment out of the bed were reported [106]. Sufficient experience exists with the use of FCC catalyst due to the extensive application in the fuels processing industry and also their

relatively low costs, making them advantageous for catalytic cracking. They are however prone to rapid deactivation due to coke formation [147].

2.2.5 Novel concepts

2.2.5.1 In-situ hydrogen removal

One promising concept for the production of hydrogen from biomass and waste gasification is the in-situ extraction of hydrogen from the syngas mixture during gasification in order to collect a pure stream of hydrogen which can be utilized in processes which require such purity grades of hydrogen such as fuel cells. This can be achieved via separation of hydrogen from the gas mixture using a permeable membrane [244]. Some promising research findings on the integration of membrane separation technology with gasification for hydrogen production have been reported [245-246].

2.2.5.2 In-situ CO₂ removal

The in-situ capture of CO₂ produced during gasification is actively being researched because it presents an opportunity to produce a gas stream with less CO₂ as well as shift the gasification reaction equilibrium towards the production of more H₂. CaO has been reported to be a promising solid sorbent for CO₂ capture and is actively being researched for this purpose [171, 247-248].

References

1. Demirbas, A., *Biomass resource facilities and biomass conversion processing for fuels and chemicals*. Energy Conversion and Management, 2001. **42**(11): p. 1357-1378.
2. Dufour, A., Girods, P., Masson, E., Rogaume, Y. and Zoulalian, A., *Synthesis gas production by biomass pyrolysis: Effect of reactor temperature on product*

- distribution*. International Journal of Hydrogen Energy, 2009. **34**(4): p. 1726-1734.
3. Kantarelis, E., Donaj, P., Yang, W. and Zabaniotou, A., *Sustainable valorization of plastic wastes for energy with environmental safety via High-Temperature Pyrolysis (HTP) and High-Temperature Steam Gasification (HTSG)*. Journal of Hazardous Materials, 2009. **167**(1-3): p. 675-684.
 4. Buah, W.K., Cunliffe, A.M. and Williams, P.T., *Characterization of Products from the Pyrolysis of Municipal Solid Waste*. Process Safety and Environmental Protection, 2007. **85**(5): p. 450-457.
 5. Garcia, A.N., Font, R. and Marcilla, A., *Gas Production by Pyrolysis of Municipal Solid Waste at High Temperature in a Fluidized Bed Reactor*. Energy & Fuels, 1995. **9**(4): p. 648-658.
 6. Ferdous, D., Dalai, A.K., Bej, S.K., Thring, R.W. and Bakhshi, N.N., *Production of H₂ and medium Btu gas via pyrolysis of lignins in a fixed-bed reactor*. Fuel Processing Technology, 2001. **70**(1): p. 9-26.
 7. Williams, E.A. and Williams, P.T., *Analysis of products derived from the fast pyrolysis of plastic waste*. Journal of Analytical and Applied Pyrolysis, 1997. **40-41**: p. 347-363.
 8. Williams, P.T., Besler, S. and Taylor, D.T., *The pyrolysis of scrap automotive tyres: The influence of temperature and heating rate on product composition*. Fuel, 1990. **69**(12): p. 1474-1482.
 9. Elbaba, I.F., Wu, C. and Williams, P.T., *Catalytic Pyrolysis-Gasification of Waste Tire and Tire Elastomers for Hydrogen Production*. Energy & Fuels, 2010. **24**(7): p. 3928-3935.
 10. Aylon, E., Fernandez-Colino, A., Navarro, M.V., Murillo, R., Garcia, T. and Mastral, A.M., *Waste Tire Pyrolysis: Comparison between Fixed Bed Reactor and Moving Bed Reactor*. Industrial & Engineering Chemistry Research, 2008. **47**(12): p. 4029-4033.
 11. Velghe, I., Carleer, R., Yperman, J. and Schreurs, S., *Study of the pyrolysis of municipal solid waste for the production of valuable products*. Journal of Analytical and Applied Pyrolysis, 2011. **92**(2): p. 366-375.
 12. Miskolczi, N., Buyong, F., Angyal, A., Williams, P.T. and Bartha, L., *Two stages catalytic pyrolysis of refuse derived fuel: Production of biofuel via syncrude*. Bioresource Technology, 2010. **101**(22): p. 8881-8890.
 13. Dawei, A., Zhimin, W., Shuting, Z. and Hongxing, Y., *Low-temperature pyrolysis of municipal solid waste: influence of pyrolysis temperature on the characteristics of solid fuel*. International Journal of Energy Research, 2006. **30**(5): p. 349-357.
 14. Phan, A.N., Ryu, C., Sharifi, V.N. and Swithenbank, J., *Characterisation of slow pyrolysis products from segregated wastes for energy production*. Journal of Analytical and Applied Pyrolysis, 2008. **81**(1): p. 65-71.
 15. Bridgwater, A.V., *Renewable fuels and chemicals by thermal processing of biomass*. Chemical Engineering Journal, 2003. **91**(2-3): p. 87-102.
 16. Balat, M., *Potential importance of hydrogen as a future solution to environmental and transportation problems*. International Journal of Hydrogen Energy, 2008. **33**(15): p. 4013-4029.
 17. Brem, G., *PyRos Technology for Flash Pyrolysis: Integrated reactor and filter concept*. 2006, TNO Science and Industry. p. 1 - 24.

18. Zubtsov, V.M., Pian, C.C.P. and Yoshikawa, K., *Potential applications of high-temperature air/steam-blown gasification and pyrolysis systems*. Energy, 2005. **30**(11-12): p. 2229-2242.
19. Dounit, S., Hemati, M. and Andreux, R., *Modelling and experimental validation of a fluidized-bed reactor freeboard region: Application to natural gas combustion*. Chemical Engineering Journal, 2008. **140**(1-3): p. 457-465.
20. Iamarino, M., Chirone, R., Lisi, L., Pirone, R., Salatino, P. and Russo, G., *Cu/[gamma]-Al₂O₃ catalyst for the combustion of methane in a fluidized bed reactor*. Catalysis Today, 2002. **75**(1-4): p. 317-324.
21. Vamvuka, D., Pitharoulis, M., Alevizos, G., Repouskou, E. and Pentari, D., *Ash effects during combustion of lignite/biomass blends in fluidized bed*. Renewable Energy, 2009. **34**(12): p. 2662-2671.
22. Yan, R., Liang, D.T. and Tsen, L., *Case studies--Problem solving in fluidized bed waste fuel incineration*. Energy Conversion and Management, 2005. **46**(7-8): p. 1165-1178.
23. García, A.N., Font, R. and Marcilla, A., *Kinetic study of the flash pyrolysis of municipal solid waste in a fluidized bed reactor at high temperature*. Journal of Analytical and Applied Pyrolysis, 1995. **31**: p. 101-121.
24. Bridgwater, A.V., *Thermal conversion of biomass and waste: The status*. 2001.
25. Zhang, H., Xiao, R., Huang, H. and Xiao, G., *Comparison of non-catalytic and catalytic fast pyrolysis of corncob in a fluidized bed reactor*. Bioresource Technology, 2009. **100**(3): p. 1428-1434.
26. Xianwen, D., Chuangzhi, W., Haibin, L. and Yong, C., *The Fast Pyrolysis of Biomass in CFB Reactor*. Energy & Fuels, 2000. **14**(3): p. 552-557.
27. Chen, G., Sjoestrom, K. and Bjoernbom, E., *Pyrolysis/gasification of wood in a pressurized fluidized bed reactor*. Industrial & Engineering Chemistry Research, 1992. **31**(12): p. 2764-2768.
28. Janse, A.M.C., Maarten Biesheuvel, P., Prins, W. and van Swaaij, W.P.M., *A novel interconnected fluidised bed for the combined flash pyrolysis of biomass and combustion of char*. Chemical Engineering Journal, 1999. **75**(2): p. 121-130.
29. Olazar, M., Alvarez, S., Aguado, R. and José, M.J.S., *Spouted Bed Reactors*. 2003. p. 845-852.
30. Garcia, L., Salvador, M.L., Arauzo, J. and Bilbao, R., *Influence of Catalyst Weight/Biomass Flow Rate Ratio on Gas Production in the Catalytic Pyrolysis of Pine Sawdust at Low Temperatures*. Industrial & Engineering Chemistry Research, 1998. **37**(10): p. 3812-3819.
31. Wang, Z., Huang, H., Li, H., Wu, C., Chen, Y. and Li, B., *Pyrolysis and Combustion of Refuse-Derived Fuels in a Spouting Moving Bed Reactor*. Energy & Fuels, 2001. **16**(1): p. 136-142.
32. Hernández, M.d.R., Gómez, A., García, Á.N., Agulló, J. and Marcilla, A., *Effect of the temperature in the nature and extension of the primary and secondary reactions in the thermal and HZSM-5 catalytic pyrolysis of HDPE*. Applied Catalysis A: General, 2007. **317**(2): p. 183-194.
33. Chen, G., Andries, J., Spliethoff, H., Fang, M. and van de Enden, P.J., *Biomass gasification integrated with pyrolysis in a circulating fluidised bed*. Solar Energy, 2004. **76**(1-3): p. 345-349.

34. Bahng, M.-K., Mukarakate, C., Robichaud, D.J. and Nimlos, M.R., *Current technologies for analysis of biomass thermochemical processing: A review*. Analytica Chimica Acta, 2009. **651**(2): p. 117-138.
35. Sadakata, M., Takahashi, K., Saito, M. and Sakai, T., *Production of fuel gas and char from wood, lignin and holocellulose by carbonization*. Fuel, 1987. **66**(12): p. 1667-1671.
36. Bitowft, B., Andersson, L.A. and Bjerle, I., *Fast pyrolysis of sawdust in an entrained flow reactor*. Fuel, 1989. **68**(5): p. 561-566.
37. Zanzi, R., Sjöström, K. and Björnbom, E., *Rapid high-temperature pyrolysis of biomass in a free-fall reactor*. Fuel, 1996. **75**(5): p. 545-550.
38. Li, S., Xu, S., Liu, S., Yang, C. and Lu, Q., *Fast pyrolysis of biomass in free-fall reactor for hydrogen-rich gas*. Fuel Processing Technology, 2004. **85**(8-10): p. 1201-1211.
39. Zhang, Y., Kajitani, S., Ashizawa, M. and Oki, Y., *Tar destruction and coke formation during rapid pyrolysis and gasification of biomass in a drop-tube furnace*. Fuel, 2010a. **89**(2): p. 302-309.
40. Zanzi, R., Sjöström, K. and Björnbom, E., *Rapid pyrolysis of agricultural residues at high temperature*. Biomass and Bioenergy, 2002. **23**(5): p. 357-366.
41. Couhert, C., Commandré, J.-M. and Salvador, S., *Failure of the component additivity rule to predict gas yields of biomass in flash pyrolysis at 950 °C*. Biomass and Bioenergy, 2009. **33**(2): p. 316-326.
42. Dupont, C., Commandré, J.-M., Gauthier, P., Boissonnet, G., Salvador, S. and Schweich, D., *Biomass pyrolysis experiments in an analytical entrained flow reactor between 1073 K and 1273 K*. Fuel, 2008. **87**(7): p. 1155-1164.
43. Wei, L., Xu, S., Zhang, L., Zhang, H., Liu, C., Zhu, H. and Liu, S., *Characteristics of fast pyrolysis of biomass in a free fall reactor*. Fuel Processing Technology, 2006. **87**(10): p. 863-871.
44. Sun, S., Tian, H., Zhao, Y., Sun, R. and Zhou, H., *Experimental and numerical study of biomass flash pyrolysis in an entrained flow reactor*. Bioresource Technology, 2010. **101**(10): p. 3678-3684.
45. Zhang, L., Xu, S., Zhao, W. and Liu, S., *Co-pyrolysis of biomass and coal in a free fall reactor*. Fuel, 2007. **86**(3): p. 353-359.
46. Lu, H., Ip, E., Scott, J., Foster, P., Vickers, M. and Baxter, L.L., *Effects of particle shape and size on devolatilization of biomass particle*. Fuel, 2010. **89**(5): p. 1156-1168.
47. Goyal, H.B., Seal, D. and Saxena, R.C., *Bio-fuels from thermochemical conversion of renewable resources: A review*. Renewable and Sustainable Energy Reviews, 2008. **12**(2): p. 504-517.
48. Day, M., Shen, Z. and Cooney, J.D., *Pyrolysis of auto shredder residue: experiments with a laboratory screw kiln reactor*. Journal of Analytical and Applied Pyrolysis, 1999. **51**(1-2): p. 181-200.
49. Li, A.M., Li, X.D., Li, S.Q., Ren, Y., Chi, Y., Yan, J.H. and Cen, K.F., *Pyrolysis of solid waste in a rotary kiln: influence of final pyrolysis temperature on the pyrolysis products*. Journal of Analytical and Applied Pyrolysis, 1999. **50**(2): p. 149-162.
50. Lemort, F., Soudais, Y., Moga, L. and Blazeck, Y., *Heat treatment of chlorinated waste in a rotating kiln: Problems with intermediate reaction products and solutions applied*. International Journal of Engineering Science, 2006. **44**(15-16): p. 1071-1081.

51. Serrano, D.P., Aguado, J., Escola, J.M. and Garagorri, E., *Conversion of low density polyethylene into petrochemical feedstocks using a continuous screw kiln reactor*. Journal of Analytical and Applied Pyrolysis, 2001. **58-59**: p. 789-801.
52. Guéhenneux, G., Baussand, P., Brothier, M., Poletiko, C. and Boissonnet, G., *Energy production from biomass pyrolysis: a new coefficient of pyrolytic valorisation*. Fuel, 2005. **84**(6): p. 733-739.
53. Fortuna, F., Cornacchia, G., Mincarini, M. and Sharma, V.K., *Pilot-scale experimental pyrolysis plant: Mechanical and operational aspects*. Journal of Analytical and Applied Pyrolysis, 1997. **40-41**: p. 403-417.
54. Sobeih, K.L., Baron, M. and Gonzalez-Rodriguez, J., *Recent trends and developments in pyrolysis-gas chromatography*. Journal of Chromatography A, 2008. **1186**(1-2): p. 51-66.
55. Wagenaar, B.M., Prins, W. and van Swaaij, W.P.M., *Pyrolysis of biomass in the rotating cone reactor: modelling and experimental justification*. Chemical Engineering Science, 1994. **49**(24, Part 2): p. 5109-5126.
56. Fagbemi, L., Khezami, L. and Capart, R., *Pyrolysis products from different biomasses: application to the thermal cracking of tar*. Applied Energy, 2001. **69**(4): p. 293-306.
57. Unapumnuk, K., Lu, M. and Keener, T.C., *Carbon Distribution from the Pyrolysis of Tire-Derived Fuels*. Industrial & Engineering Chemistry Research, 2006. **45**(26): p. 8757-8764.
58. Zabaniotou, A., Ioannidou, O. and Skoulou, V., *Rapeseed residues utilization for energy and 2nd generation biofuels*. Fuel, 2008. **87**(8-9): p. 1492-1502.
59. Zabaniotou, A. and Ioannidou, O., *Evaluation of utilization of corn stalks for energy and carbon material production by using rapid pyrolysis at high temperature*. Fuel, 2008. **87**(6): p. 834-843.
60. Balat, M., *Hydrogen-Rich Gas Production from Biomass via Pyrolysis and Gasification Processes and Effects of Catalyst on Hydrogen Yield*. 2008, Taylor & Francis. p. 552 - 564.
61. Demirbas, M.F., *Hydrogen from Various Biomass Species via Pyrolysis and Steam Gasification Processes*. 2006, Taylor & Francis. p. 245 - 252.
62. Williams, P.T., *Waste Treatment and Disposal*. 2nd Edition ed. 2005: John Wiley & Sons, Ltd. 380.
63. Dou, B., Park, S., Lim, S., Yu, T.-U. and Hwang, J., *Pyrolysis Characteristics of Refuse Derived Fuel in a Pilot-Scale Unit*. Energy & Fuels, 2007. **21**(6): p. 3730-3734.
64. Nahil, M.A. and Williams, P.T., *Recycling of carbon fibre reinforced polymeric waste for the production of activated carbon fibres*. Journal of Analytical and Applied Pyrolysis, 2011. **91**(1): p. 67-75.
65. Demirbas, A., *Yields of hydrogen-rich gaseous products via pyrolysis from selected biomass samples*. Fuel, 2001. **80**(13): p. 1885-1891.
66. He, M., Xiao, B., Liu, S., Hu, Z., Guo, X., Luo, S. and Yang, F., *Syngas production from pyrolysis of municipal solid waste (MSW) with dolomite as downstream catalysts*. Journal of Analytical and Applied Pyrolysis, 2009. **87**(2): p. 181-187.
67. Demirbas, A., *Hydrogen Production via Pyrolytic Degradation of Agricultural Residues*. 2005, Taylor & Francis. p. 769 - 775.

68. Onay, O., *Influence of pyrolysis temperature and heating rate on the production of bio-oil and char from safflower seed by pyrolysis, using a well-swept fixed-bed reactor*. Fuel Processing Technology, 2007. **88**(5): p. 523-531.
69. Acikgoz, C., Onay, O. and Kockar, O.M., *Fast pyrolysis of linseed: product yields and compositions*. Journal of Analytical and Applied Pyrolysis, 2004. **71**(2): p. 417-429.
70. Demirbas, A., *Pyrolysis of municipal plastic wastes for recovery of gasoline-range hydrocarbons*. Journal of Analytical and Applied Pyrolysis, 2004. **72**(1): p. 97-102.
71. Greenhalf, C.E., Nowakowski, D.J., Harms, A.B., Titiloye, J.O. and Bridgwater, A.V., *Sequential pyrolysis of willow SRC at low and high heating rates – Implications for selective pyrolysis*. Fuel, 2012. **93**(0): p. 692-702.
72. Belgiorno, V., De Feo, G., Della Rocca, C. and Napoli, R.M.A., *Energy from gasification of solid wastes*. Waste Management, 2003. **23**(1): p. 1-15.
73. Wagland, S.T., Kilgallon, P., Coveney, R., Garg, A., Smith, R., Longhurst, P.J., Pollard, S.J.T. and Simms, N., *Comparison of coal/solid recovered fuel (SRF) with coal/refuse derived fuel (RDF) in a fluidised bed reactor*. Waste Management, 2011. **31**(6): p. 1176-1183.
74. Flamme, S. and Geiping, J., *Quality standards and requirements for solid recovered fuels: a review*. Waste Management & Research, 2012. **30**(4): p. 335-353.
75. Bridgwater, A.V., *Waste incineration and pyrolysis*. Resource Recovery and Conservation, 1980. **5**(1): p. 99-115.
76. Luo, S., Xiao, B., Hu, Z. and Liu, S., *Effect of particle size on pyrolysis of single-component municipal solid waste in fixed bed reactor*. International Journal of Hydrogen Energy, 2010. **35**(1): p. 93-97.
77. Helsen, L., Van den Bulck, E., Mullens, S. and Mullens, J., *Low-temperature pyrolysis of CCA-treated wood: thermogravimetric analysis*. Journal of Analytical and Applied Pyrolysis, 1999. **52**(1): p. 65-86.
78. Lv, D., Xu, M., Liu, X., Zhan, Z., Li, Z. and Yao, H., *Effect of cellulose, lignin, alkali and alkaline earth metallic species on biomass pyrolysis and gasification*. Fuel Processing Technology, 2010. **91**(8): p. 903-909.
79. Sørum, L., Grønli, M.G. and Hustad, J.E., *Pyrolysis characteristics and kinetics of municipal solid wastes*. Fuel, 2001. **80**(9): p. 1217-1227.
80. Grammelis, P., Basinas, P., Malliopoulou, A. and Sakellariopoulos, G., *Pyrolysis kinetics and combustion characteristics of waste recovered fuels*. Fuel, 2009. **88**(1): p. 195-205.
81. Grieco, E.M. and Baldi, G., *Pyrolysis of polyethylene mixed with paper and wood: Interaction effects on tar, char and gas yields*. Waste Management, 2012. **32**(5): p. 833-839.
82. Bhaskar, T., Hall, W.J., Mitan, N.M.M., Muto, A., Williams, P.T. and Sakata, Y., *Controlled pyrolysis of polyethylene/polypropylene/polystyrene mixed plastics with high impact polystyrene containing flame retardant: Effect of decabromo diphenylethane (DDE)*. Polymer Degradation and Stability, 2007. **92**(2): p. 211-221.
83. Wang, G., Li, W., Li, B. and Chen, H., *TG study on pyrolysis of biomass and its three components under syngas*. Fuel, 2008. **87**(4-5): p. 552-558.
84. Pindoria, R.V., Megaritis, A., Messenböck, R.C., Dugwell, D.R. and Kandiyoti, R., *Comparison of the pyrolysis and gasification of biomass: effect*

- of reacting gas atmosphere and pressure on Eucalyptus wood.* Fuel, 1998. **77**(11): p. 1247-1251.
85. Çaglar, A. and Demirbas, A., *Hydrogen rich gas mixture from olive husk via pyrolysis.* Energy Conversion and Management, 2002. **43**(1): p. 109-117.
 86. Demirbas, A., *Gaseous products from biomass by pyrolysis and gasification: effects of catalyst on hydrogen yield.* Energy Conversion and Management, 2002. **43**(7): p. 897-909.
 87. Williams, P.T. and Besler, S., *Polycyclic aromatic hydrocarbons in waste derived pyrolytic oils.* Journal of Analytical and Applied Pyrolysis, 1994. **30**(1): p. 17-33.
 88. Piskorz, J., Radlein, D. and Scott, D.S., *On the mechanism of the rapid pyrolysis of cellulose.* Journal of Analytical and Applied Pyrolysis, 1986. **9**(2): p. 121-137.
 89. Guoxin, H., Hao, H. and Yanhong, L., *Hydrogen-Rich Gas Production from Pyrolysis of Biomass in an Autogenerated Steam Atmosphere.* Energy & Fuels, 2009. **23**(3): p. 1748-1753.
 90. Beis, S.H., Onay, Ö. and Koçkar, Ö.M., *Fixed-bed pyrolysis of safflower seed: influence of pyrolysis parameters on product yields and compositions.* Renewable Energy, 2002. **26**(1): p. 21-32.
 91. Meesri, C. and Moghtaderi, B., *Lack of synergetic effects in the pyrolytic characteristics of woody biomass/coal blends under low and high heating rate regimes.* Biomass and Bioenergy, 2002. **23**(1): p. 55-66.
 92. Seebauer, V., Petek, J. and Staudinger, G., *Effects of particle size, heating rate and pressure on measurement of pyrolysis kinetics by thermogravimetric analysis.* Fuel, 1997. **76**(13): p. 1277-1282.
 93. Cetin, E., Gupta, R. and Moghtaderi, B., *Effect of pyrolysis pressure and heating rate on radiata pine char structure and apparent gasification reactivity.* Fuel, 2005. **84**(10): p. 1328-1334.
 94. Karaduman, A., Şimşek, E.H., Çiçek, B. and Bilgesü, A.Y., *Flash pyrolysis of polystyrene wastes in a free-fall reactor under vacuum.* Journal of Analytical and Applied Pyrolysis, 2001. **60**(2): p. 179-186.
 95. Lede, J., *The Cyclone: A Multifunctional Reactor for the Fast Pyrolysis of Biomass.* Industrial & Engineering Chemistry Research, 2000. **39**(4): p. 893-903.
 96. Yang, H., Yan, R., Chen, H., Lee, D.H., Liang, D.T. and Zheng, C., *Pyrolysis of palm oil wastes for enhanced production of hydrogen rich gases.* Fuel Processing Technology, 2006. **87**(10): p. 935-942.
 97. Baumlin, S., Broust, F., Bazer-Bachi, F., Bourdeaux, T., Herbinet, O., Toutie Ndiaye, F., Ferrer, M. and Lédé, J., *Production of hydrogen by lignins fast pyrolysis.* International Journal of Hydrogen Energy, 2006. **31**(15): p. 2179-2192.
 98. Cozzani, V., Nicolella, C., Rovatti, M. and Tognotti, L., *Modeling and Experimental Verification of Physical and Chemical Processes during Pyrolysis of a Refuse-Derived Fuel.* Industrial & Engineering Chemistry Research, 1996. **35**(1): p. 90-98.
 99. Lu, Q., Zhang, Y., Tang, Z., Li, W.-z. and Zhu, X.-f., *Catalytic upgrading of biomass fast pyrolysis vapors with titania and zirconia/titania based catalysts.* Fuel, 2010. **89**(8): p. 2096-2103.

100. Milne, T.A. and Evans, R.J., *Biomass gasification "tars": their nature, formation and conversion*. 1998, NREL, Golden, CO, USA, Report no. NREL/TP-570-25357.
101. Mun, T.-Y., Seon, P.-G. and Kim, J.-S., *Production of a producer gas from woody waste via air gasification using activated carbon and a two-stage gasifier and characterization of tar*. *Fuel*, 2010. **89**(11): p. 3226-3234.
102. Zhang, R., Brown, R.C., Suby, A. and Cummer, K., *Catalytic destruction of tar in biomass derived producer gas*. *Energy Conversion and Management*, 2004. **45**(7-8): p. 995-1014.
103. Han, J. and Kim, H., *The reduction and control technology of tar during biomass gasification/pyrolysis: An overview*. *Renewable and Sustainable Energy Reviews*, 2008. **12**(2): p. 397-416.
104. Encinar, J.M., González, J.F., Martínez, G. and Román, S., *Catalytic pyrolysis of exhausted olive oil waste*. *Journal of Analytical and Applied Pyrolysis*, 2009. **85**(1-2): p. 197-203.
105. Zhang, L., Xu, C. and Champagne, P., *Overview of recent advances in thermo-chemical conversion of biomass*. *Energy Conversion and Management*, 2010. **51**(5): p. 969-982.
106. Devi, L., Ptasinski, K.J. and Janssen, F.J.J.G., *A review of the primary measures for tar elimination in biomass gasification processes*. *Biomass and Bioenergy*, 2003. **24**(2): p. 125-140.
107. Dufour, A., Celzard, A., Fierro, V., Martin, E., Broust, F. and Zoulalian, A., *Catalytic decomposition of methane over a wood char concurrently activated by a pyrolysis gas*. *Applied Catalysis A: General*, 2008. **346**(1-2): p. 164-173.
108. Bridgwater, A.V., *The technical and economic feasibility of biomass gasification for power generation*. *Fuel*, 1995. **74**(5): p. 631-653.
109. Umeki, K., Yamamoto, K., Namioka, T. and Yoshikawa, K., *High temperature steam-only gasification of woody biomass*. *Applied Energy*, 2010. **87**(3): p. 791-798.
110. Skoulou, V., Swiderski, A., Yang, W. and Zabaniotou, A., *Process characteristics and products of olive kernel high temperature steam gasification (HTSG)*. *Bioresource Technology*, 2009. **100**(8): p. 2444-2451.
111. He, M., Hu, Z., Xiao, B., Li, J., Guo, X., Luo, S., Yang, F., Feng, Y., Yang, G. and Liu, S., *Hydrogen-rich gas from catalytic steam gasification of municipal solid waste (MSW): Influence of catalyst and temperature on yield and product composition*. *International Journal of Hydrogen Energy*, 2009. **34**(1): p. 195-203.
112. Li, J., Yan, R., Xiao, B., Liang, D.T. and Du, L., *Development of Nano-NiO/Al₂O₃ Catalyst to be Used for Tar Removal in Biomass Gasification*. *Environmental Science & Technology*, 2008. **42**(16): p. 6224-6229.
113. He, M., Xiao, B., Liu, S., Guo, X., Luo, S., Xu, Z., Feng, Y. and Hu, Z., *Hydrogen-rich gas from catalytic steam gasification of municipal solid waste (MSW): Influence of steam to MSW ratios and weight hourly space velocity on gas production and composition*. *International Journal of Hydrogen Energy*, 2009. **34**(5): p. 2174-2183.
114. Wu, C. and Williams, P.T., *Hydrogen Production from the Pyrolysis Gasification of Polypropylene: Influence of Steam Flow Rate, Carrier Gas Flow Rate and Gasification Temperature*. *Energy & Fuels*, 2009. **23**(10): p. 5055-5061.

115. Nemtsov, D.A. and Zabaniotou, A., *Mathematical modelling and simulation approaches of agricultural residues air gasification in a bubbling fluidized bed reactor*. Chemical Engineering Journal, 2008. **143**(1-3): p. 10-31.
116. Pröll, T. and Hofbauer, H., *H₂ rich syngas by selective CO₂ removal from biomass gasification in a dual fluidized bed system -- Process modelling approach*. Fuel Processing Technology, 2008. **89**(11): p. 1207-1217.
117. Thamavithya, M. and Dutta, A., *An investigation of MSW gasification in a spout-fluid bed reactor*. Fuel Processing Technology, 2008. **89**(10): p. 949-957.
118. Hamel, S. and Krumm, W., *Modelling and simulation of bubbling fluidized bed gasification reactors*. Fuel and Energy Abstracts, 2002. **43**(4): p. 250-250.
119. Gil, J., Aznar, M.P., Caballero, M.A., Frances, E. and Corella, J., *Biomass Gasification in Fluidized Bed at Pilot Scale with Steam-Oxygen Mixtures. Product Distribution for Very Different Operating Conditions*. Energy & Fuels, 1997. **11**(6): p. 1109-1118.
120. Lv, P., Chang, J., Xiong, Z., Huang, H., Wu, C., Chen, Y. and Zhu, J., *Biomass Air-Steam Gasification in a Fluidized Bed to Produce Hydrogen-Rich Gas*. Energy & Fuels, 2003. **17**(3): p. 677-682.
121. Koppatz, S., Pfeifer, C., Rauch, R., Hofbauer, H., Marquard-Moellenstedt, T. and Specht, M., *H₂ rich product gas by steam gasification of biomass with in situ CO₂ absorption in a dual fluidized bed system of 8 MW fuel input*. Fuel Processing Technology, 2009. **90**(7-8): p. 914-921.
122. Brage, C., Yu, Q. and Sjöström, K., *Characteristics of evolution of tar from wood pyrolysis in a fixed-bed reactor*. Fuel, 1996. **75**(2): p. 213-219.
123. Ponzio, A., Kalisz, S. and Blasiak, W., *Effect of operating conditions on tar and gas composition in high temperature air/steam gasification (HTAG) of plastic containing waste*. Fuel Processing Technology, 2006. **87**(3): p. 223-233.
124. Kan, T., Xiong, J., Li, X., Ye, T., Yuan, L., Torimoto, Y., Yamamoto, M. and Li, Q., *High efficient production of hydrogen from crude bio-oil via an integrative process between gasification and current-enhanced catalytic steam reforming*. International Journal of Hydrogen Energy, 2010. **35**(2): p. 518-532.
125. Dou, B., Rickett, G.L., Dupont, V., Williams, P.T., Chen, H., Ding, Y. and Ghadiri, M., *Steam reforming of crude glycerol with in situ CO₂ sorption*. Bioresource Technology, 2010. **101**(7): p. 2436-2442.
126. Dupont, V., Ross, A.B., Knight, E., Hanley, I. and Twigg, M.V., *Production of hydrogen by unmixed steam reforming of methane*. Chemical Engineering Science, 2008. **63**(11): p. 2966-2979.
127. Haavisto, I., ed. *Fixed Bed Gasification for Heat Production*. Biomass Gasification & Pyrolysis: State of the Art and Future Prospects, ed. Kaltschmitt, M. and Bridgwater, A.V. 1997, CPL Press: Newbury. 6.
128. Guoxin, H. and Hao, H., *Hydrogen rich fuel gas production by gasification of wet biomass using a CO₂ sorbent*. Biomass and Bioenergy, 2009. **33**(5): p. 899-906.
129. Pasel, C. and Wanzl, W., *Experimental investigations on reactor scale-up and optimisation of product quality in pyrolysis of shredder waste*. Fuel Processing Technology, 2003. **80**(1): p. 47-67.
130. Warnecke, R., *Gasification of biomass: comparison of fixed bed and fluidized bed gasifier*. Biomass and Bioenergy, 2000. **18**(6): p. 489-497.

131. McKendry, P., *Energy production from biomass (part 3): gasification technologies*. Bioresource Technology, 2002. **83**(1): p. 55-63.
132. Roll, H. and Hedden, K., *Entrained flow gasification of coarsely ground Chinese reed*. Chemical Engineering and Processing: Process Intensification, 1994. **33**(5): p. 353-361.
133. Santo, U., Seifert, H., Kolb, T., Krebs, L., Kuhn, D., Wiemer, H.J., Pantouflas, E. and Zarzalis, N., *Conversion of Biomass Based Slurry in an Entrained Flow Gasifier*. 2007. p. 967-969.
134. Zhao, Y., Sun, S., Zhou, H., Sun, R., Tian, H., Luan, J. and Qian, J., *Experimental study on sawdust air gasification in an entrained-flow reactor*. Fuel Processing Technology, 2010. **91**(8): p. 910-914.
135. Zhao, Y., Sun, S., Tian, H., Qian, J., Su, F. and Ling, F., *Characteristics of rice husk gasification in an entrained flow reactor*. Bioresource Technology, 2009. **100**(23): p. 6040-6044.
136. Hernández, J.J., Aranda-Almansa, G. and Bula, A., *Gasification of biomass wastes in an entrained flow gasifier: Effect of the particle size and the residence time*. Fuel Processing Technology, 2010. **91**(6): p. 681-692.
137. Fantozzi, F., Colantoni, S., Bartocci, P. and Desideri, U., *Rotary Kiln Slow Pyrolysis for Syngas and Char Production From Biomass and Waste --- Part II: Introducing Product Yields in the Energy Balance*. Journal of Engineering for Gas Turbines and Power, 2007. **129**(4): p. 908-913.
138. Donatelli, A., Iovane, P. and Molino, A., *High energy syngas production by waste tyres steam gasification in a rotary kiln pilot plant. Experimental and numerical investigations*. Fuel, 2010. **89**(10): p. 2721-2728.
139. Efika, C., Wu, C. and Williams, P.T., *Syngas Production from Pyrolysis-Catalytic Steam Reforming of Waste Biomass in a Continuous Screw Kiln Reactor*. Journal of Analytical and Applied Pyrolysis, 2012(0).
140. Galvagno, S., Casciaro, G., Casu, S., Martino, M., Mingazzini, C., Russo, A. and Portofino, S., *Steam gasification of tyre waste, poplar, and refuse-derived fuel: A comparative analysis*. Waste Management, 2009. **29**(2): p. 678-689.
141. Demirbas, A., *Hydrogen Production from Carbonaceous Solid Wastes by Steam Reforming*. 2008a, Taylor & Francis. p. 924 - 931.
142. Kalinci, Y., Hepbasli, A. and Dincer, I., *Biomass-based hydrogen production: A review and analysis*. International Journal of Hydrogen Energy, 2009. **34**(21): p. 8799-8817.
143. Kirubakaran, V., Sivaramakrishnan, V., Nalini, R., Sekar, T., Premalatha, M. and Subramanian, P., *A review on gasification of biomass*. Renewable and Sustainable Energy Reviews, 2009. **13**(1): p. 179-186.
144. Blanco, P.H., Wu, C., Onwudili, J.A. and Williams, P.T., *Characterization and evaluation of Ni/SiO₂ catalysts for hydrogen production and tar reduction from catalytic steam pyrolysis-reforming of refuse derived fuel*. Applied Catalysis B: Environmental, 2013. **134-135**(0): p. 238-250.
145. Li, J., Yin, Y., Zhang, X., Liu, J. and Yan, R., *Hydrogen-rich gas production by steam gasification of palm oil wastes over supported tri-metallic catalyst*. International Journal of Hydrogen Energy, 2009. **34**(22): p. 9108-9115.
146. Gao, N., Li, A., Quan, C. and Gao, F., *Hydrogen-rich gas production from biomass steam gasification in an updraft fixed-bed gasifier combined with a porous ceramic reformer*. International Journal of Hydrogen Energy, 2008. **33**(20): p. 5430-5438.

147. Abu El-Rub, Z., Bramer, E.A. and Brem, G., *Review of Catalysts for Tar Elimination in Biomass Gasification Processes*. Industrial & Engineering Chemistry Research, 2004. **43**(22): p. 6911-6919.
148. He, M., Xiao, B., Hu, Z., Liu, S., Guo, X. and Luo, S., *Syngas production from catalytic gasification of waste polyethylene: Influence of temperature on gas yield and composition*. International Journal of Hydrogen Energy, 2009a. **34**(3): p. 1342-1348.
149. Tomishige, K., Asadullah, M. and Kunimori, K., *Syngas production by biomass gasification using Rh/CeO₂/SiO₂ catalysts and fluidized bed reactor*. Catalysis Today, 2004. **89**(4): p. 389-403.
150. Wang, T., Chang, J., Cui, X., Zhang, Q. and Fu, Y., *Reforming of raw fuel gas from biomass gasification to syngas over highly stable nickel-magnesium solid solution catalysts*. Fuel Processing Technology, 2006. **87**(5): p. 421-428.
151. Domine, M.E., Iojoiu, E.E., Davidian, T., Guilhaume, N. and Mirodatos, C., *Hydrogen production from biomass-derived oil over monolithic Pt- and Rh-based catalysts using steam reforming and sequential cracking processes*. Catalysis Today, 2008. **133-135**: p. 565-573.
152. Demirbas, A., *Hazelnut Shell to Hydrogen-Rich Gaseous Products via Catalytic Gasification Process*. Energy Sources, Part A: Recovery, Utilization, and Environmental Effects, 2004. **26**(1): p. 25-33.
153. Wu, C., Huang, Q., Sui, M., Yan, Y. and Wang, F., *Hydrogen production via catalytic steam reforming of fast pyrolysis bio-oil in a two-stage fixed bed reactor system*. Fuel Processing Technology, 2008. **89**(12): p. 1306-1316.
154. Miyazawa, T., Kimura, T., Nishikawa, J., Kado, S., Kunimori, K. and Tomishige, K., *Catalytic performance of supported Ni catalysts in partial oxidation and steam reforming of tar derived from the pyrolysis of wood biomass*. Catalysis Today, 2006. **115**(1-4): p. 254-262.
155. Guan, Y., Luo, S., Liu, S., Xiao, B. and Cai, L., *Steam catalytic gasification of municipal solid waste for producing tar-free fuel gas*. International Journal of Hydrogen Energy, 2009. **34**(23): p. 9341-9346.
156. Asadullah, M., Miyazawa, T., Ito, S.-i., Kunimori, K., Yamada, M. and Tomishige, K., *Catalyst development for the gasification of biomass in the dual-bed gasifier*. Applied Catalysis A: General, 2003. **255**(2): p. 169-180.
157. Kobayashi, N., Tanaka, M., Piao, G., Kobayashi, J., Hatano, S., Itaya, Y. and Mori, S., *High temperature air-blown woody biomass gasification model for the estimation of an entrained down-flow gasifier*. Waste Management, 2009. **29**(1): p. 245-251.
158. Sheth, P.N. and Babu, B.V., *Production of hydrogen energy through biomass (waste wood) gasification*. International Journal of Hydrogen Energy, 2010. **35**(19): p. 10803-10810.
159. Sun, S., Zhao, Y., Tian, H., Ling, F. and Su, F., *Experimental study on cyclone air gasification of wood powder*. Bioresource Technology, 2009a. **100**(17): p. 4047-4049.
160. Bridgwater, A.V., Elliott, D.C., Fagernäs, L., Gifford, J.S., Mackie, K.L. and Toft, A.J., *The nature and control of solid, liquid and gaseous emissions from the thermochemical processing of biomass*. Biomass and Bioenergy, 1995a. **9**(1-5): p. 325-341.
161. Maroño, M., Sánchez, J.M. and Ruiz, E., *Hydrogen-rich gas production from oxygen pressurized gasification of biomass using a Fe-Cr Water Gas Shift catalyst*. International Journal of Hydrogen Energy, 2010. **35**(1): p. 37-45.

162. Zhou, J., Chen, Q., Zhao, H., Cao, X., Mei, Q., Luo, Z. and Cen, K., *Biomass-oxygen gasification in a high-temperature entrained-flow gasifier*. *Biotechnology Advances*, 2009. **27**(5): p. 606-611.
163. Gil, J., Corella, J., Aznar, M.P. and Caballero, M.A., *Biomass gasification in atmospheric and bubbling fluidized bed: Effect of the type of gasifying agent on the product distribution*. *Biomass and Bioenergy*, 1999. **17**(5): p. 389-403.
164. Iliuta, I., Leclerc, A. and Larachi, F., *Allothermal steam gasification of biomass in cyclic multi-compartment bubbling fluidized-bed gasifier/combustor - New reactor concept*. *Bioresource Technology*, 2010. **101**(9): p. 3194-3208.
165. Hanaoka, T., Sasaki, H., Sakanishi, K. and Edashige, Y., *Syngas Production by Woody Biomass Gasification with a CO₂/O₂ Mixture*. *Journal of the Japan Institute of Energy*, 2009. **88**(10): p. 862-868.
166. Gordillo, G. and Annamalai, K., *Adiabatic fixed bed gasification of dairy biomass with air and steam*. *Fuel*, 2010. **89**(2): p. 384-391.
167. González, J.F., Román, S., Bragado, D. and Calderón, M., *Investigation on the reactions influencing biomass air and air/steam gasification for hydrogen production*. *Fuel Processing Technology*, 2008. **89**(8): p. 764-772.
168. Luo, S., Xiao, B., Guo, X., Hu, Z., Liu, S. and He, M., *Hydrogen-rich gas from catalytic steam gasification of biomass in a fixed bed reactor: Influence of particle size on gasification performance*. *International Journal of Hydrogen Energy*, 2009. **34**(3): p. 1260-1264.
169. Gómez-Barea, A., Arjona, R. and Ollero, P., *Pilot-Plant Gasification of Olive Stone: a Technical Assessment*. *Energy & Fuels*, 2004. **19**(2): p. 598-605.
170. Xiao, R., Jin, B., Zhou, H., Zhong, Z. and Zhang, M., *Air gasification of polypropylene plastic waste in fluidized bed gasifier*. *Energy Conversion and Management*, 2007. **48**(3): p. 778-786.
171. Florin, N.H. and Harris, A.T., *Enhanced hydrogen production from biomass with in situ carbon dioxide capture using calcium oxide sorbents*. *Chemical Engineering Science*, 2008. **63**(2): p. 287-316.
172. Yan, F., Luo, S.-y., Hu, Z.-q., Xiao, B. and Cheng, G., *Hydrogen-rich gas production by steam gasification of char from biomass fast pyrolysis in a fixed-bed reactor: Influence of temperature and steam on hydrogen yield and syngas composition*. *Bioresource Technology*, 2010. **101**(14): p. 5633-5637.
173. Gao, N., Li, A. and Quan, C., *A novel reforming method for hydrogen production from biomass steam gasification*. *Bioresource Technology*, 2009. **100**(18): p. 4271-4277.
174. Ono, A., Kurita, M., Nagashima, T. and Horio, M., *Evaluation of waste pyrolysis characteristics in a pressurized fluidized bed reactor*. *Waste Management*, 2001. **21**(5): p. 451-456.
175. Qin, Y., Huang, H., Wu, Z., Feng, J., Li, W. and Xie, K., *Characterization of tar from sawdust gasified in the pressurized fluidized bed*. *Biomass and Bioenergy*, 2007. **31**(4): p. 243-249.
176. Feroso, J., Arias, B., Plaza, M.G., Pevida, C., Rubiera, F., Pis, J.J., García-Peña, F. and Casero, P., *High-pressure co-gasification of coal with biomass and petroleum coke*. *Fuel Processing Technology*, 2009. **90**(7-8): p. 926-932.
177. Valin, S., Ravel, S., Guillaudeau, J. and Thiery, S., *Comprehensive study of the influence of total pressure on products yields in fluidized bed gasification of wood sawdust*. *Fuel Processing Technology*, 2010. **91**(10): p. 1222-1228.

178. Knight, R.A., *Experience with raw gas analysis from pressurized gasification of biomass*. Biomass and Bioenergy, 2000. **18**(1): p. 67-77.
179. Xu, C., Donald, J., Byambajav, E. and Ohtsuka, Y., *Recent advances in catalysts for hot-gas removal of tar and NH₃ from biomass gasification*. Fuel, 2010. **89**(8): p. 1784-1795.
180. Srinakruang, J., Sato, K., Vitidsant, T. and Fujimoto, K., *A highly efficient catalyst for tar gasification with steam*. Catalysis Communications, 2005. **6**(6): p. 437-440.
181. Simell, P.A., Hepola, J.O. and Krause, A.O.I., *Effects of gasification gas components on tar and ammonia decomposition over hot gas cleanup catalysts*. Fuel, 1997. **76**(12): p. 1117-1127.
182. Davidian, T., Guilhaume, N., Iojoiu, E., Provendier, H. and Mirodatos, C., *Hydrogen production from crude pyrolysis oil by a sequential catalytic process*. Applied Catalysis B: Environmental, 2007. **73**(1-2): p. 116-127.
183. Wu, C. and Williams, P.T., *Nickel-based catalysts for tar reduction in biomass gasification*. Biofuels, 2011. **2**(4): p. 451-464.
184. Yung, M.M., Jablonski, W.S. and Magrini-Bair, K.A., *Review of Catalytic Conditioning of Biomass-Derived Syngas*. Energy & Fuels, 2009. **23**(4): p. 1874-1887.
185. Clause, O., Gazzano, M., Trifiro, F., Vaccari, A. and Zatorski, L., *Preparation and thermal reactivity of nickel/chromium and nickel/aluminium hydrotalcite-type precursors*. Applied Catalysis, 1991. **73**(2): p. 217-236.
186. Wu, C. and Williams, P.T., *Hydrogen production by steam gasification of polypropylene with various nickel catalysts*. Applied Catalysis B: Environmental, 2009. **87**(3-4): p. 152-161.
187. García, L., Salvador, M.L., Arauzo, J. and Bilbao, R., *Catalytic Steam Gasification of Pine Sawdust. Effect of Catalyst Weight/Biomass Flow Rate and Steam/Biomass Ratios on Gas Production and Composition*. Energy & Fuels, 1999. **13**(4): p. 851-859.
188. Garcia, L., Salvador, M.L., Arauzo, J. and Bilbao, R., *CO₂ as a gasifying agent for gas production from pine sawdust at low temperatures using a Ni/Al coprecipitated catalyst*. Fuel Processing Technology, 2001. **69**(2): p. 157-174.
189. Minowa, T. and Ogi, T., *Hydrogen production from cellulose using a reduced nickel catalyst*. Catalysis Today, 1998. **45**(1-4): p. 411-416.
190. Furusawa, T. and Tsutsumi, A., *Comparison of Co/MgO and Ni/MgO catalysts for the steam reforming of naphthalene as a model compound of tar derived from biomass gasification*. Applied Catalysis A: General, 2005. **278**(2): p. 207-212.
191. Rapagnà, S., Jand, N. and Foscolo, P.U., *Catalytic gasification of biomass to produce hydrogen rich gas*. International Journal of Hydrogen Energy, 1998. **23**(7): p. 551-557.
192. Freni, S., Cavallaro, S., Mondello, N., Spadaro, L. and Frusteri, F., *Production of hydrogen for MC fuel cell by steam reforming of ethanol over MgO supported Ni and Co catalysts*. Catalysis Communications, 2003. **4**(6): p. 259-268.
193. Furusawa, T., Sato, T., Sugito, H., Miura, Y., Ishiyama, Y., Sato, M., Itoh, N. and Suzuki, N., *Hydrogen production from the gasification of lignin with nickel catalysts in supercritical water*. International Journal of Hydrogen Energy, 2007. **32**(6): p. 699-704.

194. Inaba, M., Murata, K., Saito, M. and Takahara, I., *Hydrogen Production by Gasification of Cellulose over Ni Catalysts Supported on Zeolites*. *Energy & Fuels*, 2006. **20**(2): p. 432-438.
195. Seok, S.-H., Choi, S.H., Park, E.D., Han, S.H. and Lee, J.S., *Mn-Promoted Ni/Al₂O₃ Catalysts for Stable Carbon Dioxide Reforming of Methane*. *Journal of Catalysis*, 2002. **209**(1): p. 6-15.
196. Benito, M., García, S., Ferreira-Aparicio, P., Serrano, L.G. and Daza, L., *Development of biogas reforming Ni-La-Al catalysts for fuel cells*. *Journal of Power Sources*, 2007. **169**(1): p. 177-183.
197. Moliner, R., Echegoyen, Y., Suelves, I., Lázaro, M.J. and Palacios, J.M., *Ni-Mg and Ni-Cu-Mg catalysts for simultaneous production of hydrogen and carbon nanofibers: The effect of calcination temperature*. *International Journal of Hydrogen Energy*, 2008. **33**(6): p. 1719-1728.
198. Świerczyński, D., Libs, S., Courson, C. and Kiennemann, A., *Steam reforming of tar from a biomass gasification process over Ni/olivine catalyst using toluene as a model compound*. *Applied Catalysis B: Environmental*, 2007. **74**(3-4): p. 211-222.
199. Yang, X., Xu, S., Xu, H., Liu, X. and Liu, C., *Nickel supported on modified olivine catalysts for steam reforming of biomass gasification tar*. *Catalysis Communications*, 2010. **11**(5): p. 383-386.
200. Zhao, Z., Lakshminarayanan, N., Kuhn, J.N., Senefeld-Naber, A., Felix, L.G., Slimane, R.B., Choi, C.W. and Ozkan, U.S., *Optimization of thermally impregnated Ni-olivine catalysts for tar removal*. *Applied Catalysis A: General*, 2009. **363**(1-2): p. 64-72.
201. Courson, C., Makaga, E., Petit, C. and Kiennemann, A., *Development of Ni catalysts for gas production from biomass gasification. Reactivity in steam- and dry-reforming*. *Catalysis Today*, 2000. **63**(2-4): p. 427-437.
202. Corujo, A., Yermán, L., Arizaga, B., Brusoni, M. and Castiglioni, J., *Improved yield parameters in catalytic steam gasification of forestry residue; optimizing biomass feed rate and catalyst type*. *Biomass and Bioenergy*, 2010. **34**(12): p. 1695-1702.
203. Wang, T.J., Chang, J., Wu, C.Z., Fu, Y. and Chen, Y., *The steam reforming of naphthalene over a nickel-dolomite cracking catalyst*. *Biomass and Bioenergy*, 2005. **28**(5): p. 508-514.
204. Srinakruang, J., Sato, K., Vitidsant, T. and Fujimoto, K., *Highly efficient sulfur and coking resistance catalysts for tar gasification with steam*. *Fuel*, 2006. **85**(17-18): p. 2419-2426.
205. Sharma, A., Nakagawa, H. and Miura, K., *Uniform dispersion of Ni nano particles in a carbon based catalyst for increasing catalytic activity for CH₄ and H₂ production by hydrothermal gasification*. *Fuel*, 2006. **85**(17-18): p. 2396-2401.
206. Boxiong, S., Chunfei, W., Cai, L., Binbin, G. and Rui, W., *Pyrolysis of waste tyres: The influence of USY catalyst/tyre ratio on products*. *Journal of Analytical and Applied Pyrolysis*, 2007. **78**(2): p. 243-249.
207. Chang, J.-S., Park, S.-E. and Chon, H., *Catalytic activity and coke resistance in the carbon dioxide reforming of methane to synthesis gas over zeolite-supported Ni catalysts*. *Applied Catalysis A: General*, 1996. **145**(1-2): p. 111-124.

208. Garcia, L., French, R., Czernik, S. and Chornet, E., *Catalytic steam reforming of bio-oils for the production of hydrogen: effects of catalyst composition*. Applied Catalysis A: General, 2000. **201**(2): p. 225-239.
209. Aznar, M.P., Caballero, M.A., Gil, J., Martín, J.A. and Corella, J., *Commercial Steam Reforming Catalysts To Improve Biomass Gasification with Steam–Oxygen Mixtures. 2. Catalytic Tar Removal*. Industrial & Engineering Chemistry Research, 1998. **37**(7): p. 2668-2680.
210. Czernik, S., French, R., Feik, C. and Chornet, E., *Hydrogen by Catalytic Steam Reforming of Liquid Byproducts from Biomass Thermoconversion Processes*. Industrial & Engineering Chemistry Research, 2002. **41**(17): p. 4209-4215.
211. Wang, D., Czernik, S., Montané, D., Mann, M. and Chornet, E., *Biomass to Hydrogen via Fast Pyrolysis and Catalytic Steam Reforming of the Pyrolysis Oil or Its Fractions*. Industrial & Engineering Chemistry Research, 1997. **36**(5): p. 1507-1518.
212. Garcia, L., Benedicto, A., Romeo, E., Salvador, M.L., Arauzo, J. and Bilbao, R., *Hydrogen Production by Steam Gasification of Biomass Using Ni–Al Coprecipitated Catalysts Promoted with Magnesium*. Energy & Fuels, 2002. **16**(5): p. 1222-1230.
213. Youn, M.H., Seo, J.G., Kim, P. and Song, I.K., *Role and effect of molybdenum on the performance of Ni-Mo/ γ -Al₂O₃ catalysts in the hydrogen production by auto-thermal reforming of ethanol*. Journal of Molecular Catalysis A: Chemical, 2007. **261**(2): p. 276-281.
214. Youn, M.H., Seo, J.G., Kim, P., Kim, J.J., Lee, H.-I. and Song, I.K., *Hydrogen production by auto-thermal reforming of ethanol over Ni/ γ -Al₂O₃ catalysts: Effect of second metal addition*. Journal of Power Sources, 2006. **162**(2): p. 1270-1274.
215. Profeti, L.P.R., Dias, J.A.C., Assaf, J.M. and Assaf, E.M., *Hydrogen production by steam reforming of ethanol over Ni-based catalysts promoted with noble metals*. Journal of Power Sources, 2009. **190**(2): p. 525-533.
216. Profeti, L.P.R., Ticianelli, E.A. and Assaf, E.M., *Production of hydrogen via steam reforming of biofuels on Ni/CeO₂–Al₂O₃ catalysts promoted by noble metals*. International Journal of Hydrogen Energy, 2009. **34**(12): p. 5049-5060.
217. Lu, Y., Li, S., Guo, L. and Zhang, X., *Hydrogen production by biomass gasification in supercritical water over Ni/[γ]-Al₂O₃ and Ni/CeO₂-[γ]-Al₂O₃ catalysts*. International Journal of Hydrogen Energy, 2010b. **35**(13): p. 7161-7168.
218. Tomishige, K., Kimura, T., Nishikawa, J., Miyazawa, T. and Kunimori, K., *Promoting effect of the interaction between Ni and CeO₂ on steam gasification of biomass*. Catalysis Communications, 2007. **8**(7): p. 1074-1079.
219. Arauzo, J., Radlein, D., Piskorz, J. and Scott, D.S., *Catalytic Pyrogasification of Biomass. Evaluation of Modified Nickel Catalysts*. Industrial & Engineering Chemistry Research, 1997. **36**(1): p. 67-75.
220. Choudhary, V.R., Uphade, B.S. and Mamman, A.S., *Oxidative Conversion of Methane to Syngas over Nickel Supported on Commercial Low Surface Area Porous Catalyst Carriers Precoated with Alkaline and Rare Earth Oxides*. Journal of Catalysis, 1997. **172**(2): p. 281-293.

221. Zhang, T. and Amiridis, M.D., *Hydrogen production via the direct cracking of methane over silica-supported nickel catalysts*. Applied Catalysis A: General, 1998. **167**(2): p. 161-172.
222. Bartholomew, C.H., *Sintering kinetics of supported metals: new perspectives from a unifying GPLE treatment*. Applied Catalysis A: General, 1993. **107**(1): p. 1-57.
223. Trimm, D.L. and Calvin, H.B.a.J.B.B., *Thermal Stability of Catalyst Supports*, in *Studies in Surface Science and Catalysis*. 1991, Elsevier. p. 29-51.
224. Bartholomew, C.H. and Farrauto, R.J., *Fundamentals of Industrial Catalytic Processes*. 2nd Edition ed. 2006: John Wiley & Sons Inc.
225. Agnelli, M., Kolb, M. and Mirodatos, C., *Co Hydrogenation on a Nickel Catalyst .: I. Kinetics and Modeling of a Low-Temperature Sintering Process*. Journal of Catalysis, 1994. **148**(1): p. 9-21.
226. Bartholomew, C.H., *Mechanisms of catalyst deactivation*. Applied Catalysis A: General, 2001. **212**(1-2): p. 17-60.
227. Maxted, E.B., *The Poisoning of Metallic Catalysts*, in *Advances in Catalysis*. 1951, Academic Press. p. 129-178.
228. Elliott, D., Peterson, K., Muzatko, D., Alderson, E., Hart, T. and Neuenschwander, G., *Effects of trace contaminants on catalytic processing of biomass-derived feedstocks*. Applied Biochemistry and Biotechnology, 2004. **115**(1): p. 807-825.
229. Aguayo, A.T., Gayubo, A.G., Erena, J., Atutxa, A. and Bilbao, J., *Coke Aging and Its Incidence on Catalyst Regeneration*. Industrial & Engineering Chemistry Research, 2003. **42**(17): p. 3914-3921.
230. Pham, H.N., Reardon, J. and Datye, A.K., *Measuring the strength of slurry phase heterogeneous catalysts*. Powder Technology, 1999. **103**(2): p. 95-102.
231. Dayton, D., *A review of the literature on catalytic biomass tar destruction: Milistone completion report*. 2002, National Renewable Energy Laboratory: Cole Boulevard.
232. Olivares, A., Aznar, M.P., Caballero, M.A., Gil, J., Frances, E. and Corella, J., *Biomass Gasification: Produced Gas Upgrading by In-Bed Use of Dolomite*. Industrial & Engineering Chemistry Research, 1997. **36**(12): p. 5220-5226.
233. Vassilatos, V., Taralas, G., Sjöström, K. and Björnbom, E., *Catalytic cracking of tar in biomass pyrolysis gas in the presence of calcined dolomite*. 1992. p. 1008-1013.
234. Corella, J., Aznar, M.-P., Gil, J. and Caballero, M.A., *Biomass Gasification in Fluidized Bed: Where To Locate the Dolomite To Improve Gasification?* Energy & Fuels, 1999. **13**(6): p. 1122-1127.
235. Tamhankar, S.S., Tsuchiya, K. and Riggs, J.B., *Catalytic cracking of benzene on iron oxide-silica: catalyst activity and reaction mechanism*. Applied Catalysis, 1985. **16**(1): p. 103-121.
236. Simell, P.A., Leppälähti, J.K. and Bredenberg, J.B.s., *Catalytic purification of tarry fuel gas with carbonate rocks and ferrous materials*. Fuel, 1992. **71**(2): p. 211-218.
237. Chembukulam, S.K., Dandge, A.S., Rao, N.L.K., Seshagiri, K. and Vaidyeswaran, R., *Smokeless fuel from carbonized sawdust*. Industrial & Engineering Chemistry Product Research and Development, 1981. **20**(4): p. 714-719.

238. Turn, S., Kinoshita, C., Ishimura, D., Zhou, J., Hiraki, T. and Masutani, S., *Control of alkali species in gasification systems*. 2000, Hawaii Natural Energy Institute: Honolulu.
239. Suzuki, T., Ohme, H. and Watanabe, Y., *Alkali metal catalyzed carbon dioxide gasification of carbon*. *Energy & Fuels*, 1992. **6**(4): p. 343-351.
240. Rolin, A., Tichard, C., Masson, D. and Deglise, X., *Catalytic conversion of biomass by fast pyrolysis*. *Journal of Analytical and Applied Pyrolysis*, 1983. **5**(2): p. 151-166.
241. Sutton, D., Kelleher, B. and Ross, J.R.H., *Review of literature on catalysts for biomass gasification*. *Fuel Processing Technology*, 2001. **73**(3): p. 155-173.
242. Lizzio, A.A. and Radovic, L.R., *Transient kinetics study of catalytic char gasification in carbon dioxide*. *Industrial & Engineering Chemistry Research*, 1991. **30**(8): p. 1735-1744.
243. Regina Oliveira de Souza, T., Modesto de Oliveira Brito, S. and Martins Carvalho Andrade, H., *Zeolite catalysts for the water gas shift reaction*. *Applied Catalysis A: General*, 1999. **178**(1): p. 7-15.
244. Prasad, P. and Elnashaie, S.S.E.H., *Coupled Steam and Oxidative Reforming for Hydrogen Production in a Novel Membrane Circulating Fluidized-Bed Reformer*. *Industrial & Engineering Chemistry Research*, 2003. **42**(20): p. 4715-4722.
245. Abashar, M.E.E., Alhabdan, F.M. and Elnashaie, S.S.E.H., *Staging Distribution of Oxygen in Circulating Fast Fluidized-Bed Membrane Reactors for the Production of Hydrogen*. *Industrial & Engineering Chemistry Research*, 2007. **46**(17): p. 5493-5502.
246. Karellas, S., Kakaras, E., Papadopoulos, T., Schäfer, C. and Karl, J., *Hydrogen production from allothermal biomass gasification by means of palladium membranes*. *Fuel Processing Technology*, 2008. **89**(6): p. 582-588.
247. Stevens Jr, R.W., Shamsi, A., Carpenter, S. and Siriwardane, R., *Sorption-enhanced water gas shift reaction by sodium-promoted calcium oxides*. *Fuel*, 2010. **89**(6): p. 1280-1286.
248. Acharya, B., Dutta, A. and Basu, P., *An investigation into steam gasification of biomass for hydrogen enriched gas production in presence of CaO*. *International Journal of Hydrogen Energy*, 2010. **35**(4): p. 1582-1589.

CHAPTER 3. MATERIALS AND METHODS

3.1 Materials

3.1.1 Solid waste (RDF)

The real world municipal solid wastes (MSW) used in this research were in the form of densified refuse derived fuel (RDF). The RDF samples were obtained as pellets of approximately 16 mm diameter and 80 mm length were obtained from a UK MSW treatment facility.

In order to increase the sample homogeneity, the RDF pellets were thoroughly mixed, ground and then sieved to different particle sizes as follows; 1 mm, 2 mm, 3 mm and 3-9 mm sizes. All of the experimental tests were carried out with the 1mm particle size, while the other sizes were used to study the effect of particle size on the pyrolysis of the RDF samples. Table 3-1 shows the results of the proximate analysis and the elemental analysis of the 1mm size samples of RDF.

Table 3-1

Ultimate and proximate analysis of RDF

Ultimate analysis	wt%
C	43.5
H	5.9
N	0.6
S	nd
O (by diff, ash free)*	37.0
Proximate analysis	wt%
Moisture	4.0
Ash	13.0
Volatiles	73.0
Fixed carbon	10.0

nd: not detected

3.1.2 Simulated single components of RDF

The paper samples used to simulate the paper fraction which make up part of RDF were obtained from waste A4 printing paper. These were cut, ground and sieved to a sample size of 1 mm.

Waste packaging cardboard boxes were obtained from a recycling bin to represent the cardboard fraction of RDF. These were cut, ground and sieved to sample sizes of 1mm.

The waste plastics used for this study were real world mixed municipal plastic wastes from the treatment and recycling of municipal solid wastes. The waste plastics were recycled by Fost Plus, a recycling company in Belgium. The waste plastics were supplied in the form of flakes of approximately 5 to 10 mm sizes. The plastics had been air separated into a low density fraction and contained mainly high density polyethylene and polyethylene terephthalate. The samples were ground and sieved to 1 mm sizes for the purpose of this research.

Table 3-2 shows results of the proximate and elemental analyses of the paper, cardboard and mixed waste plastic samples.

Table 3-2

Ultimate and proximate analysis of RDF simulated single components			
Ultimate analysis (wt%)	Paper	Cardboard	Plastics
C	39.4	40.6	69.8
H	5.4	5.7	11
N	0.6	0.5	0.5
S	nd	nd	nd
O (by diff, ash free)*	44.6	47.2	13.7
Proximate analysis (wt%)			
Moisture	5.0	5.0	1.0
Ash	10.0	6.0	5.0
Volatiles	68.0	71.0	91.0
Fixed carbon	17.0	18.0	3.0

nd: not detected

3.1.3 Waste wood

The wood sample used for this study, were supplied in the form of waste wood pellets of approximately 6 mm diameter and 14 mm length. These wood pellets were compressed from waste saw dust from wood processing by Liverpool Wood Pellets Ltd, a UK company. The wood pellets were then ground and sieved to about 1 mm particle size, which was used for most of this research. In order to investigate the effects of particle size, 3 other size ranges were also obtained using the necessary sieves as follows: 2mm, 3 mm and 3 – 9 mm. Table 3-3 shows the results of the proximate analysis and the elemental analysis of the 1mm wood sample.

Table 3-3

Ultimate and proximate analysis of wood	
Ultimate analysis	wt%
C	46.6
H	5.8
N	0.4
S	nd
O (by diff, ash free)*	38.2
Proximate analysis	wt%
Moisture	7.0
Ash	2.0
Volatiles	76.0
Fixed carbon	15.0

nd: not detected

3.1.4 Simulated single components of waste wood

The cellulose utilized for this research was in the form of microcrystalline powders of particle size < 180 µm and were supplied by Avocado Research Chemicals, UK.

Hemicellulose as a single component of wood was investigated for this study in the form of xylan powder of particle size < 180 µm and was supplied by Sigma Aldrich, UK.

Kraft alkali lignin was utilized for this study, in form of powder of particle size < 180 μm and was supplied by Sigma Aldrich, UK.

Table 3-4 shows results of the proximate and elemental analyses of the cellulose, xylan and lignin samples.

Table 3-4

Ultimate and proximate analysis of wood simulated single components			
Ultimate analysis (wt%)	Cellulose	Xylan	Lignin
C	41.7	40.3	61.3
H	5.9	5.5	5.1
N	0.4	0.4	1.1
S	nd	nd	0.7
O (by diff, ash free)*	52.0	49.8	27.7
Proximate analysis (wt%)			
Moisture	5.0	6.0	4.0
Ash	nd	4.0	4.0
Volatiles	82.0	73.0	56.0
Fixed carbon	13.0	17.0	36.0

nd: not detected

3.1.5 Researched catalysts and CO₂ sorbents

The catalysts researched in this study were all nickel based catalysts supported on alumina support, which were prepared in the university of Leeds laboratories. The alumina was obtained from Catal International Ltd, a UK company, and these were supplied as γ -alumina (Al₂O₃) spheres of approximate diameters of 4 to 5 mm. The BET surface area of the as supplied alumina spheres was 7.62 m² g⁻¹.

NiO/Al₂O₃ catalysts with 5 wt%, 10 wt% and 20 wt% of Ni were prepared by a wetness method, using the γ -alumina spheres and the appropriate concentration of aqueous solution of Ni(NO₃)₂*6H₂O. The mixture was dried overnight at 105 °C followed by calcination at 500 °C for 3hrs in an air atmosphere. The same drying and calcination procedures as stated above were used for all the catalysts.

NiO/CeO₂/Al₂O₃ catalyst with a loading of 20 wt% of Ni and 5 wt% CeO₂ was prepared by a co-impregnation method. The γ -alumina spheres were impregnated with an aqueous solution of a mixture of Ni(NO₃)₂*6H₂O and Ce(NO₃)₃.

NiO/La₂O₃/Al₂O₃ catalyst with a loading of 20 wt% of Ni and 5 wt% La₂O₃ was prepared by a co-impregnation method. The γ -alumina spheres were impregnated with an aqueous solution of a mixture of Ni(NO₃)₂*6H₂O and La(NO₃)₃.

NiO/MgO/Al₂O₃ catalyst with a loading of 20 wt% of Ni and 5 wt% MgO was prepared by a co-impregnation method. The γ -alumina spheres were impregnated with an aqueous solution of a mixture of Ni(NO₃)₂*6H₂O and Mg(NO₃)₂.

NiO/CuO/Al₂O₃ catalyst with a loading of 20 wt% of Ni and 5 wt% CuO was prepared by a co-impregnation method. The γ -alumina spheres were impregnated with an aqueous solution of a mixture of Ni(NO₃)₂*6H₂O and Cu(NO₃)₂.

NiO/MnO/Al₂O₃ catalyst with a loading of 20 wt% of Ni and 5 wt% MnO was prepared by a co-impregnation method. The γ -alumina spheres were impregnated with an aqueous solution of a mixture of Ni(NO₃)₂*6H₂O and Mn(NO₃)₂.

NiO/CoO/Al₂O₃ catalyst with a loading of 20 wt% of Ni and 5 wt% CoO was prepared by a co-impregnation method. The γ -alumina spheres were impregnated with an aqueous solution of a mixture of Ni(NO₃)₂*6H₂O and Co(NO₃)₂.

NiO/CaO/Al₂O₃ catalyst/CO₂ sorbent with a loading of 20 wt% of Ni and 5 wt% CaO was prepared by a co-impregnation method. The γ -alumina spheres

were impregnated with an aqueous solution of a mixture of $\text{Ni}(\text{NO}_3)_2 \cdot 6\text{H}_2\text{O}$ and $\text{Ca}(\text{NO}_3)_2$.

$\text{NiO}/\text{Al}_2\text{O}_3+\text{CaO}$ catalyst/ CO_2 sorbents which contained 2g, 5g and 10g of CaO and 38g of $\text{NiO}/\text{Al}_2\text{O}_3$ were prepared by thoroughly mixing the required mass of dry CaO powder with the prepared $\text{NiO}/\text{Al}_2\text{O}_3$ catalyst of 20 wt% Ni loading. The CaO powder was supplied by Johnson Matthey.

3.2 Fixed bed reactor

3.2.1 Fixed bed reactor setup

A fixed bed reactor was utilized in this study to conduct experiments to investigate the effects of operating conditions on the products yields as well as the gas and hydrogen yield, from the pyrolysis of RDF, waste wood and their single components. The operating conditions which were investigated include: heating rate, temperature and sample particle size. The fixed bed reactor designed and utilized for this study was made up of a horizontal stainless steel cylindrical tube of length 650 mm and internal diameter of 11 mm. The reactor was heated externally by an electrical tube furnace which provides a heated zone of length 450 mm and was easily controlled to provide the desired final temperature and heating. The sample was introduced to the reactor via a sample boat, which was a cylindrical tube with a cup at its end for holding the sample.

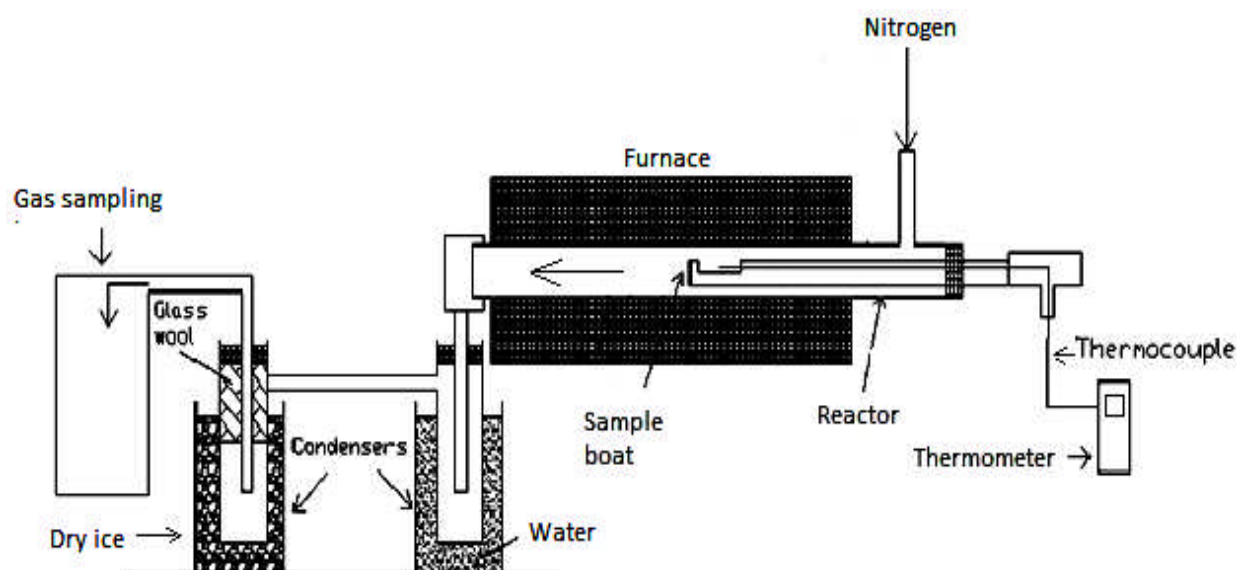


Figure 3-1 Schematic of the fixed bed reactor

The sample boat was designed to be easily, horizontally inserted into and withdrawn from one end of the reactor, placing the cup at the centre of the reactor's heated zone for effective heating. A thermocouple was also integrated into the sample boat, designed to be placed concentric to the walls of the sample boat, thereby providing the temperature at the centre of the sample. The reactor was continually purged with nitrogen so that volatile products could be transported through a pair of condensers where the condensable vapours were condensed, and the non-condensable gases were collected in a sampling bag. A schematic diagram and photograph of the reactor are shown in figures 3-1 and 3-2 respectively. Prior to the start and at the end of every experiment, the reactor tube, sample boat and condensers were weighed and the data recorded.

3.2.2 Fixed bed experimental procedure

Experiments were performed with 1 g of the investigated sample loaded onto the sample boat and inserted into the reactor which was continually purged with nitrogen. Experiments were performed at flow rates of 50, 100 and 200 ml min⁻¹ and indicated that there were no notable impacts from varying the nitrogen flow rates, therefore a flow rate of 100 ml min⁻¹ was selected for all experiments on the fixed bed reactor. The volatiles residence time within the

reactor was estimated to be 9 seconds. The reactor was heated to the desired final temperatures (700, 800 and 900 °C) and at the desired furnace heating rates which were found to be very close to the heating rate for the sample as measured by the thermocouple. The experiment at fast heating rate was achieved by heating the reactor up to temperature before introducing the sample into the hot zone. The heating rate was determined by the equation 3.1.

$$dT/dt = (T_2 - T_1) / (t_2 - t_1) \quad (\text{equation 3.1})$$

Where T_2 is the final pyrolysis temperature, T_1 is the initial sample temperature and $t_2 - t_1$ is the time taken from the start of the experiment until the sample attained final temperature.



Figure 3-2 Photograph of the horizontal fixed bed reactor

For both fast and slow pyrolysis experiments, the samples were allowed to achieve the final pyrolysis temperature and were held at this temperature for 20 min before the heaters were switched off. Pyrolysis volatile products were purged from the reactor by the nitrogen flow into two sets of glass condensers, one was immersed in water and the other with a glass wool trap was immersed in dry ice in order to trap the liquid products. The non-condensable gases were finally collected in a 25 L Tedlar™ sampling bag for

off-line analysis by gas chromatography. Gas collection was continued 20 min after the heaters were switched off in order ensure complete gas collection.

Solid products remained in the sample boat and were weighed and collected for analysis after the reactor cooled. The weight of the solid products were determined by the difference in the reactor and sample boat weight before and after experiments, while that of the oil products were determined by the difference in the condenser weights before and after experiments.

3.2.3 Validation of the fixed bed reactor

In order to validate and optimize the fixed reaction system, initial tests were carried out using RDF samples for fast pyrolysis to a final temperature of 800 °C at fast heating rates of approximately 350 °C min⁻¹. Figure 3-3 shows a temperature profile of the internal walls of the reactor at the furnace temperature of 850 °C. This shows a 50 °C temperature difference between the furnace heater and the reactor wall and this was taken into account during experiments. The temperature profile also shows an isothermal zone between the reactor hot zones of 15cm and 35 cm. The samples were therefore always placed at the middle of the isothermal zone at 25cm of the reactor hot zone. Table 3-5 shows data from the initial testing of the reactor.

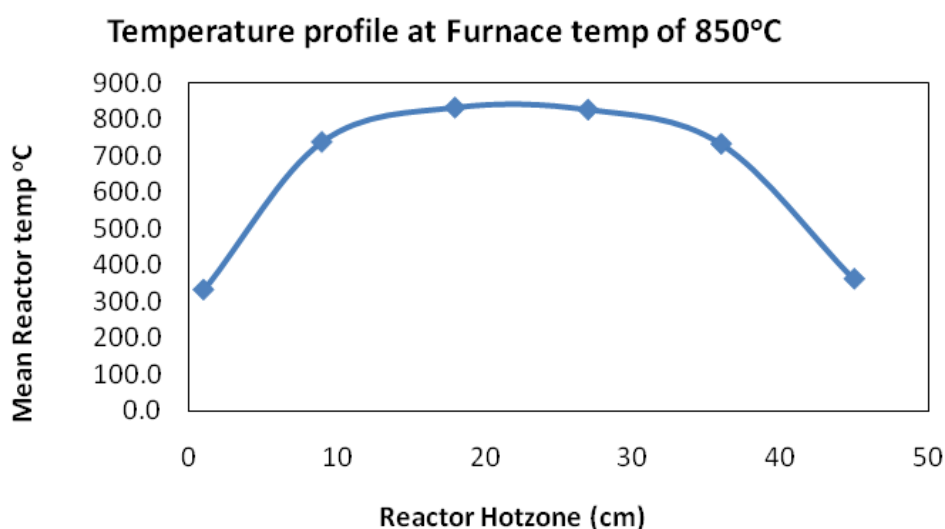


Figure 3-3 Temperature profile of the fixed bed reactor

Table 3-5

Validation of the fixed bed reactor for RDF pyrolysis

	Exp 1	Exp 2	Exp 3	Exp 4	Mean	STDEV
Pyrolysis temperature (°C)	800	800	800	800		
Nitrogen flow rate (mL/min)	100	100	100	100		
Mass of sample (g)	1	1	1	1		
Products	Yield (wt% of RDF)					
Gas	43.2	42.7	46.3	46.9	44.8	1.84
solid	23.5	27.6	23.5	22.8	24.3	1.90
Oil	27.5	29.1	27.0	23.0	26.6	2.25
Balance	94.2	99.4	96.8	92.7	95.8	2.67
Gas composition (N ₂ free)	Yield (vol %)					
H ₂	16.6	17.0	16.6	17.4	16.9	0.33
CO	40.3	40.2	40.6	34.9	39.0	2.47
CO ₂	9.6	14.1	9.7	13.7	11.8	2.13
CH ₄	17.5	15.2	17.6	16.1	16.6	1.00
C ₂ - C ₄	15.9	13.5	15.6	17.8	15.7	1.52

Exp: Experiment, STDEV: standard deviation

The data in Table 3-5 shows that the process conditions within the fixed bed reactor were reproducible for pyrolysis. Furthermore during this study several experimental repetitions were carried out throughout the research at regular intervals in order to check for and ensure the accuracy of data.

3.3 Continuous screw kiln reactor

3.3.1 Screw kiln reactor setup

A continuous screw kiln reactor was designed and utilized in this study to investigate the effects of operating conditions on the two stage pyrolysis and steam pyrolysis-gasification of waste wood. The operating conditions investigated included: the effects of temperature, steam, catalysts and CaO as a CO₂ sorbent. The continuous screw kiln reactor used in this study had four main elements as follows; a waste feed mechanism, a first stage screw kiln reactor which was a pyrolysis stage, and a second stage fixed bed reactor which was a catalytic reformer. The screw kiln reactor was 540 mm long x 62

mm diameter, constructed of stainless steel and heated externally by an electrical furnace to a fixed pyrolysis temperature. The second stage fixed bed catalytic reformer was 360 mm high x 46 mm diameter, constructed of stainless steel and was also heated externally by an electric furnace to provide a fixed gasification temperature.

The feed mechanism was made up of a feedstock hopper which could be sealed and could hold up to 4kg of feedstock. It was connected to a rotary feeder which was operated by an electric motor. The rotary feeder and electric motor ensured continuous feed of material to the first stage reactor and the feed rate could be varied by varying the speed of the electric motor. The first stage reactor was made up of a horizontal cylindrical tube with a screw shaft which rotated along the length of the reactor. Waste was fed into the first stage screw kiln reactor via gravity from the feed hopper and was pyrolyzed as it was moved along the horizontal length of the reactor by the effect of the screw rotation. The reactor had a main control panel with display controllers and interfaces for controlling its operations. Figure 3-4 shows a schematic of the continuous feed screw kiln reactor.

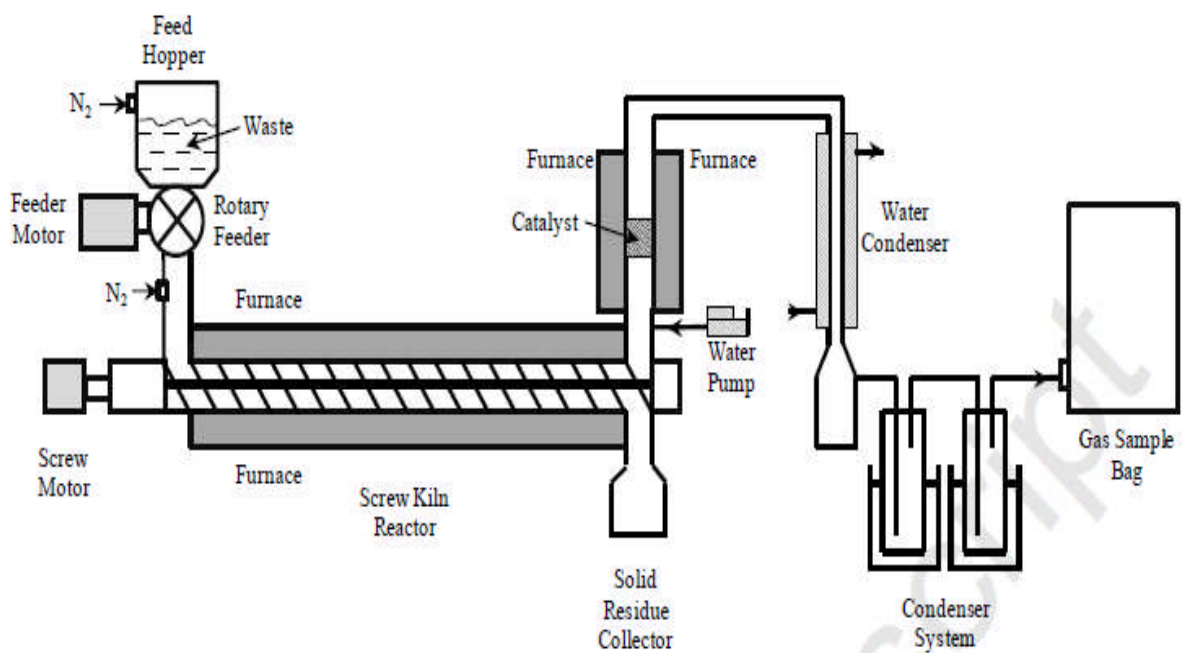


Figure 3-4 Schematic of the continuous screw kiln reactor

The reaction system was continuously purged with nitrogen which was supplied via two inlets, one at the top of the feed hopper and another inlet before the first reactor. The screw shaft was connected to an electric motor which controlled its rotation and the sample throughput. The shaft also sits on top of bearings at its ends which were water cooled to prevent damage to the bearings. Gaseous products from pyrolysis in the screw kiln were transported via the nitrogen purge to the second stage vertical fixed bed reactor which was a catalytic reactor. The second stage fixed bed reactor had a water injection inlet and a catalyst bed. Product gases from the fixed bed reactor were channelled through a series of condensers and into a sampling gas bag for off-line GC analysis. The reactor had a solid residue collector at the end of the first stage reactor.

3.3.2 Development and modification of the screw kiln reactor

The screw kiln reactor had to undergo an initial testing, development phase and modifications before finally being used for this study.

Initial tests on the reactor system highlighted the following issues which needed to be addressed in order to make it suitable for experimentation:

- The two independent electric furnaces which heated the first stage reactor were noted to heat the reactor un-equally, resulting in non-isothermal regions within the reactor.
- The design of the catalyst bed in the second stage fixed bed reactor allowed gases from the first stage to by-pass the packed catalytic bed from the sides without being cracked.
- The catalyst bed could only hold a very limited quantity of catalysts.
- The mass flow of vapours and steam through the catalyst bed resulted in an entrainment of the sand and powdered catalysts bed materials initially tested, rendering the catalytic bed almost ineffective.

- The electric furnace which heated the fixed bed reactor did not deliver fixed isothermal heating during tests, resulting in continuous temperature fluctuations.
- The volume of the stainless steel water cooled condenser was insufficient to contain the condensed liquids.

The results of the initial tests are shown in table 3-6 and 3-7. Table 3-6 shows results for the reproducibility tests of the continuous screw kiln reactor for pyrolysis and gasification. Steam gasification tests were carried out with a steam to biomass ratio of 0.4. The results in table 3-6 show that conditions within the reactor were not reproducible during the initial pyrolysis and gasification tests. Both the product yields and the gas product compositions were found to vary between each pyrolysis gasification experimental repetition.

Table 3-6

Results from pyrolysis and gasification during reactor initial tests

	Pyrolysis			Steam gasification only		
	Run1	Run2	Run3	Run1	Run2	Run3
Screw kiln temperature (°C)	500	500	500	500	500	500
Fixed bed temperature (°C)	800	800	800	800	800	800
Nitrogen flow rate (mL min ⁻¹)	300	300	300	300	300	300
Mass of sample (g)	40	40	40	40	40	40
Sample feed rate (g min ⁻¹)	8	8	8	8	8	8
Steam to biomass ratio	0	0	0	0.4	0.4	0.4
	Products			Yield (wt% of waste wood)		
Gas	27.5	19.4	21.4	42.4	34.2	26.3
Solid	23.1	28.2	34.0	23.8	22.5	26.8
Oil (by difference)	49.4	52.4	44.6	33.8	43.3	46.9
	Gas composition (N ₂ free)			Yield (vol %)		
H ₂	14.4	12.3	12.4	18.0	17.5	16.3
CO	52.2	54.6	54.4	46.5	46.5	48.3
CO ₂	13.1	13.2	12.2	15.0	14.2	14.4
CH ₄	13.3	14.0	14.7	12.3	13.2	13.1
C ₂ - C ₄	7.0	5.9	6.3	8.2	8.6	7.9

Table 3-7

Effects of varying steam to biomass ratio during gasification

Steam gasification only				
Screw kiln temperature (°C)	500	500	500	500
Fixed bed temperature (°C)	800	800	800	800
Nitrogen flow rate (mL min ⁻¹)	300	300	300	300
Mass of sample (g)	40	40	40	40
Sample feed rate (g min ⁻¹)	8	8	8	8
Steam to biomass ratio	0.2	0.4	0.6	0.8
Products	Yield (wt% of waste wood)			
Gas	32.0	42.4	31.2	38.4
Solid	26.4	23.8	24.8	26.0
Oil (by difference)	41.6	33.8	44.1	35.6
Gas composition (N ₂ free)	Yield (vol %)			
H ₂	14.5	18.0	14.3	7.0
CO	48.7	46.5	47.8	52.9
CO ₂	14.5	15.0	14.9	16.2
CH ₄	13.3	12.3	13.5	14.1
C ₂ - C ₄	8.9	8.2	9.5	9.8

Table 3-7 shows results from investigating the effects of varying the steam to biomass ratio for steam gasification. The steam to biomass ratios investigated were: 0.2, 0.4, 0.6 and 0.8. The results show that there was no trend for both the product yields and the gas compositions, with varying the steam to biomass ratio, indicating inconsistencies within the reactor.

In order to address the issues stated above, the continuous screw kiln system was modified as shown in figure 3-5. Figure 3-5 shows a photograph of the reactor and a schematic diagram of the catalytic fixed bed after modifications. The following modifications were made to the continuous screw kiln reaction system:

- The electric furnaces for the first stage and second stage reactors were replaced with furnaces which could provide a more accurate temperature and heating programme.

- The catalytic fixed bed was redesigned to increase the catalyst capacity of the bed as well as prevent gases from by-passing the catalyst bed.
- The particle sizes of the sand bed was initially 50 and 180 μm was increased to between 212 and 300 μm , and powdered catalysts were replaced with more dense spheres of sizes between 4 to 5 mm, to prevent bed material loss by entrainment.
- The stainless steel condenser was replaced with one with larger dimensions and therefore more holding capacity.

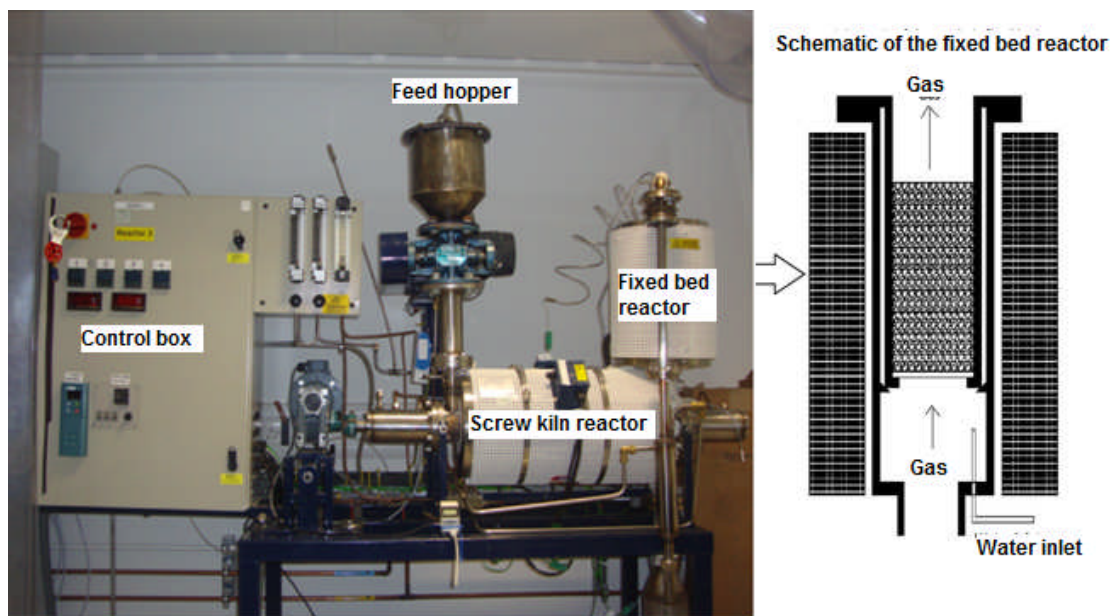


Figure 3-5 Photograph and schematic of continuous screw kiln after modifications.

3.3.3 Screw kiln experimental procedure

Prior to starting up the system, 40g of the feedstock was loaded into the feed hopper and all connections tightly sealed to avoid leakages. Carrier gas flow was initiated to purge and maintain an inert atmosphere, and cooling water supply to the shaft bearings and first condenser were initiated from a dedicated cooling system, and the flow rates set once the reactor was powered on. The nitrogen gas flow out of the reactor was then set to 300 mL min^{-1} and checked via an electronic flow meter and recorded. After this, the

reactor temperature program was set and its heating was started. Once the desired temperatures for the reactors had been achieved, the screw kiln was switched on and its rotation speed was programmed. The feed mechanism was then switched on and feeding rate programmed to start feeding the waste wood to the first stage.

Fast pyrolysis of the waste wood took place in the horizontal screw-kiln reactor which was pre-heated to 500 °C or 700 °C when the waste was fed into the reactor and the rotating motion of the screw within the reactor transported it through the reactor. The waste wood feeding rate used in this work was 0.48 kg hr⁻¹ (8 g min⁻¹) and the solids residence time within the screw kiln pyrolysis reactor was 40 s. The solid char product was collected in a solids collection pot.

The released pyrolysis vapours were then transported by the nitrogen gas purge to the second stage vertical fixed bed reactor which was maintained at a fixed temperature of 700 °C, 800 °C or 900 °C, where steam and or catalytic reforming of the pyrolysis vapours occurred. Water required for the steam reforming was injected via an inlet at the base of the fixed bed reactor, using a syringe pump. Water injection was started 2 min before the start of sample feed and was stopped 2 min after the end of sample feed in order to provide the appropriate steam atmosphere. For catalytic steam reforming experiments, 40 g of the catalyst supported on quartz wool was placed in the fixed bed. While 40 g of sand of sizes between 212 and 300 µm, supported on quartz wool, was used for only steam reforming experiments, in order to reproduce any non-catalytic effects of the bed such as heat transfer and particulate filtration. The catalyst was activated in-situ by the pyrolysis gases.

The product gases from the fixed bed reactor were channelled through a series of cold traps made up of a stainless steel water cooled condenser designed as part of the reactor and cooled by the dedicated refrigerated cooling system flowing water at 10 °C. Two glass condensers were immersed in water and 2 glass condensers were immersed in dry ice in order to collect

the condensable liquid product. The product gases were finally passed through an activated carbon filter and an electronic flow meter before being collected in a 100 L Tedlar™ sampling bag for analysis by gas chromatography.

The reactor temperatures, sample feed, screw-kiln rotation and product gas volume flow were measured every second with a National Instrument™ data logger and was monitored and recorded on a computer via Lab-view software. The reactor operating conditions including the pyrolysis temperature, the gasification temperature, the sample feed rate, the solids and gas residence times and the steam flow rate were kept constant for all experiments. Experiments were carried out twice in order to determine the repeatability of each experiment and the reliability of the gasification system, at the same conditions.

3.3.4 Validation of the modified screw kiln reactor

Prior to the validation of the screw kiln system, the waste feeder and the screw kiln shaft were calibrated without any heating for feeding the sample of waste wood. Table 3-8 shows data from the calibration of the waste feed hopper and the kiln screw at room temperature.

Table 3-8

Calibration of the feed hopper and kiln screw for waste wood			
Feed hopper		Kiln screw	
Motor setting	Feed rate (g min ⁻¹)	Motor setting	Residence time (sec)
10	4	10	150
20	8	20	85
30	13	30	46
40	18	40	34

Tests were carried out for pyrolysis without steam, at a first stage reactor temperature of 500 °C and second stage reactor temperature of 800 °C. Also

for steam only gasification at a first stage reactor temperature of 700 °C, second stage reactor temperature of 800 °C and steam to biomass ratio of 0.41 (water injection rate of 0.33 ml min⁻¹). All tests were carried out using waste wood samples of sizes between 3 to 9 mm, at a feed rate of 8 g min⁻¹ and the bed material used was sand of particle sizes between 212 and 300 µm, supported on quartz wool. Table 3-9 shows data from the reactor validation tests.

Table 3-9

Validation of the continuous screw kiln reactor for waste wood

	Pyrolysis					Steam gasification only			
	Exp 1	Exp 2	Exp 3	Mean	STDV	Exp 1	Exp 2	Mean	STDV
Screw kiln temperature (°C)	500	500	500			700	700		
Fixed bed temperature (°C)	800	800	800			800	800		
Nitrogen flow rate (mL min ⁻¹)	300	300	300			300	300		
Mass of sample (g)	40	40	40			40	40		
Sample feed rate (g min ⁻¹)	8	8	8			8	8		
Water injection rate (g min ⁻¹)	-	-	-			3.3	3.3		
Steam to biomass ratio	-	-	-			0.4	0.4		
	Products					Yield (wt% of waste wood)			
Gas	19.4	21.4	19.5	20.1	0.94	46.6	46.3	46.5	0.16
solid	35.7	34.0	36.5	35.4	1.05	12.5	13.0	12.7	0.25
Liquid (by difference)	44.9	44.6	44.0	44.5	0.35	40.9	40.7	40.8	0.09
	Gas composition (N ₂ free)					Yield (vol %)			
H ₂	12.3	12.4	13.1	12.6	0.38	14.6	14.7	14.6	0.03
CO	54.6	54.4	54.3	54.4	0.15	54.7	59.2	56.9	2.27
CO ₂	13.2	12.2	12.6	12.6	0.39	12.4	11.0	11.7	0.74
CH ₄	14.0	14.7	13.2	14.0	0.60	12.5	10.9	11.7	0.80
C ₂ - C ₄	5.9	6.3	6.8	6.4	0.37	5.8	4.3	5.1	0.76

Exp: experiment, **STDV:** standard deviation,

Table 3-9 shows that the process conditions in the continuous screw kiln reactor were reproducible for both pyrolysis and gasification of the waste wood samples. Careful inspection showed that there were no noticeable gas leaks or solids collection elsewhere in the reactor. The liquid product was

therefore determined by the difference of the wt% of gas and solids from a balance of 100%.

3.4 Gas Analysis

3.4.1 GC/TCD and GC/FID

Non-condensable gaseous products collected in the Tedlar™ sample gas bag were analysed by gas chromatography (GC). A Varian 3380GC with dual packed columns and dual thermal conductivity detectors (GC/TCD) was used to analyse and determine the permanent gases (H₂, CO, O₂, N₂ and CO₂). The column for CO₂ analysis was 2 m length by 2 mm diameter with Haysep 80 – 100 mesh packing material. Analysis for H₂, CO, O₂ and N₂ was carried out in a second column of 2m length by 2 mm diameter packed with 60 – 80 mesh molecular sieve.



Figure 3-6 Photograph of a Varian GC with TCD and FID.

The GC oven was held at 40 °C during the analysis while the detector oven and filament temperatures were at 120 °C and 160 °C respectively and the

carrier gas for both columns was Argon. The total analysis time for CO₂ was 7 min while for the other permanent gases was 10 min. A second Varian 3380 GC with a flame ionization detector (GC/FID) was used to analyse and determine the hydrocarbons (C₁ – C₄) in Nitrogen carrier gas. The column was 2 m length by 2mm diameter, packed with Haysep 80 – 100 mesh. The GC oven temperature was set to 60 °C for 3 min and ramped to 100 °C at 5 °C min⁻¹ held for 3 min and finally heated to 120 °C at 20 °C min⁻¹ held for 17 min. The total analysis time was 21 min. Other researchers have used similar off-line GC analysis [1-3]. Figure 3-6 above shows a photograph of a Varian GC with TCD and FID.

3.4.2 Determination of sampled gas concentration

Each of the component gases were eluted at unique retention times in the appropriate GC and temperature programme, making them easily identifiable as shown in figures 3-7 to 3-10. In order to determine the concentration of the sampled gases, the response factors of standard gases of known concentrations, purchased from Scientific and Technical gases Ltd, were compared with the response from the GCs (TCD and FID) of the sampled gases and a relationship was determined. The standard gases obtained were: permanent gases (which contained 1 vol% CO, 1 vol% CO₂, 1 vol% H₂, 1 vol% O₂ and balance N₂), alkane gases (which contained 1 vol% CH₄, 1 vol% C₂H₆, 1 vol% C₃H₈, 1 vol% C₄H₁₀ and balance N₂) and alkene gases (which contained 1 vol% C₂H₄, 1 vol% C₃H₆, 2 vol% C₄H₈ & C₄H₆ and balance N₂).

1 ml of the gas (standard or sample) was injected into the GCs, the elution of each component gas in the respective GC generated a peak. The response factors were determined by calculating the area under the respective peak and sample gas concentration was determined by equation 3.2 below

$$C_{\text{sample}} = C_{\text{standard}} \times A_{\text{sample}} / A_{\text{standard}} \quad (\text{equation 3.2})$$

Where C_{sample} is the concentration of the sample gas, C_{standard} is the concentration of the respective standard gas, A_{sample} is the peak area of the sample gas and A_{standard} is the peak area of the respective standard gas.

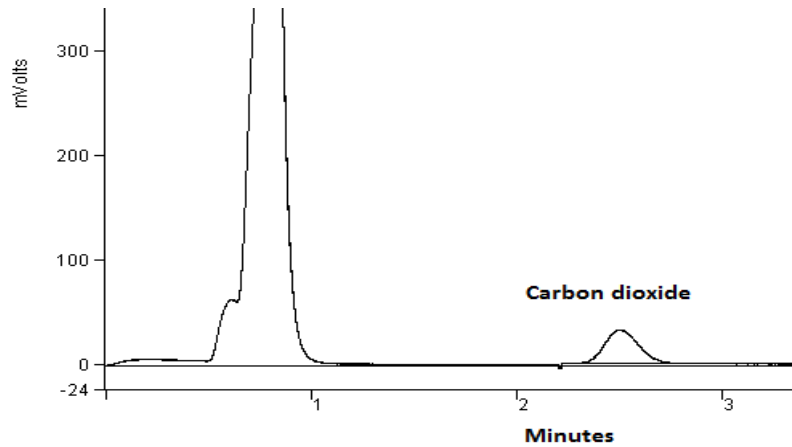


Figure 3-7 Example output GC chromatogram showing CO₂

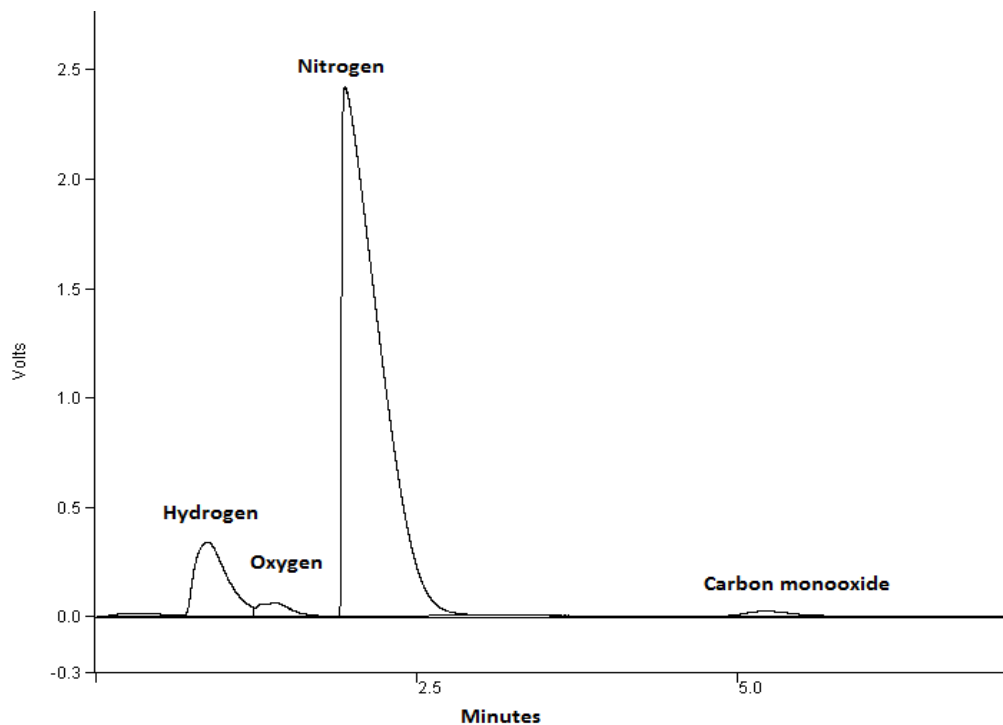


Figure 3-8 Example GC output chromatogram showing H₂, O₂, N₂ and CO

For accuracy a total of 3 sample gas injections were analysed for each sample and an average of the 3 determined concentrations were used for calculations. The concentration was used to determine the total gas volume, mass as well as the gross calorific value (GCV) of the gases by using a

designed spreadsheet which took account of factors such as the nitrogen flow rate during experiments, the total gas collection time and the calorific value (CV) of the individual gas components.

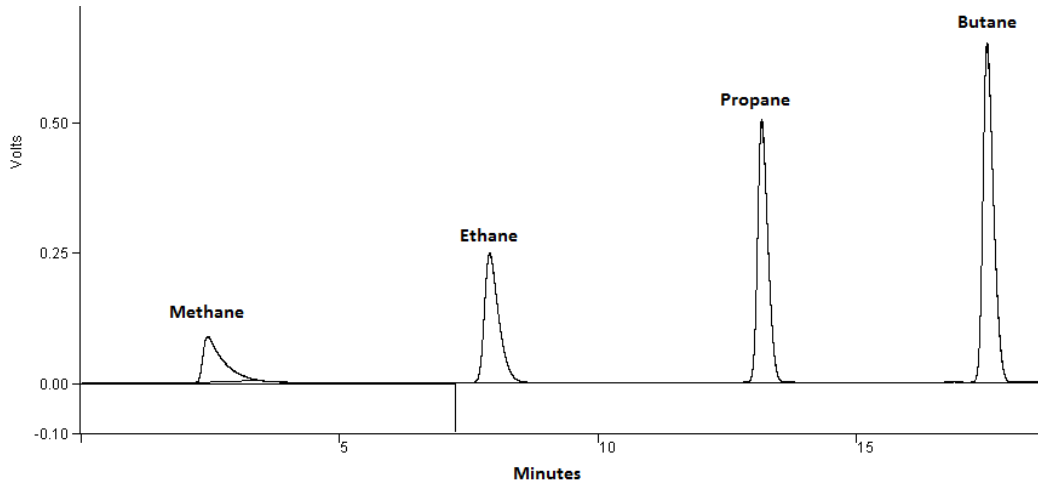


Figure 3-9 Example GC output chromatogram showing the alkane gases

The GCV of the gases were calculated from the equation 3.3 below

$$GCV = CV_m / Z_m \quad (\text{equation 3.3})$$

Where CV_m is the sum of the products of the mole fractions and the calorific values of the individual gases and Z_m is the compressibility factor of the gases.

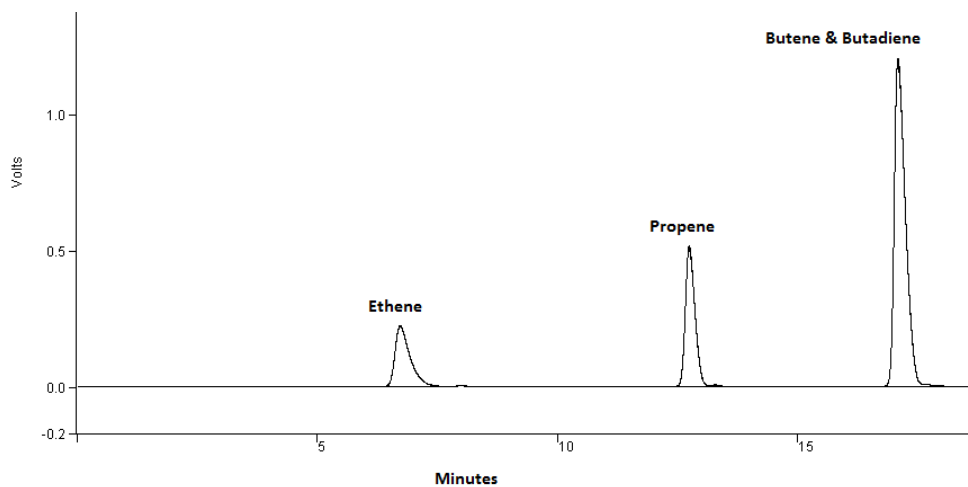


Figure 3-10 Example GC output chromatogram showing the alkene gases

3.5 Oil analysis

The liquid products condensed in the condensers for each experiment were weighed and then collected for analysis by gas chromatography/mass spectrometry (GC/MS) and Fourier transforms infra-red (FTIR).

3.5.1 Fourier transforms infra-red (FTIR) spectrometry

The raw oil samples obtained from pyrolysis were analysed by Fourier transforms infra-red spectrometry using a ThermoScientific, Nicolet iS10 spectrometer in order to determine the chemical functional groups in the oils. A very small quantity of the oil sample was smeared on the equipment's sample disc. An infra-red spectrum was produced and was compared with characteristic infrared spectra of known organic functional groups in the database. This method has been used by other researchers [4-5]. Figure 3-11 shows a photograph of the ThermoScientific Nicolet iS10 spectrometer.



Figure 3-11 Photograph of the ThermoScientific Nicolet iS10 spectrometer

3.5.2 Gas chromatography/mass spectrometry (GC/MS)

Before analysis in the GC/MS/MS, the oil product was dried by a packed column of sodium sulphate to remove water. The liquids were collected from the condensers using dichloromethane (DCM) solvent, dried and their volume concentrated down to 10 ml by extracting the DCM via vacuum evaporation. The samples were then separated into an aliphatic fraction dissolved in n-hexane and an aromatic and oxygenated fraction dissolved in DCM using a packed column containing a sorbent which was a mix of silica and alumina, designed to fractionate aliphatic and aromatics from petroleum hydrocarbons, supplied by Biotage. This involved washing the vessel containing evaporated extract first in n-hexane and passing solution through the packed column and then washing the vessel with DCM and passing the solution through the column and finally flushing the column thoroughly with DCM. The extracted solutions were then vacuum evaporated to about 2ml. Appropriate dilutions of the prepared oil samples were made prior to GC/MS analysis.



Figure 3-12 Photograph of the Varian 3800-GC/MS

The extracts were then analysed on a GC/MS/MS instrument using the external standard method. The GC/MS/MS system consisted of a Varian 3800-GC coupled to a Varian Saturn 2200 ion trap MS/MS equipment shown in figure 5-12 above. The column used was a 30m x 0.25mm inner diameter Varian VF-5ms (DB-5 equivalent), while the carrier gas was helium, at a constant flow rate of 1 ml min⁻¹. The GC injector was held at 290 °C. the oven temperature programme was as follows; 40 °C, held for 2 min and ramped to 280 °C at a rate of 5 °C min⁻¹ and then held at 280 °C for 10 min., the transfer line temperature was 280 °C, manifold was at 120 °C and the trap temperature was held at 200 °C. Spectral searches on the installed NIST2008 library were used to qualitatively identify the major 'unknown' compounds in the oil products.

Many of the detected peaks were identified and quantified however due to the overlapping of certain species as well as possibly low concentration level below the GC/MS detection levels, not all peaks could be identified and quantified.

3.6 Solids analysis

3.6.1 Thermogravimetric analysis of solids

The thermogravimetric analyses of solids (fresh samples and process products) were carried out in order to determine their thermal behaviour in terms of weight loss in relation to temperature and from which a proximate analysis was determined. The proximate analysis provided data on the moisture, volatile, fixed carbon and ash content of the samples. The thermogravimetric analysis was carried out using a Stanton-Redcroft thermogravimetric analyser (TGA). The TGA was made up of an aluminium pan held in a micro balance which was coupled to a precisely controlled furnace. The procedure involved placing a known quantity of the sample into the aluminium pan which was suspended in the micro balance within the furnace. Figure 3-13 shows a photograph of the Stanton-Redcroft TGA.



Figure 3-13 Photograph of the Stanton-Redcroft TGA

The TGA temperature programme was set to heat the sample from 25 °C to 110 °C at a heating rate of 25 °C min⁻¹ and a hold time of 10 mins in nitrogen, then to 900 °C at 25 °C min⁻¹ for 20 min in nitrogen and finally to 910 °C at 10 °C min⁻¹ for 20 min in air. During the programme, the micro balance recorded the weight change of the sample and this was stored on a computer. Figure 3-14 shows a characteristic thermogram and a first order differential for the decomposition of the RDF samples using the above TGA and temperature program.

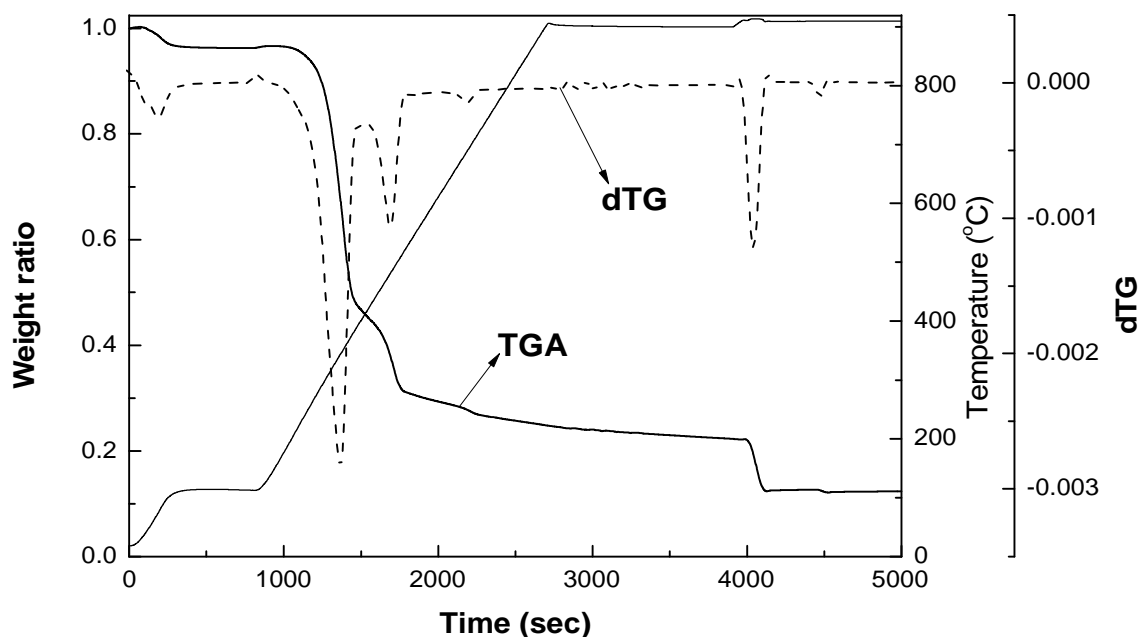


Figure 3-14 Thermogram for RDF

The weight ratio was determined by equation 3.4 below.

$$\text{Weight ratio} = (W_i - W_c) / W_i \quad (\text{equation 3.4})$$

Where W_i is the initial sample weight and W_c is the change in sample weight.

3.6.2 Elemental (CHNSO) analysis

Elemental analysis of samples to determine their carbon, hydrogen, nitrogen and sulphur contents were carried out by the flash combustion method with a Carlo Erba Flash EA 112 elemental analyser. About 3 mg of the sample was weighed into a tin capsule, folded and the reactors auto-sampler for analysis. In the reactor, the sample was combusted at 1800 °C in excess oxygen and high purity helium gas. The product gases were passed and separated in a chromatographic column with a TCD. The TCD determined and quantified the carbon, hydrogen, nitrogen and sulphur contents of the product gas using standards. The oxygen content was determined by the ash free difference. A similar method has been used before [6].

3.6.3 Bomb calorimetric analysis

The GCV of the fresh and produced solids were determined using a bomb calorimeter. The calorimetric equipment was a Parr 6200 Isooperibol calorimeter. The method involved combusting a known quantity of the sample in pure oxygen. The heat generated from combustion raised the temperature of the bomb wall and the measured mass of water in the surrounding jacket, and these temperature changes were measured. The GCV was then determined by equation 3.5.

$$\text{GCV} = (M_w \times C_w \times dT) + k \quad (\text{equation 3.5})$$

Where M_w is the mass of water, C_w is the specific heat of water, dT is the change in temperature and K is the bomb constant. Figure 3-15 shows a photograph of the Parr 6200 Isooperibol calorimeter.



Figure 3-15 Photograph of the Parr Isooperibol calorimeter

3.7 Catalyst analysis

3.7.1 Brunauer, Emmett and Teller (BET) surface area analysis

The (BET) surface area of the catalysts were measured by the Brunauer, Emmett and Teller (BET) method via nitrogen adsorption using a Quantachrome Corporation (FL, US) Autosorb 1-C instrument shown in figure 5-16. This was achieved by measuring the quantity of the adsorbate (nitrogen)

adsorbed onto or desorbed from the solid sample at different equilibrium vapour pressures by the static volumetric method. A known quantity of nitrogen was admitted or removed from the solid sample structure which was maintained at a constant temperature of $-196\text{ }^{\circ}\text{C}$ which was the critical temperature of nitrogen. During the adsorption or desorption pressure changes occur within the sample walls until equilibrium is achieved and these changes are measured. At the equilibrium pressure, the quantity of nitrogen which is adsorbed or desorbed is determined by the difference between the amount of nitrogen required to fill the space around the sample and the amount of nitrogen admitted or removed. The data from the adsorption and desorption of nitrogen onto and from the solid sample at constant temperature and at a range of pressures can be used to plot adsorption and desorption isotherms, from which the surface area of sample can be determined.



Figure 3-16 Photograph of the Quantachrome BET equipment

Known masses of the samples between 0.5 to 1 g were first degassed under vacuum at $120\text{ }^{\circ}\text{C}$ for 3 hrs to ensure gradual release of moisture and other adsorbed species from the solid sample, before nitrogen adsorption-desorption. The isotherms from adsorption-desorption were then analysed by the BET method in order to determine the surface area. Figure 3-17 below shows an example multi point BET plot for Ni Al_2O_3 catalyst sample.

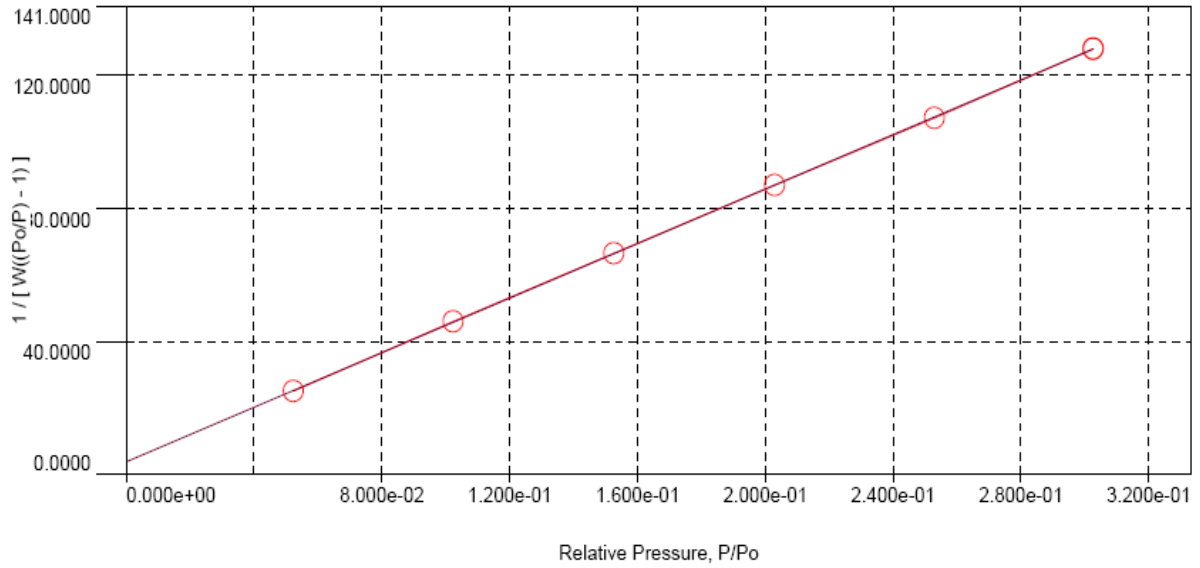


Figure 3-17 Example BET plot for the Ni Al₂O₃ catalyst

The BET equation proposed by Brunauer et al [7] is as shown in equation 3.6.

$$1 / v((P_0/P)-1) = (1/V_m \cdot C) + (C-1 / V_m \cdot C) \times (P/P_0) \quad (\text{equation 3.6})$$

Where v is the volume of adsorbed gas at relative pressure (P/P_0) (cm^3), P is pressure, P_0 is the saturated vapour pressure, V_m is the volume of adsorbate adsorbed when the entire adsorbent surface is covered with a complete unimolecular layer (cm^3), and C is the BET constant.

V_m can be obtained from a combination of the slope and the intercept with the Y axis of the BET plot as shown in equations 3.7, 3.8 and 3.9 below.

$$\text{Slope} = (C - 1) / (V_m \cdot C) \quad (\text{equation 3.7})$$

$$\text{Intercept} = 1 / (V_m \cdot C) \quad (\text{equation 3.8})$$

$$V_m = 1 / (\text{Slope} + \text{Intercept}) \quad (\text{equation 3.9})$$

The total surface area of the sample can be determined from equation 3.10 below.

$$S = (V_m \cdot N_a \cdot A) / V \quad (\text{equation 3.10})$$

Where A is the molecular cross sectional area of the adsorbate (m^2), N_a is Avogadro's number ($6.023 \times 10^{23} \text{ mole}^{-1}$) and V is the molar volume of the adsorbate ($\text{cm}^3 \text{ mole}^{-1}$).

The BET surface area of the sample can then be determined by equation 3.11.

$$S_{\text{BET}} = S / W \quad (\text{equation 3.11})$$

Where W is the weight of the sample (g).

3.7.2 Temperature programmed oxidation (TPO-FTIR)

Reacted catalysts were analysed by temperature programmed oxidation (TPO) using a Stanton-Redcroft Thermogravimetric analyser interfaced with a Thermoscientific, Nicolet iS10 spectrometer in order to investigate the properties of the carbon deposits on the reacted catalysts. A known quantity of the reacted catalyst was placed into the aluminium pan which was suspended in the micro balance within the furnace of the TGA. The TGA was then heated up in a flow of 50 ml^{-1} of air according to a set temperature programme while the catalyst weight change was recorded. The product gases were channelled to the FTIR for analysis in order to analyse the CO_2 from the combustion of carbon deposits on the catalyst. The temperature programme was set to heat the sample at $15 \text{ }^\circ\text{C min}^{-1}$ to a final temperature of $800 \text{ }^\circ\text{C}$ with the a dwell time of 10 min. Figure 3-18 shows an example TPO-FTIR for the reacted $\text{Ni Al}_2\text{O}_3$ catalyst.

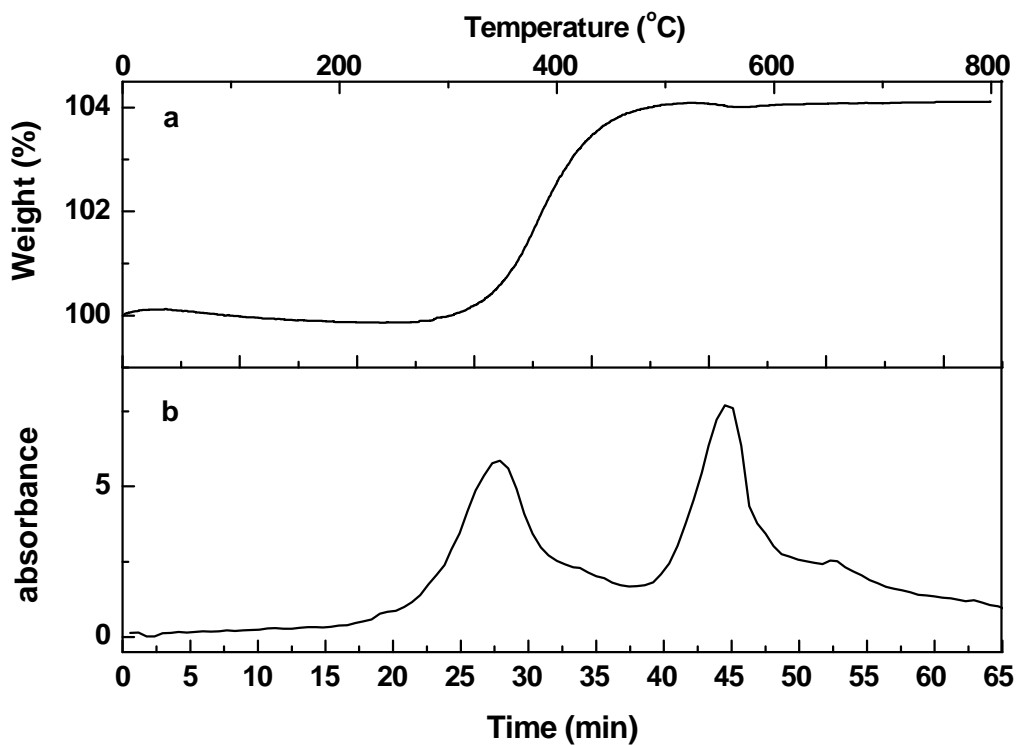


Figure 3-18 TPO-FTIR of spent Ni Al₂O₃ catalyst: (a) TPO (b) FTIR

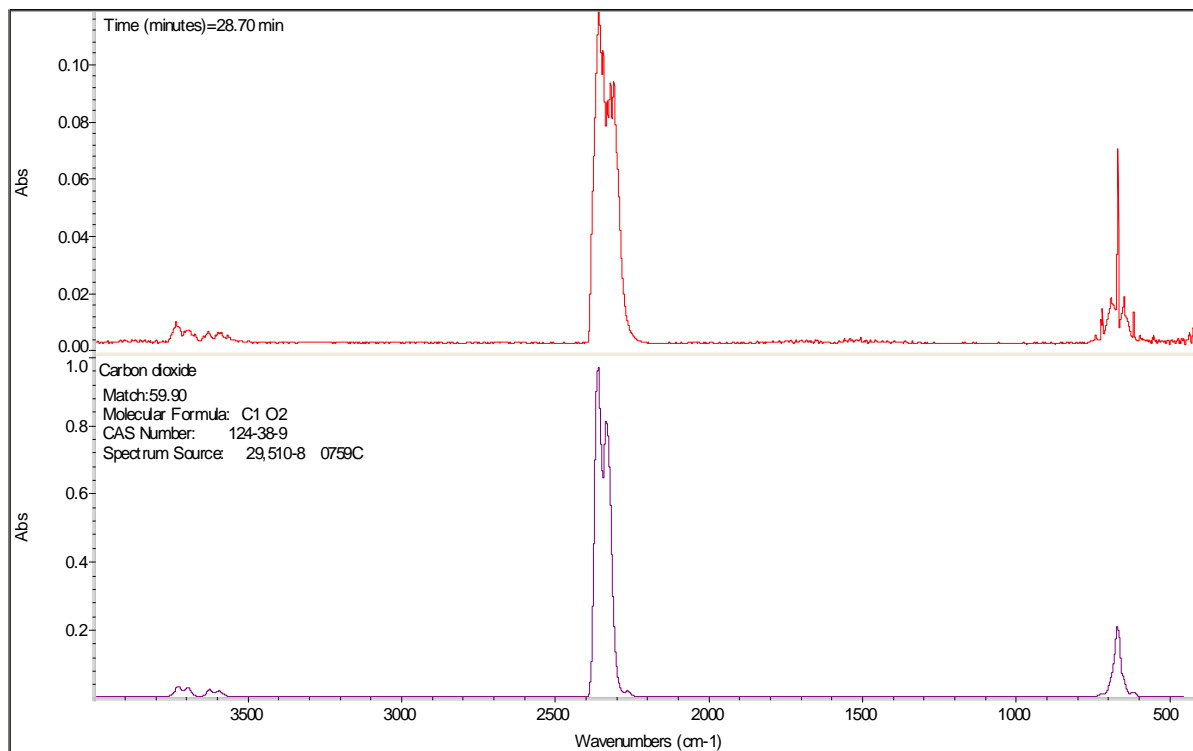


Figure 3-19 CO₂ spectra from the FTIR and library match.

Figure 3-19 shows an example spectra for CO₂ as measured by the FTIR analyser, compared against a library spectra for CO₂ gas, and the figure shows a match between both spectra. This provided a confirmation that the spectra from the FTIR was for CO₂ produced from the combustion of carbon deposits on the reacted catalysts.

3.7.3 X-ray diffraction (XRD)

X-ray diffraction (XRD) analysis was carried out on the fresh and reacted catalysts using a Bruker D8, using Cu α 1 radiation X-ray tube (shown in figure 3-20), scanning from 20° to 80° (2 θ). This was used to determine the crystallographic structure by determining the diffraction peak position of the compounds in the powders and comparing their diffraction pattern against a standard database. The catalyst samples were ground into powders, loaded on sample holders and loaded into the machine holder. The data from the analyser was collected by XRD wizard data acquisition software. Phase identification was carried out with Highscore software using the International centre for diffraction data powder diffraction files (ICDD PDF2) database. Figure 3-21 shows an example of the XRD spectra for the fresh and reacted Ni Al₂O₃ catalyst. Once the diffraction patterns had been determined, a Reitveld simulation analysis of the diffraction pattern was done using the Highscore software, in order to estimate the quantities of each compound in the powder. This method was used to evaluate the contents of the fresh catalysts in order to determine if they had been synthesized properly.

The diffraction peak position is a product of the atomic bond distance in the crystal which is determined by Bragg's law (equation 3.12) [8-9].

$$\text{Bragg's Law: } \lambda = 2 d_{hkl} \sin\theta \quad (\text{equation 3.12})$$

Where λ is the X-ray wavelength, d_{hkl} is calculated by the lattice parameters of the unit cell (its size and shape and can be gotten from publications) and 2θ is the specific diffraction peak angle.

The Reitveld method uses a combination of Bragg's law and an atomic scattering factor to simulate ideal diffraction patterns for the powder. The atomic scattering factor defines the efficiency of scattering from a group of electrons in an atom and can be determined from databases such as the inorganic crystal structure database (ICSD).

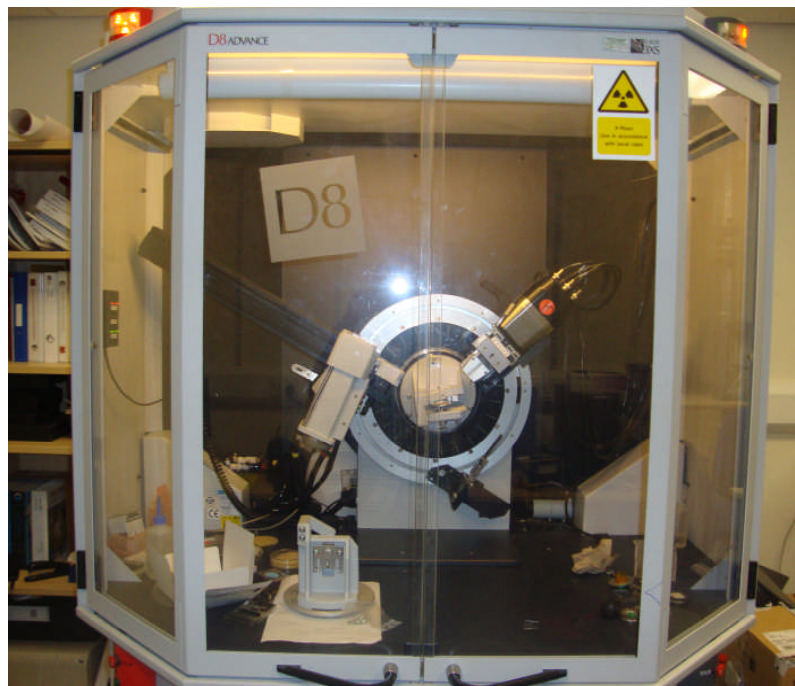


Figure 3-20 Photograph of the Bruker D8

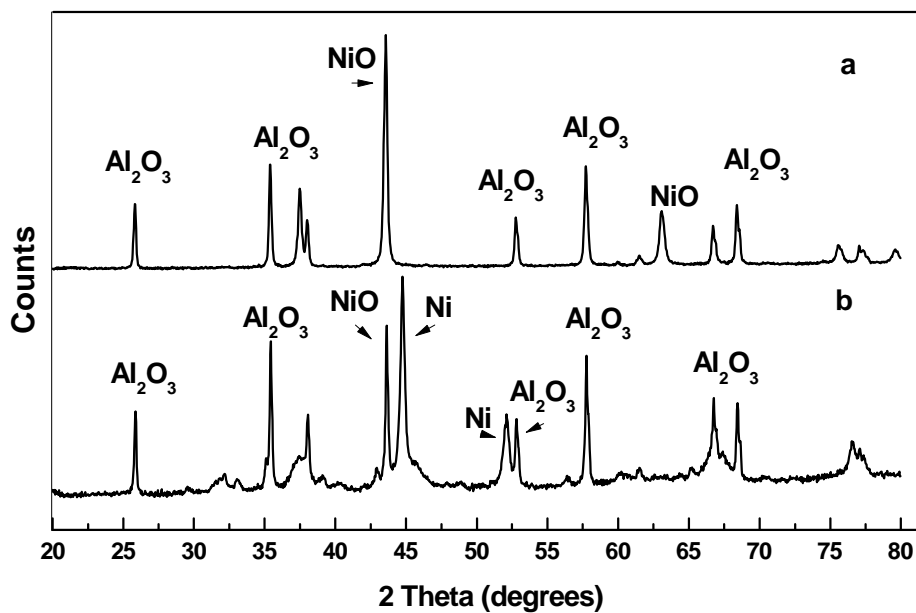


Figure 3-21 XRD spectra for Ni Al₂O₃: (a) Fresh (b) Reacted

3.7.4 Scanning electron microscopy (SEM)

High resolution (SEM) scanning electron microscopy was carried out on the fresh and spent catalysts using a LEO 1530 instrument shown in figure 3-22. An image of the catalysts surface was obtained by scanning their surface with a high-energy beam of electrons.

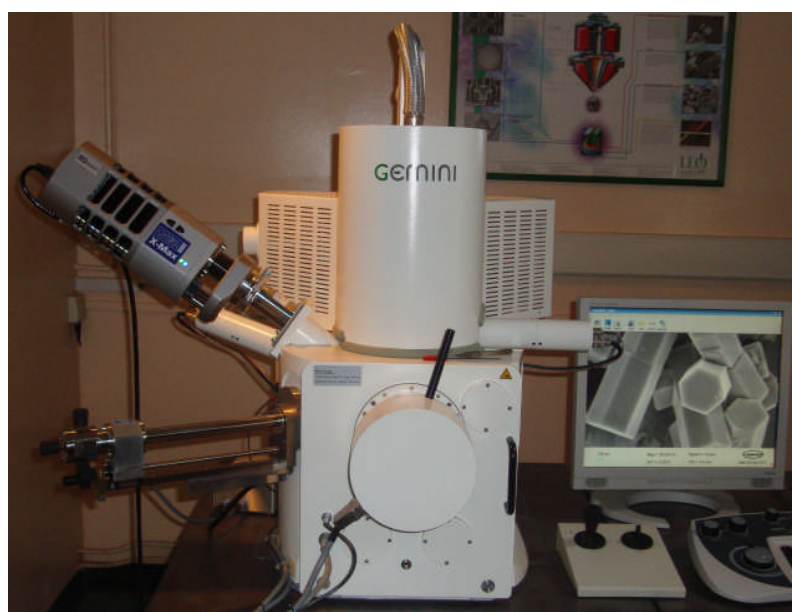


Figure 3-22 Photograph of the LEO 1530 SEM instrument

The catalysts were prepared by mounting them with adhesive on a flat stand and short bursts of pressurized air were used to clear loose particles from their surface. The sample was then coated with a 10 nm layer of platinum. The samples were mounted and fastened in the analyser sample holder for analysis under vacuum, at an accelerating voltage of 3 KV and at a distance of 3 – 8 mm from the electron gun.

3.7.5 Transmission electron microscopy (TEM) and energy dispersive X-ray spectroscopy (EDXS)

Transmission electron microscopy (TEM) was carried out on the fresh and reacted catalysts using a Philips CM200 shown in figure 3-23. A high

resolution image of the sample was obtained by transmitting a beam of electrons through an ultra thin specimen. The interaction of the electrons with the sample forms an image which was then magnified and focused onto an imaging device. Samples for the TEM analysis were scrapped off the surface of the sphere catalysts before being dispersed in methanol and then deposited on a copper grid which was covered with a perforated carbon membrane.



Figure 3-23 Photograph of the Philips CM200 TEM-EDXS equipment

The same equipment coupled to an (EDXS) energy dispersive X-ray spectroscope, was used to investigate the elemental distribution and surface morphology of the fresh and reacted catalyst. The EDXS equipment could detect X-rays according to their energy using a semi-conductor detector. The energy from the X-ray is converted into current pulses proportional to the photon energy by a lithium-drifted silicon crystal disc. The spectral data is collected by a computer and compared against a library of elements. The EDXS microscope was operated at an accelerating voltage of 20 KV and a working distance of 8 mm.

References

1. He, M., Xiao, B., Liu, S., Hu, Z., Guo, X., Luo, S. and Yang, F., *Syngas production from pyrolysis of municipal solid waste (MSW) with dolomite as downstream catalysts*. Journal of Analytical and Applied Pyrolysis, 2009. **87**(2): p. 181-187.
2. Wu, C. and Williams, P.T., *Hydrogen Production from the Pyrolysis Gasification of Polypropylene: Influence of Steam Flow Rate, Carrier Gas Flow Rate and Gasification Temperature*. Energy & Fuels, 2009. **23**(10): p. 5055-5061.
3. Luo, S., Xiao, B., Hu, Z. and Liu, S., *Effect of particle size on pyrolysis of single-component municipal solid waste in fixed bed reactor*. International Journal of Hydrogen Energy, 2010. **35**(1): p. 93-97.
4. Williams, E.A. and Williams, P.T., *Analysis of products derived from the fast pyrolysis of plastic waste*. Journal of Analytical and Applied Pyrolysis, 1997. **40-41**: p. 347-363.
5. Buah, W.K., Cunliffe, A.M. and Williams, P.T., *Characterization of Products from the Pyrolysis of Municipal Solid Waste*. Process Safety and Environmental Protection, 2007. **85**(5): p. 450-457.
6. Wei, L., Xu, S., Zhang, L., Zhang, H., Liu, C., Zhu, H. and Liu, S., *Characteristics of fast pyrolysis of biomass in a free fall reactor*. Fuel Processing Technology, 2006. **87**(10): p. 863-871.
7. Brunauer, S., Emmett, P.H. and Teller, E., *Adsorption of Gases in Multimolecular Layers*. Journal of the American Chemical Society, 1938. **60**(2): p. 309-319.
8. Young, R.A., ed. *The Rietveld method*. Monographs on crystallography, ed. Crystallography, I.U.o. 1995, Oxford university press: New York.
9. Will, G., *Powder diffraction: the Rietveld method and the two stage method to determine and refine crystal structures from powder diffraction data*. 2006, New York: Springer.

CHAPTER 4. Pyrolysis of Refuse Derived Fuel (RDF) and waste wood

4.1 RDF and waste wood characteristics

4.1.1 RDF characteristics

The elemental analysis of RDF presented in Table 3-1 indicated a high oxygen content (37 wt%), which is typical of RDF [1, 2], mostly as a result of the chemically bound oxygen in the lignocellulosic fractions such as the paper, cardboard etc that make up RDF.

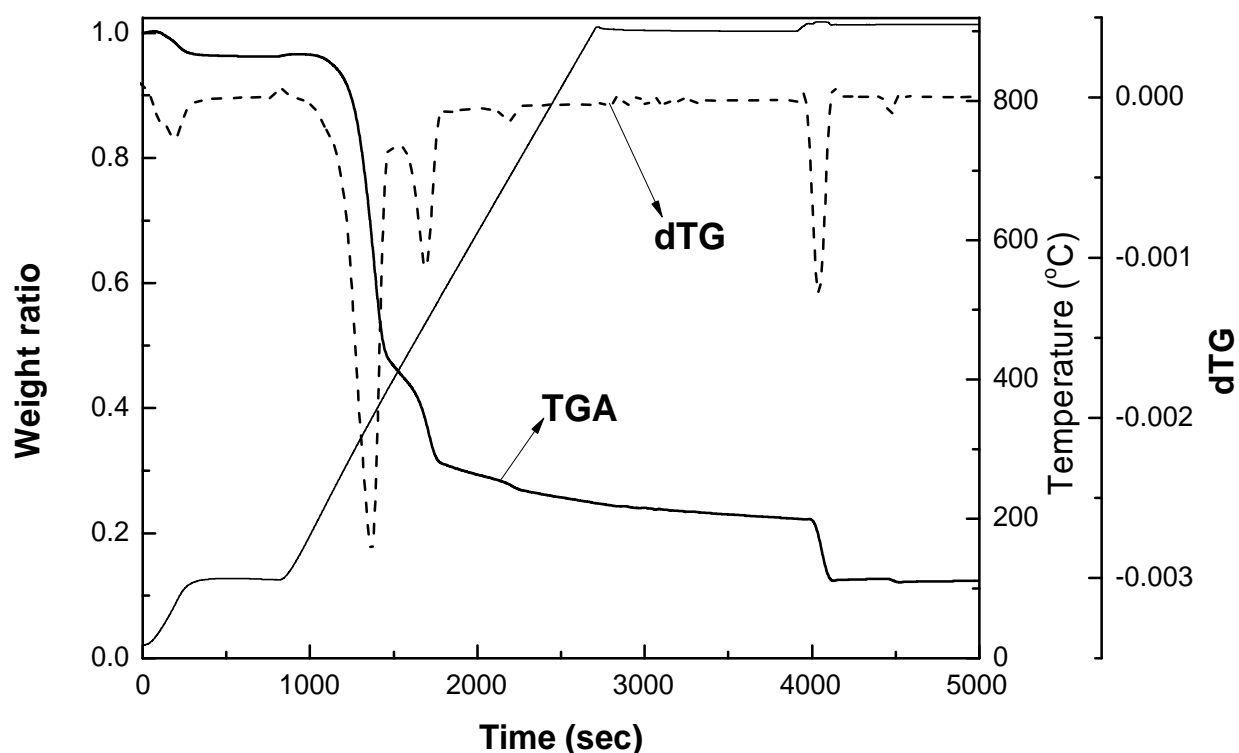


Figure 4-1 The thermal degradation of RDF in the TGA

The thermal degradation behaviour of the RDF sample is depicted in figure 4-1, which shows the rate of weight loss, the derivative weight loss curve (dTG) and temperature with reference to time. The dTG in figure 4-1 shows four major peaks. The peak at the 100 °C region represents weight loss due to moisture release while the peak at the 910 °C temperature region represents

weight loss due to the combustion of fixed carbon. The two peaks between 200 and 425 °C, and between 425 to 565 °C, represent the decomposition of the volatiles in RDF. The degradation of lignocellulosic matter has been reported to take place around the temperature ranges of 200 to 400 °C [2, 3] while plastic decomposition was reported to occur around the ranges 425 to 565 °C [1, 4]. The thermal degradation behaviour of the RDF at the TGA conditions appeared to be a combination of the individual degradation behaviours of its lignocellulosic and plastic components.

4.1.2 Waste wood characteristics

The proximate and elemental analysis for the waste wood is shown in Table 3-3. Figure 4-2 below shows the thermal degradation behaviour of the wood sample. The thermal degradation of biomass has been extensively researched [5-8] and biomass has been reported to mostly be made up of cellulose, hemi-cellulose and lignin. The degradation behaviour of biomass has also been reported to be as a result of the combined effects of the degradation of its cellulose, hemi-cellulose and lignin contents [3, 5, 8].

The plot in figure 4-2 shows the rate of weight loss, the derivative (dTG) curve and temperature with reference to time. Four major degradation peaks are depicted in the dTG curve as follows: the first peak at the temperature region of 100 °C is as a result of moisture loss from the wood. The second peak, between the temperature ranges of 200 and 450 °C, appears to represent the major volatile loss, and is actually mostly a combination of two degradation peaks; the smaller peak between 200 and 300 °C is assigned to the decomposition of hemicellulose while the peak between 300 and 450 °C is assigned to cellulose decomposition. The degradation of hemi-cellulose and cellulose from wood have been reported to occur between 200 to 350 °C and between 250 to 450 °C, respectively [3, 8]. The degradation of lignin occurs gradually throughout the degradation of the wood [3, 5, 8], because it is more thermally stable. Lignin degradation evolves less volatiles than cellulose and hemicellulose, and the associated degradation peak is overshadowed by the

degradation peak of cellulose in wood, resulting in a lack of an independent sharp degradation peak for lignin in the TGA shown in figure 4-2.

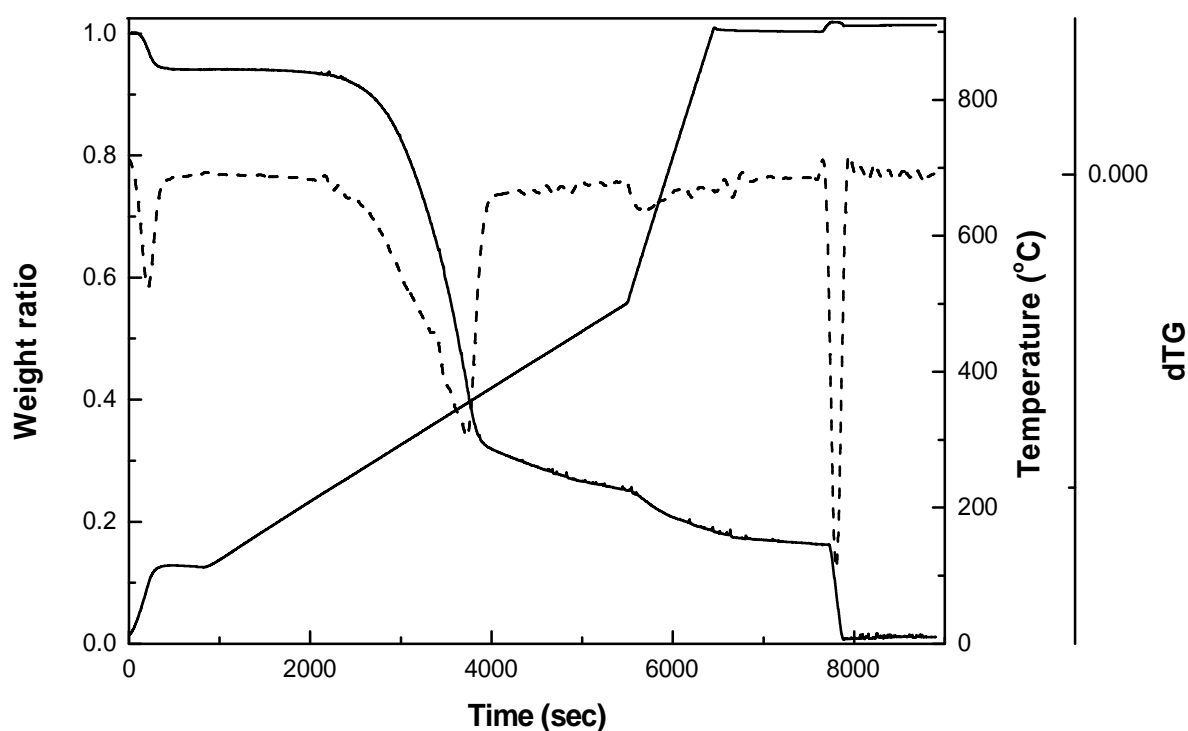


Figure 4-2 The thermal degradation of waste wood in the TGA

4.2 The influence of slow and fast heating on the pyrolysis of RDF and its single components

The pyrolysis of wastes at high temperature has been reported to enhance total conversion, gas yield and hydrogen production. This chapter further investigates the effects of process conditions such as the heating rate, the final pyrolysis temperature and the particle size, during the pyrolysis of wastes in the fixed bed reactor described in section 3.2.1. RDF as a model compound for municipal waste and some of its major single components such as paper, cardboard and waste plastics were investigated with the aim of identifying the effects of the process conditions on their gas and hydrogen yield as well as the contributions of the components to the product yields.

4.2.1 Product yields

The samples mentioned above were tested in the horizontal fixed bed reactor to investigate the effects of different heating rates (5, 20, 90, and ≈ 350 °C min^{-1}) on pyrolysis. About 1 g of sample was used for each experiment at a pyrolysis temperature of 800 °C. The carrier gas flow rate was 100 ml min^{-1} and the particle size of the samples was 1mm.

The result of the pyrolysis of RDF and its investigated single components (paper, cardboard and plastics) to a final temperature of 800 °C at different heating rates is summarized in table 4-1. As explained in Chapter 3, the experiments at the fast heating rate of ≈ 350 °C min^{-1} were conducted by heating the reactor up to the required process temperature and then inserting the sample via the sample boat into the heated reactor. While experiments at the lower heating rates of 5, 20 and 90 °C min^{-1} , were conducted by placing the sample in the reactor and then heating up to the desired temperature and at the desired heating rate controlled by the furnace.

The heating rates for the different samples during the fast heating experiments as determined by equation 3.1 were: RDF 350 °C min^{-1} , paper 330 °C min^{-1} , cardboard 325 °C min^{-1} and plastics 320 °C min^{-1} . It is important to note that these figures represent an estimated average heating for the sample and not the actual heating because the heating rate of individual particles would vary depending on factors such as; location in the sample holder/boat i.e. samples on the outer surface of the pile would experience higher heating rates compared to sample at the centre or at the bottom of the holder, the size of the individual particle i.e. smaller particles would experience higher heating rates compared to larger particles.

Table 4-1

Products from the slow and fast heating of RDF and its components at 800 °C

Yield	Heating rates °C min ⁻¹											
	5			20	90				≈ 350			
	RDF	paper	plastics	RDF	RDF	paper	cardboard	plastics	RDF	paper	cardboard	plastics
Gas	14.4	22.2	9.7	15.4	16.6	22.4	17.4	11.9	46.9	52.2	51.6	57.0
solid	25.0	23.6	6.0	24.1	23.0	18.9	24.5	5.5	22.8	18.0	22.6	4.0
Oil	55.0	50.9	84.0	53.0	51.1	49.1	49.1	81.8	23.0	22.0	18.9	30.0
Balance	94.4	96.7	99.7	92.5	90.7	90.4	91.0	99.2	92.7	92.2	93.1	91.0
Gas composition wt% sample												
H ₂	0.4	0.4	0.2	0.4	0.4	0.4	0.3	0.1	0.7	0.9	0.8	0.5
CO	4.4	7.1	nd	4.5	4.7	8.4	6.7	1.4	18.7	27.7	28.8	3.0
CO ₂	8.2	14.2	6.1	8.8	9.3	12.8	9.3	2.7	11.5	16.0	12.3	3.8
CH ₄	0.6	0.5	nd	0.7	0.8	0.5	0.6	0.6	4.9	3.4	4.4	7.0
C ₂ - C ₄	0.8	nd	3.4	0.9	1.4	0.4	0.4	7.1	11.0	4.2	5.4	42.8
Gas composition vol%												
H ₂	32.8	23.2	27.5	30.3	29.0	22.0	24.0	15.3	17.4	20.1	17.6	10.6
CO	26.3	31.9	nd	26.2	25.6	37.0	36.4	12.5	34.9	46.5	48.3	5.0
CO ₂	30.9	40.6	47.7	32.2	32.0	35.8	32.2	15.5	13.7	17.1	13.1	4.1
CH ₄	6.7	4.2	nd	7.5	7.9	3.8	5.6	9.3	16.1	10.0	12.9	20.4
C ₂ H ₄	0.5	nd	1.5	0.7	1.6	0.4	0.5	16.8	11.3	4.5	5.8	36.1
C ₂ H ₆	1.0	nd	2.5	1.1	1.3	0.5	0.6	7.0	1.0	0.6	0.8	4.8
C ₃ H ₆	0.5	nd	6.5	0.6	1.0	0.2	0.3	11.9	1.8	0.6	0.8	13.4
C ₃ H ₈	0.9	nd	3.9	0.8	0.8	0.2	0.2	3.8	0.4	0.1	0.2	0.7
C ₄ H ₈ & C ₄ H ₆	0.3	nd	6.9	0.3	0.6	0.1	0.2	6.2	1.0	0.3	0.4	4.6
C ₄ H ₁₀	0.2	nd	3.7	0.3	0.2	nd	0.1	1.7	*	nd	nd	0.1

nd: not detected, *: less than 0.1

The pyrolysis of RDF just like biomass always yields three major product fractions: gases, liquids and solids [9]. However, the pyrolysis process can be designed in order to optimize the production of the product fraction of choice. Controlling the heating rate is one of such methods and its effect is shown in Table 4-1 which shows the variations in the product yields when the RDF samples were pyrolyzed at heating rates of 5, 20, 90 and 350 °C min⁻¹ to a final temperature of 800 °C and held at this temperature for 20 min. Table 4-1 suggests a definite trend of the gas, oil and solid yields, with increasing heating rate at the process conditions defined by the reactor design. This was due to the increased intensification of the temperature effects as the heating rate increased. Gas yield increased from 14.4 to 46.9 wt % while oil yield decreased from 55 to 23 wt% with increasing heating rate. The solids residue showed a continuous decreasing trend in yield with increasing heating rate from 5 to 350 °C min⁻¹, probably as result of the thermal degradation of higher molecular weight hydrocarbons within the residue [10].

The higher gas yields and lower oil yields noted for RDF at the heating rate of ≈ 350 °C min⁻¹ compared to the yields at the lower heating rates, was as a result of the secondary thermal cracking of the primary pyrolysis vapour. High heating rates and longer residence times combined with high temperatures have been reported to increase gas production from pyrolysis of waste [11, 12]. During pyrolysis at the fast heating rate of ≈ 350 °C min⁻¹, the pyrolysis vapours from the primary thermal decomposition of the RDF were released into the high temperature atmosphere within the reactor, which when combined with the long residence time of about 9 sec, initiated the secondary cracking of the vapours to yield lighter molecular weight hydrocarbons and more gases. Garcia et al [12, 13] have investigated the effects of residence time on the pyrolysis of MSW and their works indicated that volatile residence times (above 1 seconds) favours secondary pyrolytic cracking reactions which results in higher gas yields.

Table 4-1 also shows that the same trend for RDF was observed for its single components investigated, with the change in heating rate. More liquid

products were yielded during pyrolysis at the lower heating rates (5 and 90 °C min⁻¹) at 800 °C for the paper, cardboard and waste plastic samples while at the heating rate of ≈ 350 °C min⁻¹, the highest yielded products are gaseous products due enhanced thermal degradation reactions. At the lower heating rates of 5 and 90 °C min⁻¹, the oil product collected from the waste plastic pyrolysis was made up of mostly semi-solid waxes and some fluid oil as expected [14, 15]. The cellulosic wastes; paper and cardboard, yielded more gaseous products compared to the plastic wastes at the heating rates of 5 and 90 °C min⁻¹, however at the heating rate of ≈ 350 °C min⁻¹, the plastic waste produced the most gaseous yield. Marcilla et al [16] reported similar product yields for the slow and fast pyrolysis of HDPE in a fluidized bed. This is the case because of the nature of plastics which have almost no ash and fixed carbon compared to paper and cardboard. During pyrolysis of the plastic wastes at the heating rates of 5 and 90 °C min⁻¹, the released volatiles were easily swept out of the reactor hot zone by the carrier gas and resulted in the formation of mostly oils. This was not the case for the RDF, paper and cardboard which have a fixed carbon and ash structure that can hinder vapour release therefore allowing for some degree of vapour cracking to yield gases [17]. However during pyrolysis at the heating rate of ≈ 350 °C min⁻¹ the easily released vapours from plastic decomposition are released into the high temperature reactor therefore promoting the thermal cracking of its long chain polymers to yield more gases. The RDF, paper and cardboard volatiles were also released into an atmosphere which promotes secondary cracking, during their pyrolysis at ≈ 350 °C min⁻¹, but the higher volatile content of the plastic wastes results in higher gas yield [17].

During the experiment at the heating rate of ≈ 350 °C min⁻¹, the RDF yielded the highest quantity of solids, probably due to presence of dirt and in-organics as well as the formation of fixed carbon. The cardboard yielded the second highest solid yield, due to its higher fixed carbon content, followed by paper and then plastics. The higher quantity of solids yields from the other samples compared to the plastic wastes is due to the formation of char. The higher tendency of RDF, paper and cardboard samples to form char has been

reported to be as a result of their content of cyclic groups which can react with hydrogen atoms within their structure to yield char [18].

4.2.2 Gas composition and hydrogen yield

The effect of heating rate on the composition of the pyrolysis gas, in this study, is also shown in Table 4-1. This shows an increase (on a mass basis) across the detected compositional fractions that make up the gas products, with increasing heating rate. The volumetric composition (vol%) in table 4-1 shows a reduction in the hydrogen yield with increasing heating rate however this does not mean that the quantity of hydrogen produced reduced but this is as a result of the increased production of other gases, mostly CO.

The highest mass yields of the different gases were produced at the highest heating rate due to the promotion of secondary thermal cracking. The degradation of polymers which occurs during pyrolysis has been explained to be as a result of free radical degradation via different mechanisms: random scission, side group scission, monomer reversion and a combination of any of the former [19]. For example during the pyrolysis of higher alkanes, the carbon-carbon bonds randomly cleave along the chain to produce smaller alkyl radicals [20]. The degradation mechanism or mechanisms which will be applicable during the pyrolysis of polymers are dictated by factors such as, the weakest chemical bond within the polymer and the stability of the resultant product molecule.

During the experiment at the heating rate of $\approx 350 \text{ }^\circ\text{C min}^{-1}$, the initial products of the different degradation reactions during RDF pyrolysis were concurrently released into the hot reactor atmosphere where further thermal degradation and other reactions took place. Reactions such as auto-thermal gasification [21], the Boudouard reaction, methane dry reforming reactions [22], recombination and dis-proportionation reactions [20] have been proposed for pyrolysis products. The complex combination of reactions and interactions during the pyrolysis of RDF at the heating rate of $\approx 350 \text{ }^\circ\text{C min}^{-1}$ and at high temperature, coupled with the secondary thermal cracking of the primary

pyrolysis vapours due to the long vapour residence time in the fixed bed reactor, could result in a different gas composition compared to that attained for pyrolysis at 5, 20 and 90 °C min⁻¹ as suggested by table 4-1. The CO₂ content in the gas increased with the heating rate, and this has been explained to be as a result of the promoted decomposition of carboxylic groups [23]. In addition the yield of CO increased with increasing heating rate, and can be attributed mainly to the promoted secondary decomposition of oxygenated functional groups [24-26] such as carbonyl, hydroxyl and ether.

The paper, cardboard and plastic samples also showed an increased trend in gas and hydrogen mass yield with increased heating rate. The increase in gas and hydrogen yield for these samples is mainly also as a result of the cracking of the heavier liquid hydrocarbons. This is obvious from the highly reduced quantities of the liquid pyrolysis fraction produced at the heating rate of ≈ 350 °C min⁻¹, while the yield of the solid fractions only reduced slightly. Table 4-2 shows details of the hydrogen production (mol g⁻¹) and the gas production (m³ g⁻¹) for the investigated samples. Table 4-2 shows that during the experiment at the heating rate of ≈ 350 °C min⁻¹, the paper sample produced the highest hydrogen yield, followed by the cardboard, followed by the RDF and finally the plastic sample. This also agrees with the mass yields shown in Table 4-1. The volumetric gas production (m³ g⁻¹) appears to be fairly similar across the different samples at the heating rate of ≈ 350 °C min⁻¹.

At the lower heating rates (5, 20, 90 °C min⁻¹), the product gases from the RDF, paper and cardboard samples was composed mainly of CO₂, followed by CO. Similar results were obtained by other researchers [27, 28] for the pyrolysis of different segregated wastes at low heating rates. However at the heating rate of ≈ 350 °C min⁻¹, the most abundant gaseous product was CO for the earlier stated samples. This gives an indication that for these samples which have a lignocellulosic content CO₂ is a major product of their oxygenated contents primary decomposition while most of the CO yield is as a result of secondary degradation reactions [23, 25, 26].

Table 4-2

Hydrogen and total gas production per gram of the samples

Heating rates (°C min ⁻¹)	H ₂ mol g ⁻¹ x 1000			
	RDF	paper	cardboard	plastic
≈ 350	3.43	4.26	3.75	2.26
90	1.91	1.78	1.58	0.61
20	1.88	nd	nd	nd
5	1.97	1.84	nd	0.80
	gas production m ³ g ⁻¹ x 1000			
	RDF	paper	cardboard	plastic
≈ 350	0.47	0.48	0.48	0.48
90	0.15	0.18	0.15	0.09
20	0.14	nd	nd	nd
5	0.13	0.18	nd	0.07

nd: not determined

The gaseous products from the plastics did not show the same compositional characteristics as the other samples. At the heating rate of 5 °C min⁻¹ the most abundant gaseous compound was CO₂, followed by hydrogen. No CO and CH₄ were detected for the plastic sample at this heating rate. The gas products at the other heating rates for plastics are different in their components. The most abundant gases detected were CH₄ and the C₂ – C₄ gases, especially ethane and propene. There is also the noted presence of CO and CH₄ in the product gases at these heating rates.

Hall et al [29] examined the individual gas release with time and temperature from the pyrolysis of mixed plastics from waste electrical and electronic equipment (WEEE). Their results showed that the initial gas released during degradation was CO₂, the other gases especially CO and the hydrocarbons were released at a later degradation peak. The analysis of the gas compositions at the different heating rates for the plastic sample can give an idea of the release of species during its degradation. The degradation of the plastics would have initiated by its melting and bond cleavage to yield long chain polymers (mostly liquids and some gases) and CO₂ (from oxygenates) and solids. Further degradation of these materials impacted by the more severe temperature conditions during pyrolysis at ≈ 350 °C min⁻¹, resulted in a

further degradation of the long chain polymers into more stable shorter chain hydrocarbons (liquids and gases) and other gases (CO, CO₂ and H₂).

The product gas from RDF shown in table 4-1 indicated that its composition was as a result of the combination of the decomposition products of its lignocellulosic and plastic fractions. For example a larger proportion of its contents of mostly CO, H₂ and CO₂ are likely as a result of contributions from the pyrolytic degradation of lignocellulosic materials, while a large proportion of its hydrocarbon gases are likely as a result of the contribution of plastic pyrolysis. Greico et al [30] pyrolyzed different mixtures of polyethylene with paper and wood. They concluded that the presence of the lignocellulosic materials gave rise to an increase of CO and CO₂, while the presence of polyethylene gave rise to an increase of the hydrocarbons.

The CO and hydrocarbon contents of RDF make it a likely feedstock for the water gas shift and the hydrocarbon reforming reactions during steam gasification for hydrogen production.

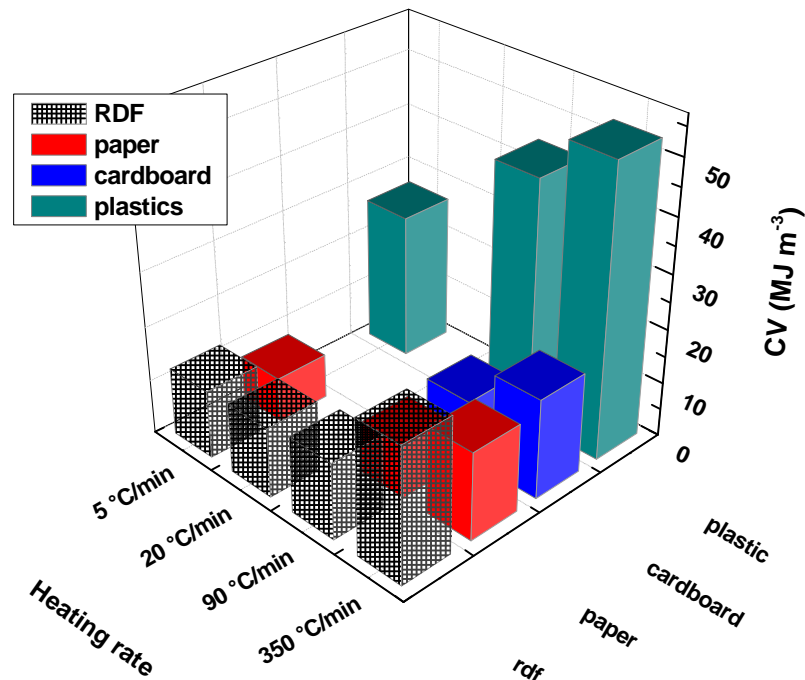


Figure 4-3 Effect of heating rate on product gas CV

The CV of the product gases from the different samples pyrolysis with respect to heating rate is shown in figure 4-3 above. The CV of the product gases

from the pyrolysis of all samples increased with increasing heating rate. This was mostly due to more gases, especially methane and C₂-C₄ hydrocarbon gases, being produced as a result of higher conversion of the volatiles at the elevated heating rates. The CV of the gas from RDF ranges between 12.5 and 24.8 MJ m⁻³, for paper it ranges between 8.2 and 16.1 MJ m⁻³, for cardboard it ranges between 10.8 and 18.3 MJ m⁻³, and for the plastics it ranges between 26.8 and 52.9 MJ m⁻³.

4.2.3 Composition of oil products

The liquid products from the pyrolysis of MSW have been reported to be very complex in nature [1, 27, 31, 32] and contain a mixture of oxygenated and non-oxygenated hydrocarbons. In order to investigate the effects of the heating rate on the pyrolysis oil, the oils from the pyrolysis of RDF paper and plastics, at the different heating rates were analysed by FTIR (RDF only) and GC/MS/MS. Figure 4-4 shows the spectra from the FTIR analysis of RDF pyrolysis oil.

Figure 4-4 shows a comparison between the FTIR spectra for the liquids from pyrolysis at heating rates of 5 and 350 °C min⁻¹ to a final temperature of 800 °C, and provides information on the functional group composition of the pyrolysis liquids. The spectra shows the presence of polycyclic, monocyclic and substituted aromatic groups in the absorption peaks between 675 to 900 cm⁻¹ and 1572 to 1625 cm⁻¹. The peaks from 950 to 1325 cm⁻¹ represent C-O stretching and O-H deformation, indicating the presence of primary, secondary, tertiary alcohols and phenols. Peaks between 1350 to 1475 cm⁻¹ and 2800 to 3000 cm⁻¹ represent C-H deformation and indicates the presence of alkanes. The presence of alkenes is indicated by the C=C stretching vibrations between peaks 1625 and 1675 cm⁻¹. C=O stretching vibrations are indicated by the peaks between 1650 and 1850 cm⁻¹, while O-H vibrations are indicated by the broad peaks between 3050 and 3600 cm⁻¹, and a combination of these peaks suggests the presence of carboxylic acids and their derivatives. A comparison of both spectra clearly shows differences in the intensities of the different functional group peaks, indicating as expected a

difference in the composition of the liquids as a result of the different heating rates.

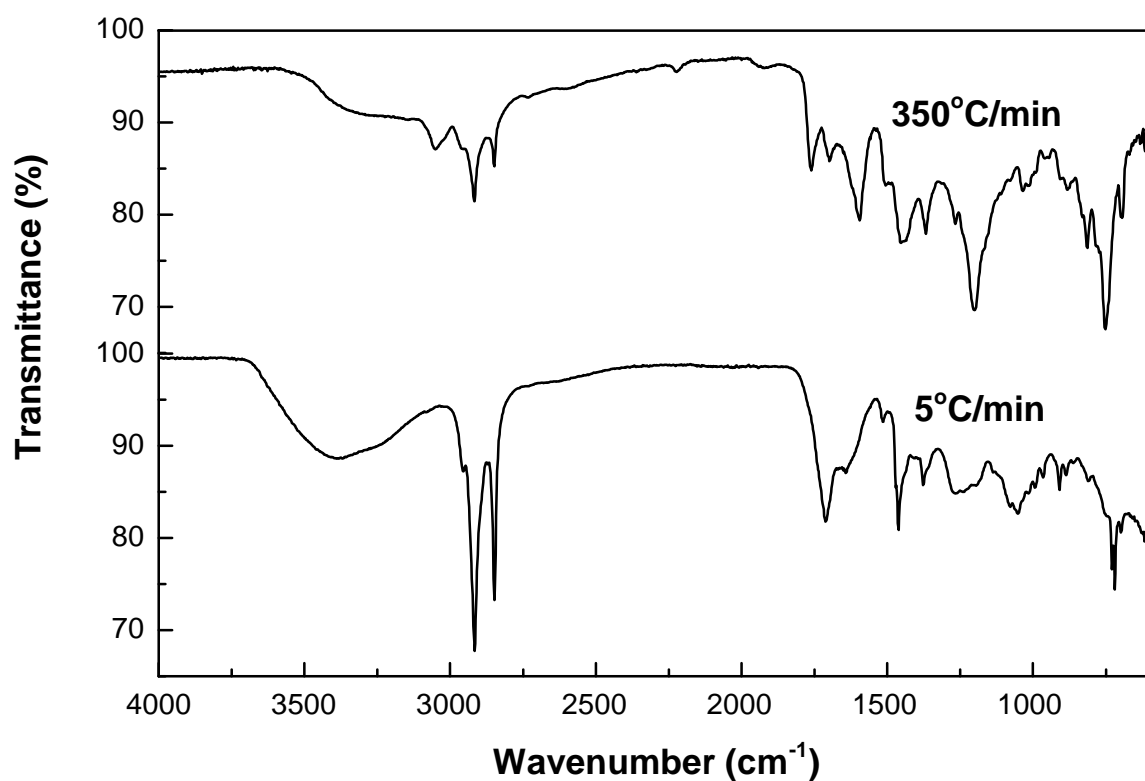


Figure 4-4 FTIR spectrogram of oil from the pyrolysis of RDF at 5 and 350 °C min⁻¹

Table 4-3

Detected oil compounds from RDF, paper and plastics pyrolysis at different heating rates

Heating rate °C min ⁻¹	5			20	90	≈ 350		
	RDF	paper	plastics	RDF	RDF	RDF	paper	plastic
Oil compounds	Oxygenates							
Cyclopentanone	***	*	*	*	*	*		***
Furfural	**	**						
pyran						***		
Phenol	***							
o-Cresol	*					***		
Acetophenone	***	*	*		**	*	*	**
p-cresol	**	*			*			
m-cresol	**	*			*			
2-Methoxyphenol	*	*						
2-Ethylphenol	*					*		
2,4-Dimethylphenol	*					*		
3/4-Ethylphenol	*	***						
2,3,5-Trimethylphenol	*	*						
Dibenzofuran			***		***	*		*
2-Phenylphenol			*	**	***			

Table 4-3 continues

Aromatics								
Alphamethylstyrene	*	*	*	***	*	*		
Betamethylstyrene		*	*		*			
Indene	*	*	*	*	***	*	***	
Naphthalene	*	*	**	*	****	*	***	
2-Methylnaphthalene					****	***	****	
1-Methylnaphthalene					****	***		
Biphenyl	*	*	*	**	*	***	***	****
2-Ethyl-naphthalene			**		**			
1-Ethyl-naphthalene			***		***		***	
2,6-Dimethylnaphthalene					*	*	**	
1,4-Dimethylnaphthalene			***	*	**	****	*	
2,2-Diphenylpropane			*	*		**		
Fluorene	*	*	*	*	*	***	**	****
1,3-Diphenylpropane	*	***	*	***	***			*
Phenanthrene	*		*	*	**	***	***	****
1-Phenylnaphthalene	*		*	*				**
o-Terphenyl			*	**				
Fluoranthene	*		*	**		***	*	***
Pyrene	*		*	*	*	***	*	***
m-Terphenyl								****
1,3,5-Triphenylbenzene	*			***	****		**	
Alkanes								
Octane, C8	*	***	**	***	*	*	*	*
Nonane, C9	*		**	***	*			*
Decane, C10	*	***	***	***	*	*		*
Undecane, C11	*	***	***	***	*	*	*	*
Dodecane, C12	*	***	***	****	**	*		*
Tridecane, C13	***	***	**	***	*	*		*
Tetradecane, C14	*		*	***	*	*	*	*
Pentadecane, C15	*		**	***				*
Hexadecane, C16	*	*	*	***	*	*		*
Phytane	*	*	*	**	*			*
Hepadecane, C17	*	*	*	**	*			*
Pristane	*	***	**		*		*	*
Octadecane, C18	*	***	**	***	*			*
Nonadecane, C19	*		**	***	*			*
Eicosane, C20	*		**	***	*			*
Heneicosane, C21	*			***	*			*
Docosane, C22	*		*	***	*			*
Tricosane, C23	*		*		*			*
Tetracosane, C24	*				*			*
Pentacosane, C25	*			***	*			*
Hexacosane, C26	*		*		*			*
Octacosane, C28	*		*	***				*
Nonacosane, C29	*			***				*
Triacontane	*		*	***	*			*
Hentriacontane, C31	*		*	***	*			*
Dotriacontane, C32	*	***	**	***	*			*
Trtriacontane, C33	*	***	**		*			*
Tetratriacontane, C34	*		**	***	*			*
Pentatriacontane, C35	*		**		*			*
Hexatriacontane, C36	*		**	***	*			*
Heptatriacontane, C37	*				*			*

Table 4-3 continues	Alkenes						
Octene, C8	****	**	**	***	**	****	**
Nonene, C9	****	*	***	***	**		**
Decene, C10	****	*	**	**	**		**
Undecene, C11		**	*	*			**
Dodecene, C12		**	*	*	***		**
Tridecene, C13	**	****	**	**	*		**
Tetradecene, C14		****	**	**	*	*	***
Pentadecene, C15		***	*	**			***
Hexadecene, C16		***	*	**		***	***
Phytene	***	***	*	*			*
Hepadecene, C17		***	*	*			*
Pristene	***	***	**	**			***
Octadecene, C18		*	*	*			**
Nonadecene, C19		***	**	**			**
Eicosene, C20	*	***	***	**			**
Heneicosene, C21	***	****	**	*			***
Docosene, C22		***	***	***			***
Tricosene, C23		***	**	**			***
Tetracosene, C24		****	**	**			***
Pentacosene, C25		***	**	**			**
Hexacosene, C26		****	**	**			***
Octacosene, C28		**	*	***			
Nonacosene, C29		***	**	***			
Triacontene		***	*				
Dotriacontene, C32		****	*	**			
Tritriacontene, C33		**		*			
Tetratriacontene, C34		**		**			
Pentatriacontene, C35		**		***			

more * indicates higher concentration

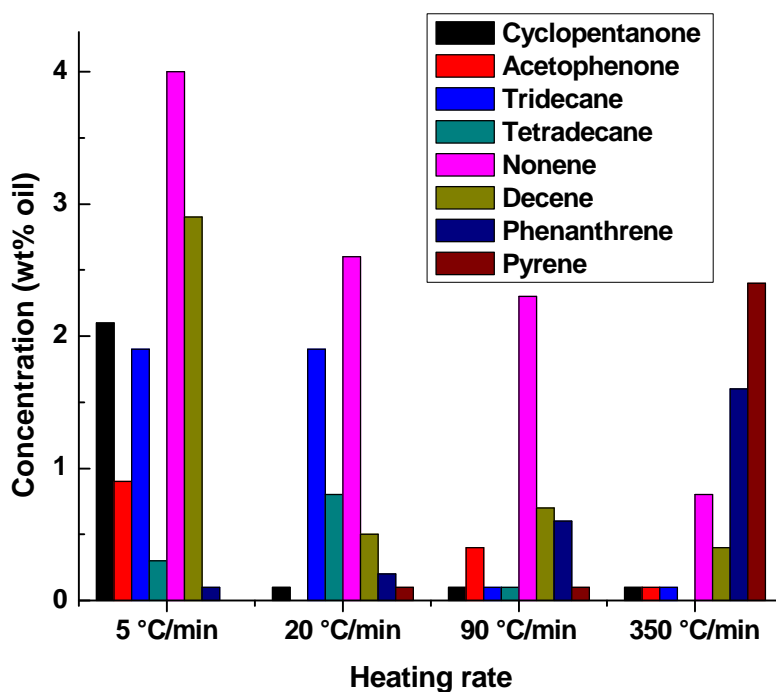


Figure 4-5 Effects of heating rate on oil compounds from RDF pyrolysis

The results of the GC/MS/MS analysis are presented in Table 4-3, which shows the compounds detected from the liquids obtained from the pyrolysis of the RDF, paper and plastics at different heating rates. The relative abundances of these compounds in the pyrolysis liquid are also shown and represented by asterisk (*). Increasing number of asterisks signifies increasing concentration of a particular compound. Table 4-3 shows that with increasing heating rate, the quantity of the detected oxygenates, alkanes and alkenes decreases while the quantity of aromatics increase for the pyrolysis of RDF. This trend is also supported by figure 4-5 which shows the effect of heating rate on selected oil compounds representative of oxygenate, aliphatic and aromatic oil compounds from RDF pyrolysis. Figure 4-5 shows a decrease in the detected concentrations of acetophenone, tridecane and decene, and an increase in the concentration of phenanthrene, with increasing heating rate from 5 to ≈ 350 °C min⁻¹.

Table 4-3 also shows that in the oil from RDF pyrolysis at 5 °C min⁻¹, more alkanes, alkenes and oxygenates were detected compared to the oil from pyrolysis at ≈ 350 °C min⁻¹. This is in agreement with the FTIR spectra in Figure 4-4 which shows higher peak intensities for peaks between 1350 to 1475 cm⁻¹, 1625 to 1675 cm⁻¹ and between peaks 950 to 1325 cm⁻¹, for the pyrolysis at 5 °C min⁻¹ compared to the pyrolysis at 350 °C min⁻¹, corresponding to the presence of more aliphatic hydrocarbons and oxygenates in the liquid from pyrolysis of RDF at 5 °C min⁻¹ compared to that at ≈ 350 °C min⁻¹. Miskolczi et al [33] also detected the presence of alkanes and alkenes from RDF pyrolysis at 550 °C. Figure 4-4 also shows an increase in the intensity of the indicative peaks for the monocyclic, polycyclic and substituted aromatic groups, in the spectra for the liquid from pyrolysis at 350 °C min⁻¹ compared to that at 5 °C min⁻¹. Phan et al [27] detected increases in the presence of aromatics in the oil from waste pyrolysis at 700 °C. While Ates et al [34] also reported an increase in the yield of single and multi-ringed aromatic groups with increasing temperature up to 800 °C from the pyrolysis of corncob. Figures 4-6 and 4-7 show the chromatograms for the GC/MS

analysis of the oil samples produced from RDF at slow ($5\text{ }^{\circ}\text{C min}^{-1}$) and fast heating rates ($\approx 350\text{ }^{\circ}\text{C min}^{-1}$).

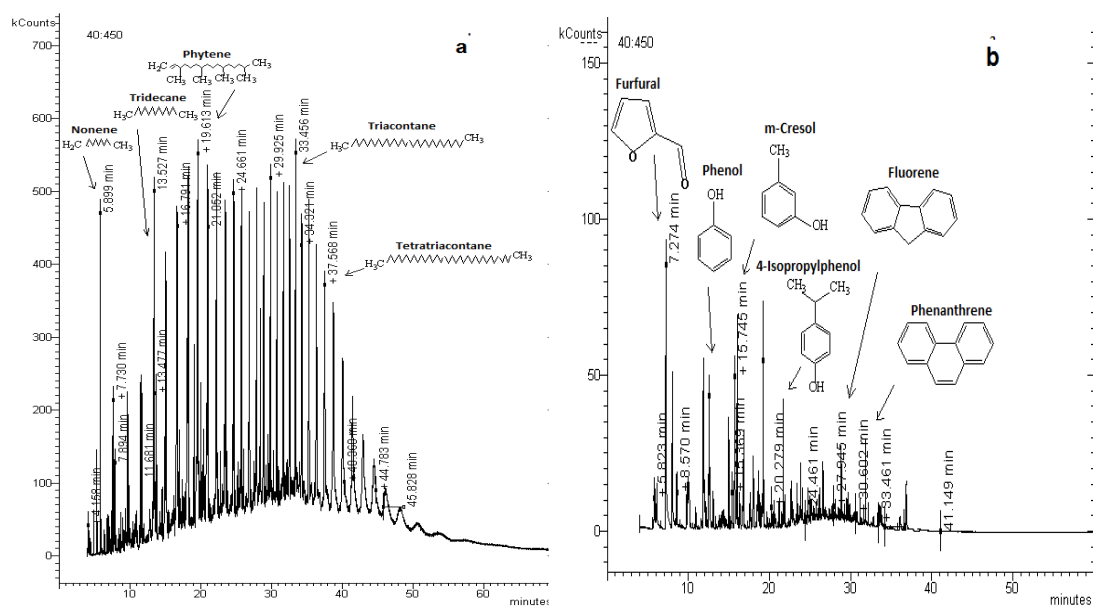


Figure 4-6. GC/MS chromatography of liquid from pyrolysis of RDF at $5\text{ }^{\circ}\text{C/min}^{-1}$; (a) GC/MS Chromatography of aliphatics (b) GC/MS Chromatography of oxygenates and aromatics.

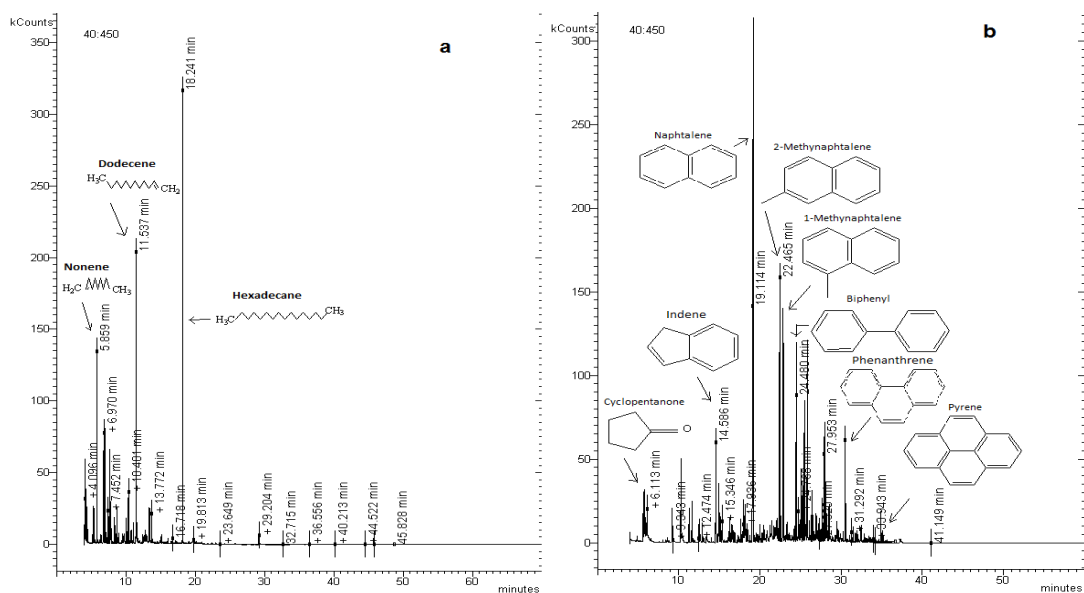


Figure 4-7. GC/MS chromatography of liquid from pyrolysis of RDF at $\approx 350\text{ }^{\circ}\text{C/min}^{-1}$; (a) GC/MS Chromatography of aliphatics (b) GC/MS Chromatography of oxygenates and aromatics.

Table 4-3 shows an increase in the number of aromatics detected in the oil from pyrolysis at $\approx 350\text{ }^{\circ}\text{C min}^{-1}$, compared to the oil from RDF pyrolysis at $5\text{ }^{\circ}\text{C min}^{-1}$. This suggests that fast heating rate pyrolysis caused an intensification of the high temperature effects, resulting in the formation of more aromatic compounds. The aromatic compounds were produced from reactions which involved initially the conversion of alkanes to alkenes, then the conversion of alkenes to monocyclic aromatic compounds via Diels-Alder cyclization reactions [35, 36], and then finally the conversion of monocyclic compounds to polycyclic compounds, as explained later in section 4-4-1. These reactions have been reported to be favoured by high temperature, long residence times and high heating rates. This could explain the predominance of aromatic compounds in the oil from RDF pyrolysis at $350\text{ }^{\circ}\text{C min}^{-1}$ compared to the predominance of mostly alkanes and alkenes in the oil from RDF pyrolysis at $5\text{ }^{\circ}\text{C min}^{-1}$.

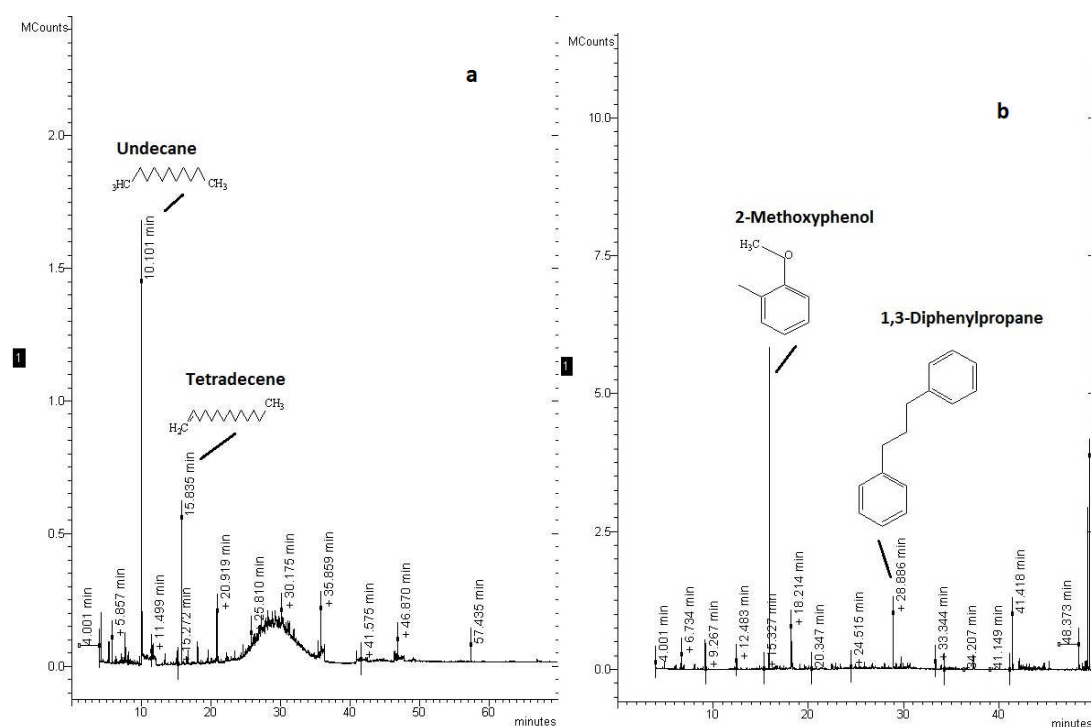


Figure 4-8. GC/MS chromatography of liquid from pyrolysis of paper at $5\text{ }^{\circ}\text{C/min}^{-1}$; (a) GC/MS Chromatography of aliphatics (b) GC/MS Chromatography of oxygenates and aromatics.

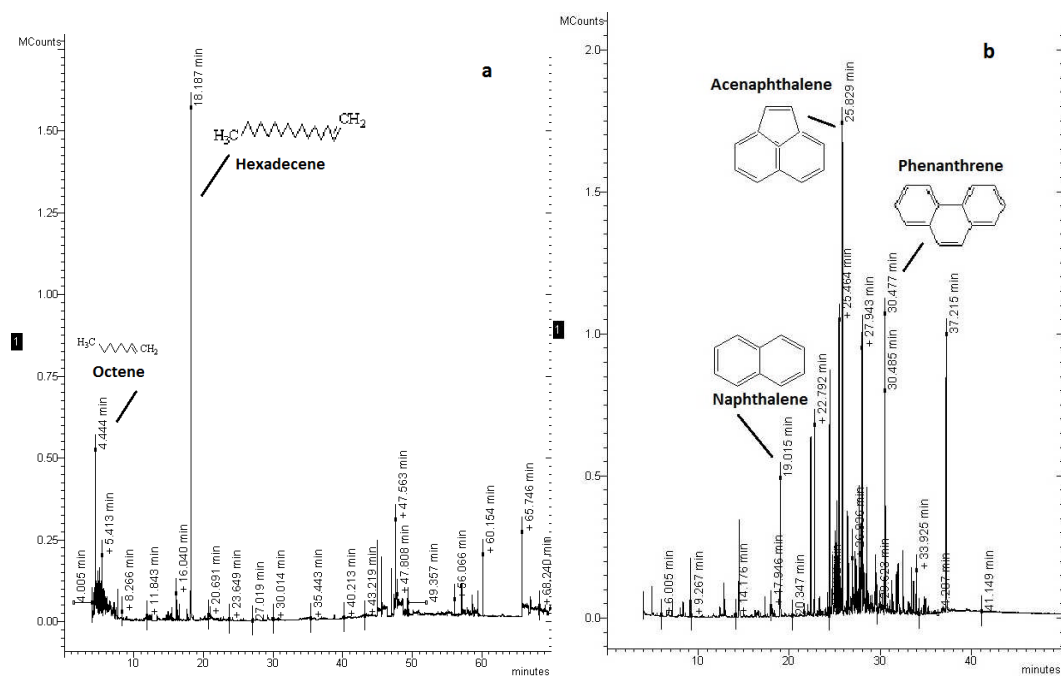
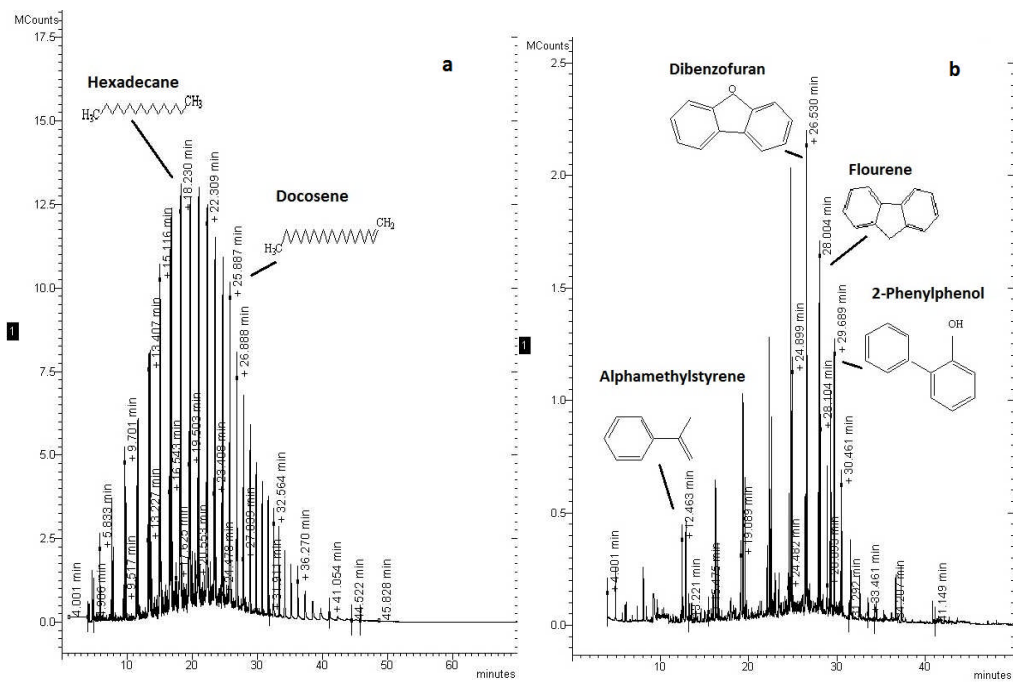


Figure 4-9. GC/MS chromatography of liquid from pyrolysis of paper at ≈ 350 $^{\circ}\text{C}/\text{min}^{-1}$; (a) GC/MS Chromatography of aliphatics (b) GC/MS Chromatography of oxygenates and aromatics.

Table 4-3 also shows data for the pyrolysis of paper and plastics at $5^{\circ}\text{C min}^{-1}$ and at $\approx 350^{\circ}\text{C min}^{-1}$. The data shows that the paper and plastic samples exhibited similar trends to RDF under pyrolysis at $5^{\circ}\text{C min}^{-1}$ and at $\approx 350^{\circ}\text{C min}^{-1}$, in terms of the compounds detected. For the paper sample, the oil product from pyrolysis at $5^{\circ}\text{C min}^{-1}$ contained mostly alkenes, alkanes and oxygenates, while the oil product from pyrolysis at $\approx 350^{\circ}\text{C min}^{-1}$, contained mostly aromatics and alkenes. Other researchers have investigated oil products from paper pyrolysis [37-39] and detected similar compounds.

The pyrolysis of the waste plastic sample at $5^{\circ}\text{C min}^{-1}$, yielded an oil product from which mostly alkenes and alkanes were detected, while pyrolysis at the heating rate of $\approx 350^{\circ}\text{C min}^{-1}$, yielded an oil product from which mostly aromatics and alkenes were detected. Similar products have been detected by other researchers in the oil from plastic pyrolysis [15, 40]. Williams et al [40] detected the presence of aromatics at temperatures above 650°C for plastic pyrolysis in a fluidised bed.



The analysis of the components of the individual oil products from the pyrolysis of RDF and its single components of paper (cellulosic) and plastics can give an idea into the contributions of these single components to the oil products from RDF pyrolysis. The oil product from the slow pyrolysis of RDF can be linked to its cellulosic contents e.g. the paper fractions which contributed to most of its oxygenated content and its plastic content which contributed to most of its aliphatic content. The oil product from the pyrolysis of the three samples at the heating rate of $\approx 350 \text{ }^\circ\text{C min}^{-1}$, contained mostly aromatic compounds and suggests that the aromatic content of the oil from RDF pyrolysis was as result of the contributions of both the cellulosic and plastic fractions. However the RDF oil contained some alkenes and alkanes and this can be linked to its plastic contents due to the high concentration of alkenes and alkanes in the oil from plastic pyrolysis at a heating rate of $\approx 350 \text{ }^\circ\text{C min}^{-1}$. Figures 4-8 to 4-11 show chromatograms for the GC/MS analysis of the oil samples produced from paper and plastics pyrolysis at the heating rates of 5 and $\approx 350 \text{ }^\circ\text{C min}^{-1}$.

4.2.4 Solid product characteristics

Table 4-1 shows the effects of the different heating rates on the solid residues from the pyrolysis of RDF and its simulated single components at $800 \text{ }^\circ\text{C}$. During pyrolysis, as the heating rate was increased from 5 to $350 \text{ }^\circ\text{C min}^{-1}$ the solids yield showed a decreasing trend for the RDF, paper, cardboard and plastic samples. This reduction suggests that higher heating rate influences the solids yields [3] by encouraging the complete degradation and release of any trapped volatiles within the solid residue structure. The GCV of the solid product from RDF pyrolysis at the heating rate of $5 \text{ }^\circ\text{C min}^{-1}$ is higher at 18.45 MJ Kg^{-1} , compared with a CV of 16.37 MJ Kg^{-1} at the heating rate of $\approx 350 \text{ }^\circ\text{C min}^{-1}$. This difference could be as a result of lower ash content per mass basis [27] and residual volatile matter within the structure of the solid produced from pyrolysis at $5 \text{ }^\circ\text{C min}^{-1}$. The BET surface area for the solid products from RDF pyrolysis at the lowest and highest heating rates were measured, and indicates that the solids produced from pyrolysis at $5 \text{ }^\circ\text{C min}^{-1}$, had a higher

surface area ($170 \text{ m}^2\text{g}^{-1}$) than the solids from pyrolysis at $\approx 350 \text{ }^\circ\text{C min}^{-1}$ ($84 \text{ m}^2\text{g}^{-1}$). This suggests that during the pyrolysis at $\approx 350 \text{ }^\circ\text{C min}^{-1}$, the thermal shock impacted on the RDF sample caused the volatiles to be violently released from the RDF structure [41], thereby destroying the internal pore structure of the solid product, compared to that from pyrolysis at $5 \text{ }^\circ\text{C min}^{-1}$, where the volatiles gradually exited the structure of the RDF.

4.2.5 Influence of other process conditions

In this section the results of the investigations of process conditions such as the final temperature and the particle size used for RDF are presented and discussed. The effects of these conditions on gas yield, gas characteristics and components are discussed. Experiments to investigate the effects of temperature were carried out using RDF samples of 1mm particle size.

4.2.5.1 Effects of final pyrolysis temperature

The effect of the different final pyrolysis temperatures investigated on the product yields from RDF pyrolysis is shown in Table 4-4. These tests were carried out at fast heating rates ($\approx 350 \text{ }^\circ\text{C min}^{-1}$), to the final temperatures of 700, 800 and 900 $^\circ\text{C}$ and at slow heating ($90 \text{ }^\circ\text{C min}^{-1}$) to the same final temperatures. A careful look at the tabulated results reveals a trend in the product yields with increasing temperature. Essentially the oil and solid yields decreased while the gas yield increased with increasing temperature for both the slow and fast heating rate experiments. Similar trends in product yields with increasing pyrolysis temperature have been reported by other researchers as well [4, 42-46]. At 900 $^\circ\text{C}$ with heating rate of $\approx 350 \text{ }^\circ\text{C min}^{-1}$, the gas yield increased to 52.3 wt%, solids yield reduces to 21 wt%, while the liquid yield remained apparently unchanged at 23 wt%. It appears that the increased gas yield at 900 $^\circ\text{C}$ was therefore mostly due to further degradation of the solids at such high temperatures. This may be related to the release of trapped volatiles within char structures. The further degradation of the solids fractions of MSW at such temperatures have also been linked to the degradation of inorganics e.g. CaCO_3 contained in MSW, into CaO and CO_2

[12, 13]. This may also be responsible for some of the increase in CO₂ recorded in the gas composition from pyrolysis at 900 °C, in addition to the CO₂ produced from further degradation of oxygenated species such as oxygenated aromatics.

Table 4-4

Products from the slow and fast heating of RDF at different temperatures

wt% sample	90 °C min ⁻¹			≈ 350 °C min ⁻¹		
	700 °C	800 °C	900 °C	700 °C	800 °C	900 °C
Gas	14.0	16.6	17.7	43.6	46.9	52.3
solid	27.0	27.0	25.0	22.4	22.8	21.0
Oil	53.0	50.0	48.0	29.0	23.0	23.0
Balance	94.0	93.6	90.7	95.0	92.7	96.3
Gas composition wt% sample						
H ₂	0.3	0.4	0.4	0.4	0.7	0.8
CO	3.5	4.7	6.3	21.4	18.7	24.4
CO ₂	8.3	9.3	8.7	10.2	11.5	13.2
CH ₄	0.7	0.8	0.8	2.7	4.9	5.5
C ₂ - C ₄	1.2	1.4	1.4	8.9	11.0	8.4
Gas composition vol%						
H ₂	26.9	29.0	28.2	12.0	17.4	18.0
CO	23.1	25.6	31.9	47.6	34.9	39.9
CO ₂	35.2	32.0	27.9	14.4	13.7	13.7
CH ₄	8.7	7.9	6.8	10.3	16.1	15.7
C ₂ H ₄	1.6	1.6	1.4	7.9	11.3	10.7
C ₂ H ₆	1.5	1.3	1.2	1.8	1.0	0.5
C ₃ H ₆	1.1	1.0	1.0	3.7	1.8	0.8
C ₃ H ₈	1.0	0.8	0.8	0.5	0.4	0.2
C ₄ H ₈ & C ₄ H ₆	0.7	0.6	0.6	1.7	1.0	0.4
C ₄ H ₁₀	0.3	0.2	0.2	0.2	*	nd

nd: not detected, *: less than 0.1

During pyrolysis at the heating rate of ≈ 350 °C min⁻¹, the CV of the produced gases was 22.8, 24.8 and 21.3 MJ m⁻³ for pyrolysis at 700, 800 and 900 °C respectively. The CV for the gas produced at 900 °C decreased due cracking

of hydrocarbon gases. The CV of the gas product at 800 °C was the highest at 24.8 MJ m⁻³, indicating that this might be a good temperature for the production of an optimum heating value gas from RDF fast pyrolysis.

Table 4-5
Effect of particle size on RDF pyrolysis at 800 °C

wt% sample	particle sizes (mm)			
	1	2	3	3 - 9
Gas	46.9	44.4	42.2	43.3
solid	22.8	23.5	22.1	21.4
Oil	23.0	23.0	29.0	29.0
Balance	92.7	90.9	93.3	93.7
Gas composition wt% sample				
H ₂	0.7	0.7	0.6	0.6
CO	18.7	17.9	15.3	14.6
CO ₂	11.5	9.6	12.8	10.5
CH ₄	4.9	7.5	3.8	4.7
C ₂ - C ₄	11.0	8.7	9.6	12.8
Gas composition vol%				
H ₂	17.4	17.7	17.8	18.0
CO	34.9	33.2	33.1	29.7
CO ₂	13.7	11.4	17.6	13.6
CH ₄	16.1	24.1	14.4	16.8
C ₂ H ₄	11.3	9.2	10.3	14.3
C ₂ H ₆	1.0	1.1	1.6	1.8
C ₃ H ₆	1.8	2.2	3.2	3.8
C ₃ H ₈	0.4	0.3	0.3	0.3
C ₄ H ₈ & C ₄ H ₆	1.0	0.9	1.7	1.8
C ₄ H ₁₀	*	*	*	*

*: less than 0.1

4.2.5.2 Effects of particle size

The influence of particle size on the fast pyrolysis of RDF was investigated and the results are shown in Table 4-5. The effects of particle size on the pyrolysis of carbonaceous material has been investigated and reported by other researchers in terms of its influence on heating rate/heat transfer [12, 23, 47, 48] and its influence on extending the residence time of the pyrolyzed primary volatiles within the sample structure [17, 23], possibly encouraging secondary reactions of the volatiles and or reactions of the volatiles with the solid products of pyrolysis. Results from this present study as presented in table 4-5 did not show any significant effects with varying the sizes of the RDF samples which were pyrolysed.

The nature of RDF which is heterogeneous and made up of various fractions (plastics, inorganics, paper, cardboard and wood) compared to wood alone, suggests that increasing the particle size of the pyrolyzed samples can result in a reduction in the sample homogeneity. This may explain the lack of a trend in the product yields when RDF samples of different particle sizes were pyrolysed. The samples of larger sized particles may either be composed largely of high calorific value material like the plastics, or may be composed largely of inorganic materials of no calorific value. These would therefore influence the products of pyrolysis accordingly.

4.2.6 Conclusions

The pyrolysis of RDF and its components (paper, cardboard and waste plastics) as representatives of MSW were carried out in a fixed bed reactor where different process parameters were varied, such as the; heating rate, final pyrolysis temperature and the size of the sample, in order to investigate their effects on the product yields and compositions. The following main conclusions have been drawn:

- TGA analysis of the RDF sample indicated major volatile degradation at two temperature zones which were characteristic of the volatile

degradation temperatures of lignocellulosic (biomass derived) and plastic materials. This indicated that the RDF sample contained both lignocellulosic and plastic materials as expected.

- For the RDF, paper, cardboard and waste plastic samples, increasing the heating rate resulted in an increased gas yield, reduced liquid yield and reduced solids yield at the conditions investigated. A combination of increased heating rate, high temperature and extended vapour residence time promoted secondary decomposition of volatiles and resulted in increased gas yield as well as increased hydrogen yield from all four samples. The calorific value of the product gas was also found to increase with increasing heating rate for RDF.
- The secondary decomposition of volatile during pyrolysis at $\approx 350\text{ }^{\circ}\text{C min}^{-1}$, for the paper and cardboard samples resulted in a gas with the most abundant components as CO, while for the waste plastics the most abundant gas component were the hydrocarbon gases. This can give an insight into the contributions of these materials to the gas components from RDF pyrolysis. The high CO and hydrocarbon contents of RDF pyrolysis gas makes it a likely feedstock for the steam reforming reactions to produce hydrogen.
- FTIR and GC/MS/MS analysis showed that the oil from fast pyrolysis was found to contain mostly aromatic compounds which could be formed from the conversion of alkanes to alkenes and then to monocyclic aromatics via Diels-Alder reactions and finally to polycyclic aromatics. On the other hand the oil from slow pyrolysis ($5\text{ }^{\circ}\text{C min}^{-1}$) was found to contain mostly alkanes, alkenes and oxygenates.
- Increasing the final temperature for RDF pyrolysis at slow ($90\text{ }^{\circ}\text{C min}^{-1}$) and fast ($\approx 350\text{ }^{\circ}\text{C min}^{-1}$) heating rates resulted in an increased gas yield, reduced liquid yield and reduced solids yield at the conditions investigated. Fast pyrolysis of RDF at $800\text{ }^{\circ}\text{C}$ resulted in the

production of a gas with the highest calorific value of 24.8 MJ m^{-3} . While fast pyrolysis of RDF at $900 \text{ }^\circ\text{C}$ resulted in the highest gas and hydrogen yield.

- The particle sizes of RDF investigated in this work did not significantly impact its pyrolysis products.

4.3 Influence of slow and fast heating on the pyrolysis of waste wood and its single components

This chapter further investigates the effects of process conditions such as the heating rate, the final pyrolysis temperature and the particle size, during the pyrolysis of waste wood and its major components such as cellulose, hemicellulose (xylan) and lignin in the fixed bed reactor. The investigations were aimed at identifying the effects of these process conditions on their gas and hydrogen yield as well as the contributions of the components to the product yields.

4.3.1 Product yields

The waste wood and its single component samples were tested in the horizontal fixed bed reactor to investigate the effects of different heating rates ($5, 20, 90$ and $\approx 350 \text{ }^\circ\text{C min}^{-1}$) on pyrolysis. About 1 g of sample was used for each experiment at a pyrolysis temperature of $800 \text{ }^\circ\text{C}$. The carrier gas flow rate was 100 ml min^{-1} and the particle size of the samples was 1 mm .

Table 4-6 shows the result of the pyrolysis of waste wood and its investigated single components (cellulose, xylan and lignin) to a final temperature of $800 \text{ }^\circ\text{C}$ at the different investigated heating rates.

The pyrolysis procedure for slow and fast heating were the same as explained in section 4.1.3 earlier, for the pyrolysis of RDF. The estimated heating rates for the different samples at the fast heating experiments as determined by equation 3.1 were: wood $360 \text{ }^\circ\text{C min}^{-1}$, cellulose $320 \text{ }^\circ\text{C min}^{-1}$, xylan $340 \text{ }^\circ\text{C min}^{-1}$ and lignin $340 \text{ }^\circ\text{C min}^{-1}$.

As expected from wood pyrolysis, table 4-6 below, shows that three different major product fractions were produced from the pyrolysis of the wood sample [49-51], up to a final temperature of 800 °C, and at the chosen heating rates of 5, 20, 90 and 360 °C min⁻¹. The major products were; a gaseous fraction made up mostly of CO, H₂, CO₂, CH₄ and other lighter hydrocarbon gases (C₂ to C₄) which were collected in the sampling gas bag, a solid fraction made up mostly of char and ash which remained on the sample boat and were also deposited on the reactor wall, and a liquid fraction made mostly of a dark brown oil and some moisture which were collected in the condensers.

It is obvious from table 4-6 that varying the heating rate of pyrolysis influenced the yields of the three major products, at the parameters investigated for the wood sample. The gas yield was seen to increase from 14.5 to 54.1 wt%, with increasing heating rate while the solids yield was noted to decrease from 26.7 to 14.2 wt%, with increasing heating rate. The liquid yield was noted to initially show an increasing trend of yield from 49.5 to 57.4 wt%, with the heating rate, from 5 through to 90 °C min⁻¹. Similar results have been obtained from other researchers for the pyrolysis of pine wood [3], cherry seed [52], rice straw and saw dust [53], safflower seed [54] and biomass wastes [55] up to final temperatures of 720, 600, 700, 700 and 900 °C respectively. Williams et al [3] reported that increasing the heating rate for pine wood pyrolysis from 5 to 80 °C min⁻¹ resulted in increased production of oil and gas while reducing the yield of char. However table 4-6 shows that when the heating rate was ramped up to 360 °C min⁻¹, a sharp reduction in the liquid yield to 27.4 wt% and a resulting sharp increase in the gas yield to 57.4 wt% were recorded. Becidan et al [55] showed that, compared to the low heating rate, the higher heating rate (115 °C min⁻¹) pyrolysis of waste biomass resulted in increased gas yield and reduced liquid and char yield.

The increased gas yield during investigations at the heating rate of ≈ 350 °C min⁻¹, was as a result of the promoted secondary thermal cracking of primary pyrolysis vapours which were released quickly into the high temperature

atmosphere within the reactor due to the fast heating rate. The higher heating rate of $\approx 350 \text{ }^\circ\text{C min}^{-1}$, combined with a residence time of about 9 sec, initiated the secondary cracking of the vapours to yield lighter molecular weight hydrocarbons and more gases. The heating rate in combination with final temperature, vapour and solids residence time are very influential for controlling the product yields from pyrolysis. The heating rate impacts pyrolysis by affecting how long it takes for the sample to get to the final pyrolysis temperature.

The quantity of solids (char) produced from waste wood pyrolysis declined with the increasing heating rate as shown in Table 4-6. This is in-line with previous literatures [3, 56, 57] which reported that low heating rates resulted in more char yield from the pyrolysis of biomass, and vice-versa. The increased char yield impacted by the low heating rate pyrolysis may be explained by the proposal that the mechanism of char formation which is “cross-linking” [58, 59], is at its optimum at low temperatures (around $220 \text{ }^\circ\text{C}$). Low heating rate pyrolysis possibly promotes the char formation mechanism by extending the time the sample spends at the “optimum char formation temperature region”, thereby promoting further char formation [60] compared to higher heating rate pyrolysis.

The products of the pyrolysis of the single components of waste wood investigated, exhibited the same trend as the wood samples with increasing heating rate as shown in table 4-6. As the heating rate was increased from 5 to $90 \text{ }^\circ\text{C min}^{-1}$, the oil and gaseous products increased as a result of the release of volatiles from the solids structure, while the solid product yield decreased, for the cellulose, xylan and lignin samples. At the heating rate of $5 \text{ }^\circ\text{C min}^{-1}$ the product fraction of the highest yield for the cellulose and xylan samples was oil while that for lignin was a solid product (char). At the heating rate of $\approx 350 \text{ }^\circ\text{C min}^{-1}$, the product fraction of the highest yield for lignin was still the solid product while that for cellulose and xylan was a gaseous product.

The cellulose sample yielded the highest oil product at heating rate of 5 °C min⁻¹, and the highest gaseous product at the heating rate of ≈ 350 °C min⁻¹. This is as a result of the high volatile content of cellulose which was converted into mostly condensable oils during pyrolysis at 5 °C min⁻¹, and into mostly gases during pyrolysis at ≈ 350 °C min⁻¹. Compared to the cellulose, the xylan sample produced the higher gas and solids yields at the lower heating rates (5 and 90 °C min⁻¹), while it produced the higher solid but lower gas yield at the heating rate of ≈ 350 °C min⁻¹. Shen et al [61] reported more char formation from xylan than cellulose during pyrolysis up to 750 °C at fast heating rates.

Table 4-6

Products from the slow and fast heating of waste wood and its components at 800 °C

Yield	Heating rates °C min ⁻¹												
	5				20	90				≈ 350			
wt% sample	wood	cellulose	xylan	lignin	wood	wood	cellulose	xylan	lignin	wood	cellulose	xylan	lignin
Gas	14.5	21.0	27.1	16.4	16.6	17.5	21.3	27.3	16.5	52.9	73.1	44.4	29.3
solid	26.7	16.0	27.2	43.7	22.3	20.8	12.4	22.9	37.6	15.7	5.9	22.5	36.5
Oil	49.5	54.0	36.9	35.9	54.4	57.4	65.4	42.9	40.6	27.5	16.7	23.5	25.0
Balance	90.8	91.0	91.2	96.0	93.3	95.7	99.0	93.0	94.7	96.1	95.6	90.5	90.8
Gas composition wt% sample													
H ₂	0.4	0.4	0.6	1.0	0.4	0.4	0.3	0.6	0.7	0.8	1.4	1.0	0.8
CO	5.6	6.3	7.1	6.1	6.0	6.3	6.7	9.0	6.9	30.3	44.5	16.8	15.9
CO ₂	7.2	13.0	17.5	6.2	8.8	9.2	13.1	16.0	5.8	10.9	14.7	20.3	5.7
CH ₄	1.0	0.8	0.7	2.6	1.1	1.2	0.7	0.8	2.6	4.8	5.0	2.7	4.4
C ₂ - C ₄	0.3	0.6	1.2	0.5	0.3	0.4	0.5	0.9	0.5	6.1	7.3	3.7	2.4
Gas composition vol%													
H ₂	32.7	25.7	30.3	47.7	28.6	24.8	21.3	27.8	38.8	18.1	22.0	26.3	28.4
CO	31.0	28.4	24.4	21.4	28.6	33.3	31.5	30.6	27.1	48.7	50.2	32.9	39.0
CO ₂	25.5	37.6	38.0	13.7	31.3	28.8	39.3	34.6	14.5	11.2	10.6	25.4	9.0
CH ₄	9.6	6.6	4.4	16.0	10.1	11.2	6.0	4.5	18.2	13.6	9.9	9.1	18.9
C ₂ H ₄	0.4	0.4	0.4	0.2	0.4	0.6	0.5	0.4	0.3	5.7	4.7	3.9	2.5
C ₂ H ₆	0.5	0.5	1.4	0.5	0.6	0.7	0.6	1.2	0.6	0.8	1.3	1.2	0.8
C ₃ H ₆	0.2	0.3	0.3	0.1	0.2	0.3	0.5	0.3	0.1	1.1	0.8	0.6	0.6
C ₃ H ₈	0.1	nd	0.3	0.1	0.1	0.1	0.0	0.4	0.4	0.2	0.1	0.2	0.2
C ₄ H ₈ & C ₄ H ₆	nd	0.4	0.2	0.1	0.1	0.1	0.1	0.1	0.0	0.6	0.2	0.4	0.6
C ₄ H ₁₀	nd	0.2	0.4	0.2	0.0	0.0	0.1	0.1	0.0	0.0	0.3	0.0	0.0

nd: not detected, *: less than 0.1

Table 4-6 shows that the increased gas yield noted for the cellulose and xylan samples at the heating rate of $\approx 350 \text{ }^\circ\text{C min}^{-1}$, were as a result of the conversion of the oil products as well as the solid products (especially for cellulose). However for the lignin sample the increased gas yield was mostly as a result of the cracking of oil products. The solids yield was almost unchanged when comparing the results for lignin pyrolysis at $90 \text{ }^\circ\text{C min}^{-1}$ and at $\approx 350 \text{ }^\circ\text{C min}^{-1}$. Caballero et al [62] pyrolyzed lignin at high heating rate and temperatures up to $900 \text{ }^\circ\text{C}$ and found that the product of highest yield was char up to $800 \text{ }^\circ\text{C}$ and then gas followed by char above $800 \text{ }^\circ\text{C}$. Considering the individual pyrolysis products from the wood, cellulose, xylan and lignin samples, the production of char noted for the wood sample can be linked mostly to its content of lignin and partly from hemicellulose (xylan) [61, 63]. While its gaseous and oil products is as a result of volatiles which can be linked mostly to the woods contents of cellulose and hemicellulose which degrade more easily [63].

4.3.2 Gas composition and hydrogen yield

Further analysis of the results in Table 4-6 above gives an indication of the effect of the different heating rates on the gas products from the pyrolysis of the wood sample and its single components. The detected gases were noted to increase (on a mass basis) with increasing heating rate. The highest gas compositional mass yields were produced at the heating rate of $\approx 350 \text{ }^\circ\text{C min}^{-1}$ due to the promotion of secondary thermal cracking of the pyrolysis vapours and this is supported by the noted reduction in the quantity of liquids collected compared to the lower heating rate experiments ($5, 20$ and $90 \text{ }^\circ\text{C min}^{-1}$).

As expected, due to the high molecular oxygen content of wood ($38.2 \text{ wt}\%$ for our sample), the most abundant gaseous component produced at the highest heating rate was CO and this has been reported to be as a result of reactions such as, secondary cracking of oxygenated primary volatiles [52] and the Boudouard reaction [64]. This is further supported by the reduced yield of liquids recorded for the experiment at $360 \text{ }^\circ\text{C min}^{-1}$ compared to the other heating rate experiments. The CV of the gas produced from the test at the

heating rate of $360\text{ }^{\circ}\text{C min}^{-1}$ was also noted to be the highest (18.8 MJ m^{-3}) compared to the other heating rates. This was as a result of the increased yield of CH_4 and the other hydrocarbon gases $\text{C}_2 - \text{C}_4$ in the product gas.

For the experiments at the heating rates of 5, 20 and $90\text{ }^{\circ}\text{C min}^{-1}$ the most abundant gaseous component detected was CO_2 . Similar results have been achieved by other researchers [65, 66] for the pyrolysis of wood. The higher yield of CO_2 at these conditions has been explained to be as a result of the primary decomposition of oxygen-containing functional groups, especially the decomposition of carboxylic compounds [66] due to their highly thermal unstable nature.

In terms of total gas yield, similar trends to the wood sample were observed for the cellulose, xylan and lignin samples as the heating rate increased. The cellulose had the highest gas mass yield followed by wood, xylan and lignin. For all the samples, at the lowest heating rate investigated, the most abundant gas component was CO_2 , followed by CO. At the heating rate of $\approx 350\text{ }^{\circ}\text{C min}^{-1}$, results showed that for the wood, cellulose and lignin, the most abundant gas component was CO. For xylan the mass yield of CO more than doubled at the heating rate of $\approx 350\text{ }^{\circ}\text{C min}^{-1}$, though the CO_2 gas increased only slightly but was the most abundant gas detected on a mass basis.

The yield of CO from cellulose pyrolysis at elevated temperature and high volatile residence has been reported to be as a result of the secondary reactions of aldehyde-type compounds while its CO_2 content has been linked to the primary decomposition of oxygenates [61, 67]. The CO product from xylan pyrolysis at elevated temperature has been reported to be a secondary product of the decomposition of ring-opened intermediates and the decarbonylation of aldehyde-type compounds while its CO_2 product has been linked to the decarboxylation of the o-acetyl groups within the xylan chain [61, 68].

Yang et al [69] compared the pyrolysis of cellulose, xylan and lignin and reported that xylan produced the highest CO₂ content as a result of higher carboxylic content. The CO₂ and CO products of lignin pyrolysis have been reported to be as a result of the degradation of carbonyl, carboxyl and ether groups while at high temperature CO production is mostly as a result of the cracking of diaryl ether groups [70]. A comparison of the CO composition for the wood components at ≈ 350 °C min⁻¹ heating rate indicates that most of the CO content of wood is likely contributed by cellulosic materials.

Table 4-7

Hydrogen and total gas production per gram of samples

Heating rates (°C min ⁻¹)	H ₂ mol g ⁻¹ x 1000			
	wood	cellulose	xylan	lignin
≈ 350	4.01	6.95	4.78	4.15
90	1.64	1.61	2.92	3.52
20	1.94	nd	nd	nd
5	2.11	2.01	3.17	4.88
	gas production m ³ g ⁻¹ x 1000			
	wood	cellulose	xylan	lignin
≈ 350	0.50	0.71	0.41	0.33
90.0	0.15	0.17	0.24	0.20
20.0	0.15	nd	nd	nd
5.0	0.14	0.18	0.23	0.23

Nd: not detected

Figure 4-12 shows the CV of the product gases while table 4-7 shows the hydrogen production and gas production of the samples in relation to the heating rate. As expected the CV of the gases from the pyrolysis of all samples at ≈ 350 °C min⁻¹, was the highest due to more volume and more contents of hydrocarbon gases. Compared to the other wood components, lignin pyrolysis at ≈ 350 °C min⁻¹ produced the lowest yield of gases, however the CV of its product gas was the highest among the wood components, due to its high content of hydrocarbons especially methane. Yang et al [69] also reported higher contents of CH₄ yield from lignin compared to cellulose and hemicellulose, as result of the decomposition of its aromatic rings, side chain fragmentation and demethylation of methoxy groups [70].

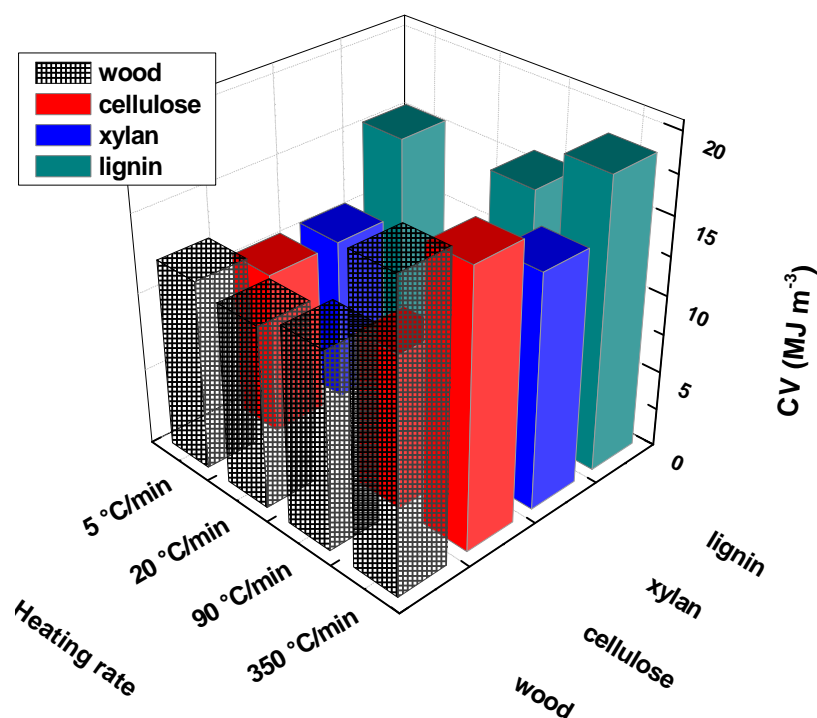


Figure 4-12 Effect of heating rate on the CV of product gases

Table 4-7 shows that during pyrolysis at $\approx 350 \text{ }^\circ\text{C min}^{-1}$, the cellulose had the highest gas production per mass of sample as expected due to its high volatile content, and it also had the highest hydrogen production per mass. However at low heating, the lignin sample had the highest hydrogen production per mass. Yang et al [69] reported similar results for the slow pyrolysis of lignin, cellulose and hemicellulose at $900 \text{ }^\circ\text{C}$. The yield of H_2 was attributed to the cracking of $\text{C}=\text{C}$ and $\text{C}=\text{H}$ aromatic bonds in the lignin. For the experiments at $\approx 350 \text{ }^\circ\text{C min}^{-1}$, in the order of increasing gas production per mass of sample, the arrangement was: lignin, xylan, wood and cellulose. While in order of increasing hydrogen production, the order was: wood, lignin, xylan and cellulose.

The CO contents of the wood pyrolysis gas and its fixed carbon content makes it a likely feedstock for the water gas shift and the carbon gasification reactions, respectively for hydrogen production.

4.3.3 Composition of the oil products

Oil samples collected in the condensers from the pyrolysis of wood, cellulose, lignin and xylan at different heating rates were analysed by FTIR (wood only) and GC/MS/MS. This was done to investigate the effects of the heating rate on the pyrolysis oils. Figure 4-13 shows the spectra from the FTIR analysis of waste wood pyrolysis oil. The spectra shown in figure 4-13 indicates the functional group characteristics of the pyrolysis oil from wood slow heating ($5\text{ }^{\circ}\text{C min}^{-1}$) and from fast heating ($\approx 350\text{ }^{\circ}\text{C min}^{-1}$), to $800\text{ }^{\circ}\text{C}$.

A comparison of both spectra clearly shows differences in the peak intensities which are representative of the different functional groups present in the oils. This indicates as expected a difference in the composition of the pyrolysis oils as a result of the different heating rates. The presence of polycyclic, monocyclic and substituted aromatic groups is indicated in the absorption peaks between 675 to 900 cm^{-1} and 1572 to 1625 cm^{-1} . The peaks from 950 to 1325 cm^{-1} represent C-O stretching and O-H deformation, indicating the presence of primary, secondary, tertiary alcohols and phenols. Peaks between 1350 to 1475 cm^{-1} and 2800 to 3000 cm^{-1} represent C-H deformation and indicates the presence of alkanes. The presence of alkenes is indicated by the C=C stretching vibrations between peaks 1625 and 1675 cm^{-1} . C=O stretching vibrations are indicated by the peaks between 1650 and 1850 cm^{-1} , while O-H vibrations are indicated by the broad peaks between 3050 and 3600 cm^{-1} , and a combination of these peaks suggests the presence of carboxylic acids and their derivatives.

Table 4-8 shows the detected compounds from the GC/MS/MS analysis of the oil products from wood, cellulose, xylan and lignin, and the relative abundance of the oil compounds indicated by asterisk, with reference to pyrolysis at the different heating rates investigated. Increasing asterisks in table 4-8 represents increasing concentration of the compound. Table 4-8 shows that for the oil product from wood pyrolysis, there was a decrease in oxygenate, alkane and alkene products as well as an increase in the aromatic products, with increasing heating rate. This is supported by figure 4-14 which shows the

effects of heating rate on selected oil compounds representing oxygenate, aliphatic and aromatic oil compounds from wood pyrolysis. Figure 4-14 showed that the concentrations of phenol, decane and hexadecane decreased from 1 – 0.1, 0.6 – 0.1 and 2 – 0.1 wt% respectively, while naphthalene increased from 0.1 – 3.2 wt%, with increasing heating rate from 5 to ≈ 350 °C min⁻¹ for the pyrolysis of wood. As the heating rate was increased, the high temperature effects were intensified, which resulted in the cracking of products such as the oxygenates and aliphatics, into gases as well into the more thermally stable aromatics via Diels-Alder reactions.

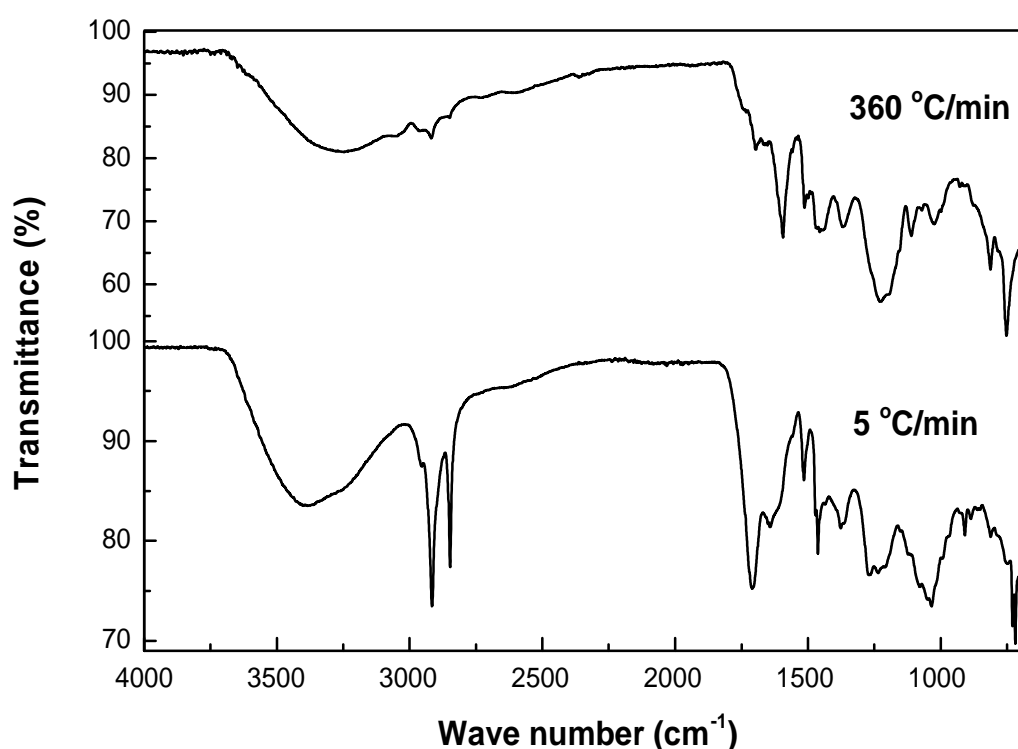


Figure 4-13 FTIR spectrogram for oil from the pyrolysis of wood at 5 and 360 °C min⁻¹

Table 4-8

Detected oil compounds from wood, cellulose, xylan and lignin pyrolysis at different heating rates

Heating rate °C min ⁻¹	5				20	90	≈ 350			
	wood	cellulose	xylan	lignin	wood	wood	wood	cellulose	xylan	lignin
Oil compounds	Oxygenates									
Cyclopentanone	***	****	****	****	***	*	**	*		
Furfural					****					
Anisole	*	*	**	**						
Phenol	***				**	**	*		*	*
Acetophenone		***	****	**		*				

Table 4-8 continues

2-Methoxyphenol					****	****				
2,4-Dimethylphenol			****							
1,2-Benzenediol					****					
2,3,5-Trimethylphenol	**	****					***		****	
4-Isopropylphenol	****	**			**					
Dibenzofuran		****		*						
Aromatics										
Styrene	*	*							****	
o-Xylene	*	*								
Alphamethylstyrene	***		*			*	**	*	**	*
Betamethylstyrene	*		*	*		*	***	***	****	**
Indane	*	*	**	*	*	*	***	*	*	*
Indene	*	*	*	*			***	***	***	
1,2,3,4-Tetramethylbenze					*					
Naphthalene	*	**	**	*	*	**	****	****	****	****
2-Methylnaphthalene			**	*	***			****		
1-Methylnaphthalene		***	**							****
Biphenyl	***	*	*	*	*	*	*	****	****	****
2-Ethyl-naphthalene				*						
1-Ethyl-naphthalene								***		
2,6-Dimethylnaphthalene	*	*	*	***	*					
1,4-Dimethylnaphthalene	**	*	**	***	***		***			****
Fluorene	***	*	*	*	*	*			****	
1,3-Diphenylpropane									**	
Phenanthrene		*		*					***	
1-Phenylnaphthalene	**									
o-Terphenyl		**								
Fluoranthene		*			*	*	*			*
Pyrene	*		*		*	*	**		*	*
m-Terphenyl			*		*					
1,3,5-Triphenylbenzene	***		**	*	***	***	***	**	****	****
Heating rate °C min ⁻¹	5				20	90	≈ 350			
	wood	cellulose	xylan	lignin	wood	wood	wood	cellulose	xylan	lignin
Alkanes										
Octane, C8		***	***	***	**	**		*	*	*
Decane, C10	***	**	**	**	**	**	*			
Undecane, C11	**	***	***	***	**	**	*	*	*	*
Dodecane, C12	***	***		***	***	***	*	*	*	*
Tridecane, C13	**				**	**	*	*	*	
Tetradecane, C14			***		**	**			*	
Pentadecane, C15				***	**				*	
Hexadecane, C16			*		*				*	*
Phytane			*	*		*		*		
Hepadecane, C17			*	*					*	*
Pristane			***					*	*	*
Octadecane, C18							*		*	*
Eicosane, C20									*	*
Docosane, C22	*									*
Tricosane, C23		**			**				*	*
Tetracosane, C24					**				*	*
Pentacosane, C25		***								
Hexacosane, C26		***								
Octacosane, C28	*	***	***	***				*		*

Table 4-8 continues

Nonacosane, C29	***		***			*		*
Triacotane		***	***		***	*		*
Hentriacotane, C31			***		***			
Dotriacotane, C32	***		***		***			
Triacotane, C33	***	***	***		***			*
Tetraacotane, C34		***	***	***	***	*	*	
Pentacotane, C35		***	***			*	*	
Hexacotane, C36	***	***	***				*	*
Heptacotane, C37		***	***	***			*	
Octacotane, C38		***	***	****			*	*
Nonacotane, C39		***			***			*
Tetraacotane, C40					***			*
Alkenes								
Octene, C8	**						****	*
Nonene, C9					***	***	**	
Decene, C10	****		***				**	
Undecene, C11		***						***
Dodecene, C12			***		***			**
Tridecene, C13			*		***			
Tetradecene, C14					***			
Pentadecene, C15						***		*
Hexadecene, C16	****					***	*	*
Eicosene, C20							**	
Tricosene, C23				***				
Octacosene, C28			***					
Nonacosene, C29			****					
Triacotene			****					
Triacotene, C33	***							
Pentacotene, C35		***					*	
Octacotene, C38		***						*

more * indicates higher concentration

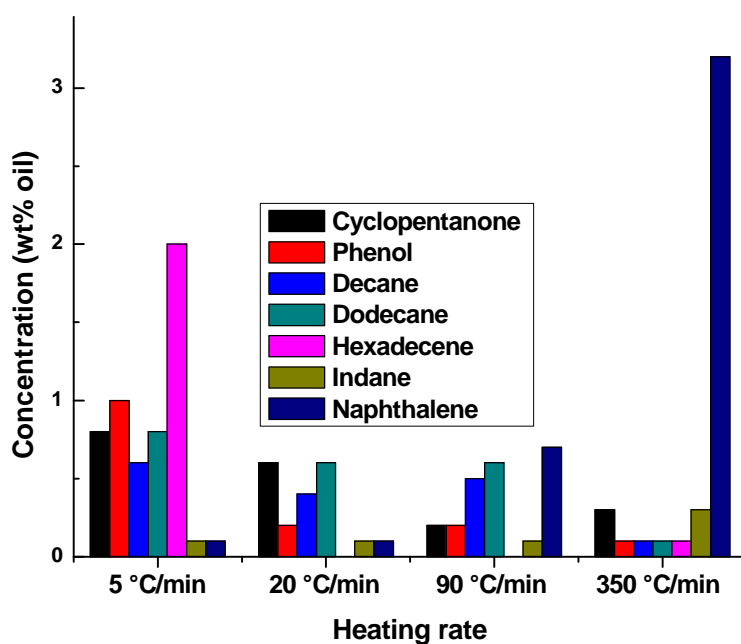


Figure 4-14 Effects of heating rate on oil compounds from wood pyrolysis

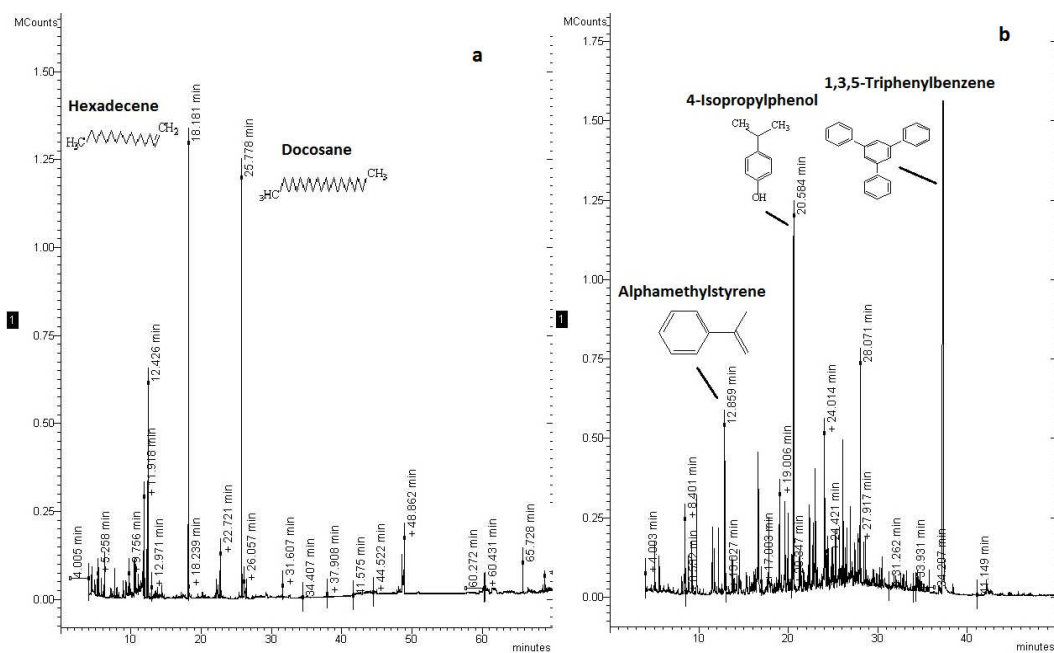


Figure 4-15. GC/MS chromatography of liquid from pyrolysis of waste wood at $5\text{ }^{\circ}\text{C}/\text{min}^{-1}$; (a) GC/MS Chromatography of aliphatics (b) GC/MS Chromatography of oxygenates and aromatics.

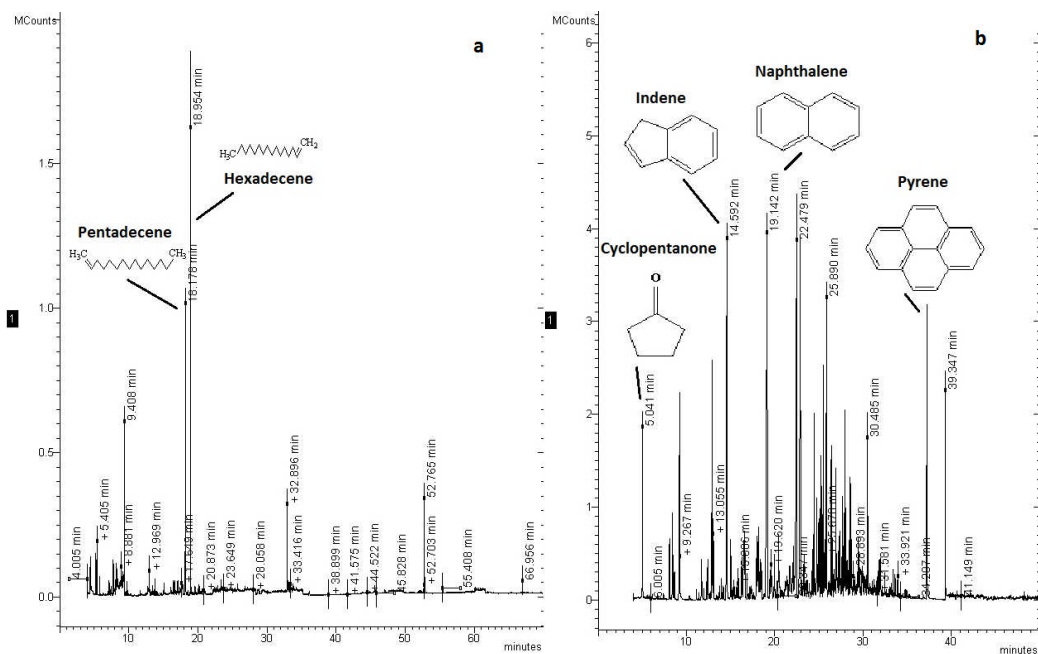


Figure 4-16. GC/MS chromatography of liquid from pyrolysis of waste wood at $\approx 350\text{ }^{\circ}\text{C}/\text{min}^{-1}$; (a) GC/MS Chromatography of aliphatics (b) GC/MS Chromatography of oxygenates and aromatics.

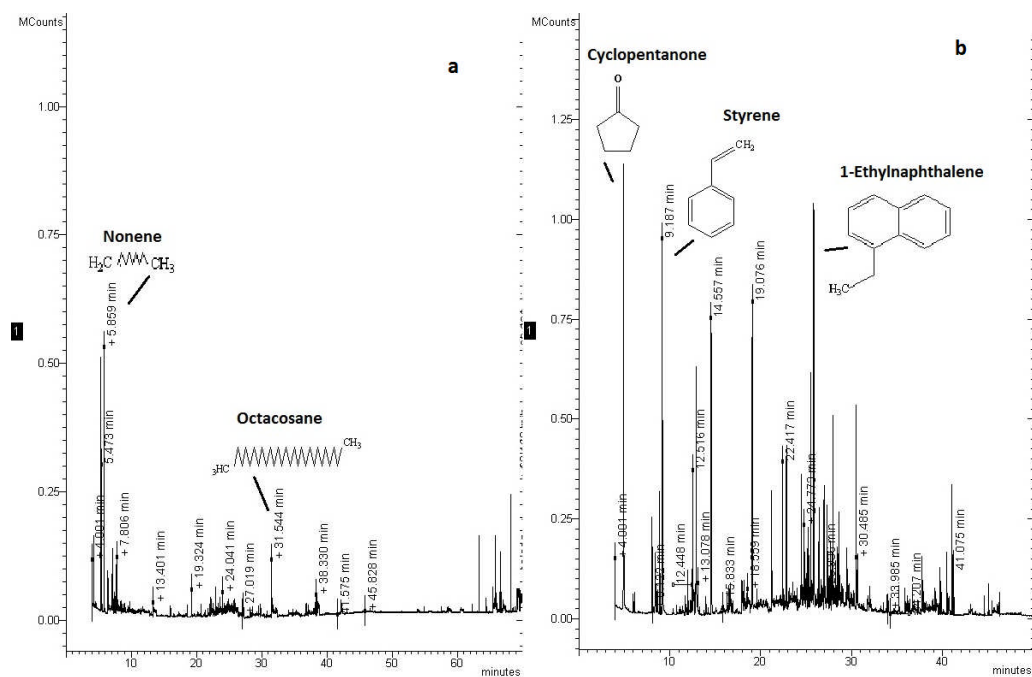


Figure 4-18. GC/MS chromatography of liquid from pyrolysis of cellulose at $\approx 350 \text{ }^\circ\text{C}/\text{min}^{-1}$; (a) GC/MS Chromatography of aliphatics (b) GC/MS Chromatography of oxygenates and aromatics.

The results of the analysis of the oil products from the pyrolysis of cellulose, xylan and lignin at 5 and $\approx 350 \text{ }^\circ\text{C}/\text{min}^{-1}$ are also shown in table 4-8. Table 4-8 indicates that the oil products from the components of wood investigated also exhibited similar trends to the wood pyrolysis oil, with varying heating rates. For pyrolysis at $5 \text{ }^\circ\text{C}/\text{min}^{-1}$, the most abundant compounds detected for the cellulose, xylan and lignin, were the oxygenate and aliphatic compounds. While during pyrolysis $\approx 350 \text{ }^\circ\text{C}/\text{min}^{-1}$, the most abundant compounds detected in the oil products from cellulose, xylan and lignin were aromatics. Windt et al [72] investigated the pyrolysis of lignin to $800 \text{ }^\circ\text{C}$ at slow and fast heating rates, and reported increased aromatics at the fast heating conditions while an abundance of oxygenates were detected at the slow heating rate. Mono-aromatic compounds are also primary decomposition products of lignin [73], and this explains its relatively higher content in the lignin derived oil at $5 \text{ }^\circ\text{C}/\text{min}^{-1}$. Shen et al [68] reported an increase in the production of ringed hydrocarbons and a decrease in oxygenates content of the pyrolysis oil with increasing pyrolysis temperature from hemicellulose. Shen et al [61] reported a decrease in the oxygenates and an increase in the ringed hydrocarbon

content of the pyrolysis oil with increasing pyrolysis temperature from cellulose.

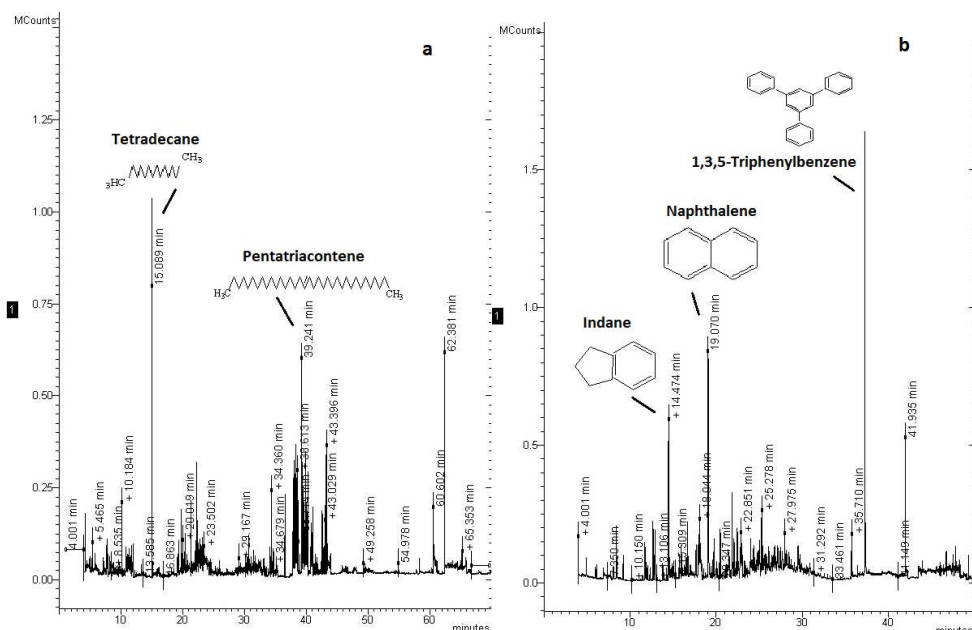


Figure 4-19. GC/MS chromatography of liquid from pyrolysis of cellulose at 5 °C/min⁻¹; (a) GC/MS Chromatography of aliphatics (b) GC/MS Chromatography of oxygenates and aromatics.

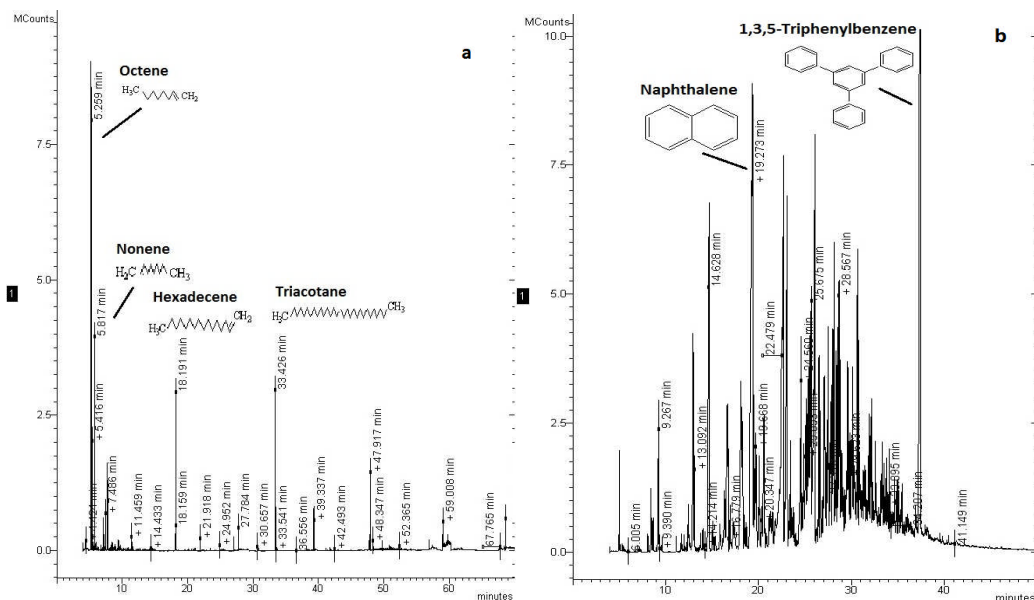


Figure 4-20. GC/MS chromatography of liquid from pyrolysis of xylan at ≈ 350 °C/min⁻¹; (a) GC/MS Chromatography of aliphatics (b) GC/MS Chromatography of oxygenates and aromatics.

The pyrolysis of the wood, cellulose, xylan and lignin samples at the heating rate of $\approx 350 \text{ }^\circ\text{C min}^{-1}$, combined with long volatile residence times, intensified the effect of the high pyrolysis temperature resulting in secondary reactions being promoted and the formation of more secondary products (aromatics). However at the heating rate of $5 \text{ }^\circ\text{C min}^{-1}$, the high temperature effect was minimized as volatiles were gradually released and swept out of the reactor before its temperature could increase to temperatures at which secondary reactions are encouraged, leading to the formation of mostly oxygenates and aliphatics. Figures 4-15 to 4-22 show the chromatograms from the GC/MS/MS analysis of the oil products from wood, cellulose, xylan and lignin pyrolysis at 5 and $\approx 350 \text{ }^\circ\text{C min}^{-1}$.

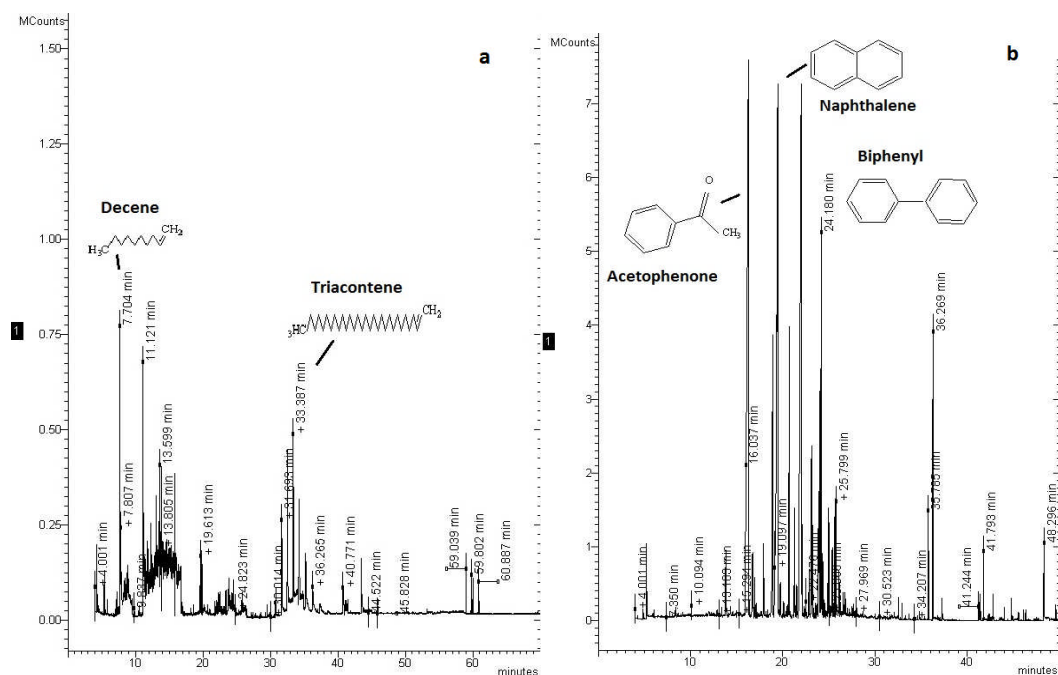


Figure 4-21. GC/MS chromatography of liquid from pyrolysis of lignin at $5 \text{ }^\circ\text{C/min}^{-1}$; (a) GC/MS Chromatography of aliphatics (b) GC/MS Chromatography of oxygenates and aromatics.

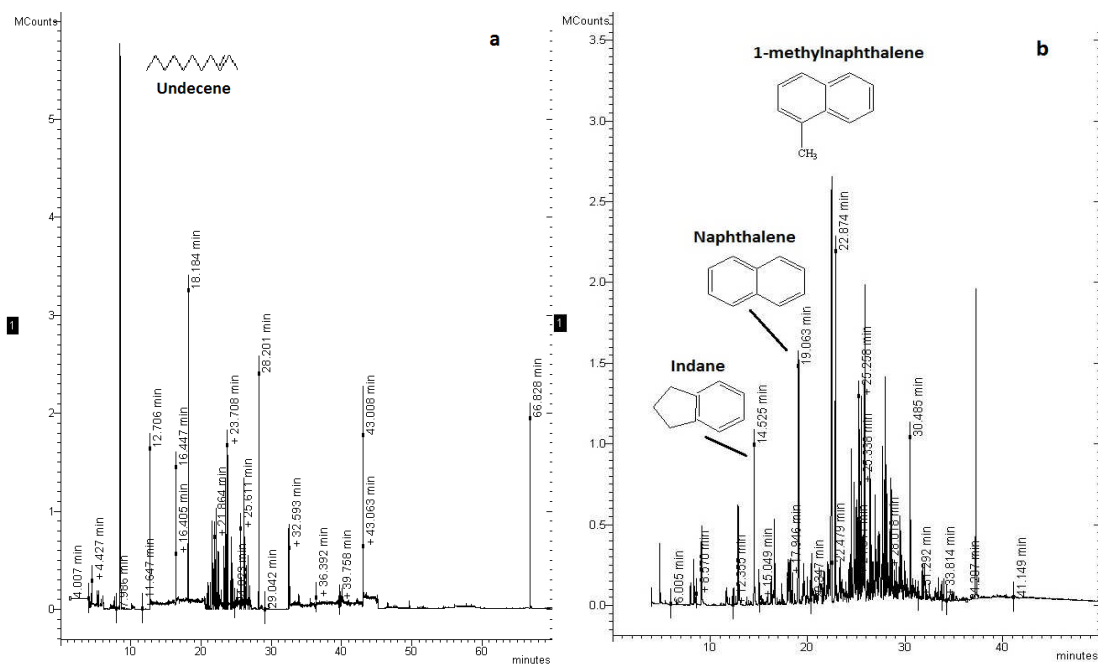


Figure 4-22. GC/MS chromatography of liquid from pyrolysis of lignin at ≈ 350 $^{\circ}\text{C}/\text{min}^{-1}$; (a) GC/MS Chromatography of aliphatics (b) GC/MS Chromatography of oxygenates and aromatics.

4.3.4 Solid product characteristics

Table 4-6 shows that with increasing heating rate, the solid product yield from the pyrolysis of the wood, cellulose, xylan and lignin samples decreased. Just as explained earlier in section 4-2-3, the increasing heating rate resulted in a release of more volatiles from the solid samples resulting in less char. The BET surface area for the solid products from wood pyrolysis at the lowest and highest heating rates were measured, and indicates that the solids from the pyrolysis at $5^{\circ}\text{C min}^{-1}$, had a higher surface area ($219\text{ m}^2\text{g}^{-1}$) than that for the solids from pyrolysis at $\approx 350^{\circ}\text{C min}^{-1}$ ($123\text{ m}^2\text{g}^{-1}$). This indicated that during pyrolysis at $\approx 350^{\circ}\text{C min}^{-1}$, the thermal shock impacted on the wood sample would have caused the volatiles to be violently released from the wood structure, thereby destroying the internal pore structure [41] of the solid product, compared to the slow pyrolysis where the volatiles gradually exit the structure of the wood sample. The GCV of the solid product from wood pyrolysis at the heating rate of $5^{\circ}\text{C min}^{-1}$ was slightly higher at 33.9 MJ Kg^{-1} ,

compared with a CV of 33.1 MJ Kg⁻¹ for the solid product from pyrolysis at the heating rate of ≈ 350 °C min⁻¹.

4.3.5 Influence of other process conditions

This section discusses the results of investigations on other process conditions such as the final temperature and the particle size used on waste wood only. The effects of these conditions on gas yield, gas characteristics and components are discussed. The experiments to investigate the effects of temperature were carried out using waste wood samples of 1mm particle size.

4.3.5.1 Effects of final pyrolysis temperature

These tests were carried out at fast heating (≈ 350 °C min⁻¹), to the final temperatures of 700, 800 and 900 °C and at slow heating (90 °C min⁻¹) to the same temperatures. The results of the different final pyrolysis temperatures investigated on the product yields from waste wood pyrolysis are shown in Table 4-9 below.

Table 4-9 shows that for both slow and fast heating, with increasing final pyrolysis temperature, the gas yield increases while the oil and solid products decrease. Other researchers have reported similar results for the pyrolysis of biomass [23, 74-75]. The effect of the increasing temperature in terms of gas production was noted to be more pronounced for the fast heating pyrolysis, due to the conversion of the pyrolysis oils to gas. The gaseous products were also noted to increase (wt%) with increased temperature as well due to the general increase in gas yield especially for the experiments at heating rate of ≈ 350 °C min⁻¹. The yield of permanent gases and methane (wt%) showed an increase with temperature while the C₂-C₄ gases showed an increase up to 800 °C and a notable decrease at 900 °C. The yield of hydrogen at 900 almost doubles, and this due to the cracking the heavier C₂-C₄ gases. For example butane was not detected at 900 °C indicating it was cracked at this temperature. The CV of the gases from the pyrolysis of waste wood at ≈ 350 °C min⁻¹ and at the final temperatures of 700, 800 and 900 °C were 18.4, 19.1

and 17.3 MJ m⁻³ respectively. The CV of the gas at 900 °C was lower due to cracking of higher hydrocarbons.

Table 4-9

Products from the slow and fast heating of wood at different temperatures

wt% sample	90 °C min ⁻¹			≈ 350 °C min ⁻¹		
	700 °C	800 °C	900 °C	700 °C	800 °C	900 °C
Gas	15.9	17.5	19.6	39.1	52.9	58.1
solid	21.6	20.8	18.0	15.8	15.7	11.0
Oil	60.8	59.4	59.0	44.6	27.5	19.0
Balance	98.3	97.7	96.6	99.5	96.0	88.1
Gas composition wt% sample						
H ₂	0.3	0.3	0.4	0.5	0.8	1.5
CO	5.6	6.2	8.2	21.7	30.3	36.2
CO ₂	8.4	8.4	9.3	9.5	10.9	10.1
CH ₄	1.1	1.2	1.3	3.2	4.8	5.2
C ₂ - C ₄	0.4	0.4	0.5	4.3	6.1	5.1
Gas composition vol%						
H ₂	23.7	24.8	25.4	16.7	18.1	27.2
CO	32.2	33.3	36.5	49.1	48.7	46.9
CO ₂	30.8	28.8	26.3	13.7	11.2	8.3
CH ₄	11.4	11.2	10.1	12.6	13.6	11.8
C ₂ H ₄	0.6	0.6	0.5	4.3	5.7	4.4
C ₂ H ₆	0.7	0.7	0.6	1.0	0.8	0.4
C ₃ H ₆	0.3	0.3	0.3	1.7	1.1	0.4
C ₃ H ₈	0.1	0.1	0.1	0.2	0.2	0.1
C ₄ H ₈ & C ₄ H ₆	0.1	0.1	0.1	0.6	0.6	0.4
C ₄ H ₁₀	*	*	*	0.1	*	nd

nd: not detected, *: less than 0.1

4.3.5.2 Effects of particle size

As explained in section 4-2-6-2 earlier, researchers have reported on the influence of particle size on the pyrolysis of carbonaceous materials in terms

of heat transfer impacts [12, 23, 47, 48] and the extension of volatile residence time within the sample structure [17, 23]. Different particle sizes (1, 2, 3 and 3 – 9mm) of the waste wood sample were pyrolyzed to 800 °C at heating rate of $\approx 350 \text{ }^\circ\text{C min}^{-1}$. Table 4-10 shows the results of the pyrolysis of the different wood sample sizes.

Table 4-10

Effect of particle size on wood pyrolysis at 800 °C

wt% sample	particle sizes (mm)			
	1	2	3	3 - 9
Gas	52.9	54.2	54.5	57.2
solid	15.7	15.4	14.3	14.2
Oil	27.5	26.9	26.7	25.5
Balance	96.0	96.5	95.5	96.8
Gas composition wt% sample				
H ₂	0.8	0.9	0.9	1.0
CO	30.3	30.1	30.0	31.4
CO ₂	10.9	12.3	13.1	13.1
CH ₄	4.8	5.0	4.9	5.6
C ₂ - C ₄	6.1	5.8	5.6	6.0
Gas composition vol%				
H ₂	18.1	19.9	20.2	19.9
CO	48.7	46.8	46.5	46.1
CO ₂	11.2	12.1	13.0	12.3
CH ₄	13.6	13.6	13.2	14.3
C ₂ H ₄	5.7	4.3	4.1	4.4
C ₂ H ₆	0.8	1.3	1.2	1.3
C ₃ H ₆	1.1	1.0	0.9	0.9
C ₃ H ₈	0.2	0.1	0.1	0.1
C ₄ H ₈ & C ₄ H ₆	0.6	0.2	0.2	0.2
C ₄ H ₁₀	*	0.6	0.6	0.5

*: less than 0.1

Table 4-10 shows that varying the sample particle sizes of the pyrolysed wood within the ranges studied, had no significant effects on the pyrolysis products.

Wei et al [23] and Lou et al [17] reported that larger particle sizes may extend the residence time of pyrolysis volatiles within the particle structure, which can promote secondary cracking of the vapours to yield more gases. This might explain the slight gas increase for the 3 to 9 mm particle however no significant conclusions can be drawn. The gas compositions for the different particle sizes were fairly similar.

4.3.6 Conclusions

The pyrolysis of waste wood and its simulated single components (cellulose, xylan and lignin) were carried out in a fixed bed reactor where different process parameters were varied, such as the; heating rate, final pyrolysis temperature and the size of the sample, in order to investigate their effects on the product yields and compositions. The following main conclusions have been drawn:

- TGA analysis of the waste wood sample indicated its volatile degradation at two temperature zones with two degradation peaks. The major volatile degradation peak which was a combination of two peaks was characteristic of the volatile degradation temperatures of hemicellulose and cellulose. The second degradation peak which was minor was characteristic of lignin degradation.
- For the wood, cellulose, xylan and lignin samples, increasing the heating rate resulted initially in an increased gas and oil yield, reduced solids yield followed finally by an increased gas yield and reduced liquid and solid yields at the conditions investigated. A combination of increased heating rate, high temperature and extended vapour residence time promoted secondary decomposition of volatiles and resulted in increased gas yield as well as increased hydrogen yield from all four samples. The calorific value of the product gas was also found to increase with increasing heating rate for wood.

- The secondary decomposition of volatiles during pyrolysis at the heating rate of $\approx 350 \text{ }^\circ\text{C min}^{-1}$, for the wood, cellulose and lignin samples resulted in a gas with the most abundant components as CO, while for the xylan the most abundant gas component was CO₂. The lignin followed by xylan produced the most char content while the cellulose produced the most CO content. The CO contents of the wood pyrolysis gas and its fixed carbon content makes it a likely feedstock for the water gas shift and the carbon gasification reactions, respectively for hydrogen production.
- FTIR and GC/MS/MS analysis showed that for the wood, cellulose, xylan and lignin, the oil from pyrolysis of the samples at a heating rate of $\approx 350 \text{ }^\circ\text{C min}^{-1}$ was found to contain mostly aromatic compounds which could be formed from the conversion of alkanes to alkenes and then to monocyclic aromatics via Dies-Alder reactions and finally to polycyclic aromatics. On the other hand the oil from pyrolysis of the samples at a heating rate of $5 \text{ }^\circ\text{C min}^{-1}$ was found to contain mostly alkanes, alkenes and oxygenates.
- Increasing the final temperature for wood pyrolysis at slow ($90 \text{ }^\circ\text{C min}^{-1}$) and fast ($\approx 350 \text{ }^\circ\text{C min}^{-1}$) heating rates resulted in an increased gas yield, reduced liquid yield and reduced solids yield at the conditions investigated. Fast pyrolysis of wood at $800 \text{ }^\circ\text{C}$ resulted in the production of the gas yield with highest calorific value of 19.1 MJ m^{-3} . While fast pyrolysis of wood at $900 \text{ }^\circ\text{C}$ resulted in the highest gas and hydrogen yield.
- Varying the particle size of the waste wood pyrolysed, between 1, 2, 3 and 3 – 9mm at the heating rate of $\approx 350 \text{ }^\circ\text{C min}^{-1}$, did not have any significant impacts on the pyrolysis products.

4.4 Mechanisms for the pyrolysis of solid wastes

The varied compositions which make up biomass wastes including MSW make it so that their pyrolytic decomposition takes place via a complex set of reactions and interactions which are not fully understood. This is evident in the complex stream of pyrolytic products especially in the pyrolysis liquids.

Sections 4.1.1 and 4.1.2 earlier looked at the thermal degradation behaviours of RDF as a model compound for MSW and a waste wood sample as a model for biomass waste and results showed that these samples degraded thermally at the TGA conditions in a manner which was as a result of the combined effects of the individual degradation of their major contents. These were the individual degradation of the lignocellulosic (cellulose, xylan and lignin) and plastics materials for the RDF, and for the waste wood sample these were the individual degradation of the cellulose, xylan and lignin contents.

This section looks at the degradation of RDF sample as a representative of solid waste degradation since this sample contains both the biomass and plastic contents.

Researchers have looked into the possibility of interactions between the lignocellulosic and plastic fractions during waste pyrolysis and have reported to have found either no interactions found [74, 75], or little interaction effects [76-78]. The possibility of interactions between the different plastic waste types [79, 80] have been investigated and both little and significant interactions were reported. Researchers have also investigated possible interactions between cellulose, hemicellulose and lignin [81, 82], results indicated little or no interactions depending on the mixture. The presence of inorganic in the ash contents of lignocellulosic materials have also been reported to possibly catalyze pyrolysis reactions [30, 83, 84]. Considering these, it is therefore very difficult to accurately predict the reaction mechanism taking place during the pyrolysis of mixed waste streams as there may be pronounced, or little or no interaction effects which may be impacted by

factors such as degree of mixing, heating rate as well as catalytic effects of inorganics .

Considering the difficulties of determining the exact degree of interactions if any for mixed waste such as RDF which contain both biomass, plastics as well as inorganic (possibly catalytic) components, this work proposes a simplistic single and multi-pathway pyrolysis mechanism for RDF based on a combination of the individual primary and secondary degradations of its lignocellulosic and plastics components and on the assumption that interaction and catalytic effects are minimal and therefore negligible. The degradation of the model compounds: cellulose, hemicellulose and lignin are proposed as representative of lignocellulosic materials, while polyethylene degradation is proposed as representative of plastic contents.

4.4.1 Degradation of cellulose, hemicellulose lignin and polyethylene

As explained earlier polymers degrade during pyrolysis mostly as a result of free radical degradation via different mechanisms such as: random scission, side group scission, monomer reversion and a combination of any of the former [19]. For example during the pyrolysis of higher alkanes, the carbon-carbon bonds randomly cleave along the chain to produce smaller alkyl radicals [20]. The degradation mechanism or mechanisms which will be applicable during the pyrolysis of polymers are dictated by factors such as, the weakest chemical bond within the polymer and the stability of the resultant product molecule. With increasing process severity in terms of temperature and volatile residence time, secondary and tertiary reactions are promoted such as Diels-Alder type mechanisms which are recombination/condensation reactions [36, 85] to form aromatics. Further Diels-Alder reactions of aromatics followed by dehydrogenation, decarboxylation or dehydroxylation reactions result in the formation of poly-aromatic compounds. Figure 4-23 shows the Diels-Alder pathway for aromatics formation from olefins

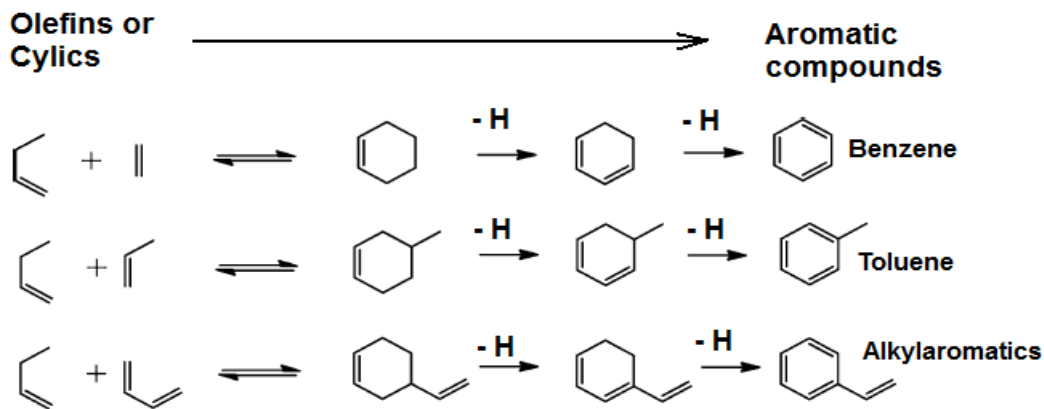


Figure 4-23 Proposed pathway for aromatic formation from olefins via Diels-Alder type reactions, from [35]

Different degradation models have been proposed for the degradation of cellulose [25, 86, 87]. A more realistic model for cellulose degradation should take into account the secondary reactions. The primary decomposition products of cellulose include: anhydrosugars such as levoglucosan [25], carbonyls, acids, primary gases such as CO_2 , and char [81]. Higher temperature results in the decomposition of volatiles into lighter volatiles such as the oxygenated compounds and alkanes, and gases. Further cracking and reactions such as the Diels-Alder reactions, result in the formation of alkenes, aromatics and gases. A detailed degradation pathway has been proposed by Greenhalf et al [60]. Figure 4-24 shows a proposed degradation pathway for cellulose.

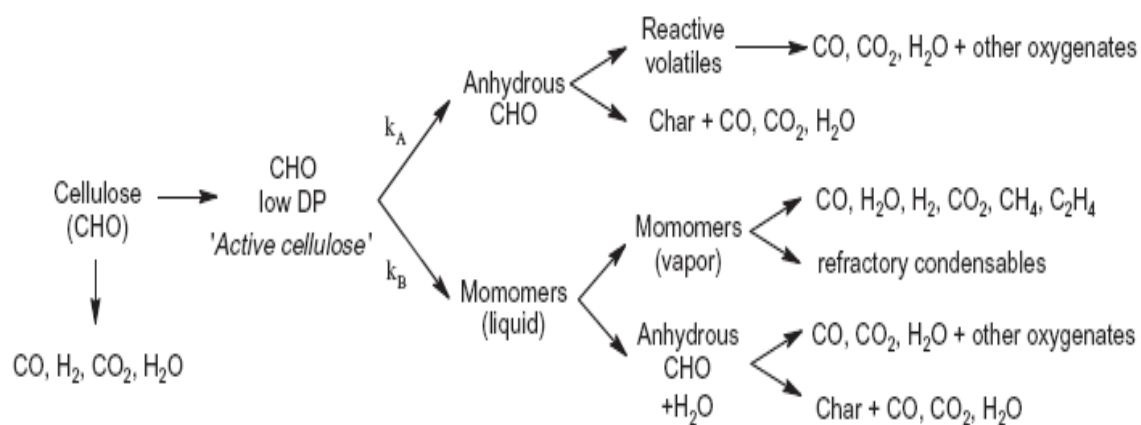


Figure 4-24 Proposed pathway for cellulose pyrolytic degradation, from [60]

The degradation of hemicellulose (xylan) has been studied and degradation mechanisms have been proposed [68, 88]. A recent work by Shen et al [68] proposed a detailed pathway for the primary and secondary decomposition of xylan. The primary decomposition products of xylan include: O-acetyl xylan, anhydroglucoses, acids, primary gases such as CO₂ and char. Further cracking and secondary reactions result in the formation of lighter volatiles and more gases. Figure 4-25 shows a proposed degradation pathway for xylan.

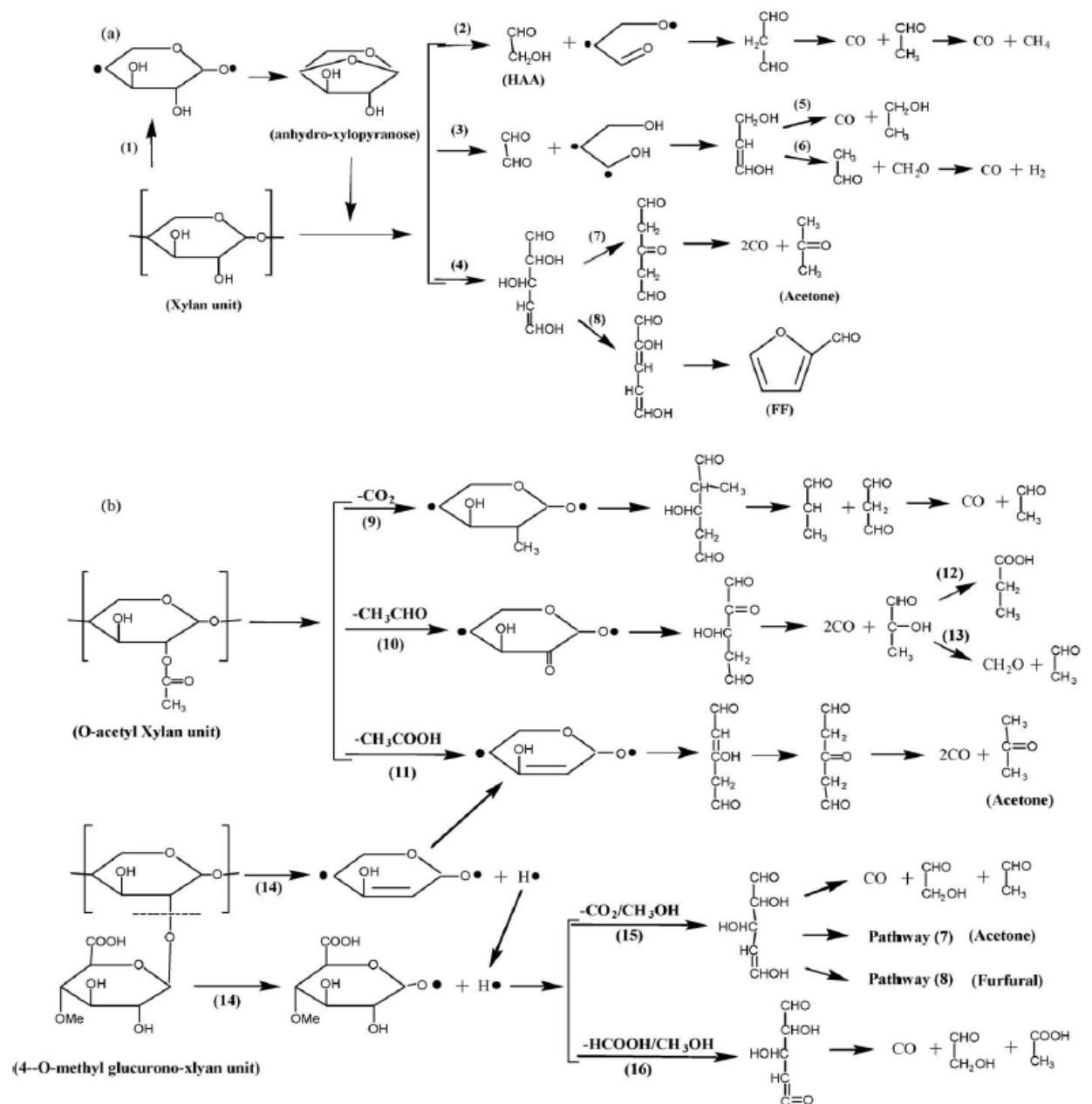


Figure 4-25 Proposed pathway for xylan pyrolytic degradation, from [68]

Lignin degradation has also been studied and decomposition pathways as well as products have been proposed [73, 89, 90]. The primary decomposition products of lignin which is an aromatic polymer includes: guaiacols, syringols, other mono-aromatic compounds and char. Secondary cracking and reactions including homolysis, results in the formation of lighter volatiles, gases such CH₄, and coke. Figure 4-26 shows a proposed degradation pathway for lignin.

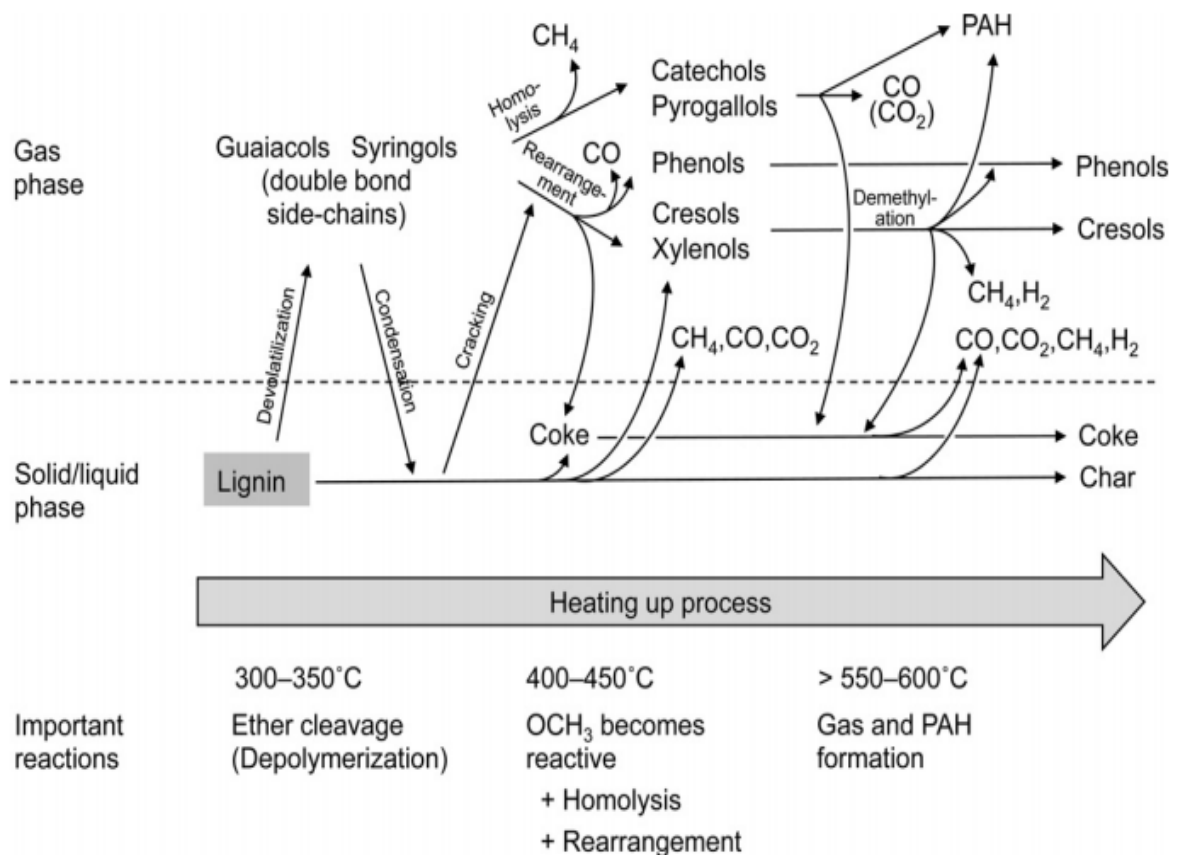
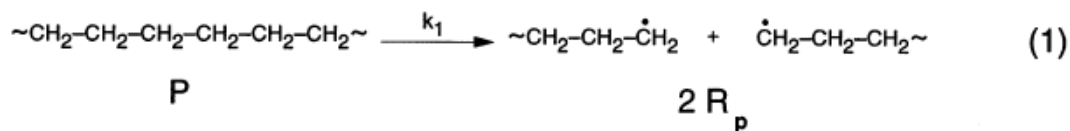


Figure 4-26 Proposed pathway for lignin degradation, from [73]

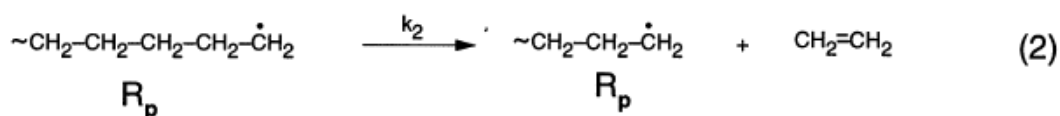
Polyethylene degradation has been extensively studied [91-94] and its decomposition pathways, primary and secondary products have been proposed. The primary decomposition products of polyethylene include condensable and gaseous olefins. Secondary cracking and reactions including re-combination and hydrogen transfer reactions result in the production of alkenes, alkanes and gases. Further secondary cracking and

Diels-Alder reactions result in more alkenes, gases and aromatics. Figure 4-27 shows the proposed degradation pathway for polyethylene.

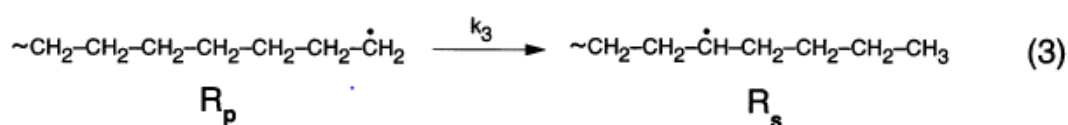
initiation:



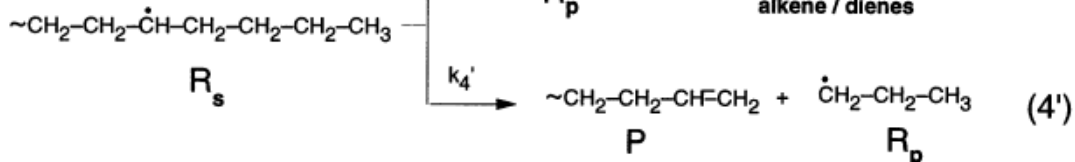
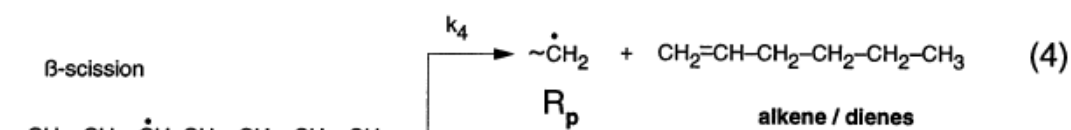
propagation:



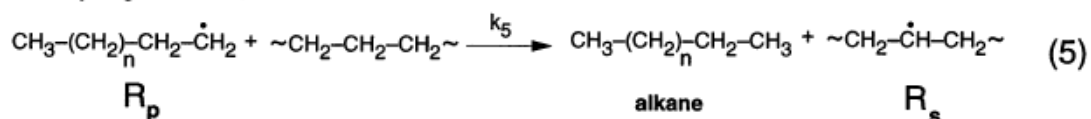
hydrogen transfer, intramolecular



β -scission



hydrogen transfer, intermolecular



termination (2nd order): recombination

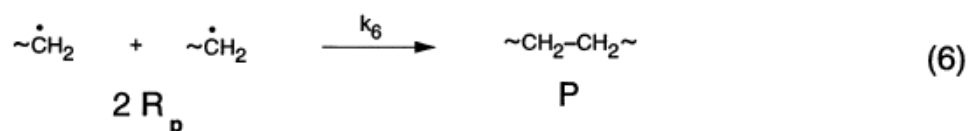


Figure 4-27 Proposed degradation pathway for polyethylene from [94]

References

1. Buah, W.K., A.M. Cunliffe, and P.T. Williams, *Characterization of Products from the Pyrolysis of Municipal Solid Waste*. Process Safety and Environmental Protection, 2007. **85**(5): p. 450-457.
2. Sørum, L., M.G. Grønli, and J.E. Hustad, *Pyrolysis characteristics and kinetics of municipal solid wastes*. Fuel, 2001. **80**(9): p. 1217-1227.
3. Williams, P.T. and S. Besler, *The influence of temperature and heating rate on the slow pyrolysis of biomass*. Renewable Energy, 1996. **7**(3): p. 233-250.
4. Lin, K.-S., et al., *Pyrolysis kinetics of refuse-derived fuel*. Fuel Processing Technology, 1999. **60**(2): p. 103-110.
5. Li, S., et al., *Fast pyrolysis of biomass in free-fall reactor for hydrogen-rich gas*. Fuel Processing Technology, 2004. **85**(8-10): p. 1201-1211.
6. Lapuerta, M.n., J.J. Hernández, and J.n. Rodríguez, *Kinetics of devolatilisation of forestry wastes from thermogravimetric analysis*. Biomass and Bioenergy, 2004. **27**(4): p. 385-391.
7. Fang, M.X., et al., *Kinetic study on pyrolysis and combustion of wood under different oxygen concentrations by using TG-FTIR analysis*. Journal of Analytical and Applied Pyrolysis, 2006. **77**(1): p. 22-27.
8. Zabaniotou, A., et al., *Experimental study of pyrolysis for potential energy, hydrogen and carbon material production from lignocellulosic biomass*. International Journal of Hydrogen Energy, 2008. **33**(10): p. 2433-2444.
9. Bridgwater, A.V., *Principles and practice of biomass fast pyrolysis processes for liquids*. Journal of Analytical and Applied Pyrolysis, 1999. **51**(1-2): p. 3-22.
10. shafizadeh, F., *Chemistry of pyrolysis and combustion of wood*. Progress in biomass conversion, 1982.
11. Bridgwater, A.V., *Waste incineration and pyrolysis*. Resource Recovery and Conservation, 1980. **5**(1): p. 99-115.
12. García, A.N., R. Font, and A. Marcilla, *Kinetic study of the flash pyrolysis of municipal solid waste in a fluidized bed reactor at high temperature*. Journal of Analytical and Applied Pyrolysis, 1995. **31**: p. 101-121.
13. Garcia, A.N., R. Font, and A. Marcilla, *Gas Production by Pyrolysis of Municipal Solid Waste at High Temperature in a Fluidized Bed Reactor*. Energy & Fuels, 1995. **9**(4): p. 648-658.
14. Arabiourrutia, M., et al., *Characterization of the waxes obtained by the pyrolysis of polyolefin plastics in a conical spouted bed reactor*. Journal of Analytical and Applied Pyrolysis, 2012. **94**(0): p. 230-237.
15. Miranda, R., et al., *Vacuum pyrolysis of commingled plastics containing PVC II. Product analysis*. Polymer Degradation and Stability, 2001. **73**(1): p. 47-67.
16. Marcilla, A., M.d.R. Hernández, and Á.N. García, *Study of the polymer-catalyst contact effectivity and the heating rate influence on the HDPE pyrolysis*. Journal of Analytical and Applied Pyrolysis, 2007. **79**(1-2): p. 424-432.
17. Luo, S., et al., *Effect of particle size on pyrolysis of single-component municipal solid waste in fixed bed reactor*. International Journal of Hydrogen Energy, 2010. **35**(1): p. 93-97.
18. Adrados, A., et al., *Pyrolysis behavior of different type of materials contained in the rejects of packaging waste sorting plants*. Waste Management, 2013. **33**(1): p. 52-59.

19. Wampler, T.P., ed. *Applied pyrolysis handbook*. 2nd ed. 2007, Taylor & Francis group: USA. 288.
20. Streitwieser, A., C.H. Heathcock, and E.M. Kosower, *Introduction to organic chemistry*. 4th ed. 1992, USA: Macmillan Publishing Company. 1256.
21. Guoxin, H., H. Hao, and L. Yanhong, *Hydrogen-Rich Gas Production from Pyrolysis of Biomass in an Autogenerated Steam Atmosphere*. *Energy & Fuels*, 2009. **23**(3): p. 1748-1753.
22. Kantarelis, E., et al., *Sustainable valorization of plastic wastes for energy with environmental safety via High-Temperature Pyrolysis (HTP) and High-Temperature Steam Gasification (HTSG)*. *Journal of Hazardous Materials*, 2009. **167**(1-3): p. 675-684.
23. Wei, L., et al., *Characteristics of fast pyrolysis of biomass in a free fall reactor*. *Fuel Processing Technology*, 2006. **87**(10): p. 863-871.
24. Williams, P.T. and S. Besler, *Polycyclic aromatic hydrocarbons in waste derived pyrolytic oils*. *Journal of Analytical and Applied Pyrolysis*, 1994. **30**(1): p. 17-33.
25. Piskorz, J., D. Radlein, and D.S. Scott, *On the mechanism of the rapid pyrolysis of cellulose*. *Journal of Analytical and Applied Pyrolysis*, 1986. **9**(2): p. 121-137.
26. Ahmed, I. and A.K. Gupta, *Syngas yield during pyrolysis and steam gasification of paper*. *Applied Energy*, 2009. **86**(9): p. 1813-1821.
27. Phan, A.N., et al., *Characterisation of slow pyrolysis products from segregated wastes for energy production*. *Journal of Analytical and Applied Pyrolysis*, 2008. **81**(1): p. 65-71.
28. Wu, C.-H., C.-Y. Chang, and C.-H. Tseng, *Pyrolysis products of uncoated printing and writing paper of MSW*. *Fuel*, 2002. **81**(6): p. 719-725.
29. Hall, W.J. and P.T. Williams, *Analysis of products from the pyrolysis of plastics recovered from the commercial scale recycling of waste electrical and electronic equipment*. *Journal of Analytical and Applied Pyrolysis*, 2007. **79**(1-2): p. 375-386.
30. Grieco, E.M. and G. Baldi, *Pyrolysis of polyethylene mixed with paper and wood: Interaction effects on tar, char and gas yields*. *Waste Management*, 2012. **32**(5): p. 833-839.
31. Cozzani, V., et al., *A Fundamental Study on Conventional Pyrolysis of a Refuse-Derived Fuel*. *Industrial & Engineering Chemistry Research*, 1995. **34**(6): p. 2006-2020.
32. Desbène, P.L., et al., *Analysis of biomass pyrolysis oils by a combination of various liquid chromatographic techniques and gas chromatography-mass spectrometry*. *Journal of Chromatography A*, 1991. **553**(0): p. 211-221.
33. Miskolczi, N., et al., *Two stages catalytic pyrolysis of refuse derived fuel: Production of biofuel via syncrude*. *Bioresource Technology*, 2010. **101**(22): p. 8881-8890.
34. Ates, F. and M.A. Isikdag, *Influence of temperature and alumina catalyst on pyrolysis of corncob*. *Fuel*, 2009. **88**(10): p. 1991-1997.
35. Koo, J.-K., S.-W. Kim, and Y.-H. Seo, *Characterization of aromatic hydrocarbon formation from pyrolysis of polyethylene-polystyrene mixtures*. *Resources, Conservation and Recycling*, 1991. **5**(4): p. 365-382.
36. Cypres, R., *Aromatic-Hydrocarbons Formation during Coal Pyrolysis*. *Fuel Processing Technology*, 1987. **15**(0): p. 1-15.

37. Galletti, G.C., et al., *Pyrolysis products as markers in the chemical characterization of paperboards from waste paper and wheat straw pulps*. *Bioresource Technology*, 1997. **60**(1): p. 51-58.
38. Wu, C.-H., et al., *Pyrolysis product distribution of waste newspaper in MSW*. *Journal of Analytical and Applied Pyrolysis*, 2003. **67**(1): p. 41-53.
39. Hajaligol, M., B. Waymack, and D. Kellogg, *Low temperature formation of aromatic hydrocarbon from pyrolysis of cellulosic materials*. *Fuel*, 2001. **80**(12): p. 1799-1807.
40. Williams, P.T. and E.A. Williams, *Fluidised bed pyrolysis of low density polyethylene to produce petrochemical feedstock*. *Journal of Analytical and Applied Pyrolysis*, 1999. **51**(1-2): p. 107-126.
41. Zanzi, R., K. Sjöström, and E. Björnbom, *Rapid high-temperature pyrolysis of biomass in a free-fall reactor*. *Fuel*, 1996. **75**(5): p. 545-550.
42. Dou, B., et al., *Pyrolysis Characteristics of Refuse Derived Fuel in a Pilot-Scale Unit*. *Energy & Fuels*, 2007. **21**(6): p. 3730-3734.
43. Cozzani, V., et al., *Modeling and Experimental Verification of Physical and Chemical Processes during Pyrolysis of a Refuse-Derived Fuel*. *Industrial & Engineering Chemistry Research*, 1996. **35**(1): p. 90-98.
44. He, M., et al., *Syngas production from pyrolysis of municipal solid waste (MSW) with dolomite as downstream catalysts*. *Journal of Analytical and Applied Pyrolysis*, 2009. **87**(2): p. 181-187.
45. Demirbas, A., *Yields of hydrogen-rich gaseous products via pyrolysis from selected biomass samples*. *Fuel*, 2001. **80**(13): p. 1885-1891.
46. Karaduman, A., et al., *Flash pyrolysis of polystyrene wastes in a free-fall reactor under vacuum*. *Journal of Analytical and Applied Pyrolysis*, 2001. **60**(2): p. 179-186.
47. Zanzi, R., K. Sjöström, and E. Björnbom, *Rapid pyrolysis of agricultural residues at high temperature*. *Biomass and Bioenergy*, 2002. **23**(5): p. 357-366.
48. Xianwen, D., et al., *The Fast Pyrolysis of Biomass in CFB Reactor*. *Energy & Fuels*, 2000. **14**(3): p. 552-557.
49. Balat, M., *Hydrogen-Rich Gas Production from Biomass via Pyrolysis and Gasification Processes and Effects of Catalyst on Hydrogen Yield*, 2008, Taylor & Francis. p. 552 - 564.
50. Bridgwater, A.V., *Renewable fuels and chemicals by thermal processing of biomass*. *Chemical Engineering Journal*, 2003. **91**(2-3): p. 87-102.
51. Demirbas, A., *Biomass resource facilities and biomass conversion processing for fuels and chemicals*. *Energy Conversion and Management*, 2001. **42**(11): p. 1357-1378.
52. Duman, G., et al., *The slow and fast pyrolysis of cherry seed*. *Bioresource Technology*, 2011. **102**(2): p. 1869-1878.
53. Chen, G., et al., *Biomass pyrolysis/gasification for product gas production: the overall investigation of parametric effects*. *Energy Conversion and Management*, 2003. **44**(11): p. 1875-1884.
54. Beis, S.H., Ö. Onay, and Ö.M. Koçkar, *Fixed-bed pyrolysis of safflower seed: influence of pyrolysis parameters on product yields and compositions*. *Renewable Energy*, 2002. **26**(1): p. 21-32.
55. Becidan, M., Ø. Skreiberg, and J.E. Hustad, *Products distribution and gas release in pyrolysis of thermally thick biomass residues samples*. *Journal of Analytical and Applied Pyrolysis*, 2007. **78**(1): p. 207-213.

56. Ayllón, M., et al., *Influence of temperature and heating rate on the fixed bed pyrolysis of meat and bone meal*. Chemical Engineering Journal, 2006. **121**(2–3): p. 85-96.
57. Williams, P.T., S. Besler, and D.T. Taylor, *The pyrolysis of scrap automotive tyres: The influence of temperature and heating rate on product composition*. Fuel, 1990. **69**(12): p. 1474-1482.
58. Weinstetn, M. and A. Broido, *Pyrolysis-Crystallinity Relationships in Cellulose*. Combustion Science and Technology, 1970. **1**(4): p. 287-292.
59. Hoekstra, E., et al., *Fast pyrolysis in a novel wire-mesh reactor: Decomposition of pine wood and model compounds*. Chemical Engineering Journal, 2012. **187**(0): p. 172-184.
60. Greenhalf, C.E., et al., *Sequential pyrolysis of willow SRC at low and high heating rates – Implications for selective pyrolysis*. Fuel, 2012. **93**(0): p. 692-702.
61. Shen, D.K., S. Gu, and A.V. Bridgwater, *The thermal performance of the polysaccharides extracted from hardwood: Cellulose and hemicellulose*. Carbohydrate Polymers, 2010. **82**(1): p. 39-45.
62. Caballero, J.A., R. Font, and A. Marcilla, *Study of the primary pyrolysis of Kraft lignin at high heating rates: yields and kinetics*. Journal of Analytical and Applied Pyrolysis, 1996. **36**(2): p. 159-178.
63. Burhenne, L., et al., *The effect of the biomass components lignin, cellulose and hemicellulose on TGA and fixed bed pyrolysis*. Journal of Analytical and Applied Pyrolysis, 2013(0).
64. Radlein, D., ed. *Study of Levoglucosan*. Fast Pyrolysis of Biomass: A Handbook, ed. A.V. Bridgwater, et al. Vol. 2. 2002, CPL Press: Newbury, UK. 165.
65. Beaumont, O. and Y. Schwob, *Influence of physical and chemical parameters on wood pyrolysis*. Industrial & Engineering Chemistry Process Design and Development, 1984. **23**(4): p. 637-641.
66. Meesri, C. and B. Moghtaderi, *Lack of synergetic effects in the pyrolytic characteristics of woody biomass/coal blends under low and high heating rate regimes*. Biomass and Bioenergy, 2002. **23**(1): p. 55-66.
67. Li, S., et al., *Real-time evolved gas analysis by FTIR method: an experimental study of cellulose pyrolysis*. Fuel, 2001. **80**(12): p. 1809-1817.
68. Shen, D.K., S. Gu, and A.V. Bridgwater, *Study on the pyrolytic behaviour of xylan-based hemicellulose using TG-FTIR and Py-GC-FTIR*. Journal of Analytical and Applied Pyrolysis, 2010. **87**(2): p. 199-206.
69. Yang, H., et al., *Characteristics of hemicellulose, cellulose and lignin pyrolysis*. Fuel, 2007. **86**(12–13): p. 1781-1788.
70. Wang, S., et al., *Comparison of the pyrolysis behavior of lignins from different tree species*. Biotechnology Advances, 2009. **27**(5): p. 562-567.
71. Yu, Q., et al., *Temperature impact on the formation of tar from biomass pyrolysis in a free-fall reactor*. Journal of Analytical and Applied Pyrolysis, 1997. **40–41**(0): p. 481-489.
72. Windt, M., et al., *Micro-pyrolysis of technical lignins in a new modular rig and product analysis by GC-MS/FID and GC x GC-TOFMS/FID*. Journal of Analytical and Applied Pyrolysis, 2009. **85**(1–2): p. 38-46.
73. Asmadi, M., H. Kawamoto, and S. Saka, *Gas- and solid/liquid-phase reactions during pyrolysis of softwood and hardwood lignins*. Journal of Analytical and Applied Pyrolysis, 2011. **92**(2): p. 417-425.

74. Kim, M.R., et al., *The Thermochemical Processing of Municipal Solid Wastes: Thermal Events and the Kinetics of Pyrolysis*. Energy Sources, Part A: Recovery, Utilization, and Environmental Effects, 2010. **32**(13): p. 1207-1214.
75. Zheng, J., et al., *Pyrolysis characteristics of organic components of municipal solid waste at high heating rates*. Waste Management, 2009. **29**(3): p. 1089-1094.
76. Caglar, A. and B. Aydinli, *Isothermal co-pyrolysis of hazelnut shell and ultra-high molecular weight polyethylene: The effect of temperature and composition on the amount of pyrolysis products*. Journal of Analytical and Applied Pyrolysis, 2009. **86**(2): p. 304-309.
77. Dong, C., et al., *The pyrolysis of sawdust and polyethylene in TG and U-shape tube reactor*. Waste Management, 2007. **27**(11): p. 1557-1561.
78. Jakab, E., G. Várhegyi, and O. Faix, *Thermal decomposition of polypropylene in the presence of wood-derived materials*. Journal of Analytical and Applied Pyrolysis, 2000. **56**(2): p. 273-285.
79. Williams, P.T. and E.A. Williams, *Interaction of Plastics in Mixed-Plastics Pyrolysis*. Energy & Fuels, 1998. **13**(1): p. 188-196.
80. Faravelli, T., et al., *Kinetic modeling of the thermal degradation of polyethylene and polystyrene mixtures*. Journal of Analytical and Applied Pyrolysis, 2003. **70**(2): p. 761-777.
81. Hosoya, T., H. Kawamoto, and S. Saka, *Solid/liquid- and vapor-phase interactions between cellulose- and lignin-derived pyrolysis products*. Journal of Analytical and Applied Pyrolysis, 2009. **85**(1-2): p. 237-246.
82. Hosoya, T., H. Kawamoto, and S. Saka, *Cellulose-hemicellulose and cellulose-lignin interactions in wood pyrolysis at gasification temperature*. Journal of Analytical and Applied Pyrolysis, 2007. **80**(1): p. 118-125.
83. Lv, D., et al., *Effect of cellulose, lignin, alkali and alkaline earth metallic species on biomass pyrolysis and gasification*. Fuel Processing Technology, 2010. **91**(8): p. 903-909.
84. Helsen, L., et al., *Low-temperature pyrolysis of CCA-treated wood: thermogravimetric analysis*. Journal of Analytical and Applied Pyrolysis, 1999. **52**(1): p. 65-86.
85. Fairburn, J.A., L.A. Behie, and W.Y. Svrcek, *Ultrapyrolysis of n-hexadecane in a novel micro-reactor*. Fuel, 1990. **69**(12): p. 1537-1545.
86. Radlein, D., J. Piskorz, and D.S. Scott, *Fast pyrolysis of natural polysaccharides as a potential industrial process*. Journal of Analytical and Applied Pyrolysis, 1991. **19**(0): p. 41-63.
87. Antal, M.J., Jr. and G. Varhegyi, *Cellulose Pyrolysis Kinetics: The Current State of Knowledge*. Industrial & Engineering Chemistry Research, 1995. **34**(3): p. 703-717.
88. Di Blasi, C. and M. Lanzetta, *Intrinsic kinetics of isothermal xylan degradation in inert atmosphere*. Journal of Analytical and Applied Pyrolysis, 1997. **40-41**(0): p. 287-303.
89. Alén, R., E. Kuoppala, and P. Oesch, *Formation of the main degradation compound groups from wood and its components during pyrolysis*. Journal of Analytical and Applied Pyrolysis, 1996. **36**(2): p. 137-148.
90. Kawamoto, H., M. Ryoritani, and S. Saka, *Different pyrolytic cleavage mechanisms of β -ether bond depending on the side-chain structure of lignin dimers*. Journal of Analytical and Applied Pyrolysis, 2008. **81**(1): p. 88-94.

91. Kiran, E. and J.K. Gillham, *Pyrolysis–molecular weight chromatography–vapor-phase infrared spectrophotometry: A new on-line system for analysis of polymers. I. Instrumentation.* Journal of Applied Polymer Science, 1976. **20**(4): p. 931-947.
92. Kiran, E. and J.K. Gillham, *Pyrolysis-molecular weight chromatography: A new on-line system for analysis of polymers. II. Thermal decomposition of polyolefins: Polyethylene, polypropylene, polyisobutylene.* Journal of Applied Polymer Science, 1976. **20**(8): p. 2045-2068.
93. Ballice, L., *A kinetic approach to the temperature-programmed pyrolysis of low- and high-density polyethylene in a fixed bed reactor: determination of kinetic parameters for the evolution of n-paraffins and 1-olefins.* Fuel, 2001. **80**(13): p. 1923-1935.
94. Bockhorn, H., et al., *Kinetic study on the thermal degradation of polypropylene and polyethylene.* Journal of Analytical and Applied Pyrolysis, 1999. **48**(2): p. 93-109.

CHAPTER 5. PYROLYSIS AND GASIFICATION OF WASTE WOOD IN A SCREW KILN REACTOR

5.1 Influence of process conditions on the two stage pyrolysis and steam only gasification of waste wood.

The waste wood sample was investigated for two stage pyrolysis only and steam only gasification in the screw-kiln reactor. The effect of pyrolysis temperature was investigated for the two stage pyrolysis of the waste wood.

The process conditions investigated for the steam gasification experiments were the effect of different second stage reactor temperatures (700, 800, 900 °C) and the effects of different steam to waste wood ratios (0.2, 0.4, 0.8 and 1). Experiments were carried out using samples of particle sizes of 3mm to 9mm, however an experiment was also conducted using samples of 3mm particle size for two stage pyrolysis in order to investigate its effect on the products. The experimental procedure detailed in section 3.3.3 was used for all experiments.

5.1.1 Effects of temperature during two stage pyrolysis of waste wood

The effects of varying the first stage reactor temperatures (500 and 700 °C) while keeping the second stage fixed bed reactor temperature at 800 °C, as well as varying the second stage fixed bed reactor temperature (700, 800 and 900 °C) while keeping the first stage reactor temperature at 700 °C were investigated in order to identify the temperature effects on the pyrolysis product yields and gas compositions. Table 5-1 shows results from varying the pyrolysis temperatures.

5.1.1.1 Product yields

Table 5-1 shows that increasing the first stage reactor temperature from 500 to 700 °C while keeping the second stage reactor temperature at 800 °C resulted in increased gas yields while the solid and oil yield reduced. Table 5-1 also shows that increasing the second stage reactor temperature from 700 to 900 °C while keeping the first stage temperature at 700 °C had no significant impacts on the product yields.

Table 5-1

Effects of varying first and second stage temperatures during pyrolysis

Screw kiln temperature (°C)	500 ^a	500	700	700	700
Fixed bed temperature (°C)	800	800	700	800	900
Sample feed rate (g min ⁻¹)	8	8	8	8	8
Products	Yield (wt % of waste wood)				
Gas	42.9	19.5	48.1	49.3	49.6
Solid	17.5	36.5	12.8	15.3	12.8
Oil (by difference)	39.6	44.0	39.1	35.5	37.6
Gas composition (N ₂ free)	Yield (wt % of waste wood)				
H ₂	0.3	0.2	0.6	0.6	0.7
CO	28.3	11.8	29.9	31.4	30.6
CO ₂	7.8	4.3	10.3	10.0	10.8
CH ₄	3.5	1.6	3.8	4.0	4.3
C ₂ - C ₄	3.0	1.6	3.1	3.6	3.2
Gas composition (N ₂ free)	Yield (vol %)				
H ₂	9.7	13.1	14.4	15.1	17.2
CO	60.8	54.3	55.4	55.9	53.0
CO ₂	10.7	12.6	12.1	11.3	11.9
CH ₄	13.0	13.2	12.2	12.4	13.1
C ₂ - C ₄	5.9	6.8	5.9	5.2	4.7

^a: 3mm waste wood particles,

The results show a more pronounced effect of increasing the first stage reactor temperature from 500 to 700 °C, in terms of the gas yield, than for increasing the second stage fixed bed reactor temperature from 700 to 900 °C. With increasing temperature from 500 to 700 °C the gas yield increased from 19.5 to 49.3 wt%, solids yield reduced from 36.5 to 15.3 wt% while the oil yield reduced from 44 to 35.5 wt%. This was mostly due to the conversion of

more of the solid product into gases, as well as the conversion of the produced oil to gases. At 500 °C, the waste wood samples were not completely pyrolysed leading to a higher yield of solid products however a combination of the higher temperature (700 °C) and the solids residence time within the first stage screw kiln reactor resulted in higher solids conversion. This is supported by figures 5-1 and 5-2 which shows TGA analyses for the solid product from waste wood pyrolysis at first stage reactor temperatures of 500 and 700 °C, respectively. The figures show that the solid product from pyrolysis at first stage temperature of 500 °C contained more volatiles (≈ 52 wt% of volatiles) than that from pyrolysis at 700 °C (≈ 10 wt% of volatiles).

Increasing the second stage fixed bed reactor temperature had no notable impacts on the product yield. This was probably due to high mass flow rates of volatiles through the second stage fixed bed reactor after they had been released during pyrolysis in the first stage reactor, resulting in minimal impacts of the temperature variation. A second stage fixed bed reactor temperature of 800 °C was adopted as the process temperature for further gasification experiments on reviewing the literatures [1-2].

In order to confirm the impacts of the waste wood particles sizes on the product yield, waste wood samples of 2 - 3 mm particle sizes were pyrolysed at first stage temperature of 500 °C and second stage temperature of 800 °C. The results are also shown in table 5-1. The results showed that pyrolysis of the 3mm waste wood particles produced more gas, less solids and less oil compared to the pyrolysis of the 3 – 9 mm particle size at the same conditions. The increased gas yield noted from the pyrolysis products of the 3 mm particle size was mostly due to increased solid conversion, showing that higher solids yield for the 3 – 9 mm particles was as a result of the presence of larger particles.

An operating temperature of 700 °C was therefore chosen as the optimum first stage reactor temperature for the pyrolysis of the waste wood of particle sizes of 3 – 9 mm which were used for all further experiments.

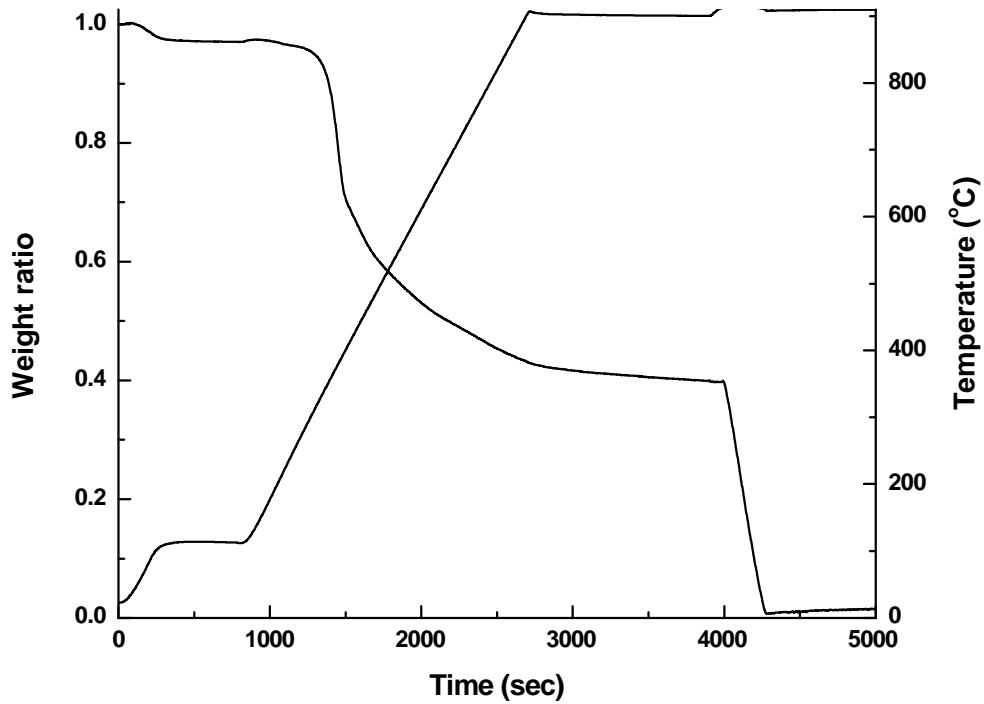


Figure 5-1 TGA analysis of solid product from first stage reactor temperature of 500 °C.

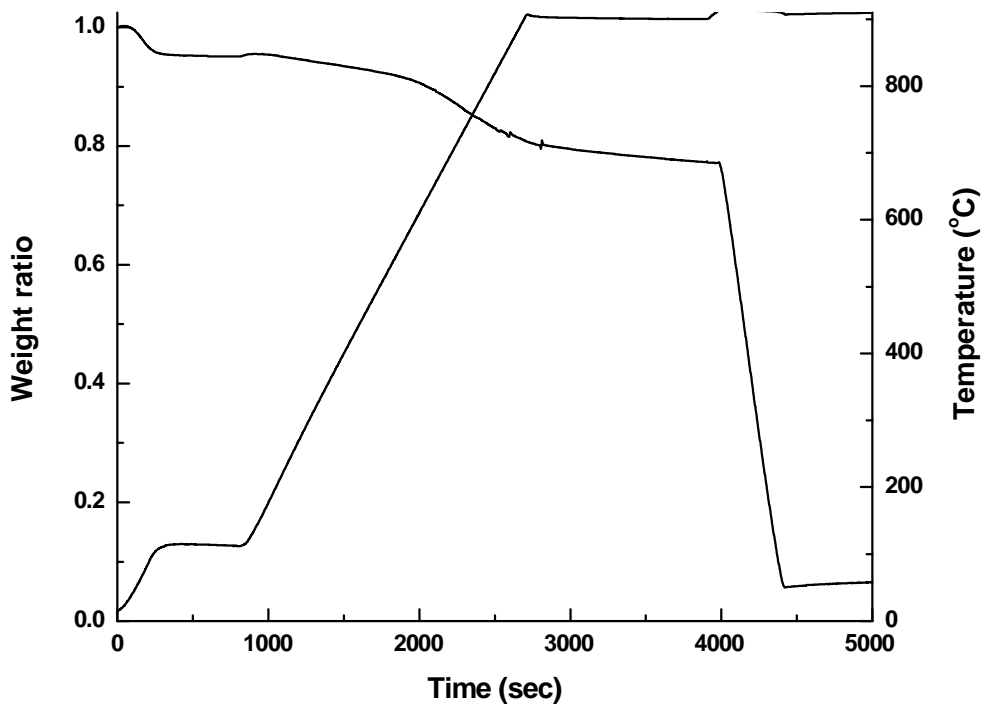


Figure 5-2 TGA analysis of solid product from pyrolysis at first stage temperature of 700 °C.

5.1.1.2 Gas composition and hydrogen yield

Increasing the first stage temperature from 500 °C to 700 °C, while keeping the second stage fixed bed temperature at 800 °C, resulted in mass yield increases as well as volumetric compositional differences in the gas components. The hydrogen yield increased from 0.2 to 0.6 wt% due to the temperature increase. Increasing the second stage temperature from 700 to 900 °C while keeping the first stage temperature at 700 °C, did not result in any notable differences in the gas composition.

The pyrolysis of waste wood samples of 2 - 3 mm particle sizes at the first stage reactor temperature of 500 °C and second stage fixed bed reactor temperature of 800 °C, resulted in a higher mass yield of each of the gas components, compared to the pyrolysis of samples of 3 – 9 mm particles sizes at the same reactor temperatures. The hydrogen yield was 0.3 wt% for the 2 - 3 mm particles compared to 0.2 wt% for the 3 – 9 mm particles for the same pyrolysis conditions. The most abundant gas component detected from all the process conditions investigated was CO as expected due to the oxygenate contents of wood [3-5].

5.1.2 Effects of temperature and steam to waste wood ratio on the steam only pyrolysis-gasification of waste wood

Steam pyrolysis-gasification of waste wood at different fixed bed reactor temperatures and at different steam to waste wood ratios were investigated in order to study the impacts of these conditions on gas and hydrogen productions, as well as to establish the optimum operating conditions for gas and hydrogen production from steam pyrolysis-gasification.

Experiments to investigate the effects of steam to waste wood ratio were carried out at a screw kiln reactor temperature of 700 °C and at a second stage fixed bed reactor temperature of 800 °C, while the steam to biomass ratio was varied between 0.2, 0.4, 0.8 and 1 by adjusting the flow rate of water

being injected by the syringe pump from 1.7, 3.3, 6.6 and 8 g min⁻¹ respectively.

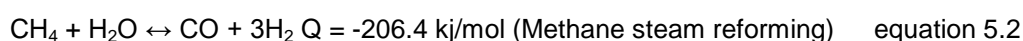
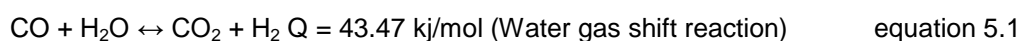
For the experiments to investigate the effects of gasification temperature, the steam to biomass ratio was kept at 0.8 (adopted from He et al [6]), the first stage screw kiln reactor temperature was kept at 700 °C while the second stage fixed bed reactor temperature was varied between 700, 800 and 900 °C.

The reactor design allowed for the gasification step which proceeds the pyrolysis reactions, to be separated. During the process only the pyrolysis volatiles are gasified, due to the reactor design, preventing the gasification of the solid char. The solid char is therefore available for other uses such as a fuel, catalyst or the production of activated carbon.

5.1.2.1 Product yields

The results of varying the steam to waste wood ratio are shown in table 5-2 which indicates that there was no strong impact on the product yield from varying the steam to biomass ratio from 0.2 to 1.

The effects of steam to waste ratio have been investigated and reported by other researchers [7-12]. [8-11, 13] reported increase in gas yield with increasing steam to feedstock ratio up to an optimal point after which no further increase was noted. The introduction of steam during gasification at high temperature promotes steam reforming reactions of hydrocarbons and the water gas shift reactions as shown in equations 5.1 and 5.2.



The endothermic nature of steam generation from water during gasification [8] could lower the reactor temperature [9] and therefore compete with the

endothermic reactions of hydrocarbon reforming, when more than the optimum quantity of steam is injected. This also explains the slightly lower gas yield for the gasification experiment compared to pyrolysis, due to the higher mass flow rate (13.5 g min^{-1}) of combined volatile and steam feed for gasification at steam to waste wood ratio of 0.8.

Increasing the gasification temperature from 700 to 900 °C had no notable impacts on the product yields as shown in table 5-2. The solid yield was unaffected by the gasification conditions due to the reactor design. Other researchers have reported increasing gas yield and decreasing oil yield with increasing gasification temperature [6, 14-15], due to the promotion of the endothermic reactions of tar cracking and steam reforming [9-11].

Table 5-2

Effects of varying the steam to waste wood ratio and second stage temperatures

Screw kiln temperature (°C)	700	700	700	700	700	700
Fixed bed temperature (°C)	800	800	800	800	700	900
Water injection rate (g min^{-1})	1.7	3.3	6.6	8.0	6.6	6.6
Steam to biomass ratio	0.2	0.4	0.8	1	0.8	0.8
Products		Yield (wt % of waste wood)				
Gas	45.6	46.6	48.6	47.8	47.7	49.1
Solid	15.5	12.5	14.3	15.2	14.0	16.5
Oil (by difference)	38.9	40.9	37.1	36.9	38.3	34.4
Gas composition (N_2 free)		Yield (wt % of waste wood)				
H_2	0.5	0.6	0.6	0.6	0.6	0.7
CO	29.0	28.7	30.3	30.1	29.3	31.2
CO_2	8.8	10.2	10.4	10.0	10.5	10.3
CH_4	3.8	3.8	3.8	3.8	3.8	4.0
$\text{C}_2 - \text{C}_4$	3.4	3.4	3.5	3.4	3.5	2.9
Gas composition (N_2 free)		Yield (vol %)				
H_2	14.4	14.6	15.0	15.0	14.6	16.2
CO	56.0	54.7	55.1	55.6	54.7	55.1
CO_2	10.8	12.4	12.1	11.7	12.4	11.6
CH_4	12.9	12.5	12.0	12.2	12.5	12.2
$\text{C}_2 - \text{C}_4$	5.9	5.8	5.7	5.6	5.8	4.9

5.1.2.2 Gas composition and hydrogen yield

Table 5-2 also shows there was little or no impacts of varying the steam to waste wood ratio on the gas composition. Li et al [9], Guan et al [10] and Gao et al [16] reported increased hydrogen production with increasing steam to feedstock ratio, for the steam gasification of palm oil wastes, MSW and biomass respectively.

When the gasification temperature was increased from 700 to 900 °C the hydrogen yields were 0.6 and 0.7 wt%, and 14.6 to 16.2 vol%, indicating that varying the gasification temperature had no significant impacts on the hydrogen yields. Increasing gasification temperature has been reported to result in increased hydrogen yield [7, 11, 15] due to the promotion of endothermic reactions at high temperature [9-10]. The other gaseous components also indicated no significant changes in yield and composition with increasing gasification temperature in the reactor.

The high mass flow rate of volatiles and steam (about 13.5 g min⁻¹ for steam to waste wood ratio of 0.8) through the fixed bed gasifier also has a high heat transfer requirement. In order to achieve a higher volatile conversion to gas, as well as higher hydrogen production, catalysts are required to promote volatile cracking, hydrocarbon reforming and the water-gas shift reaction.

5.1.3 Conclusions

The two stage pyrolysis and steam pyrolysis gasification of waste wood have been investigated in a screw kiln reactor. Different process conditions such as the first and second stage pyrolysis temperatures, gasification temperature and steam to biomass ratio were varied in order to investigate their effects on product yield, product composition and hydrogen yield. The following main conclusions have been drawn:

- Increasing the first stage pyrolysis temperature from 500 to 700 °C during two stage pyrolysis of waste wood resulted in increased gas

yield while the oil and solid yields decreased. Increasing the first stage pyrolysis temperature also impacted the gas composition from waste wood pyrolysis. The CO yield increased significantly while the hydrogen yield increased slightly.

- Increasing the second stage fixed bed reactor temperature from 700 to 900 °C during the two stage pyrolysis of waste wood had no significant impacts on the product yields and gas composition.
- Varying the steam to biomass ratio from 0.2 to 1 during the waste wood steam pyrolysis-gasification at first stage reactor temperature of 700 °C and second stage fixed bed reactor temperature of 900 °C did not have any notable impacts on the product yields and gas composition.
- Increasing the gasification temperature from 700 to 900 °C had no significant impacts on the product yields and gas composition from the steam pyrolysis gasification of waste wood.
- The solids for both two stage pyrolysis and steam pyrolysis-gasification in the screw kiln reactor were consistent due to the reactor design which prevented the gasification of solid char.

5.2 Nickel based catalytic pyrolysis-gasification of waste wood

Nickel has been widely investigated as a catalyst for steam gasification due to its high reactivity, affordability and availability [17-19]. In this section nickel based catalysts were investigated for the steam reforming of the volatiles from waste wood pyrolysis in order to study their impacts on gas yield and hydrogen yield. All catalysts were tested at screw kiln and fixed bed reactor temperature of 700 and 800 °C respectively and steam to waste wood ratio of 0.8.

The impact of varying the nickel loading on the catalyst was studied using Ni Al₂O₃ catalysts synthesised with different loadings of the nickel metal on the alumina support.

The impact of varying the catalyst to waste wood ratio was also studied using different quantities of the Ni Al₂O₃ catalyst while keeping the feed of waste wood and steam constant.

The effects of impregnating the Ni Al₂O₃ catalyst with different metal additives were also investigated in order to study their effects on catalyst activity as well as their impacts on of catalyst deactivation by coke.

5.2.1 Effects of nickel loading and catalyst to waste wood ratio

In order to study the impacts of nickel loading on the alumina support three nickel alumina catalysts annotated as Ni(5) Al₂O₃, Ni(10) Al₂O₃ and Ni(20) Al₂O₃, with different nickel loadings (5, 10 and 20 wt %), were prepared by a wetness method as described in section 3.1.5, and tested for steam pyrolysis-gasification of waste wood.

The effects of catalyst to waste wood ratio was also investigated by using different quantities (20, 40 and 80 grams) of the Ni(20) Al₂O₃ catalyst while all other conditions were kept constant.

5.2.1.1 Product yields

Results from investigating the effects of nickel loading are presented in Table 5-3. The results showed that as the nickel content on the catalyst was increased, the gas yield increased while the tar yield decreased. The gas yield increased from 55.3 to 60.0 to 81.4 wt% when the nickel loading was increased from 5 to 10 to 20 wt%, while the tar yield decreased from 30.9 to 27.5 to 2.1 wt%. As a comparison the results for the non-catalytic steam pyrolysis-gasification was also included in the table and the effect of the nickel catalytic experiment is visible. All the catalytic experiments yielded more gas and less tar than the non-catalytic steam gasification.

Similar results on the effect of nickel loading have been reported by other researchers [20-21]. Akande et al [21] reported increased gas production and activity with increased nickel loading from 10 to 15 %, while further increase of ni loading to 20 wt% yielded no further appreciable gas yield increase, for the steam reforming of ethanol. The increased gas yield from increasing the loading of nickel was due to the increased availability of active catalytic sites on the catalyst surface. This in turn made the catalyst more reactive towards steam gasification since nickel is the active catalytic component.

Investigations on the effects of catalyst to waste wood ratio as presented in Table 5-3 showed that with increasing catalyst to waste wood ratio the gas yield increased while the tar yield decreased. The gas yield increased from 71.8 to 81.4 to 88.4 wt% while the tar yield decreased from 17.2 to 2.1 to 0.1 wt% when the catalyst to waste wood ratio was increased in the range 0.5 to 1 to 2. Similar results have been reported by other researchers for the investigations of steam gasification with varying catalyst quantities [22-24]. Garcia et al [23] reported a decrease in gas yield with decreasing catalyst to biomass ratio for steam gasification of pine saw dust.

Figures 5-3 and 5-4 show the effects of nickel loading and the catalyst to waste wood ratio respectively on the gas yield (m^3 per gram of waste wood). Figures 5-3 and 5-4 show increased gas yield both with increasing nickel loading and increasing catalyst to waste wood ratio as expected. Increasing the catalyst to waste wood ratio resulted in similar effects, on the gas and tar yield, as increasing the nickel loading.

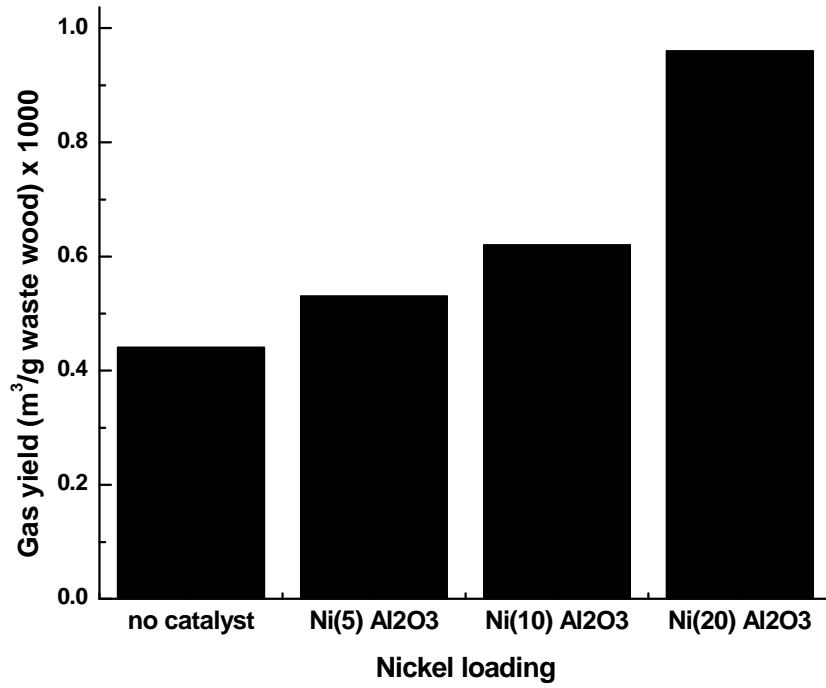


Figure 5-3 Effect of nickel loading on gas yield

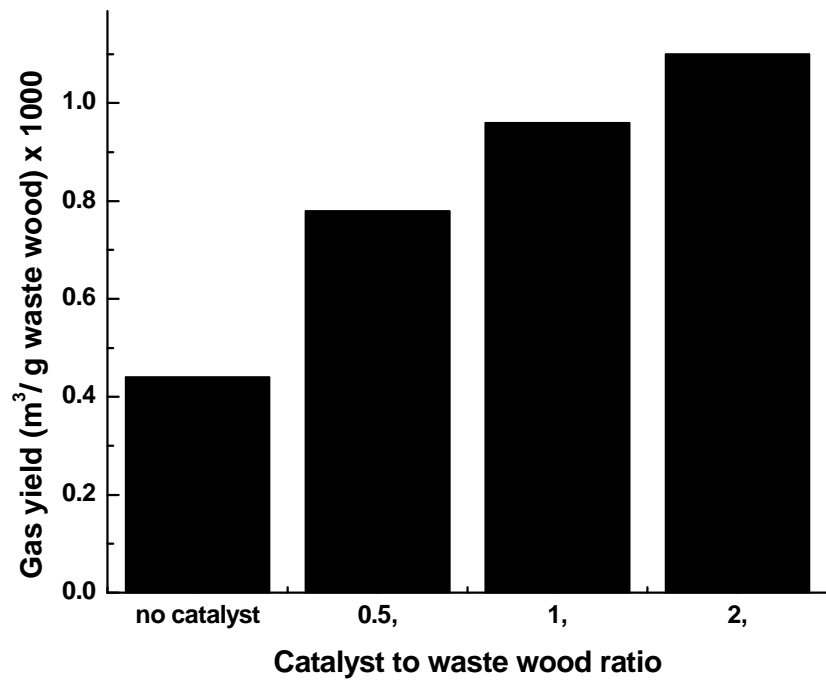


Figure 5-4 Effect of catalyst to waste wood ratio on gas yield

Table 5-3

Effects of varying the nickel loading and the catalyst to waste wood ratio

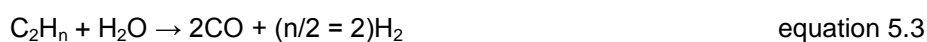
	No catalyst	Ni(5) Al ₂ O ₃	Ni(10) Al ₂ O ₃	Ni(20) Al ₂ O ₃	Ni(20) Al ₂ O ₃	Ni(20) Al ₂ O ₃
Nickel loading	-	5	10	20	20	20
catalyst to biomass ratio	-	1	1	1	0.5	2
Products	Yield (wt % of waste wood)					
Gas	48.6	55.3	60.0	81.4	71.8	88.4
Solid	14.3	13.8	12.5	16.5	11.0	11.5
Oil (by difference)	37.1	30.9	27.5	2.1	17.2	0.1
Gas composition (N ₂ free)	Yield (wt % of waste wood)					
H ₂	0.6	1.1	1.9	4.3	3.0	5.4
CO	30.3	29.7	25.6	23.3	24.6	22.6
CO ₂	10.4	17.1	26.1	51.0	39.4	59.5
CH ₄	3.8	3.9	3.6	2.0	2.5	0.9
C ₂ - C ₄	3.5	3.5	2.7	0.9	2.2	*
Gas composition (N ₂ free)	Yield (vol %)					
H ₂	15.0	23.9	34.1	49.8	42.9	54.8
CO	55.1	44.9	33.2	19.5	25.1	16.5
CO ₂	12.1	16.4	21.5	27.2	25.6	27.6
CH ₄	12.0	10.2	8.2	2.9	4.5	1.1
C ₂ - C ₄	5.7	4.6	3.1	0.6	1.9	0.0
H ₂ / CO	0.3	0.5	1.0	2.6	1.7	3.3

5.2.1.2 Gas composition and hydrogen yield

The effect of nickel loading on the gas composition and hydrogen yield were investigated and are presented in Table 5-3 and this shows that varying the nickel loading had impacts on the gas composition. Results showed that with increasing nickel loading, the hydrogen and CO₂ yield (wt% and vol%) increased while the yields of the other gases decreased. Similar results were reported by Akande et al [21] when the Ni loading was increased from 10 to 15wt% for ethanol steam reforming. The combined increased yields of hydrogen and CO₂ accompanied by a decreased yield of CO indicates an increased promotion of the water-gas shift reaction with increasing nickel loading. While the decreased yield of the hydrocarbon gases indicates that hydrocarbon steam reforming reactions as well as cracking were promoted with the increase in nickel loading. The H₂/CO ratio also increased from 0.5 to 2.6 with increased nickel loading from 5 to 20 wt%. Other researchers [25-27] have also reported increased H₂/CO ratio with increased nickel loading on an alumina support. The increased hydrogen production has been linked to the inhibition of CO forming and methanation reactions due to increased Ni loading [21]. The Ni Al₂O₃ catalyst with an Ni loading of 20 wt% yielded the highest gas and hydrogen during the steam gasification of waste wood.

Increasing the catalyst to waste wood ratio had similar effects on the gas composition and hydrogen yield, as shown also in Table 5-3. Results showed that the hydrogen and CO₂ yields (vol% and wt%) increased while the CO, CH₄ and C₂ – C₄ gases yield decreased with increasing catalyst to waste wood ratio from 0.5 to 2. This indicated both the promotion of the water-gas shift reaction as well as hydrocarbon cracking and steam reforming due to increased catalyst to waste wood ratio. Garcia et al [22] reported increase in H₂ and CO₂ and decrease in the hydrocarbon gases for the steam gasification of biomass with increasing catalyst to biomass ratio. The H₂/CO ratio also increased from 1.7 to 3.3 with increase in the catalyst to waste wood ratio. It was proposed that at low catalyst to waste wood ratios, the H₂ and CO in the reaction atmosphere which interacted with the catalyst was low, resulting in a reduced capacity to initially generate enough catalytic active sites [22]. This

in turn would have resulted in an overall reduced hydrogen production, compared to when the catalyst to waste ratio was higher, as indicated by the results in table 5-3. Bassagiannis et al [28] reported that increasing the catalyst to feedstock ratio promoted the water gas shift reaction (equation 2.5) and the hydrocarbon reforming reactions (equations 5.2 and 5.3).



Figures 5-5 and 5-6 show the effects of nickel loading and catalyst to waste wood ratio respectively on the hydrogen yield (mmol per gram of waste wood).

Increasing the catalyst to waste wood ratio, resulted in similar effects on the hydrogen production, as increasing the nickel loading, because this also increased the availability of nickel catalytically active sites. However with increasing the catalyst to waste wood ratio to 2, there was also the added advantage of more of the catalyst support being available. The bi-functional mechanism for steam reforming of oxygenates over nickel catalyst [24] proposes that steam activation takes place on the support while the activation of the organics occurs on the metal sites. As explained earlier, increasing the catalyst to waste wood ratio resulted in an increase in both the catalytic active sites available for organics activation as well as the catalyst support available for steam activation, thereby promoting the effects of the bi-functional mechanism [29-30]. These effects would promote an increased rate of organics reforming to produce mostly CO while promoting an increased activation of the hydroxyl group. The increased availability of CO and hydroxyl group will further result in an overall promotion of the water gas shift reaction and the increased production of hydrogen. This can explain the increased H₂ production as shown in table 5-3 and figure 5-6 with increasing catalyst to waste ratio.

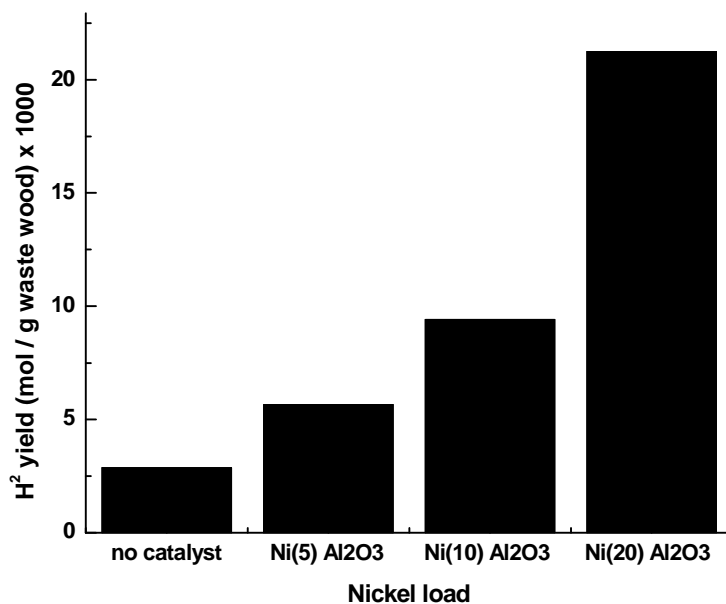


Figure 5-5 Effect of nickel loading on hydrogen yield

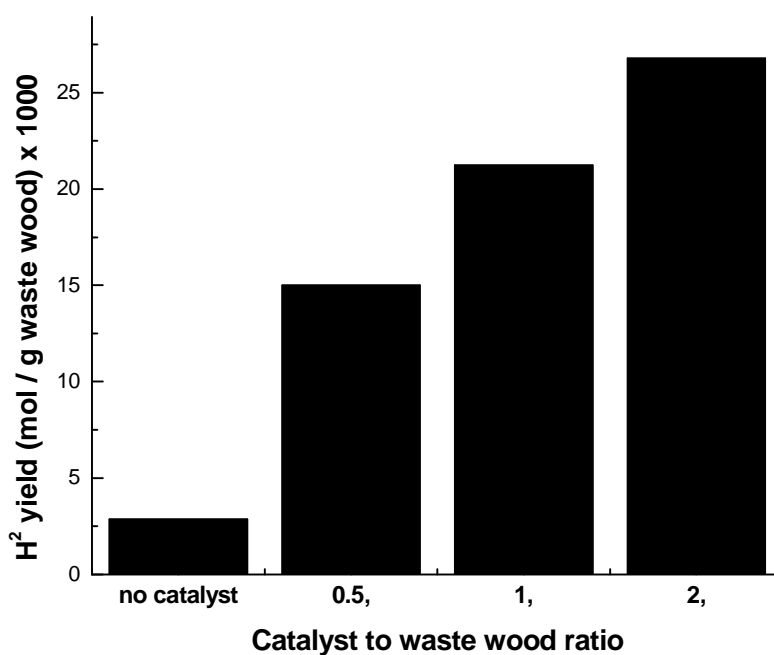


Figure 5-6 Effect of catalyst to waste wood ratio on hydrogen yield.

5.2.1.3 Effect of nickel loading and catalyst to waste wood ratio on tar yields

The tar/oil collected in the condensers from the investigations of the effects of the catalyst to waste wood ratios 0.5, 1 and 2 which were all carried out with the Ni(20) Al₂O₃ catalyst, as well the tar from the experiment investigating the

effect of the Ni(5) Al₂O₃ catalyst were collected and analysed by GC/MS in order to indentify and quantify detected compounds. Further analysis of the data provided information to support the explanations for the process that led to gas and hydrogen production in the reactor. Table 5-4 shows the detected compounds from the tar/oil analyses. The compounds detected included mostly oxygenated and aromatic tars, as well as some aliphatic compounds.

Table 5-4

Tar/oil compounds from steam pyrolysis-gasification of waste wood with Ni Al₂O₃ catalysts with different nickel loading and catalyst to waste wood ratios

Catalyst	$\mu\text{g tar g}^{-1}$ of waste wood			
	Ni(5) Al ₂ O ₃	Ni(20) Al ₂ O ₃	Ni(20) Al ₂ O ₃	Ni(20) Al ₂ O ₃
Nickel loading	5	20	20	20
catalyst to biomass ratio	1	0.5	1	2
Oil compounds	Oxygenates			
2,3,5-Trimethylphenol	197			
4-Isopropylphenol	104			
Dibenzofuran	6734			
2-Phenylphenol	548			
Oil compounds	Aromatics			
Ethylbenzene	13			
Styrene	70			
Alphamethylstyrene		60	3	1
Betamethylstyrene			17	2
Indane	71	33	0.7	<1
Indene		7533	1237	19
Naphthalene	1980	111	2157	96
2-Methylnaphthalene			2101	
Biphenyl	893	37	1157	21
2,2-Diphenylpropane	2081			
Fluorene	1843	1443.5	111	
1,3-Diphenylpropane	2188	0.0		
Phenanthrene	6863	1205		
1-Phenylnaphthalene		59		
Fluoranthene			9	
Pyrene	638	316	22	17
1,3,5-Triphenylbenzene	3159			41
Oil compounds	Alkanes			
Octane, C8	258	99	175	86
Nonacosane, C29		89		
Dotriacontane, C32		89		
Oil compounds	Alkenes			
Nonene, C9	86	176	13	
Decene, C10	99	75	19	2

Table 5-4 continues	Ni(5) Al ₂ O ₃	Ni(20) Al ₂ O ₃	Ni(20) Al ₂ O ₃	Ni(20) Al ₂ O ₃
Undecene, C11	49	12	1	
Dodecene, C12	97	17	2	
Tridecene, C13	37	3	3	
Tetradecene, C14	37	<1	5	
Hexadecene, C16	13	2	<1	
Hepadecene, C17	2		<1	
Pristene	<1			
Octadecene, C18	6			
Nonadecene, C19	2			
Eicosene, C20	<1			
Heneicosene, C21	<1			
total tar/oil $\mu\text{g g}^{-1}$ of waste wood	28066	11359	7033	284

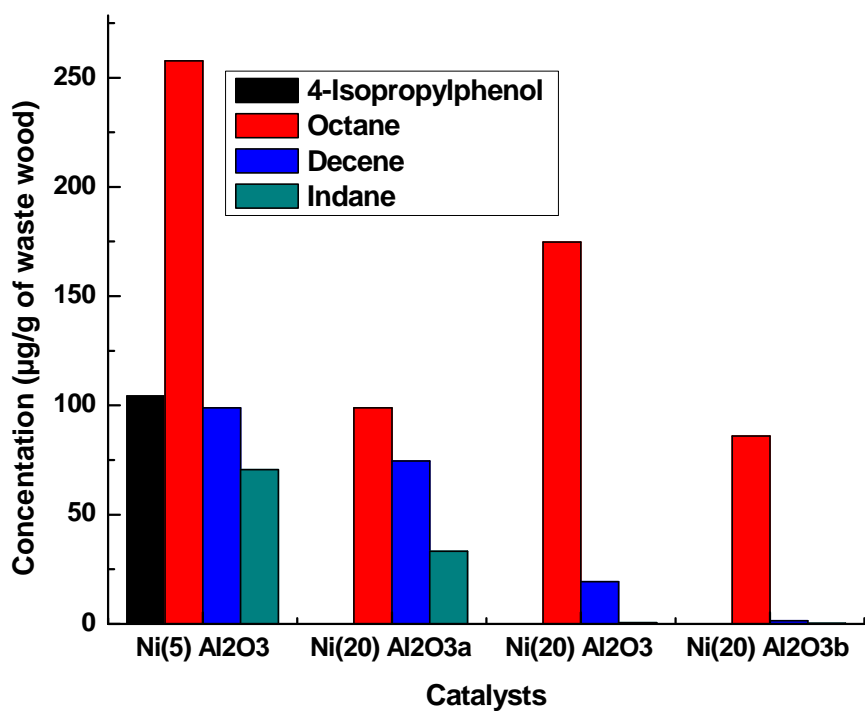


Figure 5-7 Effects of nickel catalysts on tar from waste wood steam pyrolysis-gasification

Table 5-4 shows that the total quantity of tar detected decreased with increasing catalyst to waste wood ratio, and with increasing the nickel loading from 5 to 20 wt%. The total detected tar decreased from 28 to 7 (mg of tar per g of waste wood) with increasing nickel loading, and from 11 to <1 (mg of tar per g of waste wood) with increasing catalyst to waste wood ratio. This represented a 75% reduction in tar with increasing the nickel loading, and a

97% reduction in tar with increasing the catalyst to waste wood ratio. These results are in agreement with the results in Table 5-3 which showed a decrease in tar yield in favour of gas and hydrogen yield, both with increasing the nickel loading and increasing the catalyst to waste wood ratio. Pfeifer et al [31] reported a tar yield of 0.02 g tar m⁻³ of gas for the steam gasification of biomass with a nickel based catalyst. This was comparable to a total tar/oil of about 0.01 g tar m⁻³ of gas achieved for the experiment at catalyst to waste wood ratio of 2 in this study.

The most abundant compounds detected across the samples were aromatics which are secondary products formed during the steam gasification of hydrocarbons [32]. Some of the compounds include naphthalene, phenanthrene, biphenyl and flourene, and these have been identified and reported by other researchers [33] for biomass gasification. Figure 5-7 shows the effects of increasing the Ni loading and the catalyst to waste wood ratio on selected tar compounds which were representative of oxygenate, aliphatic and aromatic compounds. As the catalyst to waste ratio was increased there was a general reduction in quantities of oxygenates, aliphatics and aromatics. The same trend was also observed when the nickel loading was increased. This suggests that increasing the catalyst to waste wood ratio and the nickel loading promoted the thermal degradation of the tar compounds from waste wood gasification as a result of increased catalyst activity [34], in favour of gas production.

5.2.1.4 Catalyst characterization

The fresh and reacted catalysts were analysed using SEM in order to investigate the catalyst surface for coke deposition. Micrographs of the fresh and reacted catalysts were also taken. The SEM images and photographs of the fresh and reacted catalysts were compared in order to identify differences on the surfaces of the catalysts due to the reactions. Figures 5-8 to 5-14 show the SEM images of the analysed fresh and reacted catalysts. The reacted catalysts from investigations of the effects of the catalyst to waste wood ratios of 0.5, 1 and 2 were annotated as Ni(20) Al₂O₃a, Ni(20) Al₂O₃ and Ni(20)

Al_2O_3 , respectively. Figures 5-15 and 5-16 show micrographs of the fresh and reacted Ni(10) Al_2O_3 catalysts.

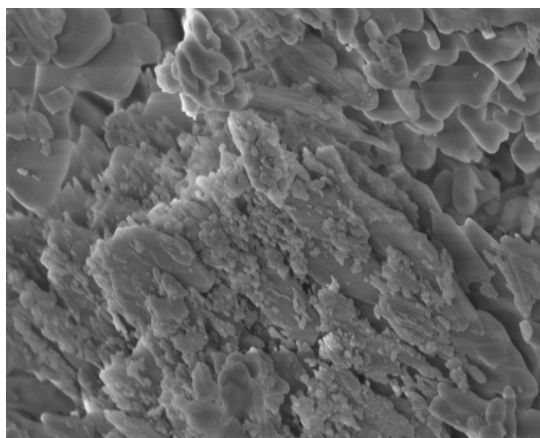


Figure 5-8 SEM of Fresh alumina

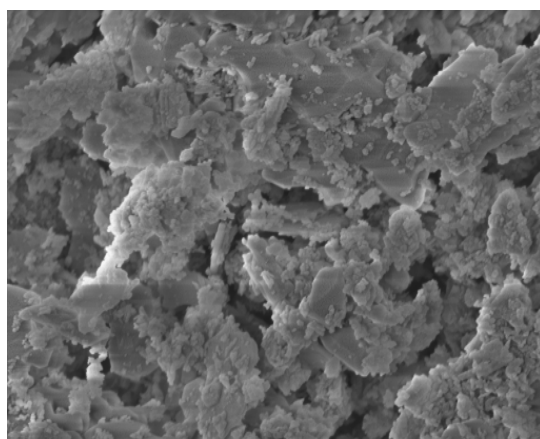


Figure 5-9 SEM of Fresh Ni(5) Al_2O_3

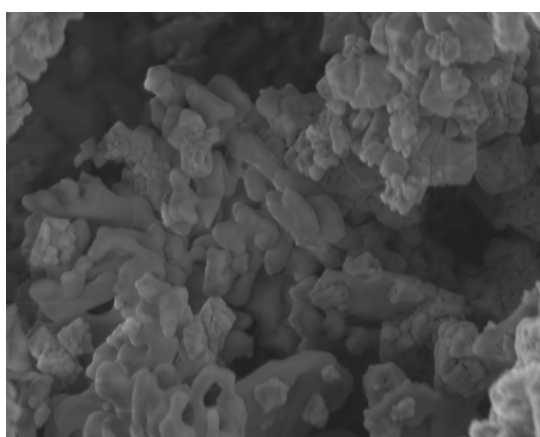


Figure 5-10 SEM of Fresh Ni(20) Al_2O_3

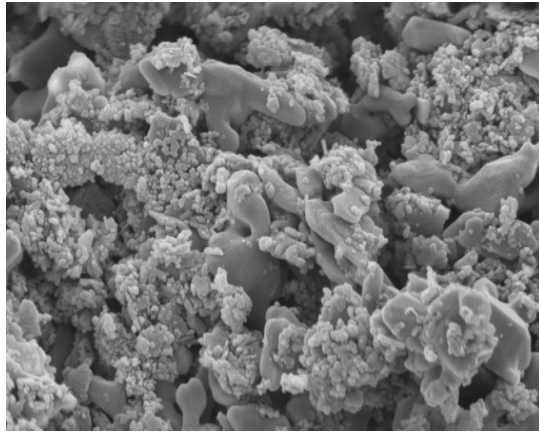


Figure 5-11 SEM of Reacted Ni(5) Al₂O₃

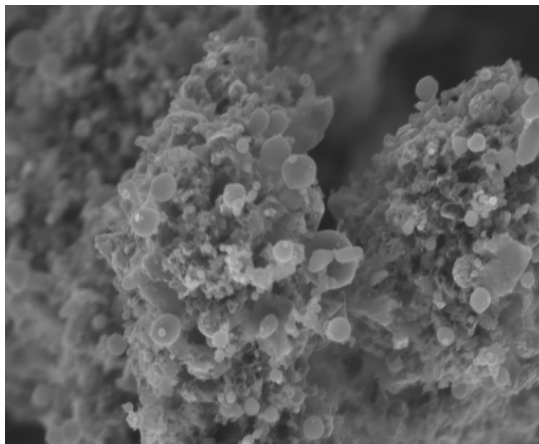


Figure 5-12 SEM of Reacted Ni(20) Al₂O₃

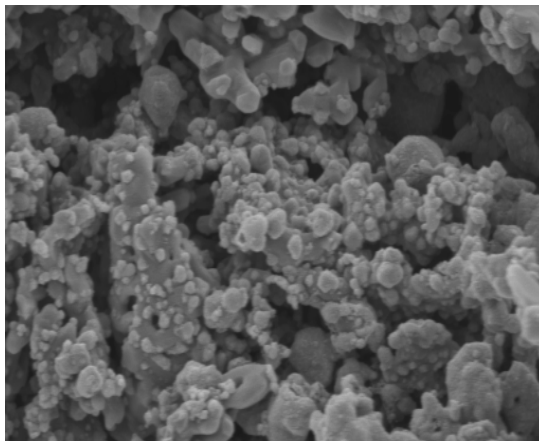


Figure 5-13 SEM of Reacted Ni(20) Al₂O₃a

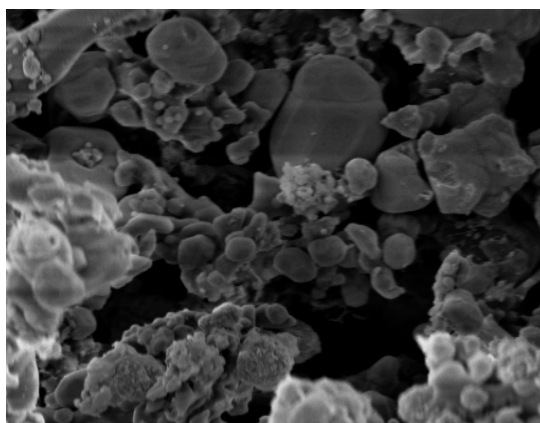


Figure 5-14 SEM of Reacted Ni(20) Al₂O₃b



Figure 5-15 Micrograph of the Fresh Ni(10) Al₂O₃



Figure 5-16 Micrograph of the Reacted Ni(10) Al₂O₃

The SEM analysis were carried out on the sphere catalysts without crushing them into powders in order to preserve the catalyst structure and therefore acquire relevant images of the “as presented” fresh and reacted catalysts.

The SEM image of the fresh as received alumina support (figure 5-7) shows multi flat layers of the alumina on the catalyst surface. The fresh Ni(5) Al₂O₃ and Ni(20) Al₂O₃ catalysts (figures 5-8 and 5-9) show the multi layers of alumina but with non-uniform spatially dispersed granular nickel particles deposited on its surface. The synthesis of supported nickel catalyst by the incipient wetness method has been reported to produce a catalyst with a non-uniform dispersion of nickel particles on the support [35]. The quantity of the nickel deposits on the catalysts appeared more for the Ni(20) Al₂O₃ catalysts than for the Ni(5) Al₂O₃ catalyst giving an indication of the difference in nickel loading.

The SEM images for the analysed reacted catalysts (figures 5-10 to 5-13), showed deposits of carbon on them. The SEM image of the reacted Ni(20) Al₂O₃ catalyst shows some amorphous carbon as well as filamentous carbon deposits. Nickel catalysts have been reported to be prone to deactivation by carbon/coke [17-18]. Amorphous carbon are the more reactive form of carbon deposits formed at low temperature (between 300 to 375 °C) and they are converted over time at higher temperature (> 650 °C) into the less reactive graphitic carbon [32] which can encapsulate the active metal surface. Filamentous carbons are formed from the precipitation of carbidic carbon, previously adsorbed on the active metal, at temperature ranges of 375 to 650 °C, and can cause the active metal to grow away from the support or it can plug access to catalyst pores thereby causing deactivation [36].

A comparison of the micrographs for the fresh and reacted Ni(20) Al₂O₃ catalysts (figures 5-14 and 5-15), showed that the reacted catalyst was discoloured by a layer of soot like black deposits which were carbon deposits. This corroborated with the detection of carbon deposits from the SEM images of the catalysts.

5.2.2 Influence of different metal additives on the catalytic activity and coke resistance of Ni Al₂O₃

From the results in section 5.2.1 above it is clear that the nickel alumina catalyst investigated promoted the steam reforming of the vapours from waste wood pyrolysis in the screw kiln reactor. However as shown by the SEM images in section 5.2.1, carbon deposition on the nickel catalyst surface is an issue for the steam reforming of biomass derived syngas with nickel and can lead to catalyst deactivation [17-19, 37].

During the steam reforming process, the severe conditions creates high pore diffusion resistance within the catalyst [32], making the catalyst surface the most available catalytic active site due to the difficulty of accessing the active sites within the porous support. The continuous deposition of un-reactive carbon and coke on the catalyst blocks-off the already difficult to access pores as well as the active sites on the surface thereby finally rendering the catalyst inactive. Different mechanisms have been proposed for the formation of carbon/coke deposits on supported metal oxide catalysts [37-40]. Carbon/coke which gets deposited on the catalyst surface are products of CO disproportionation and condensation or decomposition of hydrocarbons respectively on the catalyst surface. When formed from hydrocarbons carbon deposits are referred to coke, while when formed via CO disproportionation they are referred to as carbon [41].

During hydrocarbon decomposition on metal oxide catalysts, cracking of the hydrocarbons results in the formation of coke forming intermediates such as aromatics or olefins which undergo dehydrogenation and cyclization and finally condensation reactions into coke [32]. CO disproportionation on the metal results in the formation of amorphous carbons (atomic and polymeric carbons) which are converted at higher temperature into graphitic carbon which can encapsulate the active metal surface [32]. Some of the atomic (carbide) carbon from CO disproportionation, gets dissolved in the Ni surface and can also precipitate, and its accumulation on the metal sites can form an encapsulating layer and deactivate the catalyst [38]. The precipitation of

adsorbed atomic carbon can also result in the formation of filamentous carbon and can cause catalyst deactivation [36] as described in section 5.2.1 above.

In order to extend catalyst life it is important to reduce catalyst deactivation via carbon and coke deposits, thereby reducing the need for catalyst regeneration as well as improve process efficiency. A fundamental principle to attaining reduced carbon and coke deposition on steam reforming nickel catalysts is by ensuring that the rate of carbon and coke forming precursor gasification exceeds the rate of carbon and coke forming intermediates accumulation [32, 40, 42]. Numerous approaches to achieving this have been proposed and investigated, including:

- The integration of mobile alkali promoters on the nickel catalyst in order to remove carbon residue from the nickel surface [40, 43].
- The addition of noble metals to nickel catalysts in order to lower the carbon formation rate [41].
- The use of different oxide supports with nickel catalyst in order to inhibit the formation of filamentous carbon [44-45].
- The selective blocking or poisoning of active sites on the nickel catalyst by adsorbates such as sulphur, in order to reduce carbon deposition [46].
- The addition of metals which encourage diffusion of coke through the nickel particle and into the bulk of the catalyst thereby leaving the surface available for catalysis [42].
- The addition of metal oxides which enhance steam adsorption on the nickel catalyst thereby promoting carbon gasification [43, 47].
- The addition of metal dopants in order to increase the physical strength of the nickel catalyst [48] and prevent attrition due to the growth of carbon whiskers.
- The addition of metal oxides with high oxygen storage capacity in order to gasify carbon on the catalyst [49-50].

In the following sections the results of tests using the Ni(20) Al₂O₃ catalyst modified with different metal oxides will be discussed. The modified catalysts were prepared by adding approximately 5 wt% of the metal oxides of Ce, La, Mg, Mn, Cu and Co, to a nickel alumina catalyst also containing 20 wt% of nickel oxide, as described in section 3.1.3 earlier. The effects of the modified catalysts on hydrogen yield, gas yield as well as carbon deposition on the catalysts were studied and compared to the un-modified catalyst.

5.2.2.1 Product yields

The results of the steam pyrolysis-gasification of waste wood using the different modified catalysts as well as the results for the un-modified nickel alumina catalyst are shown in Table 5-5. In order of increasing gas yield, the sequence was Ni MgO Al₂O₃ < Ni MnO Al₂O₃ < Ni CuO Al₂O₃ < Ni Al₂O₃ < Ni La₂O₃ Al₂O₃ < Ni CoO Al₂O₃ < Ni CeO₂ Al₂O₃. It is clear that the Ni La₂O₃ Al₂O₃, Ni CoO Al₂O₃ and Ni CeO₂ Al₂O₃ catalysts improved the process gas yields compared to the un-modified Ni Al₂O₃. The Ni CuO Al₂O₃ catalyst had a slightly lower gas yield while the Ni MnO Al₂O₃ and Ni MgO Al₂O₃ catalysts had significantly lower gas yields than the Ni Al₂O₃ catalyst. The decrease in tar yield followed a similar trend with the increase in gas yields for the catalysts.

Lu et al [51] investigated a nickel alumina catalyst modified with Ce for the steam gasification of cellulose and reported an increase in gas yield with the introduction of Ce compared to the unmodified nickel alumina catalyst. Bona et al [52] investigated different nickel catalysts for the steam reforming of toluene and reported increased gas production for the catalyst containing Co compared to the nickel alumina catalyst. The integration of lanthanum to nickel alumina catalysts have been reported to increase gas yield for the steam gasification of saw dust [53] and bio oil [54]. Bimbela et al [55] investigated the effects of different loadings of copper on a nickel alumina catalyst for the steam reforming of model pyrolysis oil compounds and reported that a 5 wt% copper loading resulted in the highest gas yield.

Table 5-5

Effects of different metal additives on nickel catalytic activity

Catalyst	Ni(20) Al ₂ O ₃	Ni CeO ₂ Al ₂ O ₃	Ni MgO Al ₂ O ₃	Ni MnO Al ₂ O ₃	Ni La ₂ O ₃ Al ₂ O ₃	Ni CuO Al ₂ O ₃	Ni CoO Al ₂ O ₃
Products	Yield (wt % of waste wood)						
Gas	81.4	86.0	61.0	70.5	85.5	78.7	85.7
Solid	16.5	12.5	14.2	11.3	13.0	13.8	13.0
Oil (by difference)	2.1	1.5	24.8	18.2	1.5	7.5	1.3
Gas composition	Yield (wt % of waste wood)						
H ₂	4.3	4.9	1.5	2.6	4.4	3.4	4.3
CO	23.3	21.9	32.9	28.1	23.7	26.8	26.3
CO ₂	51.0	56.4	20.1	34.3	54.1	43.9	52.1
CH ₄	2.0	1.9	3.4	3.1	2.7	2.9	2.2
C ₂ - C ₄	0.9	0.9	3.1	2.4	0.5	1.7	0.8
Gas composition	Yield (vol %)						
H ₂	49.8	52.6	27.2	38.3	49.1	43.7	48.0
CO	19.5	16.8	44.1	30.2	19.1	24.6	21.4
CO ₂	27.2	27.5	17.1	23.5	27.7	25.7	26.9
CH ₄	2.9	2.5	8.0	5.8	3.7	4.6	3.2
C ₂ - C ₄	0.6	0.6	3.6	2.2	0.4	1.4	0.6
H ₂ / CO	2.6	3.1	0.6	1.3	2.6	1.8	2.3

Koike et al investigated the effects of different loadings of manganese on a nickel alumina catalyst for the steam reforming of cedar wood and reported increased gas yield for a 10 and 20 wt% loading of manganese compared to the un-promoted catalyst. Arauzo et al [56-57] reported reduced gas yield while Garcia et al [22] reported increased gas yield for the steam gasification of biomass when magnesium was added to a nickel alumina catalyst.

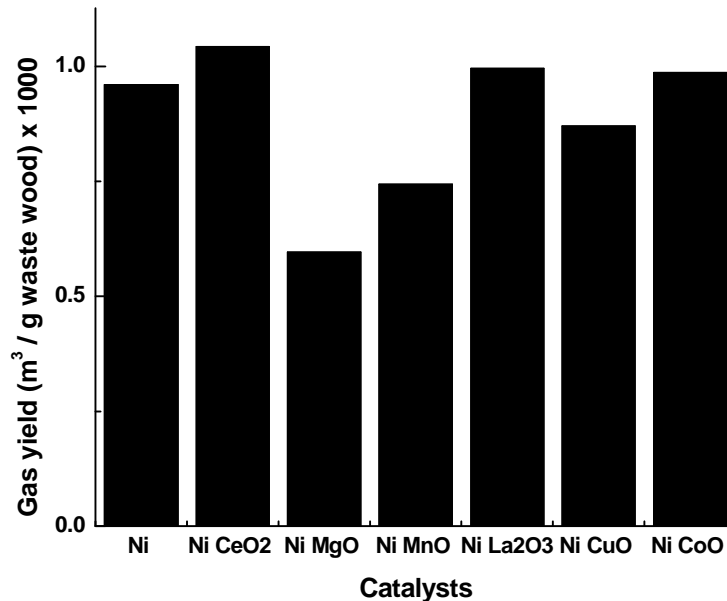


Figure 5-17 Effect of different metal additives on gas yield

Figure 5-17 shows the gas yield (m³ per gram of waste wood) from the steam pyrolysis-gasification of waste wood with the different catalyst. The figure also shows that the lowest gas yield was achieved when the catalyst doped with magnesium was used, while the highest gas yield was achieved when the catalyst doped with cerium was used.

The effects of the different metals on the gas composition are discussed in detail in section 5.2.2.2 below.

5.2.2.2 Gas composition and hydrogen yield

The addition of the different metals resulted in differences in the product gas composition as shown in Table 5-5. The hydrogen yield (vol%) increased in the order Ni MgO Al₂O₃ < Ni MnO Al₂O₃ > Ni CuO Al₂O₃ < Ni CoO Al₂O₃ < Ni

$\text{La}_2\text{O}_3 \text{ Al}_2\text{O}_3 < \text{Ni Al}_2\text{O}_3 < \text{Ni CeO}_2 \text{ Al}_2\text{O}_3$. The CO_2 yield followed a similar increasing trend as H_2 for the different catalysts, while the CO , CH_4 and $\text{C}_2 - \text{C}_4$ gases yield followed an opposite trend. For the $\text{Ni La}_2\text{O}_3 \text{ Al}_2\text{O}_3$, $\text{Ni Al}_2\text{O}_3$ and $\text{Ni CeO}_2 \text{ Al}_2\text{O}_3$ catalysts, the increased hydrogen yield was due to a promotion of the hydrocarbon reforming as well as the water-gas shift reactions, compared to the other catalysts, as evidenced by the increased yield of H_2 and CO_2 accompanied by the decreased yield of the other gases.

The $\text{Ni CeO}_2 \text{ Al}_2\text{O}_3$ catalyst exhibited the highest selectivity towards hydrogen production as a result of the presence of CeO_2 . The modification of nickel catalysts with CeO_2 have been reported to promote hydrogen production [26-27, 58-59]. However excessive loading of CeO_2 into the nickel catalyst has also been reported to reduce hydrogen yield [49, 59] possibly due to sintering of CeO_2 at high concentrations [60]. The interaction of CeO_2 within the catalyst has also been reported to promote carbon gasification on the catalyst thereby reducing catalyst deactivation by coking compared to un-promoted nickel catalysts [26-27]. CeO_2 can promote the oxidation of adsorbed carbon containing species such as CO and CH_4 on the catalyst, due to its surface oxygen vacancies which can be restored or released with change in environment [61-62]. This surface oxygen vacancy of CeO_2 promoted the dissociation and mobility of oxygen intermediates from the steam, making them available to oxidize the adsorbed carbon species as well as re-oxidise the CeO_2 oxygen deficiency [63], thus promoting gasification and hydrogen yield as well as increasing the rate of carbon gasification compared to its deposition therefore possibly reducing deactivation by coke.

The gas composition as a result of adding lanthanum was similar to that for the un-promoted catalyst. The mass of hydrogen produced was slightly more for the lanthanum promoted catalyst, compared to the un-promoted catalyst, however the nickel alumina catalyst had slightly higher hydrogen volume concentration. The effects of promoting nickel steam reforming catalysts with lanthanum has been investigated and reported to increase the yield of carbon containing gases [53-54] while reducing the catalyst activity towards hydrogen

production [53]. Bona et al [52] investigated the influence of different lanthanum contents in a nickel alumina catalyst for toluene steam reforming and reported higher individual mass gas yield including hydrogen, for the optimum lanthanum content, compared to an un-promoted catalyst. However less mol concentration of hydrogen were noted for the product gases from the promoted catalyst compared to the un-promoted catalyst. Lanthanum forms a $\text{Ni-La}_2\text{O}_2\text{CO}_3$ phase in the catalyst which limits catalyst activity but encourages the reaction of carbon species deposited on the nickel with oxy-carbonates such as CO_2 to yield CO [64], thus yielding more CO but also reducing carbon deposits on the catalyst. The presence of lanthanum also promotes the CO_2 reforming of CH_4 [52, 64].

The addition of cobalt also resulted in a gas composition similar to the un-promoted nickel catalyst at the chosen reaction conditions. The mass of hydrogen yield was the same as the un-promoted catalyst, however the (vol %) concentration of hydrogen was less for the cobalt promoted catalyst. The presence of cobalt in nickel alumina catalysts have been reported to promote hydrogen production during biomass and tar gasification [25, 52, 65]. Though no significant differences were noted in this work, it is suggested that the synergy between the Ni and Co metal is responsible for its activity towards hydrogen production [25]. The presence of Co can also reduce the deposition of carbon on the catalyst however it may deactivate due to Co oxidation [66]. Other researchers reported that Ni and Co bimetallic catalysts were effective for the gasification of oxygenates [67-68].

The hydrogen yield (on a mass and volume basis) for the product gas from the copper promoted catalyst was notably less than the nickel alumina catalyst. Other researchers [65, 69-70] however have reported hydrogen yield increase for a copper promoted nickel catalyst compared to an un-promoted catalyst for methane, ethanol and glucose gasification. Cu addition is reported to have reduced catalyst sintering effects, while increasing carbon deposition on the promoted catalyst compared to the un-promoted catalyst [65]. On the other hand Khzouz et al [69] reported a reduction in carbon deposit for a

copper promoted catalyst compared to an un-promoted nickel catalyst for steam gasification.

There was a significant reduction in the hydrogen production when the catalyst was doped with Mn and Mg (more for Mg) compared to the un-doped nickel catalyst. Mn promoting of nickel alumina has been reported to enhance hydrogen production compared to an un-promoted catalyst [71]. Koike et al investigated the effect of different loadings of Mn (10 to 40 wt%) on a nickel alumina catalyst with Nickel loading of 12 wt%, for steam gasification of biomass and reported increased hydrogen production for all Mn loadings compared to the un-promoted catalyst, as well as an optimum loading for hydrogen production of 20 wt%. The nickel / manganese wt% ratios investigated were well above ours and might be a reason for the different results. It is suggested that the manganese oxide phases in the promoted catalyst has a similar effect as explained for CeO₂ by providing oxygen for the oxidation of adsorbed carbon species .

Li et al [57, 72] reported an increase in hydrogen yield for a Mg modified catalyst compared to un-modified nickel alumina for biomass gasification. Arauzo et al [56] reported a decrease in hydrogen yield when a nickel alumina catalyst was promoted with Mg during biomass gasification, which is similar to the results from this work. They proposed that the addition of Mg could modify the catalyst pore size by reducing it and possibly preventing access to large organic molecules for cracking and reforming.

The hydrogen production (mol per gram of waste wood) shown in figure 5-18, and the H₂/CO ratios shown in table 5-5 are in agreement and follow the same trends as the hydrogen yield (vol %) for the catalysts.

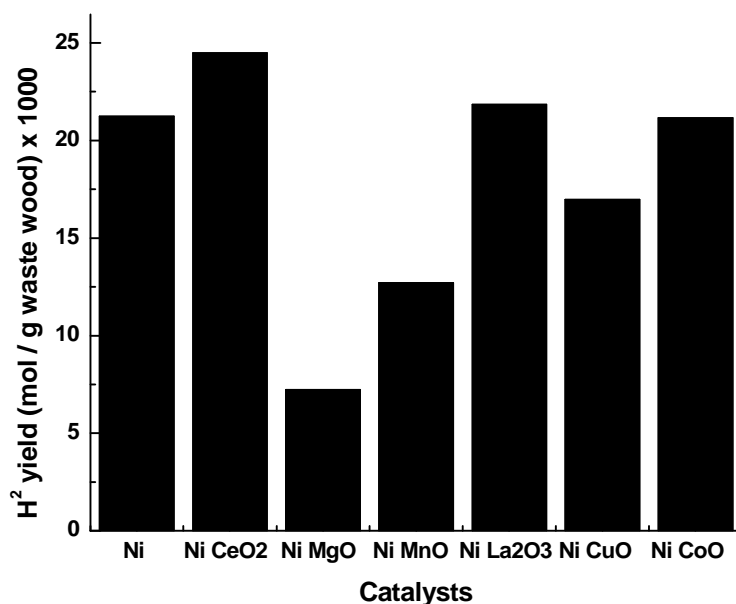


Figure 5-18 Hydrogen production (mol per g waste wood) for the catalysts

5.2.2.3 Effect of metal additives on tar yield

The tar/oil collected in the condensers from four of the investigated catalyst were collected and analysed by GC/MS in order to indentify and quantify detected compounds. The tar products from waste wood steam pyrolysis gasification with the following catalysts were analysed: Ni MgO Al₂O₃, Ni La₂O₃ Al₂O₃, and Ni CeO₂ Al₂O₃. For comparison, the previously analysed data for the tar products from gasification with the Ni Al₂O₃ catalyst were also provided. Further analysis of the data provided information to support the explanations for the process/es that led to gas and hydrogen production in the reactor. Table 5-6 shows the detected compounds from the analyses.

Table 5-6 shows the total tar detected, as well as the compounds detected in the collected and analysed tar from the four different catalytic experiments. As expected the highest total tar quantity (40.8 mg tar per g of waste wood) was detected from the product of the Ni MgO Al₂O₃ catalyst while the lowest total tar quantity (1.1 mg tar per g of waste wood) was detected from the product of the Ni CeO₂ Al₂O₃ catalyst. Results showed that integrating Ce into the Ni Al₂O₃ catalyst, resulted in an 87% total reduction compared to the tar yield from the un-promoted catalyst. Table 5-6 also indicated that the aromatic

compounds such as biphenyl, diphenylpropane, naphthalene, phenanthrene and fluorene were among the most abundant compounds. In order of decreasing total tar quantity detected the trend was Ni MgO Al₂O₃ > Ni Al₂O₃ > Ni La₂O₃ Al₂O₃ > Ni CeO₂ Al₂O₃. Figure 5-19 shows the effects of the different additives on selected tar compounds. Figure 5-19 indicated that the oxygenate, aromatic and aliphatic compounds in the tar/oil exhibited similar trends as described above for the total tar with the different catalysts. The lower tar yield of the Ni CeO₂ Al₂O₃ catalyst was as a result of its promoted catalytic activity while on the other hand the higher yield of total tar for the Ni MgO Al₂O₃ catalyst was as a result of its reduced catalytic activity during steam gasification. Miyazawa et al [73] investigated different metal additives for steam gasification of wood and reported higher tar yield for an Mg promoted catalyst, than a Ce promoted catalyst as a result of the higher catalytic activity and coking resistance of the Ce promoted catalyst.

Table 5-6

Tar compounds from steam pyrolysis-gasification of waste wood with different catalysts

Catalysts	$\mu\text{g tar g}^{-1}$ of waste wood			
	Ni Al ₂ O ₃	Ni MgO Al ₂ O ₃	Ni La ₂ O ₃ Al ₂ O ₃	Ni CeO ₂ Al ₂ O ₃
Oil compounds	Oxygenates			
2,3,5-Trimethylphenol		155		
Dibenzofuran		5537		
2-Phenylphenol		608		
Oil compounds	Aromatics			
m-Xylene			<1	
Alphamethylstyrene	3		3	<1
Betamethylstyrene	17		5	
Indane	<1	4	<1	<1
Indene	1237	2105		15
1,2,3,4-Tetramethylbenze		5		
Naphthalene	2157	3716	1880	278
2-Methylnaphthalene	2101	<1	<1	116
1-Methylnaphthalene		2016	<1	
Biphenyl	1157	1287	342	109
1,4-Dimethylnaphthalene		5684		17
2,2-Diphenylpropane		2451		
Fluorene	111	4377	54	
1,3-Diphenylpropane		6811		
Phenanthrene		4872		423
Fluoranthene	9		10	
Pyrene	22		18	11

Oil compounds		Alkanes		
Octane, C8	175	223	193	110
Nonacosane, C29		209		
Triacontane		211		
Hexatriacontane, C36		218		
Oil compounds		Alkenes		
Nonene, C9	13	101	12	2
Decene, C10	19	83	3	1
Undecene, C11	1	29	1	
Dodecene, C12	2	57	8	3
Tridecene, C13	3	20	5	<1
Tetradecene, C14	5	8		
Pentadecene, C15	<1	6		
Hexadecene, C16	<1	1	<1	<1
Phytene		<1		
Hepadecene, C17	<1	<1		
Octadecene, C18		<1		6
total oil/tar $\mu\text{g g}^{-1}$ of waste wood	7033	40793	2534	1093

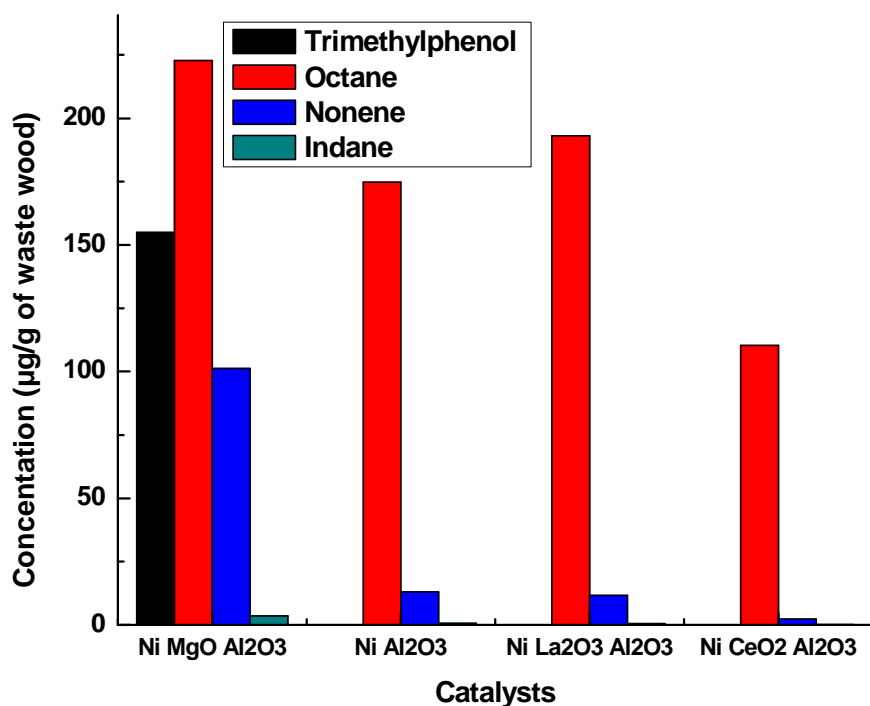


Figure 5-19 Effects of different metal promoters on tar compounds from steam pyrolysis-gasification of waste wood

5.2.2.4 Catalyst life, regeneration and re-use of the Ni Al₂O₃ and Ni CeO₂ Al₂O₃ catalysts.

The Ni Al₂O₃ and Ni CeO₂ Al₂O₃ catalysts which had the highest hydrogen yield were both continuously tested in order to investigate how long they remained active for, during a period of continuous gasification (on stream). The tests were conducted using the same experimental conditions as described earlier however each catalyst was tested for a period of about 48 minutes of continuous waste wood gasification, while gas samples were taken using gas sample bags at intervals of 6 minutes. After 48 minutes, both catalysts were regenerated by calcination in air at 750 °C for 1 hour, after which they were re-used in order to test their activity. Figures 5-20 and 5-21 show the results of the catalyst life, regeneration and re-use of the Ni Al₂O₃ and Ni CeO₂ Al₂O₃ catalysts respectively. Figure 5-22 compares the hydrogen production between the two catalysts during the tests.

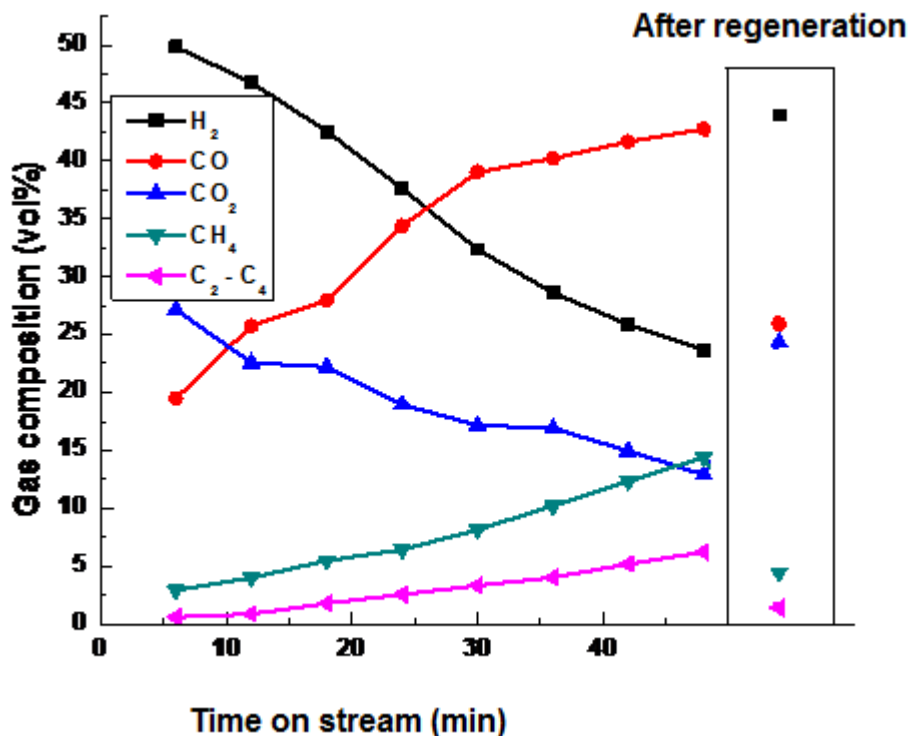


Figure 5-20 Catalyst life, regeneration and re-use test for Ni Al₂O₃

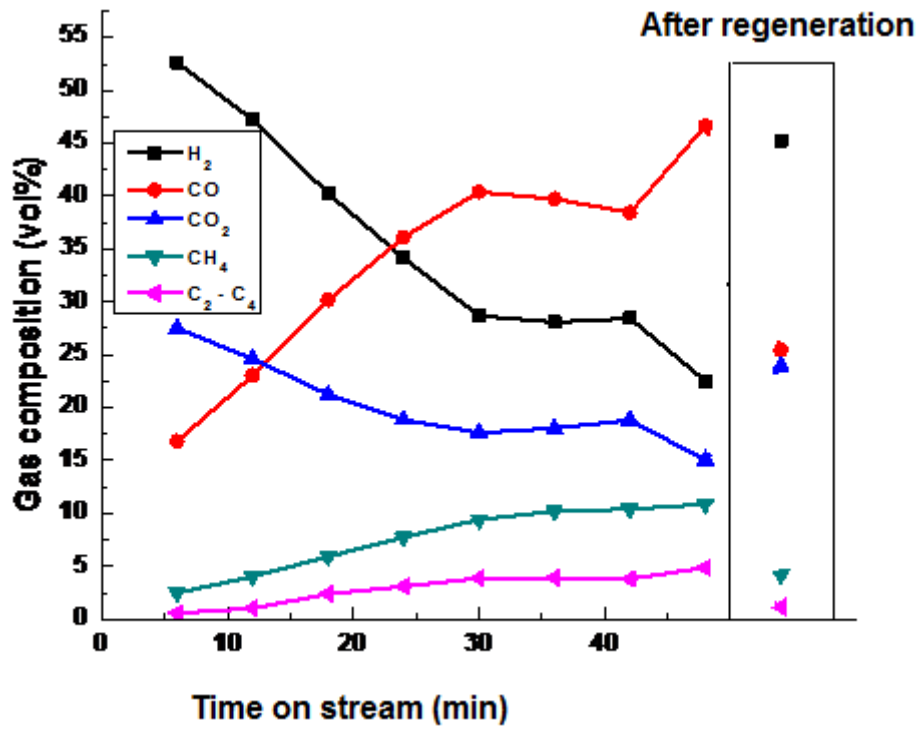


Figure 5-21 Catalyst life, regeneration and re-use test for Ni CeO₂ Al₂O₃

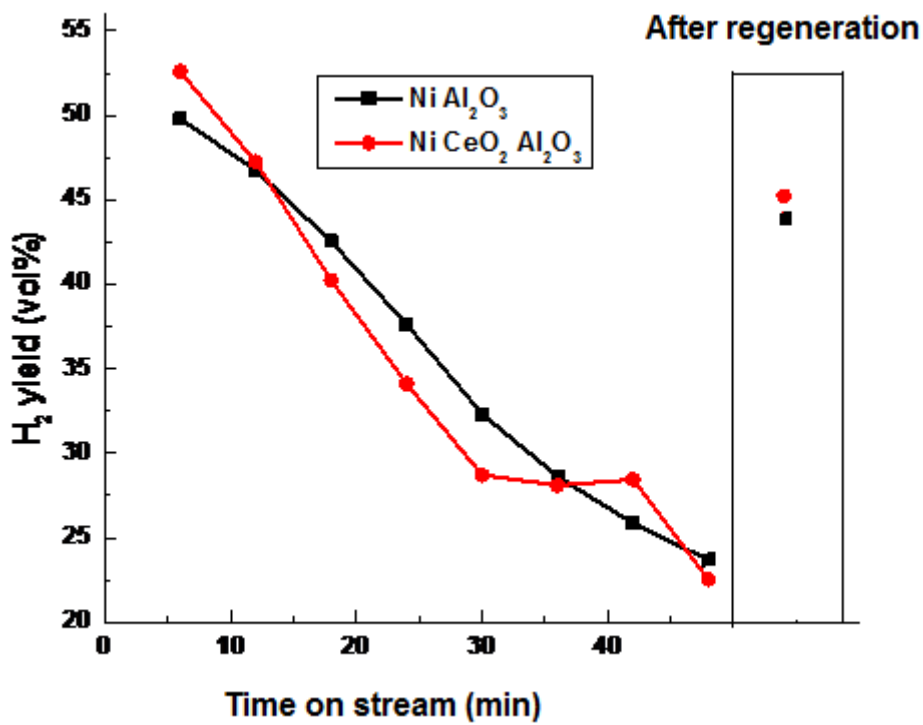


Figure 5-22 Comparison of the hydrogen yield for Ni Al₂O₃ and Ni CeO₂ Al₂O₃ during the catalyst life and re-use tests.

Analysis of the figures above indicate that the catalytic activity of both catalysts started to reduce within the first ten minutes of the life tests and exhibited a steady decline subsequently. At about 25 minutes into the life tests, the hydrogen yield for both catalysts was below 40 vol % compared to about 50 vol% at the start. This might be as a result of high mass flow of reactants through both catalysts in the reactor, combined with catalyst instability. The weight space mass velocity was estimated at 0.08 g catalyst hour / g biomass, compared to 0.14 g catalyst hour / g biomass from Li et al [72]. They reported catalytic activity loss at about 30 min as a result of poor catalyst stability and resistance against Ni particle aggregation, when a Ni Al₂O₃ catalyst was tested for the steam gasification of biomass [72]. The Ni CeO₂ Al₂O₃ catalyst exhibited higher activity than the Ni Al₂O₃ catalyst towards hydrogen production during the first 15 minutes of the life test. However after this initial period both catalysts exhibited similar activity loss. During the tests as the hydrogen yield decreased, the CO₂ yield decreased while the other gases increased.

After regeneration, the catalytic activity of both catalysts increased however not to their initial level. Figures 5-23 and 5-24 shows SEM images of the regenerated Ni Al₂O₃ and Ni CeO₂ Al₂O₃ catalysts, while figures 5-25 and 5-26 show micrographs of the regenerated Ni Al₂O₃ and Ni CeO₂ Al₂O₃ catalysts. The micrographs of both catalysts after regeneration show that they are a lighter green colour compared to the initial catalyst which shows evidence of wear. This indicates loss of nickel from the catalysts and possibly loss of cerium in the case of the Ni CeO₂ Al₂O₃ catalyst, which might be as a result of sintering or attrition. This can also provide an explanation into the slight reduction in their catalytic activity after regeneration.

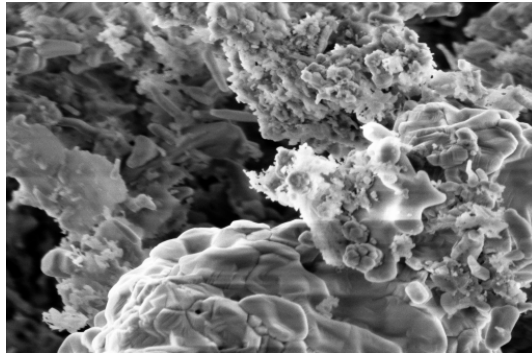


Figure 5-23 SEM of regenerated Ni Al₂O₃

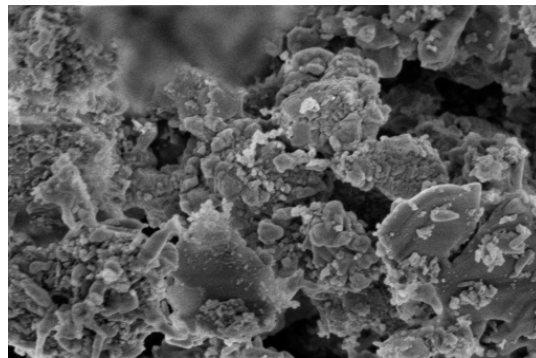


Figure 5-24 SEM of regenerated Ni CeO₂ Al₂O₃



Figure 5-25 Micrographs of regenerated Ni Al₂O₃



Figure 5-26 Micrographs of regenerated Ni CeO₂ Al₂O₃

5.2.2.5 Catalyst characterization

The fresh and reacted catalysts were characterized by a variety of analytical methods in order to study, as well as compare the effects of the process on the catalysts. All the catalysts were characterized using SEM and XRD. Selected fresh and reacted catalysts were analysed by TEM and TEM-EDXS while selected reacted catalysts were also analysed by TPO-FTIR. Pictures of the fresh and reacted catalysts were also taken for comparison.

Figure 5-27 shows the XRD pattern and a Reivelt model for the fresh Ni CeO₂ Al₂O₃ catalyst, while figure 5-28 shows the XRD patterns for the fresh and reacted Ni Al₂O₃ catalyst. The XRD patterns for the other fresh and reacted catalysts are shown in Appendices A-1 to A-6.

In order to verify that the fresh catalysts were consistent with their design the XRD pattern for the fresh Ni CeO₂ Al₂O₃ catalyst was analysed with Highscore plus software, and a Reitveld model to simulate the XRD pattern was also carried out using the software. Figure 5-27 shows a combination of the actual and simulated XRD pattern for the fresh Ni CeO₂ Al₂O₃ catalyst, and shows a very close fit between both patterns. Using a combination of the Reitveld model and the peaks for the compounds identified as described in section 3.7.3, an estimate of the proportion of each of the identified compounds was calculated and is shown also in figure 5-27. The estimate showed that the catalyst contained 21.3% NiO, 5.1% CeO₂ and 73.6% Al₂O₃, indicating that the estimated quantities were consistent with the initial catalyst design.

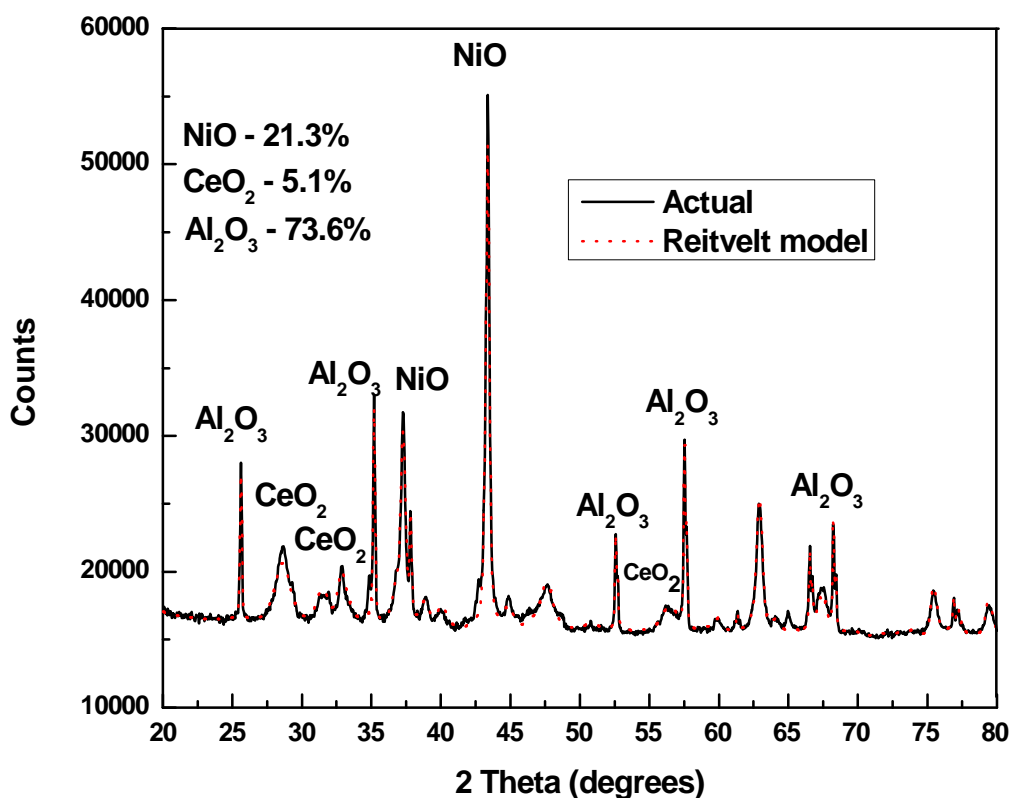


Figure 5-27 XRD pattern and Reitvelt model for the fresh Ni CeO₂ Al₂O₃ catalyst

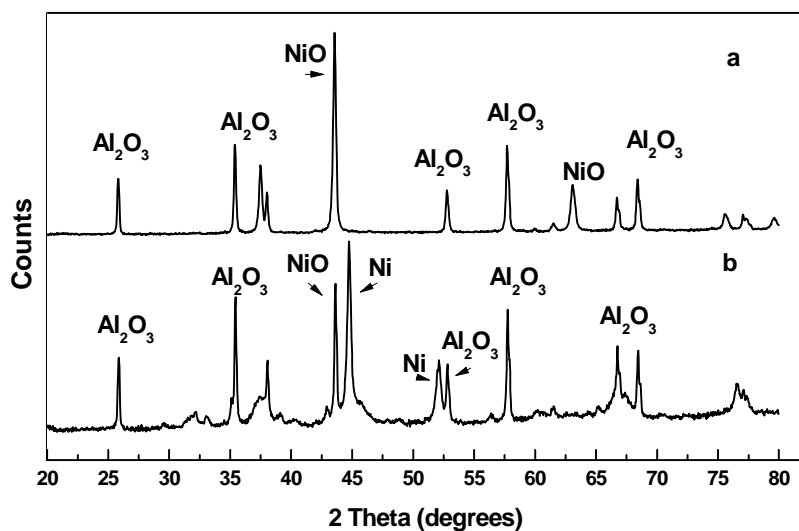


Figure 5-28 XRD patterns of the Ni Al₂O₃ catalyst: (a) fresh, (b) reacted

The XRD patterns for the fresh and reacted catalysts are shown in figure 5-28 and appendices A-1 to A-6, and shows the presence of the NiO phase for all the fresh catalysts however only the reacted catalysts show the metallic Ni

phase. This was because the fresh catalysts were not reduced prior to the experiments however during the experiments the catalysts were reduced in-situ by the syngas [49] resulting in the conversion of the NiO to the Ni phase. The metal nitrate precursor phase was not detected in any of the fresh catalyst, indicating complete decomposition into the appropriate metal oxides. The reacted La modified catalyst indicated the presence of the Al La₂O₃ phase which was not present in the fresh catalyst. The reacted Mg modified catalyst indicated the presence of the Mg Al₂O₄ phase which was not present in the fresh catalyst. The pattern for the Mn modified catalysts indicated a conversion of the Mn₂O₃ phase present in the fresh catalyst, into the Mn₃O₄ phase present in the reacted catalyst.

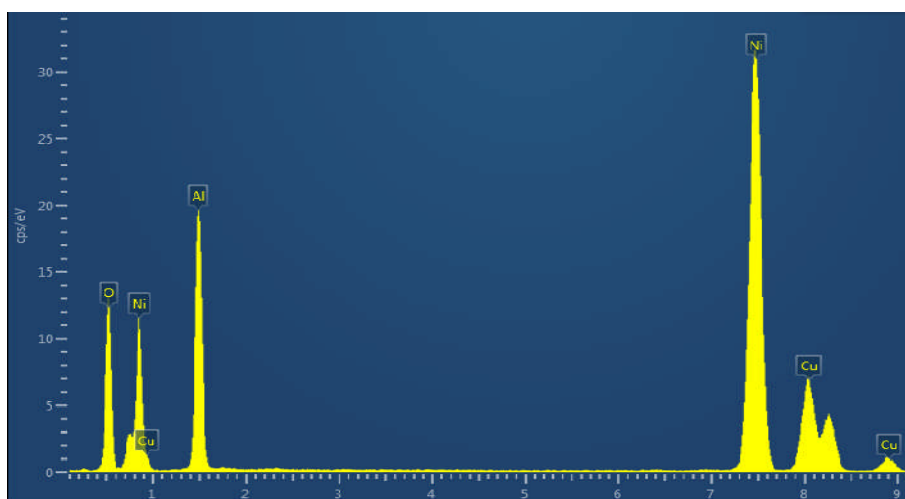


Figure 5-29 TEM-EDXS for Ni Al₂O₃

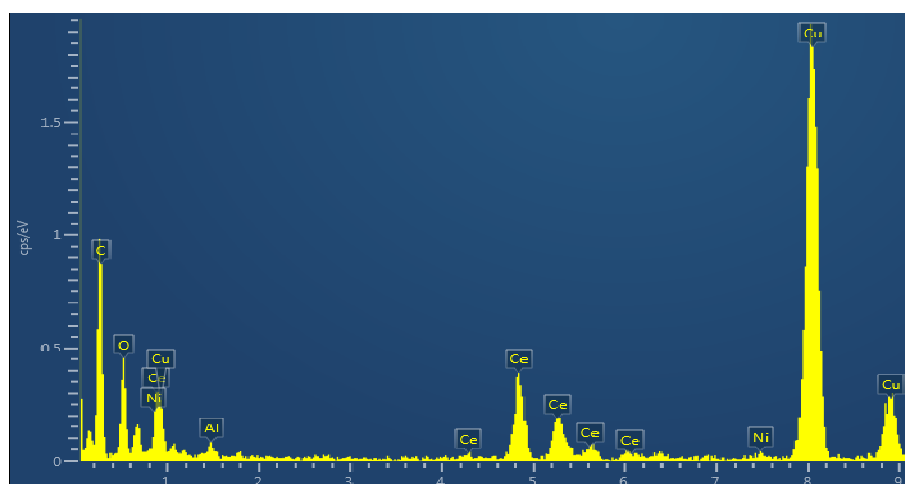


Figure 5-30 TEM-EDXS for Ni CeO₂ Al₂O₃

TEM-EDXS as shown in figures 5-29 and 5-30 as well as appendices B-1 to B-3, was performed on selected catalysts to confirm their constituents. The TEM-EDXS spectra for Ni Al₂O₃ (figure 5-29) shows the presence of Ni and Al elements while the TEM-EDXS spectra for Ni CeO₂ Al₂O₃ (figure 5-30) shows the presence of Ni, Al and Ce elements as expected. The TEM-EDXS results for the analysed catalysts were consistent with both the XRD results and the catalyst design.

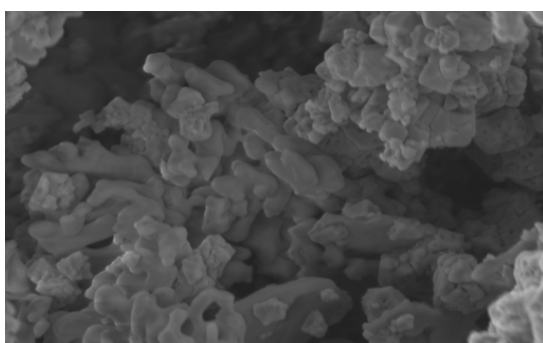


Figure 5-31 Fresh Ni Al₂O₃

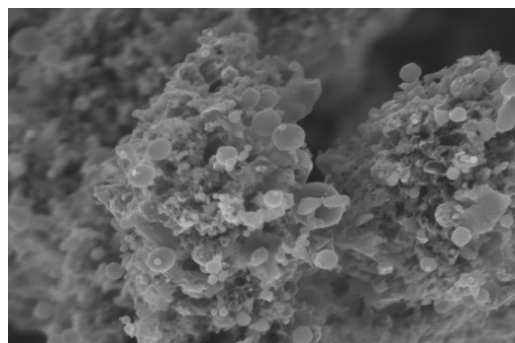


Figure 5-32 Reacted Ni Al₂O₃

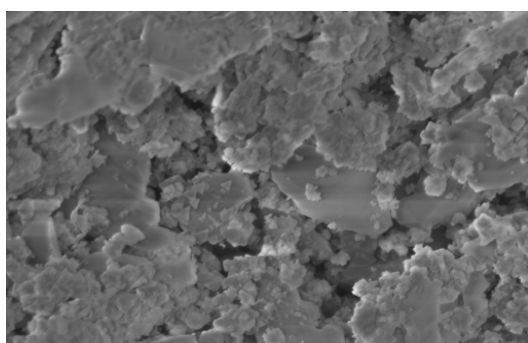


Figure 5-33 Fresh Ni CeO₂ Al₂O₃

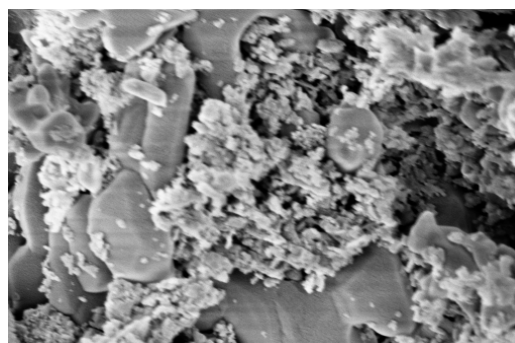


Figure 5-34 Reacted Ni CeO₂ Al₂O₃

Figures 5-31 to 5-34 show the SEM images of the fresh and reacted Ni Al₂O₃ and Ni CeO₂ Al₂O₃ catalysts. The SEM images of the other analysed catalysts are shown in appendices C-1 to C-10. The SEM images of the fresh catalysts in figure 5-31 and 5-33 show granular non-uniformly dispersed deposits of NiO and CeO₂ particles respectively, whilst the SEM images of the reacted catalysts figures 5-32 and 5-34 show carbon deposits on the catalysts surface. The carbon deposits appear concentrated around certain areas on the catalyst surface, believed to be around the surface of the metal particles.

This was confirmed by TEM images (figure 5-36 and 5-38) and TEM-EDXS mapping (figures 5-39 and 5-40). Carbon/coke deposits could form an encapsulating layer over the catalysts' active metal sites and lead to catalyst deactivation [32].

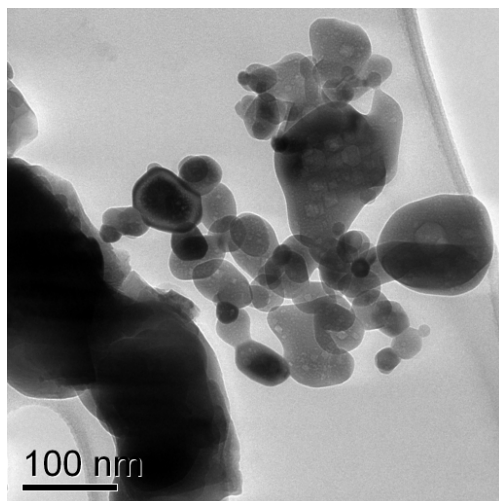


Figure 5-35 TEM image of the fresh Ni Al₂O₃

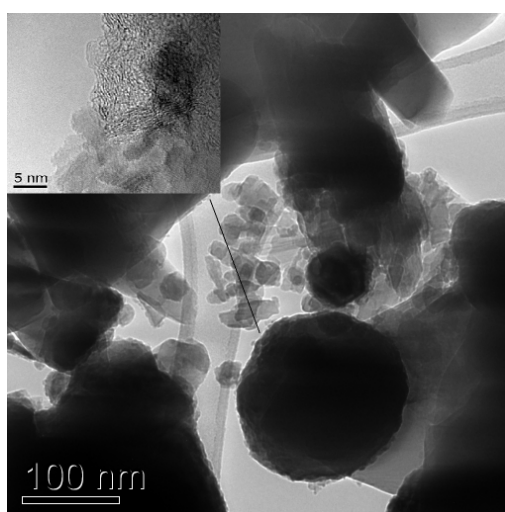


Figure 5-36 TEM image of the reacted Ni Al₂O₃

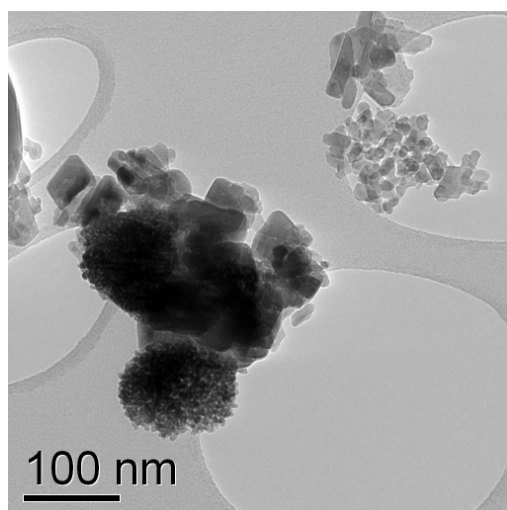


Figure 5-37 TEM image of the fresh Ni CeO₂ Al₂O₃

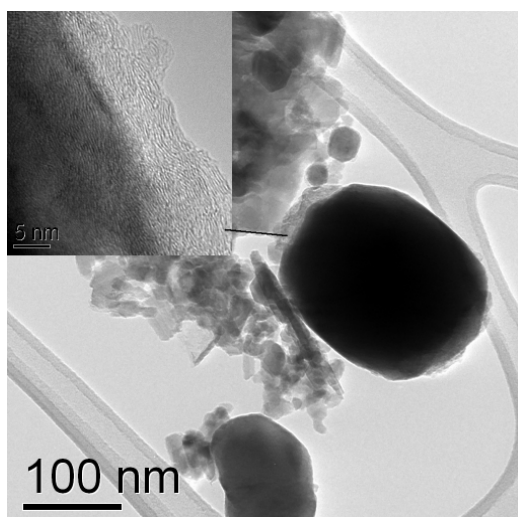


Figure 5-38 TEM image of the reacted Ni CeO₂ Al₂O₃

Figures 5-35 to 5-38 show the TEM images for the fresh and reacted Ni Al₂O₃ and Ni CeO₂ Al₂O₃ catalysts. The TEM images for the other analysed catalysts are shown in appendices D-1 to D-6.

TEM images (figure 5-35 to 5-38) and TEM-EDXS mapping (figures 5-39 and 5-40) of selected catalysts also show carbon deposits on the catalysts. The TEM images for Ni Al₂O₃ and Ni CeO₂ Al₂O₃ shown in figure 5-36 and 5-38, show graphitic carbon deposits on the nickel surface. This could block access to the catalyst pores thereby leading to catalyst deactivation. The TEM images of the fresh catalysts (figure 5-35 and 5-37) showed that the nickel

particles were of various sizes in the range 60 - 120 nm. TEM images of the reacted catalysts (figure 5-36 and 5-38) showed the presence of larger nickel particles (> 150 nm) in the catalyst structure, which indicated the aggregation of the metal particles [72]. The catalyst modified by Ce indicated less quantity of the larger Ni particle indicating stronger resistance to aggregation and this might be linked to its higher performance. The TEM-EDXS maps in figures 5-38 and 5-39 shows the element make-up of the reacted Ni Al₂O₃ and Ni CeO₂ Al₂O₃ catalysts respectively as well as an indication of the relative location of these elements on the surface of the catalyst. The TEM-EDXS maps for the catalysts analysed (figures 5-39 and 5-40 and appendices E-1 to E-3) indicated that elemental carbon was co-located or concentrated in the same areas as the nickel particles. This corroborates with the carbon deposits on the Ni metal surface detected in the TEM images. The TEM-EDXS maps for the catalysts modified with Ce, La and Mg shows that the metals were located over both the Ni and Al spectrum, indicating a non-biased dispersion of these metals over the nickel and alumina in the catalyst. However the EDXS map for the Co modified catalyst (appendix E-1) shows a concentration of the Co spectrum in the same locations as the Ni spectrum indicating a strong interaction of the Ni and Co in the catalyst. This might explain the high gas yield noted for the Co promoted catalyst. Wang et al [25] indicated that a synergy existed between Ni and Co in their bi-metallic catalyst possibly caused by the simultaneous regeneration of both metals in the catalyst, and was responsible for the catalyst's activity. Andonova et al [67] reported that the synergy between Ni and Co in their bimetal catalysts was as a result of enhanced catalyst reducibility with the addition of Co.

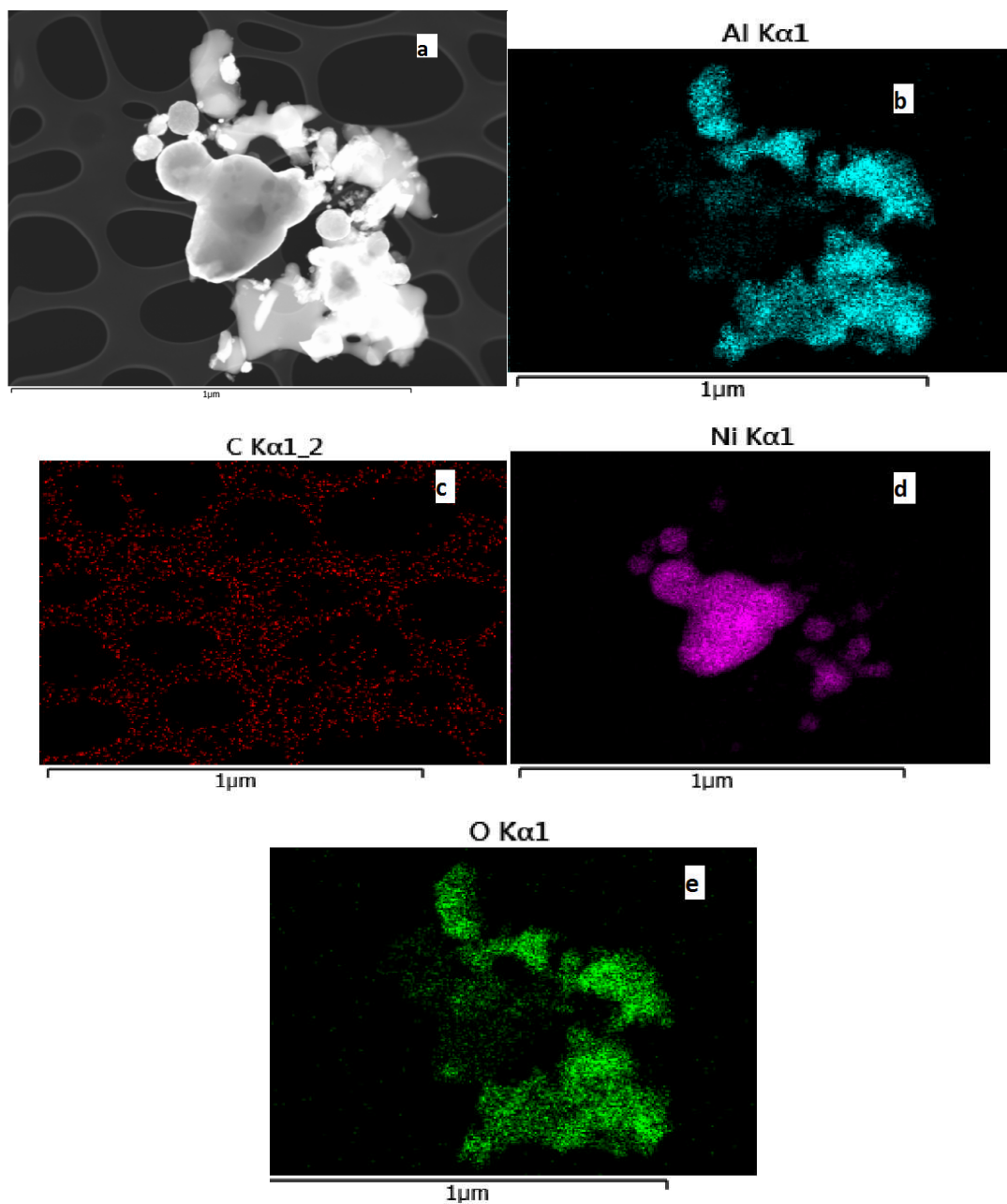


Figure 5-39 TEM-EDXS mapping for the reacted Ni Al₂O₃ catalyst showing its elemental make up and their position. (a) TEM image (b) Al spectra (c) C spectra (d) Ni spectra (e) O spectra

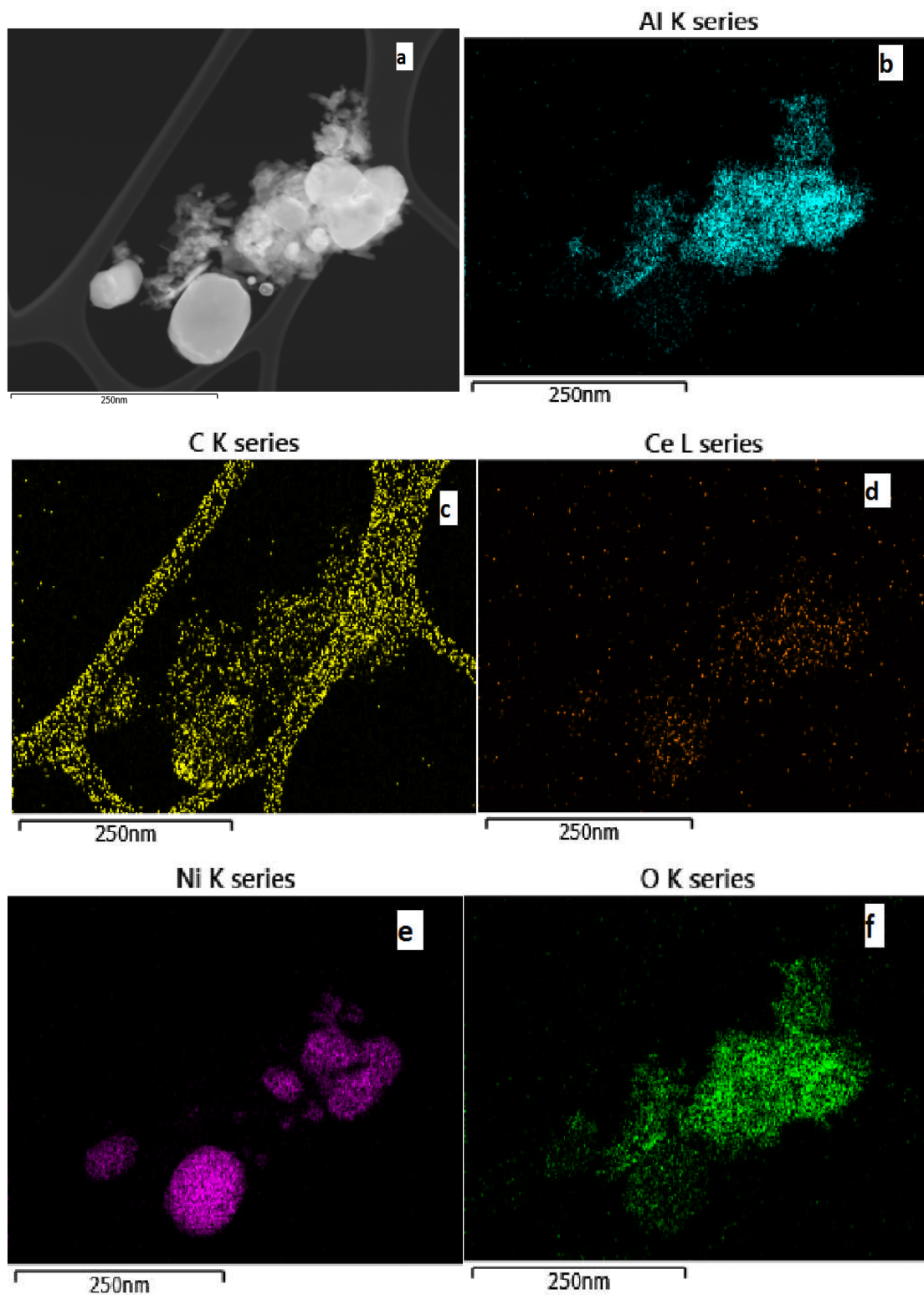


Figure 5-40 TEM-EDXS mapping for the reacted Ni CeO₂ Al₂O₃ catalyst showing its elemental make up and their position. (a) TEM image (b) Al spectra (c) C spectra (d) Ce spectra (e) Ni spectra (f) O spectra

The TPO-FTIR shown in figure 5-41 was carried out to investigate the nature of the carbon deposits on the catalyst. The thermal degradation graphs for the catalysts show an initial weight loss just above 100 °C which indicates moisture loss, however all catalysts subsequently exhibited an overall net weight gain, due to the nickel oxidation. The TGA was connected to an FTIR for analysis of the combustion gases in order to analyse the CO₂ produced.

The CO₂ evolution graph for the catalysts show three distinct CO₂ evolution peaks. The first peak which occurred around 400 °C was characteristic of the oxidation of the more reactive amorphous carbon [74]. The second peak which occurred around 500 °C was characteristic of the oxidation of filamentous carbon [74]. The peak at around 585 °C which was detectable only for the Ni Al₂O₃ catalyst was characteristic of carbon deposits with different degrees of graphitization [51]. The un-promoted catalyst had the only detectable graphitic carbon peak, as well as the second highest peak for amorphous carbon, indicating that this catalyst was the most prone to carbon deactivation. The La and Ce promoted catalysts exhibited the lowest peaks for CO₂ evolution from amorphous and filamentous carbon oxidation, indicating that they had the highest resistance to carbon deposition.

The Mn and Mg promoted catalysts had a lower amorphous carbon CO₂ peak than the un-promoted catalyst, as well as a very low peak due to filamentous carbon oxidation, indicating that these catalysts had higher carbon deposit resistance than the un-promoted catalysts. The reduced activity of these catalysts during steam gasification of waste wood was therefore not due to carbon/coke deactivation but probably due to poor catalyst stability. The Cu promoted catalyst exhibited the highest CO₂ peak for amorphous and filamentous carbon oxidation. The amorphous carbon deposits can cause catalyst deactivation when converted to graphitic carbon which can encapsulate the active metal [41]. This can explain the reduced catalytic activity of the Cu promoted catalyst. It was also observed that none of the promoted catalysts exhibited the CO₂ peak due to graphitic carbon indicating that these catalysts had better resistance to deactivation by carbon/coke, than the un-promoted catalyst. However the presence of filamentous carbon

indicated these catalysts could be prone to pore plugging or attrition/crushing by the filamentous carbon growth [32].

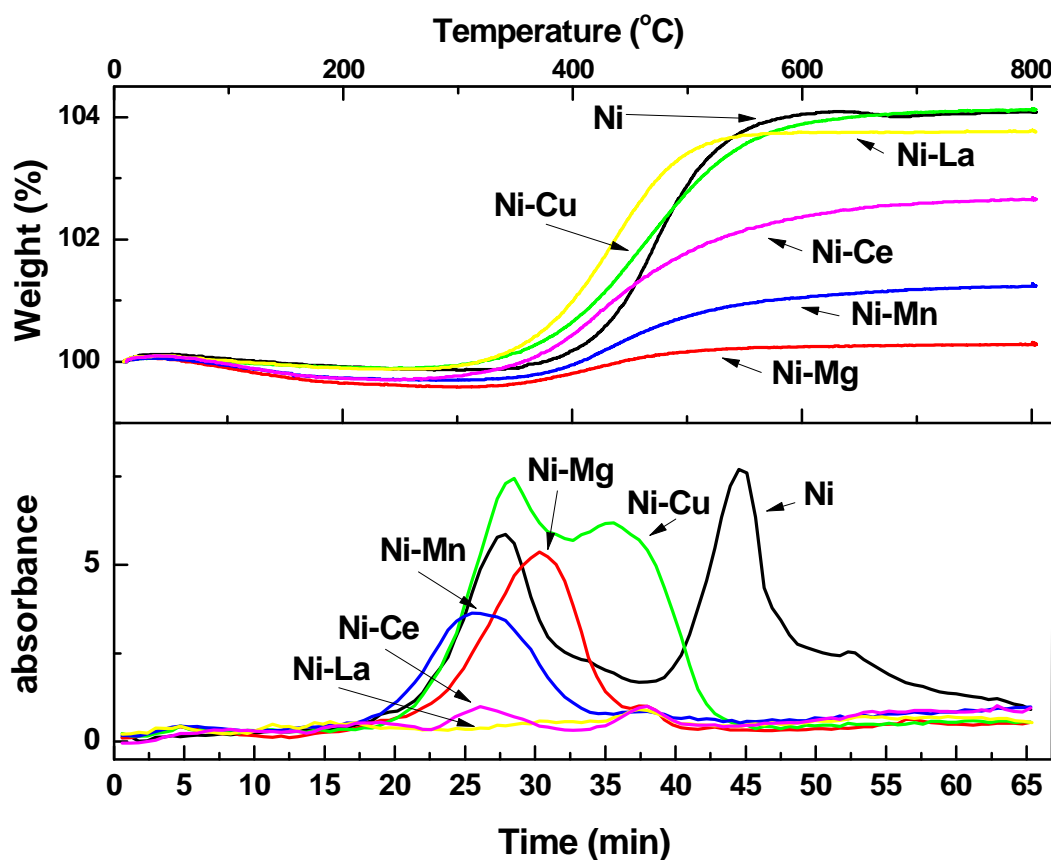


Figure 5-41 CO₂ evolution during TPO-FTIR of reacted catalysts

5.2.3 Conclusions

The steam pyrolysis-gasification of waste wood was carried out in a continuous screw kiln reactor in the presence of nickel based catalysts. Different process parameters were varied such as; the nickel loading on the catalyst, the catalyst to waste wood ratio and the modification of the nickel catalyst with different metals (Ce, La, Co, Cu, Mn and Mg), in order to investigate the effects of these parameters on gas yield, gas composition, tar yield and catalyst coke deposition resistance. The following main conclusions have been drawn:

- Increasing the nickel loading from 5 to 20 wt% on the Ni Al₂O₃ catalyst resulted in increased gas yield and reduced the tar yield by 75%, from

the steam pyrolysis-gasification of waste wood due to increased catalytic activity. Increasing the nickel loading also resulted in increased hydrogen yield, as a result of the promotion of hydrocarbon cracking and steam reforming, and water-gas shift reactions.

- Increasing the catalyst to waste wood ratio from 0.5 to 2 resulted in increased gas yield and reduced the tar yield by 97%, as well as increased hydrogen yield. This was also as a result of the promotion of hydrocarbon cracking, steam reforming, and water-gas shift reactions, due to increased availability of catalytically active sites as well as the increased availability of catalyst support on which increased organic activation and steam activation could take place respectively.
- Increasing the nickel loading and the catalyst to waste wood ratio during waste wood steam pyrolysis-gasification resulted in a decrease in the total detected tars, as well as a conversion of the tar constituents to mostly aromatics. The aromatic compounds were products from the steam reforming of hydrocarbons, which was enhanced by the catalysts.
- The SEM images of the reacted Ni Al₂O₃ catalysts showed evidence of carbon deposits on the catalyst surface which could lead to its deactivation.
- The promotion of the Ni Al₂O₃ catalyst with La, Co and Ce resulted in increased gas yields from steam pyrolysis gasification of waste wood in the order Ce > Co > La. The Ce promoted catalyst resulted in the production of the highest gas yield due to enhanced catalytic activity. The Cu, Mn and Mg promoted catalysts exhibited lower gas yield than the un-promoted catalyst in the order Cu > Mn > Mg. The Mg promoted catalyst produced the lowest gas yield due to a reduced catalytic activity.
- The promotion of the Ni Al₂O₃ catalyst with Ce resulted in a higher hydrogen yield due to its enhanced catalytic activity as well as enhanced carbon/coke gasification, while the La and Co promoted catalysts had similar hydrogen yields as the un-promoted catalyst. The

Cu, Mn and Mg promoted catalysts resulted in reduced hydrogen yields in the same order noted for their gas yields.

- The Ce and La promoted catalysts resulted in a reduction in the total detected tar by 87 and 64% respectively as a result of their enhanced activity due to the interactions of Ce and La in the catalyst. The Mg promoted catalyst resulted in an increase in the total tar detected, compared to the un-promoted catalyst, for the steam pyrolysis-gasification of waste wood due to a reduction in catalyst activity.
- The Ni CeO₂ Al₂O₃ and Ni Al₂O₃ catalyst were both deactivated after 48 minutes of the life test, possibly as a result attrition and/or sintering. The Ni CeO₂ Al₂O₃ catalyst exhibited higher catalytic activity within the first 15 minutes of the life test, as well as after regeneration due to its enhanced activity and carbon/coking resistance. The regenerated catalysts showed signs of wear due to attrition and/or sintering.
- TEM-EDXS mapping and TEM images showed carbon deposition concentrated around the nickel particles on the characterised reacted catalysts. CO₂ evolution peaks obtained by TPO-FTIR indicated the presence of peaks characteristic of the oxidation of amorphous and filamentous carbon on the promoted catalysts. The un-promoted catalyst exhibited the only detectable characteristic peak for graphitic carbon as well as the peak for amorphous carbon, indicating that it was prone to deactivation by carbon/coke encapsulation.
- The reacted Ce and La promoted catalysts exhibited negligible peaks for both amorphous and filamentous carbons, indicating higher resistance to carbon deposition as a result of enhanced gasification of carbon deposits. The reacted Cu, Mn and Mg promoted catalysts exhibited the evolution of the characteristic CO₂ peak for amorphous carbon which could be converted to graphitic carbon and cause carbon/coke deactivation. The promoted catalysts indicated higher resistance to deactivation by carbon/coke deposition, however the presence of filamentous carbon on the catalysts indicated that they were prone to deactivation by attrition/crushing or pore plugging by the filamentous carbon growth.

5.3 Nickel based steam pyrolysis-gasification of waste wood with CaO as a CO₂ sorbent

In-situ CO₂ capture with solid sorbents during gasification presents the potential of selective CO₂ removal within the gasifier thereby producing a gas stream more concentrated in hydrogen, reducing the need for expensive downstream gas purification technology as well as shifting the equilibrium of the water-gas shift reaction in favour of hydrogen production[75-76]. In addition, CO₂ capture integrated to biomass gasification could lead to the net atmospheric removal of CO₂ [77-78]. CaO has been reported as a promising solid sorbent for in-situ CO₂ capture from biomass gasification [77-79] because it can be used and regenerated for re-use via a carbonation (CO₂ adsorption) and calcination (CO₂ release) temperature swing cycle. The carbonation reaction which occurs at around 600 – 700 °C is also exothermic and can contribute to process heat, while the calcination takes place at around 800 – 900 °C [80]. CaO sorbents could play an important role in integrated gasification combined cycle (IGCC) systems where the carbonation can take place in a shift reformer, or in integrated gasification cycle (IGC) systems as described in Koppatz et al [80].

There are limitations to the use of CaO as a solid sorbent because of the fact that it suffers activity loss after some cycles of carbonation and calcination due to the degradation of micro-pore volume and surface area. However this activity loss can be reduced by the integration of magnesium and sodium into CaO sorbents [81-82]. Florin et al [77] also reviewed various methods for improving the multi-cycle performance of CaO sorbents, including: operating at mild process conditions, hydrating the sorbent after calcination and the use of nano-sized sorbent particles.

In the following section, the results of tests using CaO sorbent for in-situ CO₂ capture integrated with Ni Al₂O₃ catalyst for steam pyrolysis-gasification of waste wood are discussed. The effect of CaO integration into the catalyst

structure during synthesis, compared to its addition by solid mixing, as well as the effect of gasification temperature and CaO quantity were investigated in order to study their effects on CO₂ capture and gas composition.

5.3.1 Product yields

The activity of the Ni CaO Al₂O₃ catalyst-CO₂ sorbent prepared by co-impregnation which contained 20 wt% Ni and 5 wt% (2g) CaO was compared against that for a solid mixture containing 38 grams of Ni Al₂O₃ (20 wt% Ni) catalyst and 2 grams of CaO powder. Results of the tests are shown in Table 5-7, including the results of using only Ni Al₂O₃ for comparison.

Results indicated that there was no significant effects on the gas yield when CaO was added to the catalysts both by integration during preparation and by solid mixing, compared to the experiment using only Ni Al₂O₃. The gas yields obtained from gasification utilizing the catalyst-sorbent material prepared by co-impregnation, and that prepared by solid mixing, were similar.

The effect of the addition of different quantities of CaO powders (2, 5 and 10g, which represented 5, 12 and 21 wt% of CaO respectively) to Ni Al₂O₃ catalyst by solid mixing was investigated for the steam pyrolysis-gasification of waste wood. Results of the experiments are shown in Table 5-7 and they showed a different trend than expected. Increasing the quantity of CaO added resulted in a gradual reduction in gas yield. The gas yield reduced from 81.4 wt% when no CaO was added, to 78 wt% when 10 g of CaO was added. Hanaoka et al [83] investigated the effect of varying the CaO quantity during the steam gasification of woody biomass at 650 °C. They reported increasing gas yield with increasing the CaO content up to an optimum point after which no notable increase was recorded due to the dual action of CaO for CO₂ sorption and tar cracking.

Table 5-7Effects of CaO on in-situ CO₂ capture

Catalyst	Ni Al ₂ O ₃	Ni CaO Al ₂ O ₃	Ni Al ₂ O ₃ + CaO (2g)	Ni Al ₂ O ₃ + CaO (5g)	Ni Al ₂ O ₃ + CaO (10g)	Ni Al ₂ O ₃	Ni Al ₂ O ₃ + CaO (10g)
Fixed bed temperature (°C)	800	800	800	800	800	700	700
Products	Yield (wt % of waste wood)						
Gas	81.4	79.8	79.6	79.3	78.0	76.3	75.8
Solid	16.5	13.8	13.3	13.0	12.3	13.0	12.5
Oil (by difference)	2.1	6.4	7.2	7.7	9.7	10.7	11.7
Gas composition	Yield (wt % of waste wood)						
H ₂	4.3	4.0	3.9	3.9	3.7	3.8	3.3
CO	23.3	24.5	25.2	26.6	28.2	17.5	24.7
CO ₂	51.0	47.6	47.2	44.6	41.2	50.2	42.6
CH ₄	2.0	2.7	2.0	2.6	2.7	3.3	3.2
C ₂ - C ₄	0.9	1.0	1.1	1.6	2.2	1.6	2.1
Gas composition	Yield (vol %)						
H ₂	49.8	48.0	47.5	47.2	46.0	48.3	43.8
CO	19.5	21.1	22.2	23.1	25.0	16.0	23.5
CO ₂	27.2	26.0	26.4	24.6	23.2	29.3	25.8
CH ₄	2.9	4.1	3.1	4.0	4.2	5.2	5.3
C ₂ - C ₄	0.6	0.8	0.9	1.2	1.6	1.2	1.7
H ₂ / CO	2.6	2.3	2.1	2.0	1.8	3.0	1.9

Table 5-7 also shows the effect of steam pyrolysis-gasification with CaO at a temperature of 700 °C. For comparison, an experiment was conducted using Ni Al₂O₃ only at a gasification temperature of 700 °C. Results show that compared to similar experiments for steam pyrolysis-gasification of waste wood at 800 °C, with and without CaO addition, the gasification temperature of 700 °C resulted in lower gas yields. Acharya et al [78] reported increased gas yield with increasing temperature during biomass gasification with CaO due to increased thermal conversion of tars to gases. Table 5-7 also shows that at 700 °C, the addition of CaO resulted in lower gas yield compared to the gasification with only Ni Al₂O₃.

5.3.2 Gas composition

Table 5-7 shows that similar gas compositions including H₂ yield were produced, when CaO was added to the Ni Al₂O₃ catalyst via the different methods. The catalyst-sorbent materials with similar CaO content but derived from the different preparation methods of co-impregnation of CaO and by mixing of CaO powder with the catalyst, produced similar gas compositions. However Koboyashi et al [79] reported an increase in H₂ composition when a Ni-CaO-Al₂O₃ catalyst was used for biomass gasification compared to the absence of CaO, as a result of equation 5.4.



Increasing the quantity of CaO added to the catalyst from 2 to 10 g resulted in decrease in the yield and composition of hydrogen, accompanied by a decrease in the CO₂ as well as an increase in the CO, CH₄ and C₂ – C₄ gases. This indicated a reduction in the activity of the catalyst/sorbent. Koboyashi et al [79] reported increased hydrogen yield as well reduced CO₂ yield with increasing CaO/Catalyst ratio from 0 to 2, for the steam gasification of biomass using commercial Ni Al₂O₃ catalyst (11wt% Ni). They reported that the presence of the CaO resulted in the capture of CO₂ from the gas stream which in turn promoted a shift in the water-gas shift reaction towards the

production of more hydrogen. CaO has been reported to have chemo-affinity towards biomass derived tars [79] and is reported to be effective for tar decomposition [77]. However CaO is also reported to be deactivated by tar [84-85]. Corella et al [85] reported that due to the weak catalytic nature of CaO, its maximum tolerable limit of tar in a gasifier was in the region of ≈ 2 g of tar per m^3 of gas. Huang et al [84] reported that CaO was less active for H_2 yield and CO_2 sorption compared to Fe promoted CaO, due to deactivation by tar during biomass gasification. This could explain the reduced hydrogen yield and CO_2 sorption when the catalyst/sorbents were used during our experiments. The tar content in the pyrolysis gas which was introduced into the second stage fixed reactor would have been above the limit proposed by Corella et al [85], as shown in section 5.2.1.3 above. As a result of mixing the CaO powders with the catalyst, CaO in catalyst/sorbent would have been exposed to a high tar concentration and easily became deactivated. This does not mean that no CO_2 sorption occurred in the presence CaO. On the contrary as evidenced in the XRD patterns in section 5.3.3 below, some CO_2 capture occurred in the catalyst-sorbents however not enough to balance the overall loss of activity. It is proposed that situating the sorbent layer after the catalyst in order to reduce the tar quantity interacting with the CaO sorbent might be more effective.

In addition, researchers [86-87] have reported that carbonation reactions on the surface of pure CaO powders can induce local increase in the solid volume due to the molar volume of CaCO_3 being twice that of CaO, resulting in pore blockage and preventing access of CO_2 to powder particles below the surface. This can lead to loss of CO_2 capture capacity.

Reducing the gasification temperature to 700 °C in the presence of CaO resulted in a reduction in the H_2 yield and composition, compared to similar experiment at 800 °C, as well as compared to gasification with Ni Al_2O_3 only at 700 °C. The CO_2 and CO composition and yield of the product gas also reduced while the CH_4 and $\text{C}_2 - \text{C}_4$ gas composition increased for steam pyrolysis-gasification with the catalyst-sorbent at 700 °C compared to gasification at 800 °C. This was mostly as a result of reduced cracking

reactions due to the reduced temperature [88]. Similar trend in the gas composition was noted on comparing the results of steam pyrolysis-gasification of waste wood with Ni Al₂O₃ only, at 700 °C and 800 °C.

The carbonation process is exothermic [80], and as a result of the gasification temperature in these tests being close to the calcination temperature for CaCO₃, as the process proceeds, the exothermic carbonation reaction could add to the process heat leading to the calcination of some of the formed carbonates within the bed, resulting in CO₂ release, and further CO₂ capture by the previously calcined carbonates later. Acharya et al [78] investigated the effects of different quantities of CaO for CO₂ adsorption during the steam gasification of biomass and reported increasing H₂ and gas yield with increasing CaO quantity as a result of heat release during the exothermic carbonation reactions which promoted increased tar and char conversion.

5.3.3 Catalyst-Sorbent characterization

Fresh and reacted catalysts-sorbents were characterized by a variety of analytical methods in order to study, as well as compare the effects of the reactions on them. Selected catalysts-sorbents were characterized using XRD and TEM. Figure 5-42 shows the XRD patterns of the fresh and reacted Ni CaO Al₂O₃ catalyst-sorbent while Figure 5-43 shows a combination of XRD patterns for fresh CaO powders and the reacted catalyst-sorbents.

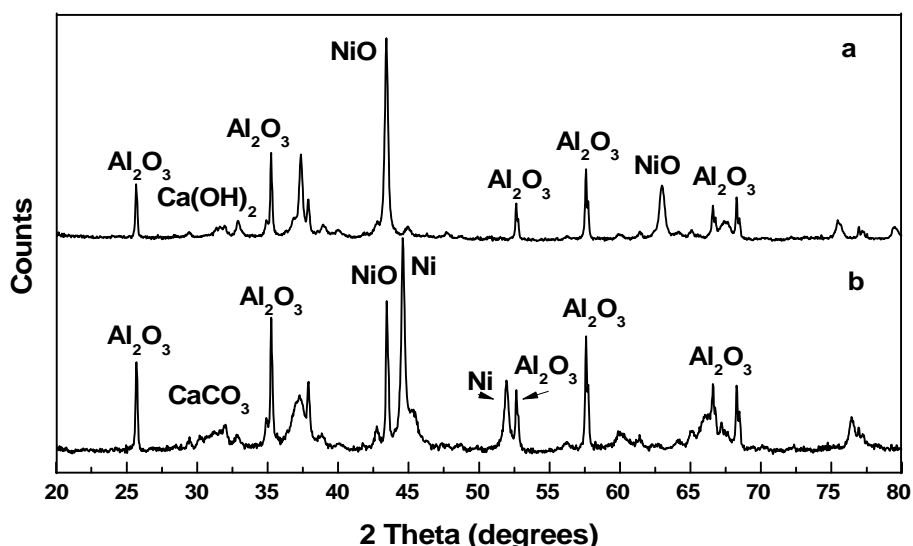


Figure 5-42 XRD patterns for Ni CaO Al₂O₃: (a) fresh (b) reacted

The XRD pattern for Ni CaO Al₂O₃ catalyst-sorbent in figure 5-42 above shows the Ca(OH)₂ and NiO phases for the fresh material while the CaCO₃ and Ni phases are only present in the reacted catalyst-sorbent. The XRD pattern for the fresh CaO in figure 5-43, shows the CaO and Ca(OH)₂ phases. The XRD pattern for the reacted Ni Al₂O₃ (figure 5-43) shows the Ni metallic phase while the catalyst-sorbent mixtures show the Ni, CaO, Ca(OH)₂, and CaCO₃ phases. The CaCO₃ phase detected is as a result of the carbonation reaction of CaO and CO₂ during the gasification process [79, 88], indicating the ability of the catalyst-sorbent to also capture CO₂ although their hydrogen yield was reduced. It therefore appears that in all cases the quantity of CO₂ adsorbed was not sufficient to balance the associated loss of nickel catalytic activity. It is suggested that separating the CaO and Ni Al₂O₃ layer in the bed or having separate beds for both materials might be more effective.

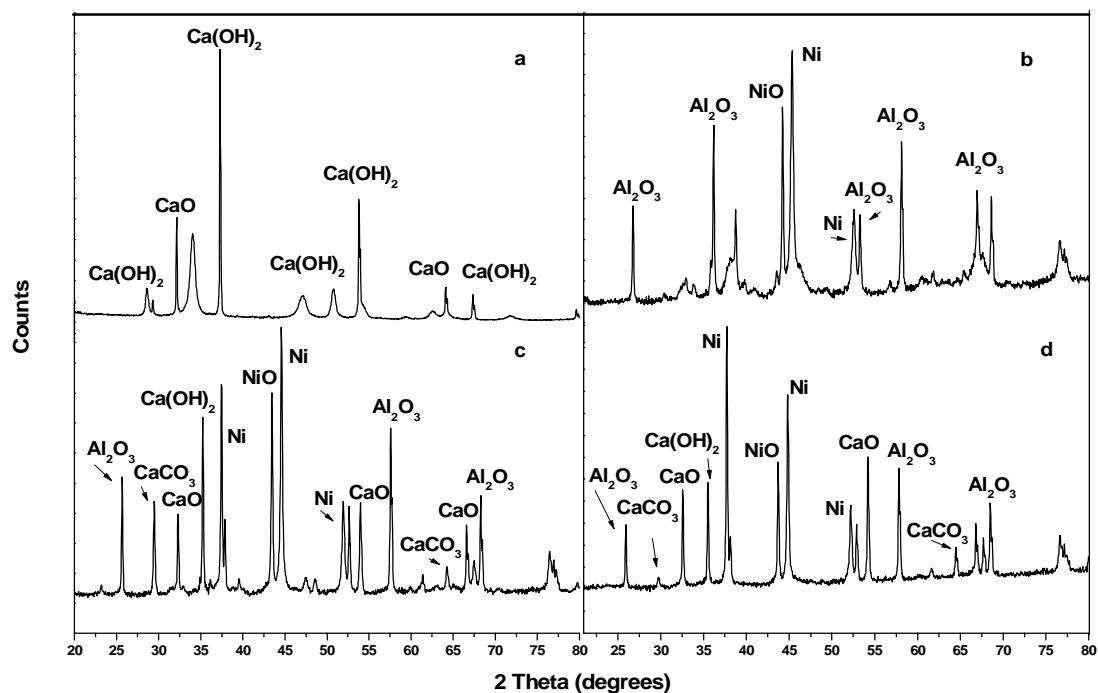


Figure 5-43 XRD patterns for Ni Al₂O₃ and CaO catalyst-sorbent: (a) fresh CaO (b) reacted Ni Al₂O₃ at 700 °C (c) reacted Ni Al₂O₃+CaO(10g) at 700 °C (d) reacted Ni Al₂O₃+CaO(10g) at 800 °C

The TEM images of the fresh and reacted catalyst-sorbents are shown in figures 5-44 to 5-46. The TEM images of the reacted catalyst-sorbents shown in figures 5-45 and 5-46 show graphitic carbon deposits on the surface of the nickel particles which could encapsulate the Ni particle and block access to the catalyst pores thereby leading to catalyst deactivation.

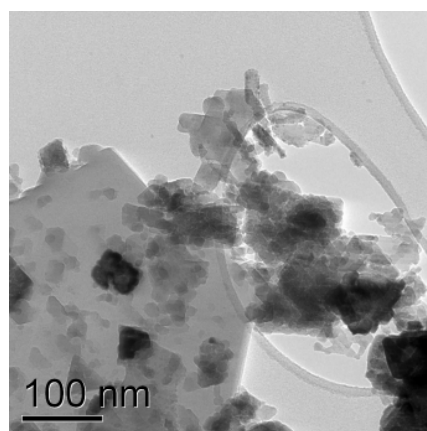


Figure 5-44 TEM image of the fresh Ni CaO Al₂O₃

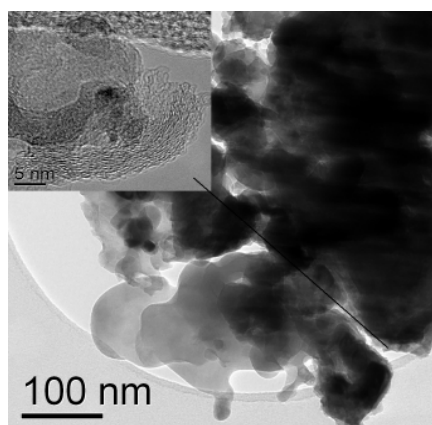


Figure 5-45 TEM image of the reacted Ni CaO Al₂O₃

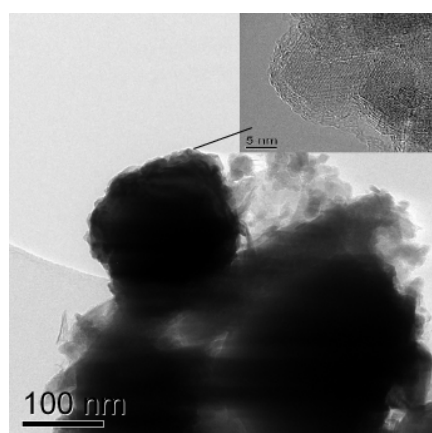


Figure 5-46 TEM image of the Ni Al₂O₃+CaO(10g) reacted at 800 °C

5.3.4 Conclusions

The steam pyrolysis-gasification of waste wood was carried out in a screw kiln reactor in the presence of nickel and calcium oxide based catalyst-sorbents. Different process parameters were varied such as; co-impregnating the CaO onto the catalyst and mixing solid CaO powder with an already synthesised Ni Al₂O₃ catalyst, varying the quantity of CaO added to the Ni Al₂O₃ catalyst, and adjusting the process temperature in order to investigate the effects of these parameters on gas yield, gas composition and CO₂ capture. The following main conclusions have been drawn:

- The use of CaO as a CO₂ sorbent, integrated into a Ni Al₂O₃ catalyst both by co-impregnation of the CaO onto the catalyst, and by mixing of

solid CaO powder with already prepared Ni Al₂O₃ catalyst, resulted in the capture of CO₂ to form CaCO₃ during the steam pyrolysis-gasification of waste wood.

- The use of the catalyst-sorbent materials containing 5 wt% of CaO prepared by CaO integration into the catalyst and by mixing CaO powders with the catalyst, had no significant impacts on the gas and hydrogen yield compared to the use of just Ni Al₂O₃ catalyst during the steam pyrolysis-gasification of waste wood. Integrating the CaO by co-impregnation and by mixing of solid CaO with the catalyst had similar effects on gas yield, hydrogen yield and gas composition.
- Increasing the CaO quantity during the steam pyrolysis gasification waste wood resulted in a gradual reduction in the gas and hydrogen yield while the CO₂ yield increased, indicating a reduction in catalytic and CO₂ sorption activity of the catalyst-sorbents. It is suggested that this was linked to the deactivation of the CaO powders by tar and could be avoided by situating the CaO powder layer after the catalyst. It is also suggested that having the CaO sorbent in a layer after the catalyst could reduce its deactivation by tar.
- Reducing the gasification temperature to 700 °C in the presence of the catalyst-sorbent resulted in reduced gas yield and hydrogen yield, compared to similar tests at 800 °C mostly due to reduced thermal cracking of heavier hydrocarbons.

References

1. Garcia, L., French, R., Czernik, S. and Chornet, E., *Catalytic steam reforming of bio-oils for the production of hydrogen: effects of catalyst composition*. Applied Catalysis A: General, 2000. **201**(2): p. 225-239.
2. Miccio, F., Piriou, B., Ruoppolo, G. and Chirone, R., *Biomass gasification in a catalytic fluidized reactor with beds of different materials*. Chemical Engineering Journal, 2009. **154**(1-3): p. 369-374.
3. Duman, G., Okutucu, C., Ucar, S., Stahl, R. and Yanik, J., *The slow and fast pyrolysis of cherry seed*. Bioresource Technology, 2011. **102**(2): p. 1869-1878.
4. Shen, D.K., Gu, S. and Bridgwater, A.V., *The thermal performance of the polysaccharides extracted from hardwood: Cellulose and hemicellulose*. Carbohydrate Polymers, 2010. **82**(1): p. 39-45.

5. Radlein, D., ed. *Study of Levoglucosan*. Fast Pyrolysis of Biomass: A Handbook, ed. Bridgwater, A.V., Czernik, S., Diebold, J., Meier, D., Oasmaa, A., Peacocke, C., Piskorz, J. and Radlein, D. Vol. 2. 2002, CPL Press: Newbury, UK. 165.
6. He, M., Hu, Z., Xiao, B., Li, J., Guo, X., Luo, S., Yang, F., Feng, Y., Yang, G. and Liu, S., *Hydrogen-rich gas from catalytic steam gasification of municipal solid waste (MSW): Influence of catalyst and temperature on yield and product composition*. International Journal of Hydrogen Energy, 2009. **34**(1): p. 195-203.
7. Wu, C., Huang, Q., Sui, M., Yan, Y. and Wang, F., *Hydrogen production via catalytic steam reforming of fast pyrolysis bio-oil in a two-stage fixed bed reactor system*. Fuel Processing Technology, 2008. **89**(12): p. 1306-1316.
8. Wu, C. and Williams, P.T., *Hydrogen Production from the Pyrolysis Gasification of Polypropylene: Influence of Steam Flow Rate, Carrier Gas Flow Rate and Gasification Temperature*. Energy & Fuels, 2009. **23**(10): p. 5055-5061.
9. Li, J., Yin, Y., Zhang, X., Liu, J. and Yan, R., *Hydrogen-rich gas production by steam gasification of palm oil wastes over supported tri-metallic catalyst*. International Journal of Hydrogen Energy, 2009. **34**(22): p. 9108-9115.
10. Guan, Y., Luo, S., Liu, S., Xiao, B. and Cai, L., *Steam catalytic gasification of municipal solid waste for producing tar-free fuel gas*. International Journal of Hydrogen Energy, 2009. **34**(23): p. 9341-9346.
11. Wei, L., Xu, S., Zhang, L., Liu, C., Zhu, H. and Liu, S., *Steam gasification of biomass for hydrogen-rich gas in a free-fall reactor*. International Journal of Hydrogen Energy, 2007. **32**(1): p. 24-31.
12. He, M., Xiao, B., Liu, S., Guo, X., Luo, S., Xu, Z., Feng, Y. and Hu, Z., *Hydrogen-rich gas from catalytic steam gasification of municipal solid waste (MSW): Influence of steam to MSW ratios and weight hourly space velocity on gas production and composition*. International Journal of Hydrogen Energy, 2009. **34**(5): p. 2174-2183.
13. Dalai, A.K., Batta, N., Eswaramoorthi, I. and Schoenau, G.J., *Gasification of refuse derived fuel in a fixed bed reactor for syngas production*. Waste Management, 2009. **29**(1): p. 252-258.
14. Luo, S., Xiao, B., Guo, X., Hu, Z., Liu, S. and He, M., *Hydrogen-rich gas from catalytic steam gasification of biomass in a fixed bed reactor: Influence of particle size on gasification performance*. International Journal of Hydrogen Energy, 2009. **34**(3): p. 1260-1264.
15. Skoulou, V., Swiderski, A., Yang, W. and Zabaniotou, A., *Process characteristics and products of olive kernel high temperature steam gasification (HTSG)*. Bioresource Technology, 2009. **100**(8): p. 2444-2451.
16. Gao, N., Li, A. and Quan, C., *A novel reforming method for hydrogen production from biomass steam gasification*. Bioresource Technology, 2009. **100**(18): p. 4271-4277.
17. Wu, C. and Williams, P.T., *Nickel-based catalysts for tar reduction in biomass gasification*. Biofuels, 2011. **2**(4): p. 451-464.
18. Yung, M.M., Jablonski, W.S. and Magrini-Bair, K.A., *Review of Catalytic Conditioning of Biomass-Derived Syngas*. Energy & Fuels, 2009. **23**(4): p. 1874-1887.

19. Bulushev, D.A. and Ross, J.R.H., *Catalysis for conversion of biomass to fuels via pyrolysis and gasification: A review*. *Catalysis Today*, 2011. **171**(1): p. 1-13.
20. Wu, C. and Williams, P.T., *A Novel Nano-Ni/SiO₂ Catalyst for Hydrogen Production from Steam Reforming of Ethanol*. *Environmental Science & Technology*, 2010. **44**(15): p. 5993-5998.
21. Akande, A.J., Idem, R.O. and Dalai, A.K., *Synthesis, characterization and performance evaluation of Ni/Al₂O₃ catalysts for reforming of crude ethanol for hydrogen production*. *Applied Catalysis A: General*, 2005. **287**(2): p. 159-175.
22. Garcia, L., Benedicto, A., Romeo, E., Salvador, M.L., Arauzo, J. and Bilbao, R., *Hydrogen Production by Steam Gasification of Biomass Using Ni–Al Coprecipitated Catalysts Promoted with Magnesium*. *Energy & Fuels*, 2002. **16**(5): p. 1222-1230.
23. García, L., Salvador, M.L., Arauzo, J. and Bilbao, R., *Catalytic Steam Gasification of Pine Sawdust. Effect of Catalyst Weight/Biomass Flow Rate and Steam/Biomass Ratios on Gas Production and Composition*. *Energy & Fuels*, 1999. **13**(4): p. 851-859.
24. Bimbela, F., Oliva, M., Ruiz, J., García, L. and Arauzo, J., *Catalytic steam reforming of model compounds of biomass pyrolysis liquids in fixed bed: Acetol and n-butanol*. *Journal of Analytical and Applied Pyrolysis*, 2009. **85**(1–2): p. 204-213.
25. Wang, L., Li, D., Koike, M., Watanabe, H., Xu, Y., Nakagawa, Y. and Tomishige, K., *Catalytic performance and characterization of Ni–Co catalysts for the steam reforming of biomass tar to synthesis gas*. *Fuel*, 2012(0).
26. Kimura, T., Miyazawa, T., Nishikawa, J., Kado, S., Okumura, K., Miyao, T., Naito, S., Kunimori, K. and Tomishige, K., *Development of Ni catalysts for tar removal by steam gasification of biomass*. *Applied Catalysis B: Environmental*, 2006. **68**(3-4): p. 160-170.
27. Tomishige, K., Kimura, T., Nishikawa, J., Miyazawa, T. and Kunimori, K., *Promoting effect of the interaction between Ni and CeO₂ on steam gasification of biomass*. *Catalysis Communications*, 2007. **8**(7): p. 1074-1079.
28. Basagiannis, A.C. and Verykios, X.E., *Steam reforming of the aqueous fraction of bio-oil over structured Ru/MgO/Al₂O₃ catalysts*. *Catalysis Today*, 2007. **127**(1–4): p. 256-264.
29. Wang, D., Montané, D. and Chornet, E., *Catalytic steam reforming of biomass-derived oxygenates: acetic acid and hydroxyacetaldehyde*. *Applied Catalysis A: General*, 1996. **143**(2): p. 245-270.
30. Takanabe, K., Aika, K.-i., Seshan, K. and Lefferts, L., *Sustainable hydrogen from bio-oil—Steam reforming of acetic acid as a model oxygenate*. *Journal of Catalysis*, 2004. **227**(1): p. 101-108.
31. Pfeifer, C. and Hofbauer, H., *Development of catalytic tar decomposition downstream from a dual fluidized bed biomass steam gasifier*. *Powder Technology*, 2008. **180**(1–2): p. 9-16.
32. Bartholomew, C.H., *Mechanisms of catalyst deactivation*. *Applied Catalysis A: General*, 2001. **212**(1-2): p. 17-60.
33. Lind, F., Seemann, M. and Thunman, H., *Continuous catalytic tar reforming of biomass derived raw gas with simultaneous catalyst regeneration*. *Industrial and Engineering Chemistry Research*, 2011. **50**(20): p. 11553-11562.

34. Li, M., Wang, X., Li, S., Wang, S. and Ma, X., *Hydrogen production from ethanol steam reforming over nickel based catalyst derived from Ni/Mg/Al hydrotalcite-like compounds*. International Journal of Hydrogen Energy, 2010. **35**(13): p. 6699-6708.
35. Efika, C., Wu, C. and Williams, P.T., *Syngas Production from Pyrolysis-Catalytic Steam Reforming of Waste Biomass in a Continuous Screw Kiln Reactor*. Journal of Analytical and Applied Pyrolysis, 2012(0).
36. Rostrup-Nielsen, J. and Trimm, D.L., *Mechanisms of carbon formation on nickel-containing catalysts*. Journal of Catalysis, 1977. **48**(1–3): p. 155-165.
37. Bartholomew, C.H. and Farrauto, R.J., *Fundamentals of Industrial Catalytic Processes*. 2nd Edition ed. 2006: John Wiley & Sons Inc.
38. Menon, P.G., *Coke on catalysts-harmful, harmless, invisible and beneficial types*. Journal of Molecular Catalysis, 1990. **59**(2): p. 207-220.
39. Eberly, P.E., Kimberlin, C.N., Miller, W.M. and Drushel, H.V., *Coke Formation on Silica-Alumina Cracking Catalysts*. Industrial & Engineering Chemistry Process Design and Development, 1966. **5**(2): p. 193-198.
40. Andrew, S.P.S., *Catalysts and Catalytic Processes in The Steam Reforming of Naphtha*. Product R&D, 1969. **8**(3): p. 321-324.
41. Bartholomew, C.H., *CARBON DEPOSITION IN STEAM REFORMING AND METHANATION*. Catalysis reviews, 1982. **24**(1): p. 67-112.
42. Trimm, D.L., *Catalyst design for reduced coking (review)*. Applied Catalysis, 1983. **5**(3): p. 263-290.
43. Rostrup-Nielsen, J.R., *Coking on nickel catalysts for steam reforming of hydrocarbons*. Journal of Catalysis, 1974. **33**(2): p. 184-201.
44. Bartholomew, C.H., Strasburg, M.V. and Hsieh, H.-Y., *Effects of Support on Carbon Formation and Gasification on Nickel during Carbon Monoxide Hydrogenation*. Applied Catalysis, 1988. **36**(0): p. 147-162.
45. Baker, R.T.K. and Chludzinski Jr, J.J., *Filamentous carbon growth on nickel-iron surfaces: The effect of various oxide additives*. Journal of Catalysis, 1980. **64**(2): p. 464-478.
46. Grabke, H.J., Möller, G.R. and Schnaas, A., *Einfluß von Schwefel auf die Aufkohlung einer CrNiFe-Legierung bei hohen Temperaturen*. Materials and Corrosion, 1979. **30**(11): p. 794-799.
47. Trimm, D.L., *Catalysts for the control of coking during steam reforming*. Catalysis Today, 1999. **49**(1–3): p. 3-10.
48. Sutton, D., Kelleher, B. and Ross, J.R.H., *Review of literature on catalysts for biomass gasification*. Fuel Processing Technology, 2001. **73**(3): p. 155-173.
49. Inaba, M., Murata, K., Saito, M. and Takahara, I., *Hydrogen Production by Gasification of Cellulose over Ni Catalysts Supported on Zeolites*. Energy & Fuels, 2006. **20**(2): p. 432-438.
50. Wang, S. and Lu, G.Q., *Role of CeO₂ in Ni/CeO₂-Al₂O₃ catalysts for carbon dioxide reforming of methane*. Applied Catalysis B: Environmental, 1998. **19**(3–4): p. 267-277.
51. Lu, Y., Li, S., Guo, L. and Zhang, X., *Hydrogen production by biomass gasification in supercritical water over Ni/[gamma]Al₂O₃ and Ni/CeO₂-[gamma]Al₂O₃ catalysts*. International Journal of Hydrogen Energy, 2010. **35**(13): p. 7161-7168.
52. Bona, S., Guillén, P., Alcalde, J.G., García, L. and Bilbao, R., *Toluene steam reforming using coprecipitated Ni/Al catalysts modified with lanthanum or cobalt*. Chemical Engineering Journal, 2008. **137**(3): p. 587-597.

53. Martinez, R., Romero, E., Garcia, L. and Bilbao, R., *The effect of lanthanum on Ni–Al catalyst for catalytic steam gasification of pine sawdust*. Fuel Processing Technology, 2004. **85**(2–3): p. 201-214.
54. Galdámez, J.R., García, L. and Bilbao, R., *Hydrogen Production by Steam Reforming of Bio-Oil Using Coprecipitated Ni–Al Catalysts. Acetic Acid as a Model Compound*. Energy & Fuels, 2005. **19**(3): p. 1133-1142.
55. Bimbela, F., Chen, D., Ruiz, J., García, L. and Arauzo, J., *Ni/Al coprecipitated catalysts modified with magnesium and copper for the catalytic steam reforming of model compounds from biomass pyrolysis liquids*. Applied Catalysis B: Environmental, 2012. **119–120**(0): p. 1-12.
56. Arauzo, J., Radlein, D., Piskorz, J. and Scott, D.S., *Catalytic Pyrogasification of Biomass. Evaluation of Modified Nickel Catalysts*. Industrial & Engineering Chemistry Research, 1997. **36**(1): p. 67-75.
57. Koike, M., Ishikawa, C., Li, D., Wang, L., Nakagawa, Y. and Tomishige, K., *Catalytic performance of manganese-promoted nickel catalysts for the steam reforming of tar from biomass pyrolysis to synthesis gas*. Fuel, 2013. **103**(0): p. 122-129.
58. Elbaba, I.F., Wu, C. and Williams, P.T., *Hydrogen production from the pyrolysis-gasification of waste tyres with a nickel/cerium catalyst*. International Journal of Hydrogen Energy, 2011. **36**(11): p. 6628-6637.
59. Wu, C. and Williams, P.T., *Ni/CeO₂/ZSM-5 catalysts for the production of hydrogen from the pyrolysis-gasification of polypropylene*. International Journal of Hydrogen Energy, 2009. **34**(15): p. 6242-6252.
60. Asadullah, M., Miyazawa, T., Ito, S.-i., Kunimori, K., Yamada, M. and Tomishige, K., *Catalyst development for the gasification of biomass in the dual-bed gasifier*. Applied Catalysis A: General, 2003. **255**(2): p. 169-180.
61. Duprez, D., *Study of surface mobility by isotopic exchange: recent developments and perspectives*, in *Studies in Surface Science and Catalysis*, Can, L. and Qin, X., Editors. 1997, Elsevier. p. 13-28.
62. Yao, H.C. and Yao, Y.F.Y., *Ceria in automotive exhaust catalysts: I. Oxygen storage*. Journal of Catalysis, 1984. **86**(2): p. 254-265.
63. Srisiriwat, N., Therdthianwong, S. and Therdthianwong, A., *Oxidative steam reforming of ethanol over Ni/Al₂O₃ catalysts promoted by CeO₂, ZrO₂ and CeO₂-ZrO₂*. International Journal of Hydrogen Energy, 2009. **34**(5): p. 2224-2234.
64. Benito, M., García, S., Ferreira-Aparicio, P., Serrano, L.G. and Daza, L., *Development of biogas reforming Ni-La-Al catalysts for fuel cells*. Journal of Power Sources, 2007. **169**(1): p. 177-183.
65. Li, S., Lu, Y., Guo, L. and Zhang, X., *Hydrogen production by biomass gasification in supercritical water with bimetallic Ni–M/γAl₂O₃ catalysts (M = Cu, Co and Sn)*. International Journal of Hydrogen Energy, 2011. **36**(22): p. 14391-14400.
66. Takanabe, K., Nagaoka, K., Nariai, K. and Aika, K.-i., *Titania-supported cobalt and nickel bimetallic catalysts for carbon dioxide reforming of methane*. Journal of Catalysis, 2005. **232**(2): p. 268-275.
67. Andonova, S., de Ávila, C.N., Arishtirova, K., Bueno, J.M.C. and Damyanova, S., *Structure and redox properties of Co promoted Ni/Al₂O₃ catalysts for oxidative steam reforming of ethanol*. Applied Catalysis B: Environmental, 2011. **105**(3–4): p. 346-360.

68. Hu, X. and Lu, G., *Investigation of steam reforming of acetic acid to hydrogen over Ni-Co metal catalyst*. Journal of Molecular Catalysis A: Chemical, 2007. **261**(1): p. 43-48.
69. Khzouz, M., Wood, J., Pollet, B. and Bujalski, W., *Characterization and activity test of commercial Ni/Al₂O₃, Cu/ZnO/Al₂O₃ and prepared Ni-Cu/Al₂O₃ catalysts for hydrogen production from methane and methanol fuels*. International Journal of Hydrogen Energy, 2013. **38**(3): p. 1664-1675.
70. Liu, Q., Liu, Z., Zhou, X., Li, C. and Ding, J., *Hydrogen production by steam reforming of ethanol over copper doped Ni/CeO₂ catalysts*. Journal of Rare Earths, 2011. **29**(9): p. 872-877.
71. Li, D., Nakagawa, Y. and Tomishige, K., *Development of Ni-Based Catalysts for Steam Reforming of Tar Derived from Biomass Pyrolysis*. Chinese Journal of Catalysis, 2012. **33**(4-6): p. 583-594.
72. Li, D., Wang, L., Koike, M., Nakagawa, Y. and Tomishige, K., *Steam reforming of tar from pyrolysis of biomass over Ni/Mg/Al catalysts prepared from hydrotalcite-like precursors*. Applied Catalysis B: Environmental, 2011. **102**(3-4): p. 528-538.
73. Miyazawa, T., Kimura, T., Nishikawa, J., Kado, S., Kunimori, K. and Tomishige, K., *Catalytic performance of supported Ni catalysts in partial oxidation and steam reforming of tar derived from the pyrolysis of wood biomass*. Catalysis Today, 2006. **115**(1-4): p. 254-262.
74. Wu, C. and Williams, P.T., *Investigation of coke formation on Ni-Mg-Al catalyst for hydrogen production from the catalytic steam pyrolysis-gasification of polypropylene*. Applied Catalysis B: Environmental, 2010. **96**(1-2): p. 198-207.
75. Dupont, V., Ross, A.B., Knight, E., Hanley, I. and Twigg, M.V., *Production of hydrogen by unmixed steam reforming of methane*. Chemical Engineering Science, 2008. **63**(11): p. 2966-2979.
76. Dou, B., Rickett, G.L., Dupont, V., Williams, P.T., Chen, H., Ding, Y. and Ghadiri, M., *Steam reforming of crude glycerol with in situ CO₂ sorption*. Bioresource Technology, 2010. **101**(7): p. 2436-2442.
77. Florin, N.H. and Harris, A.T., *Enhanced hydrogen production from biomass with in situ carbon dioxide capture using calcium oxide sorbents*. Chemical Engineering Science, 2008. **63**(2): p. 287-316.
78. Acharya, B., Dutta, A. and Basu, P., *An investigation into steam gasification of biomass for hydrogen enriched gas production in presence of CaO*. International Journal of Hydrogen Energy, 2010. **35**(4): p. 1582-1589.
79. Kobayashi, J., Kawamoto, K., Fukushima, R. and Tanaka, S., *Woody biomass and RPF gasification using reforming catalyst and calcium oxide*. Chemosphere, 2011. **83**(9): p. 1273-1278.
80. Koppatz, S., Pfeifer, C., Rauch, R., Hofbauer, H., Marquard-Moellenstedt, T. and Specht, M., *H₂ rich product gas by steam gasification of biomass with in situ CO₂ absorption in a dual fluidized bed system of 8 MW fuel input*. Fuel Processing Technology, 2009. **90**(7-8): p. 914-921.
81. Stevens Jr, R.W., Shamsi, A., Carpenter, S. and Siriwardane, R., *Sorption-enhanced water gas shift reaction by sodium-promoted calcium oxides*. Fuel, 2010. **89**(6): p. 1280-1286.
82. Rackley, S.A., *Carbon Capture and Storage*. Civil & Environmental. 2010: Butterworth-Heinemann. 1-386.

83. Hanaoka, T., Yoshida, T., Fujimoto, S., Kamei, K., Harada, M., Suzuki, Y., Hatano, H., Yokoyama, S.-y. and Minowa, T., *Hydrogen production from woody biomass by steam gasification using a sorbent*. Biomass and Bioenergy, 2005. **28**(1): p. 63-68.
84. Huang, B.-S., Chen, H.-Y., Chuang, K.-H., Yang, R.-X. and Wey, M.-Y., *Hydrogen production by biomass gasification in a fluidized-bed reactor promoted by an Fe/CaO catalyst*. International Journal of Hydrogen Energy, 2012. **37**(8): p. 6511-6518.
85. Corella, J., Toledo, J.M. and Molina, G., *Steam Gasification of Coal at Low–Medium (600–800 °C) Temperature with Simultaneous CO₂ Capture in Fluidized Bed at Atmospheric Pressure: The Effect of Inorganic Species. 1. Literature Review and Comments*. Industrial & Engineering Chemistry Research, 2006. **45**(18): p. 6137-6146.
86. Di Felice, L., Courson, C., Foscolo, P.U. and Kiennemann, A., *Iron and nickel doped alkaline-earth catalysts for biomass gasification with simultaneous tar reformation and CO₂ capture*. International Journal of Hydrogen Energy, 2011. **36**(9): p. 5296-5310.
87. Gallucci, K., Stendardo, S. and Foscolo, P.U., *CO₂ capture by means of dolomite in hydrogen production from syn gas*. International Journal of Hydrogen Energy, 2008. **33**(12): p. 3049-3055.
88. Wu, C. and Williams, P.T., *A novel Ni-Mg-Al-CaO catalyst with the dual functions of catalysis and CO₂ sorption for H₂ production from the pyrolysis-gasification of polypropylene*. Fuel, 2010. **89**(7): p. 1435-1441.

CHAPTER 6. PYROLYSIS AND PARTIAL OXIDATION OF DIFFERENT REAL WORLD WASTES IN AN INDUSTRIAL SCALE SCREW KILN REACTOR

In this study, different types of solid wastes were processed thermally in order to convert them to useful energy on an industrial scale. This study enabled comparison of the laboratory research with a real-world pyrolysis reactor. This was achieved using a pyrolysis and air-partial oxidation reactor which was located at a waste treatment facility in Selby, UK owned by Maltings Organic Treatment Ltd. The reactor termed an ST-150, was a screw-kiln reactor which could process up to 0.5 tons hr^{-1} of material at process temperatures of up to 1050 °C to produce mostly gas, solid residue and some liquid. The volatile products were used to generate the energy required to self-sustain the process, as well as provide heat energy for a compost process within the waste treatment facility. Samples of the waste feedstock and products (gas, liquid and solid residue) were analysed using; Thermogravimetric analyser, bomb calorimeter, CHNS-O analyser, GC-TCD, GC-FID and GC-MS-MS, in order to characterize the initial feedstock and investigate the effects of the process on the products.

Due to the site, materials and equipment being owned by a third party, the processes during the actual waste conversion were not within the control of the author apart from sample collection and analysis. However adequate effort was made where possible in order to standardise product sampling and analysis.

6.1 Materials and methods

The waste materials utilised in this research were available from the Maltings Organic Treatment plant in Selby. The waste materials were a mixture of 'as received' and processed organic and inorganic residual wastes including:

municipal solid waste (MSW), shredded automobile wastes (SAW), clinical wastes (non-hazardous and infectious, as defined in the literature [1-2]), waste wood, waste plastics and waste synthetic fabric (WSF). Mixtures of 50% by volume composition of MSW and waste plastics, also MSW and WSF, were also thermally processed. The WSF was a woven material utilized in industry for mopping up spills.

The MSW used for the tests was a mixture of residues from trommel screening of 'as received' MSW and composted MSW from a windrow process. The other waste materials were shredded to obtain a heterogeneous size range of approximately between 10 and 60 mm, which were fed to the reactor. The SAW contained a mixture of plastics, polyurethane foam, textile, rubber, dirt and other inorganic solids. Table 6-1 shows the results of the elemental and proximate analysis of the fresh waste materials, apart from the clinical wastes which were not characterized due to their hazardous nature.

6.1.1 Materials Characterization

Fresh feed materials were characterized before their thermal treatment, except the clinical wastes and the SAW material, due to their potentially hazardous and highly heterogeneous natures respectively. In order to increase the homogeneity of the materials prior to characterization, 1000 g of each of the waste materials were mixed. The quantity of the materials were then reduced by coning and quartering to approximately 120 g, which were then ground to an average diameter of 2mm. The ground materials were further blended and the coning and quartering process was repeated in order to obtain representative samples of approximately 8 g for each of the materials which were then characterized. The moisture, volatile, fixed carbon and ash content of the feed materials were determined by proximate analysis using a Metler thermogravimetric analyser (TGA) as described in chapter 3.

Elemental analysis to determine the carbon, hydrogen, nitrogen and sulphur contents of RDF were carried with a Carlo Erba Flash EA 112 elemental analyser, while the oxygen content was determined by difference on an ash free basis.

The calorific value (CV) of the materials was determined using a bomb calorimeter.

The characteristics of the fresh materials were determined on a dry basis due to the scale, and the accuracy of analysing a representative sample of the material. The moisture content of the as-received and processed material varied widely and was up to 40 wt%.

It should be noted that due to the constraints of the sampling regime the characteristics of the wastes may not be wholly accurate however they will provide a broad indication of their respective properties.

6.1.2 Reactor System

The test reactor used for the investigations was a commercial scale pyrolysis/partial oxidation reactor referred to as the ST-150, designed and fabricated by a company called DPS Global, a UK company in Bristol. The ST-150 could process up to 0.5 tons hr⁻¹ of a broad range of solid wastes. A schematic diagram of the reactor is shown in figure 6-1 below while figure 6-2 shows a photograph of the reactor. Figure 6-3 shows a 3D model of the reactor.

The reactor system was comprised of a waste hopper connected to a feed compactor screw which feeds the waste to the pyrolysis chamber which was made up of an externally heated tube containing a screw shaft for feeding the waste along the pyrolysis chamber, within another insulated tube. The pyrolysis chamber was 4700mm length by 390mm diameter, with an effectively heated length of 4000mm. This chamber was connected to a char, steam and air gasifier. The gasifier was connected to an oxidiser which was a refractory-lined vessel for combusting the volatile products of the process.

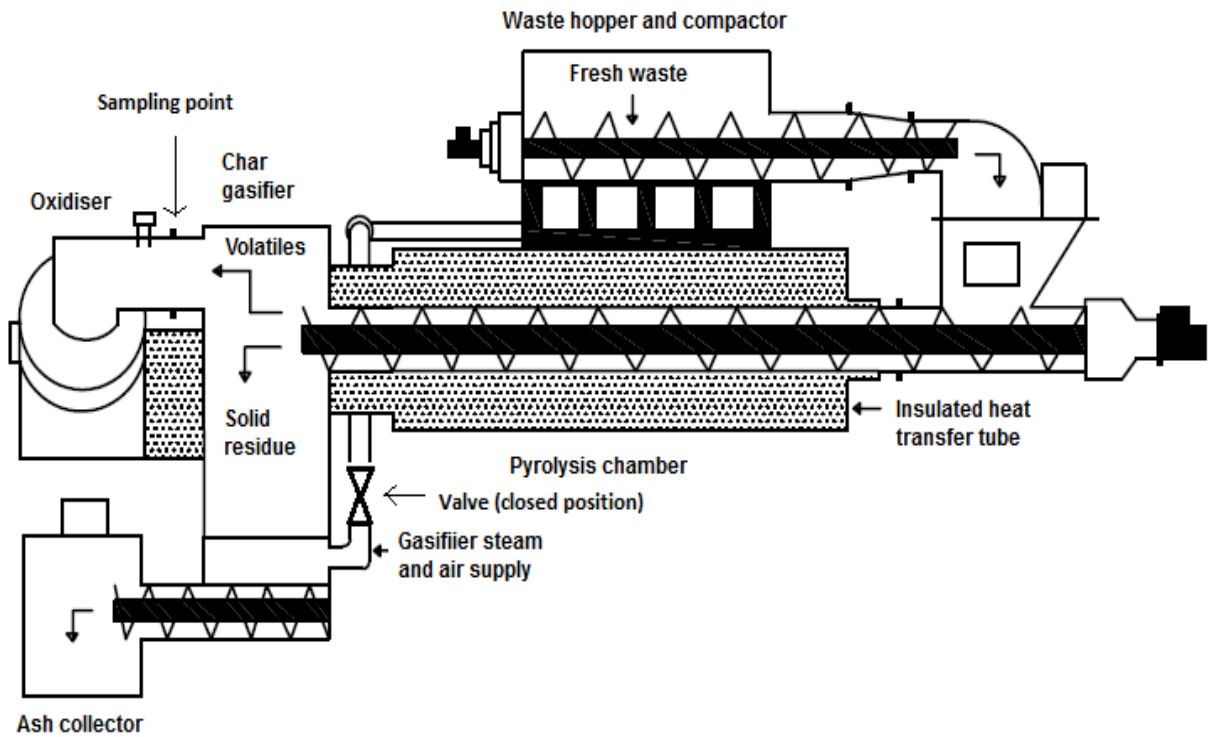


Figure 6-1 Schematic diagram of the pyrolysis/partial oxidation reactor

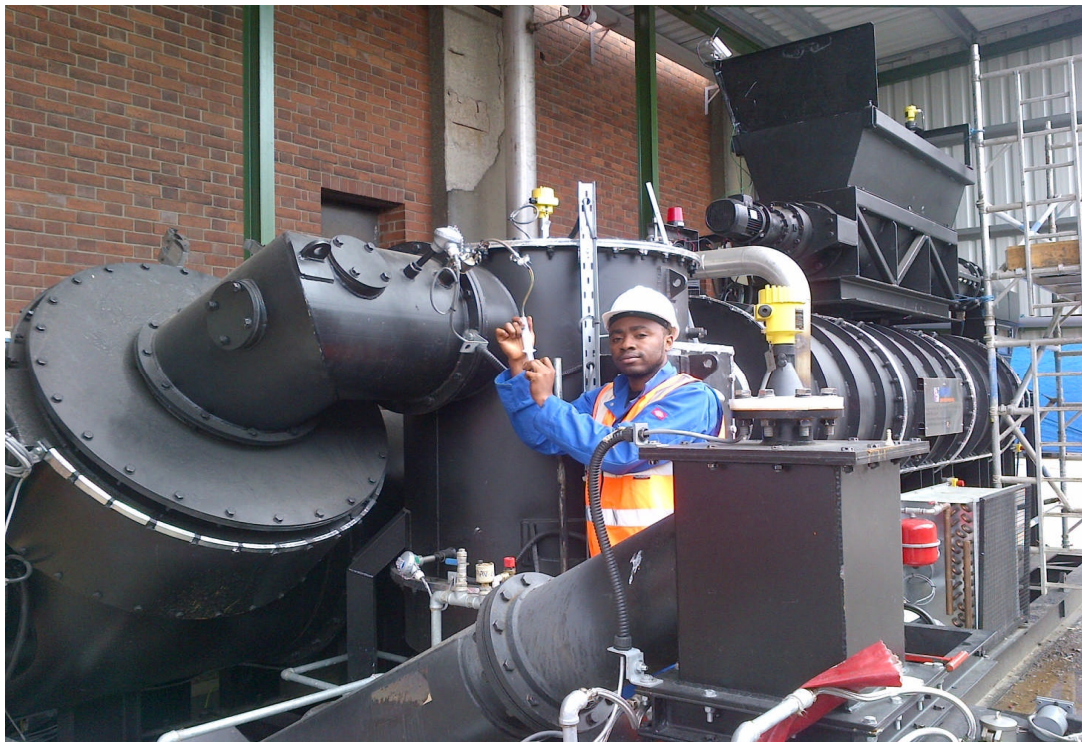


Figure 6-2 Photograph of the pyrolysis/partial oxidation reactor

The gasifier was also connected to an ash collection system. The exit of the oxidiser was connected to the outer insulated tube of the pyrolysis chamber,

which was connected at the other end to a heat exchanger system. The heat exchanger was connected to an induced draft (ID) fan which was finally connected to an exhaust system. The ID fan was responsible for pulling the exhaust gases from the oxidiser, through the pyrolysis outer tube and heat exchanger, and finally channelling the gases to the exhaust stack.

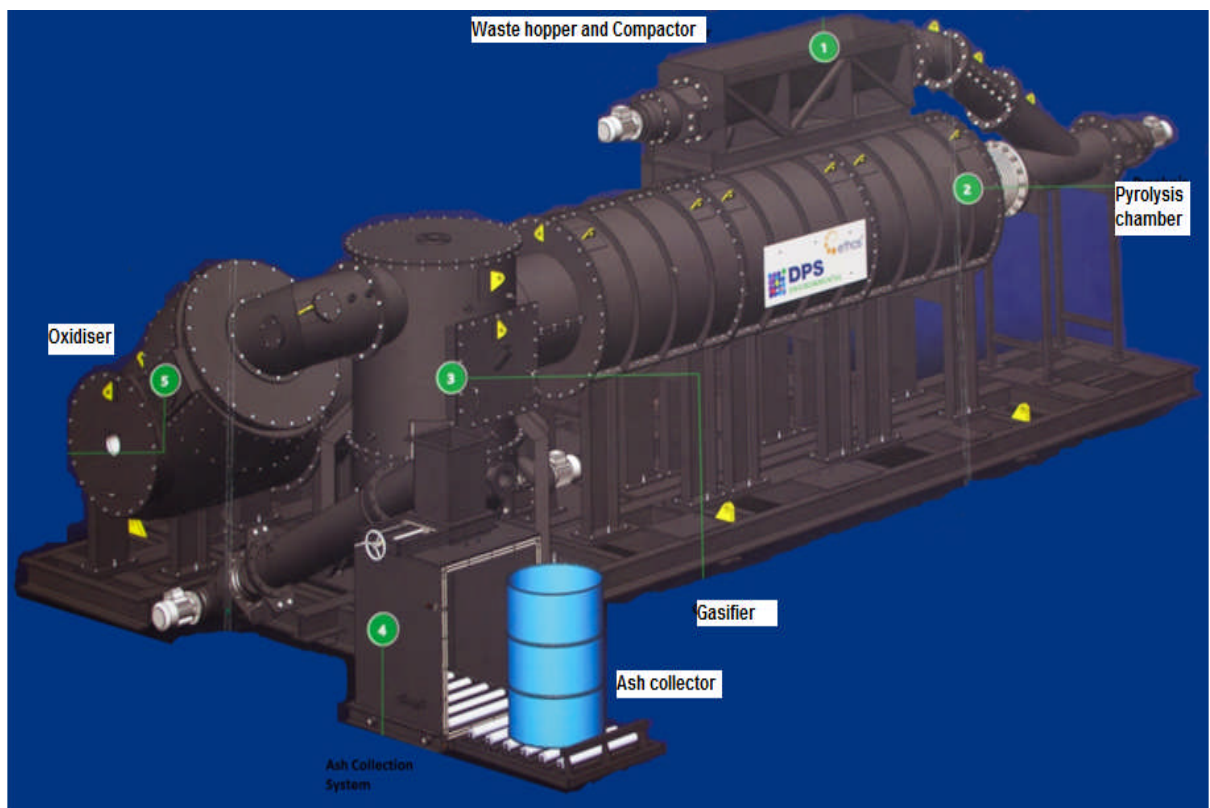


Figure 6-3 3D model of the pyrolysis/partial oxidation reactor

Experiments proceeded when the temperature of the flue gas from the oxidiser which heated up the outer pyrolysis tube reached 1050 °C when measured by a thermocouple situated at the inlet of the tube connecting the outer pyrolysis chamber to the oxidiser. The temperature of the hot flue gas measured at the exit of the outer pyrolysis chamber which was also on the same side as the waste feed inlet was 850 °C and the process temperature was taken as an average of these temperatures (950 °C). This was achieved by initially combusting propane in the oxidiser in order to achieve a temperature of approximately 1150 °C in the oxidiser. In addition to controlling the combustion process and temperature by controlling air flow into the

combustion chamber, the ID fan also maintained a negative pressure within the reactor to prevent process gases leaking out via the waste feed inlet.

When the desired process temperatures were achieved, the targeted wastes were tipped into the waste hopper which in turn fed the waste into the screw compactor system. The compactor screw was designed to compact the waste in order to eject any contained air and reduce the ingress of air into the process system by creating a continuous seal in the form of a continuous plug of the waste material during feeding. The wastes were fed at approximately $0.15 \text{ tons hr}^{-1}$. The waste was fed into the pyrolysis chamber where pyrolysis and partial oxidation took place. The waste was thermally degraded as it was transported along the length of the pyrolysis chamber by the screw shaft which was controlled by an electric motor to keep the residence time of the solids between 30 to 40 min.

The product gases and solids were transported into the gasifier. For the purpose of the tests, the gasifier system was not active, i.e. no oxidants or heat were introduced into the gasifier. The solids were transported to the ash collection vessel for storage while the volatile products were channelled into the oxidiser for combustion to gradually replace the propane until the system became self-sustaining. The temperature of the flue gas from the combustion of the pyrolysis volatiles after sustaining the pyrolysis process was sufficiently high ($800 \text{ }^{\circ}\text{C}$) and was channelled to a heat exchanger in order to reclaim the waste heat. The excess heat reclaimed by the heat exchanger was used to generate steam to provide heat to a Windrow composting process within the waste facility.

The ST-150 reactor was designed to separate the pyrolysis and gasification processes into zones by having separate pyrolysis and gasification chambers, and the pyrolysis chamber was designed to allow for pyrolysis to occur in an inert atmosphere by preventing air ingress into the chamber. However due to technical limitations and practicality which resulted in air being pulled into the

pyrolysis chamber, the process which took place in the pyrolysis chamber was a combination of pyrolysis and air partial oxidation.

Samples of the process gas were collected from a designed sampling port, using plastic syringes and a Tedlar sampling bag connected to a vacuum pump. In order to collect the condensable products, the process vapours were passed through 2 glass condensers packed with glass wool and immersed in dry ice before being pumped into the gas bag. A minimum of 6 gas samples at a 10 min interval, were taken in order to determine the reproducibility of the process. Analysis of the gas samples indicated that the process conditions were reproducible. Solid samples were also collected from the ash collection vessel after each run.

The gas, oil and solid samples that were collected were analysed as detailed in chapter 3.

The gross calorific value (GCV) of the gases were calculated from the equation 6.1 below:

$$\text{GCV} = \text{CV}_m / Z_m \quad (\text{equation 6.1})$$

Where CV_m is the sum of the products of the mole fractions and the calorific values of the individual gases, Z_m is the compressibility factor of the gases.

6.2 Results and discussion

6.2.1 Materials characteristics

Table 6-1 shows the results of the proximate, elemental and bomb calorimetric analyses of the investigated feed materials on a dry basis. The material characteristics shown for SAW were taken from literature [3] due to the highly heterogeneous nature of the feedstock. The non-hazardous clinical waste contained materials such as paper towels, rubber gloves and food waste, while the infectious clinical waste contained similar materials however

it also contained more gloves, plastic tubes and blood and tissue contaminated materials. Both clinical wastes had no sharps included.

Table 6-1.
Properties of fresh waste material

Properties of solid residue (wt%)	Waste wood	MSW + WSF	MSW + Plastic	MSW	SAW (Day et al)	Waste plastics
Moisture	4.0	4.0	1.8	4.0	2.6	1.0
Volatile	74.0	60.0	79.2	76.0	39.3	81.0
Fixed carbon	8.0	2.0	2.0	5.0	0.0	5.0
Ash content	14.0	34.0	7.0	15.0	58.1	13.0
N content	2.0	2.3	2.9	1.1	0.9	
C content	42.4	31.9	60.1	42.0	27.9	
H content	5.1	3.9	6.1	5.7	4.0	
S content	0.3	0.2	0.1	0.2	0.3	
O content	36.2	27.8	23.7	38.1	8.8	
CV (MJ Kg ⁻¹)	18.5	14.5	20.1	18.6	10.2	37.7

The waste plastics were left over packaging cartridges from coffee and tea dispensing machines (Tassimo), and contained some residual tea and coffee. The CV of the characterized materials ranged from 14.5 MJ Kg⁻¹ for the mixture of MSW and WSF, to 37.7 MJ Kg⁻¹ for the waste plastics. The results for the analyses of the mixture of MSW and plastic wastes indicated that adding plastic waste to the MSW influenced the material characteristics by mostly increasing the volatile content, reducing the ash content and thereby increasing the CV of the material.

The waste wood and MSW indicated high oxygen contents, mostly as a result of chemically bound oxygen in the cellulosic fractions. The mixture of MSW+WSF material indicated higher ash content compared to the MSW sample, indicating that the WSF material had a high inorganic content.

6.2.2 Product yields

The thermal process was designed to utilize the energy within the waste to generate the heat required for its processing by combusting the volatile products within the oxidizer and then recirculating the hot flue gases through the outer shell of the pyrolysis tube in order to harness the heat energy and sustain the process. In order to create the oxygen free environment required for pyrolysis [4-5], the design of the reactor's waste feed mechanism was such that the ingress of air into the pyrolysis chamber was limited to prevent air being sucked in freely into the chamber by the negative pressure created by the fan. However as indicated by the gas products, the atmosphere in the pyrolysis chamber was not completely inert due to design limitations.

It was therefore expected that due to the presence of air in the pyrolysis chamber of the reactor, the results obtained from the processing of the different materials would be similar to those obtained from air partial oxidation of biomass and waste in the literature [6-8]. It is important at this point to note that due to the process control limitations earlier stated, the reproducibility of the results detailed below were questionable. However the results provided an idea of the processes which occurred in the reactor during the processing of the different materials.

The thermal processing of all the investigated wastes within the ST-150 yielded mostly volatile products consisting of gases and pyrolysis liquids, and solid products. These products were as a result of the varied combination of reactions which took place within different reaction zones in the pyrolysis chamber, including; drying, preheating, pyrolysis and, air and auto-generated steam (from the moisture content of the wastes) partial oxidation [9-10]. The carbon conversion (to volatiles), determined by equation 6.2 below, for the different wastes in the pyrolysis chamber is shown in Figure 6-4.

$$C_{\text{conv}} \% = [(C_f - C_p) / C_f] \times 100 \quad (\text{equation 6.2})$$

Where C_f is the carbon content in the fresh waste material, C_p is the carbon content in the processed solid product.

Figure 6-4 shows that the waste plastics and the mixture of MSW and waste plastics indicated the highest C conversion. This was mostly because of their low ash, fixed carbon and high volatile content per mass compared to the other analysed wastes, influenced by their plastic contents.

The volatile products (gas and liquid) were collected during self-sustained processing in order to collect and analyse samples representative of running the process at steady state. Solid products were collected from the ash collection vessel after it has cooled.

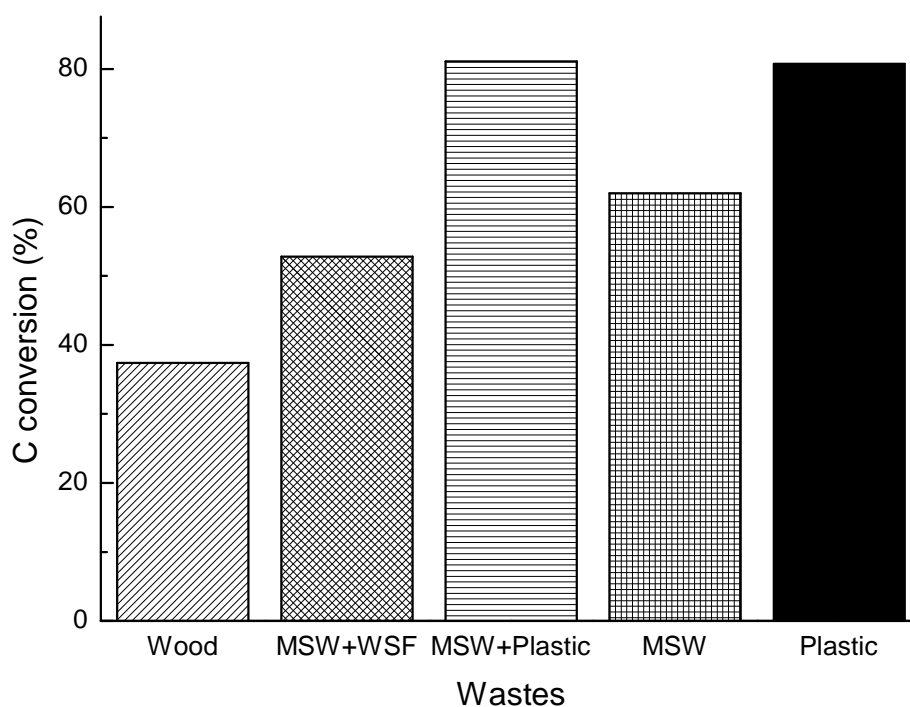


Figure 6-4 Carbon conversion for the wastes

6.2.3 Gas product and composition

Table 6-2 shows the results of the analysis of gas samples for the different wastes collected from a sampling port on the ST-150, situated just before the inlet to the oxidizer. The table shows the detected gases and their concentration in vol%. Across the gas products from the different wastes, the gas with the highest concentration detected was N₂, followed by CO₂ in most cases. The N₂ in the gases is mostly as a result of the air which enters into

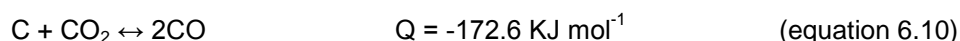
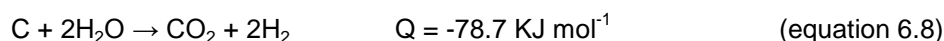
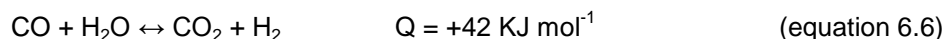
the pyrolysis chamber. Similar results have been reported from other researchers [10-13] for the air partial oxidation/gasification of carbonaceous materials.

The detected N_2 concentration was between the ranges of 44 to 89.6 vol% for the different wastes. The quantity of N_2 detected in the product gases was mostly a function of the quantity of air which escaped into the pyrolysis chamber, which was in turn impacted by the physical characteristics of the waste and its ability to form a plug during feeding. For example the infectious clinical waste was made up of materials such as paper towels, rubber gloves and tubes which when compressed formed a better seal than the SAW which contained plastics, dirt and inorganic solids which when compacted formed a porous seal. This is supported by the quantity of N_2 detected in the product gases for both materials.

The CO_2 detected in the product gases was as a result of the devolatilization of oxygenated functional groups during pyrolysis [14-15], but also due to the partial oxidation and reduction [6-8] of both pyrolysis vapours and solid carbonaceous precursors by the available oxygen in air and auto generated steam. The CO_2 content detected in the product gases for the different wastes ranged between 2.3 and 16.1 vol%, for the waste plastics and wood wastes respectively.

The major fuel gases detected which had a heating value were H_2 , CO, CH_4 and C_2H_4 . Table 6-1 also shows that for the fuel gas products across the different wastes, H_2 and CO had the highest concentrations detected. This indicates that the different wastes, considering their different characteristics were subjected to identical process conditions and underwent similar reactions. This further gives an indication of the consistency of the conversion process. The higher contents of H_2 and CO were the results of the combination of the thermal cracking and recombination reactions of primary degradation products [16-17], the oxidation of decomposition products and char which in turn increases temperature and CO_2 [18], the water-gas shift

reaction (auto-generated steam) [19] and the reduction of primary and secondary products.



Drying of the wastes took place as they were deposited unto the pyrolysis screw just at the inlet to the pyrolysis chamber. As the wastes were transported further into the chamber which was hotter, drying and preheating of the wastes took place, governed by heat transfer rates and the quantity of moisture available. Limited by heat transfer of the individual particles, the preheating phase proceeded to the devolatilization phase as the particles achieved heat transfers sufficient for bond scission and other mechanisms associated with the pyrolysis of polymers to yield primary products (equation 6.3). Heat transfer to the particles was via convection, radiation but mostly via conduction with the reactor wall and hotter particles, which was limited by the availability of contact surface due to mass flow, and the heat transfer coefficient of the waste materials.

The reactor was therefore not a fast heating reactor, however a combination of high temperature and long volatile and solid residence times allowed for secondary pyrolysis reactions to occur. This resulted in the cracking of higher hydrocarbons for example cracking of the $C_2 - C_4$ gases to yield CH_4 and H_2 , and the cracking of oxygenated functional groups to yield CO [20-21]. The available air within the reactor encouraged oxidation reactions (equations 4 and 5) evidenced by the N_2 and CO_2 in the product gases, increasing the temperature within the reactor while further encouraging the secondary pyrolysis reactions. The water-gas shift reaction via auto-thermal steam, a net

exothermic reaction was also encouraged by high temperatures and steam from the drying wastes [19] (equation 6.6), contributing to the CO₂ and H₂ yields.

The high temperature within the reactor also encouraged other reduction reactions (equations 6.7 – 6.11), further increasing the production of H₂, CO and CH₄. The rate and order of these proposed reactions within the reactor depended on factors such as temperature and oxygen availability [9] within localized zones of the reactor. Extended secondary pyrolytic cracking reactions were likely limited due to reduced vapour residence time impacted by the action of the ID fan which pulled the vapour products into the oxidiser, resulting in considerable amounts of primary and partly cracked pyrolysis products (oxygenates and aliphatics) as well as more severely cracked oil products (aromatics) being entrained in the oxidiser feed, as shown in Table 6-3 and 6-4.

The composition of the product gases influenced their CV and as a result their gas efficiency, calculated by equation 6-12. The gas products from the infectious clinical waste and the waste plastic had the highest CV of 29.8 and 19.5 Mj Kg⁻¹ respectively. This was due to the lower N₂ content in both materials, but also due to their constituent materials such as plastics, and rubber which originally have a high CV and have been shown to contain very high volatile content as shown in Table 6-1 and [22] respectively. The gas products for the SAW and MSW+WSF materials indicated the lowest CVs of 4.0 and 4.2 Mj Kg⁻¹ respectively also due to their higher content of N₂. The heating value for the product gases from MSW + plastic, MSW and non-hazardous clinical waste were similar and only slightly less than that for waste plastics. However the heating value for the product gas from the waste wood was lower (8 Mj Kg⁻¹). This could be explained by a combination of factors, the low conversion (37.5%) as a result of insufficient solids residence time possibly due to an extended drying phase, short vapour residence time resulting in limited secondary cracking reactions and therefore comparably more liquids being formed as shown in Tables 6-3 and 6-4. This could also

explain the lower gas efficiency for waste wood (43.2%) compared to MSW and MSW + plastic (88.6 and 85.7% respectively).

$$\text{Gas efficiency (\%)} = [\text{CV}_{\text{gas}} (\text{Mj Kg}^{-1}) / \text{CV}_{\text{waste}} (\text{Mj Kg}^{-1})] \times 100 \quad (\text{equation 6.12})$$

As a result of process difference due to the technical limitations of the ST-150 reactor, the results achieved from the pyrolysis of the materials in this commercial scale reactor were not comparable to the results achieved during pyrolysis using the laboratory scale continuous screw kiln reactor described in chapter five and the bench scale fixed bed reactor described in chapter four. The ST-150 pyrolysis process therefore required further development especially in order to ensure an inert atmosphere in the pyrolysis chamber.

Table 6-2

Gas products from the thermal processing of different wastes

Gas composition (vol %)	Waste wood	MSW + WSF	MSW + Plastic	MSW	Non-hazardous clinical waste	Offensive clinical waste	SAW	Waste plastics
H ₂	4.1	2.2	8.4	9.0	8.3	14.6	1.8	6.9
CO	6.9	2.4	6.7	9.4	10.7	12.5	1.9	7.7
CO ₂	16.1	7.8	14.3	4.8	14.3	11.4	3.9	2.3
CH ₄	2.3	0.8	3.8	2.8	4.9	11.7	1.1	5.2
C ₂ H ₄	0.7	0.4	2.3	3.0	4.0	4.7	0.9	4.4
C ₂ H ₆	0.2	0.1	0.4	0.6	0.5	0.4	0.1	1.2
C ₃ H ₆	0.2	0.4	0.9	2.1	1.2	0.3	0.4	5.7
C ₃ H ₈	*	*	*	0.1	0.1	0.1	*	0.2
C ₄ H ₈	0.1	0.2	0.3	0.8	0.3	0.1	0.1	2.2
C ₄ H ₁₀	0.1	*	0.2	0.4	0.3	0.1	0.1	0.6
N ₂	69.4	85.6	62.7	67.0	55.5	44.0	89.6	63.5
GCV (MJ Kg ⁻¹)	8.0	4.2	15.9	17.8	17.8	29.8	4.0	19.5
Gas efficiency (%)	43.2	28.9	85.7	88.6	nd	nd	nd	51.8

nd: not detected

Table 6-3

Oil/tar compounds from the pyrolysis/partial oxidation of different wastes

Compound	MSW + WSF	MSW + Plastic	Non-hazardous clinical Waste	Infectious clinical waste	SAW	Waste wood
Oxygenates						
Cyclopentanone	**			**	**	**
2-Methoxyphenol (guaicol)	*			**		
Dibenzofuran	*	****				
2-Phenylphenol	***					**
Aromatics						
Alphamethylstyrene	*	*	**			*
Betamethylstyrene	***		**			
Indane	*	*	*			*
Indene	*	*	***	*		*
Naphthalene	*	*	***	*	*	*
Biphenyl	***	*	***	**	**	*
1,3-Diphenylpropane	***		**			***
Phenanthrene	***		***	***	***	***
1,3,5Triphenylbenzene	*	*	*	*	*	*
Ethylbenzene				*	*	**
Styrene					*	*
2-Methylnaphthalene	***	**		*	*	*
1,4Dimethylnaphthalene	***			*	*	
Fluorene	***	*	**	***	***	***
Pyrene	**			**	*	**
2-Ethyl-naphthalene	***	***				
1-Phenyl-naphthalene	***			**		
o-Terphenyl	***			**		***
Fluoranthene	***			**		
m-Terphenyl	***			*		**
Triphenylene			****	***	**	
Alkanes						
Octane, C8		**	**	**	**	
Decane, C10	**	**	**	*	**	
Undecane, C11	**	**	***	**	**	**
Dodecane, C12	**	**	***	**	**	
Tridecane, C13	**	**	**	**	**	**
Tetradecane, C14	**		**	**	**	**
Pentadecane, C15	**	**	*	**	**	**
Hexadecane, C16	*	*	*	*	*	*
Hepadecane, C17	*	*	**		*	
Pristane	**		**		**	**
Octadecane, C18	**		**		**	
Eicosane, C20		*	**		*	
Heneicosane, C21	**		**		**	**
Docosane, C22		**	**		**	**
Tricosane, C23			**		**	**

Table 6-3 continues							
Octacosane, C28	**	**	**				**
Nonacosane, C29	**	**	**			**	**
Dotriacontane, C32	**	**					
Pentatriacontane, C35	**				**	**	
Hexatriacontane, C36	**				**	**	**
Heptatriacontane, C37		**			**		**
Nonacontane, C39					**	**	**
Alkenes							
Octene, C8	**	****	***		***	***	***
Nonene, C9	****	****	****		****	****	***
Decene, C10	****	****	****				
Undecene, C11	***	***	****				
Dodecene, C12	***	****	****		***	***	**
Tridecene, C13	***	***	****				
Tetradecene, C14	***	****	****				***
Pentadecene, C15	****	****	****				****
Hexadecene, C16	****	****	****		****	***	****
Hepadecene, C17	****	***	****		**		
Octadecene, C18	****	***	****			****	
Nonadecene, C19	****	****	****			****	***
Eicosene, C20	****	****	****			****	
Heneicosene, C21		****	****			****	
Docosene, C22	****	****	****		***		****
Tricosane, C23		****	****				****
Tetracosene, C24		****	****				****
Hentriacontene, C31		****	****		****	***	
Hexatriacontene, C36	****		****		****		

Increasing * indicates higher concentration

6.2.4 Oil products and composition

Vapours from the pyrolysis chamber were passed through 2 condensers packed with glass wool to remove particulates, and immersed in dry ice to trap the condensable vapours in the condensers. The condensable vapours which were entrained in the volatile products and trapped in the condensers are referred to here as the condensable liquid products. Any other condensable vapours still in the gas were in very negligible quantities. There was however oil condensation to be expected in the tube just before the sampling port as a result of lower temperatures around this region due to the size of the reactor.

The liquid products were composed of mostly moisture (above 70%) and the rest was a brownish liquid, referred to as oil. Such high moisture contents were also reported by Mun et al [23] for the gasification of wood wastes. The oil products for selected waste materials were extracted and analysed by GC/MS in order to identify and quantify their composition and are shown in Table 6-3. Table 6-3 shows the detected compounds in the oil/tar products from the different wastes as well as their relative abundance in the oil, indicated by asterisks (*). Increasing number of asterisks indicates increasing concentration of the detected compound. The chromatograms for the detected oil compounds are depicted in Figures 6-5 to 6-10.

Table 6-3 indicate the detected oxygenates, alkanes, alkenes and aromatic compounds, which can show the extent of pyrolysis via indication of primary products (oxygenates) secondary products (alkanes and alkenes) and extended cracking or tertiary products (aromatics) [20, 24-25] in the oil. Table 6-3 also indicates that across the investigated waste materials, alkenes are the most abundant detected oil compounds, followed by aromatic compounds. This is similar to the nature of the oil products to be expected from a fluidized bed reactor (mixture of secondary and tertiary products) [26]. It is possible that some turbulence is created within the pyrolysis chamber due to the air entering at right angle. The turbulence can result in a mixture of primary, secondary and tertiary volatile products to being extracted from the reactor.

The detected alkenes are products from the cracking of alkanes, while the aromatics are products from the cracking of alkenes and oxygenates via such reactions as Diels-Alder and de-oxygenation reactions [20, 24]. The indicated dominance of the alkene products instead of the aromatic products which should be vice-versa at the investigated reaction temperatures [12, 27-28] could support the explanation for the reduced CV of the gas products such as for wood, due to the suppression of secondary cracking reactions as a result of reduced vapour residence time.

An analysis of the aromatic products detected, indicated that the oil/tar content of the product gas was well above the limit for direct feed to gas turbines and engines due to the composition of PAHs such as phenanthrene, naphthalene, flourene and Pyrene, at concentrations which appeared higher than tolerable by such equipments [26, 29].

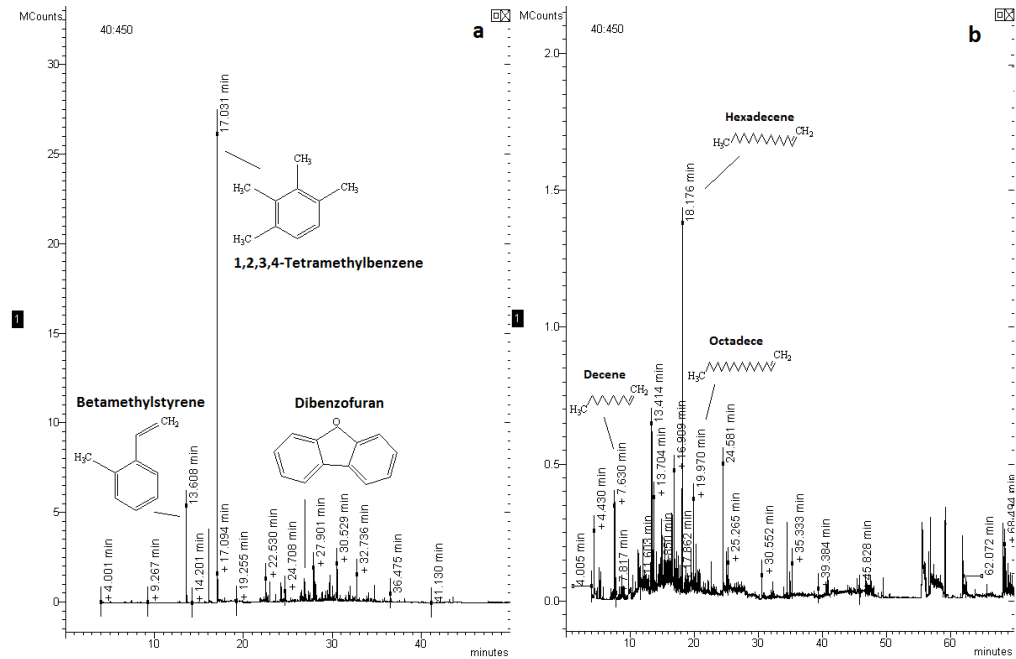


Figure 6-5 GCMS chromatograph of the oil from the processing of MSW + WSF; (a) Showing oxygenates and aromatics (b) Showing aliphatics.

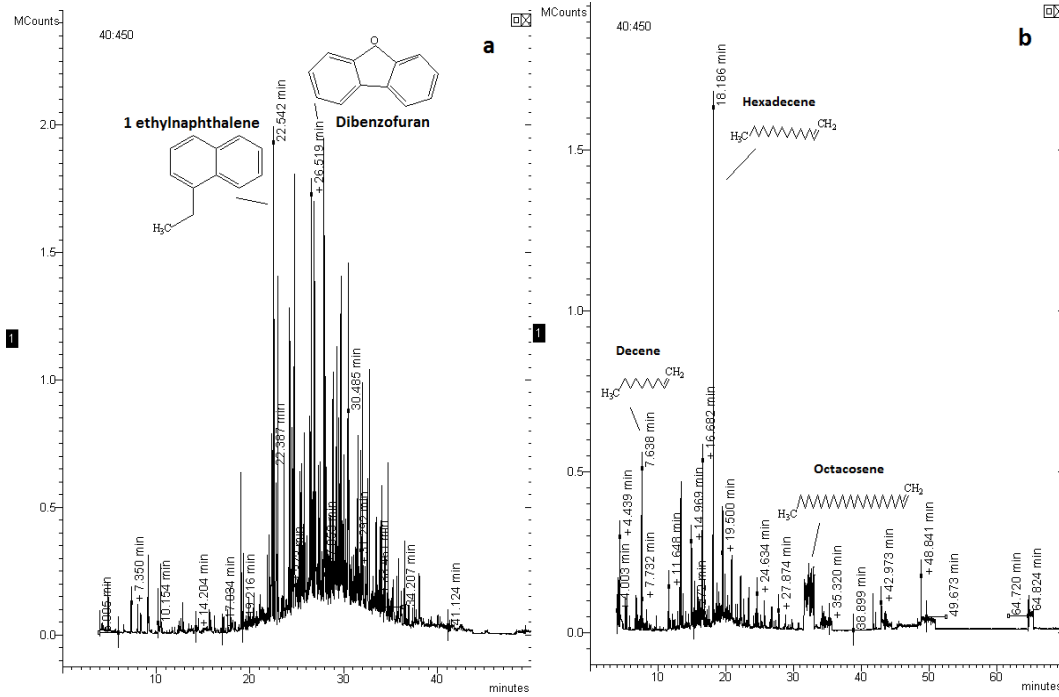


Figure 6-6 GCMS chromatograph of the oil from the processing of MSW + plastic; (a) Showing oxygenates and aromatics (b) Showing aliphatics.

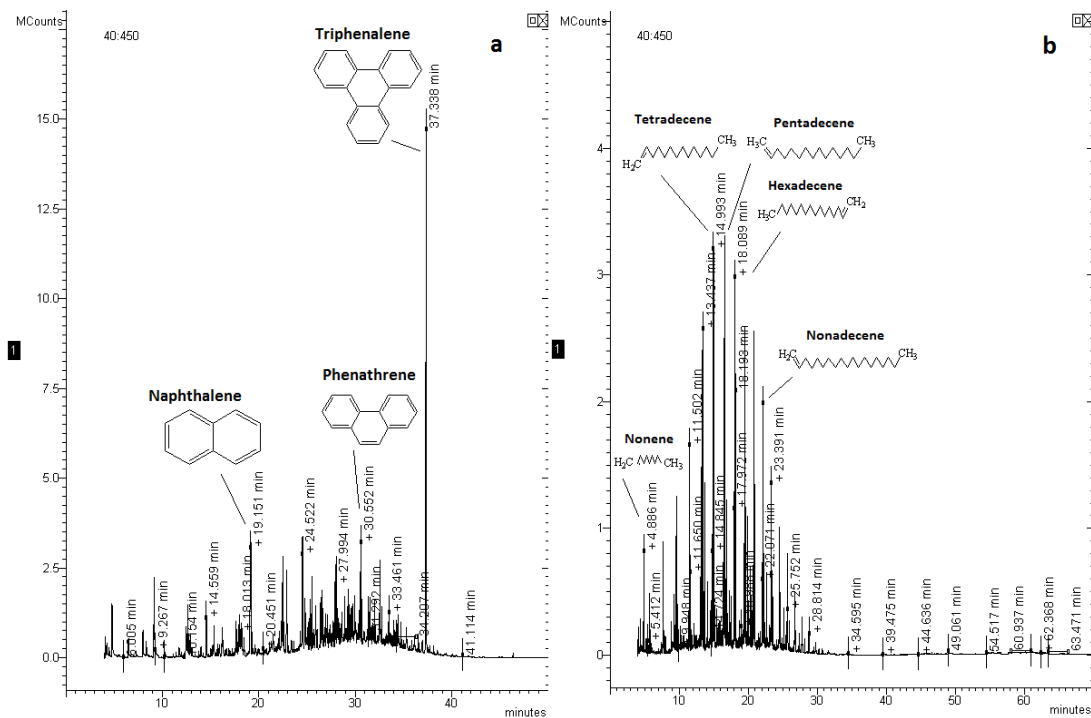


Figure 6-7 GCMS chromatograph of the oil from the processing of Clinical waste; (a) Showing oxygenates and aromatics (b) Showing aliphatics.

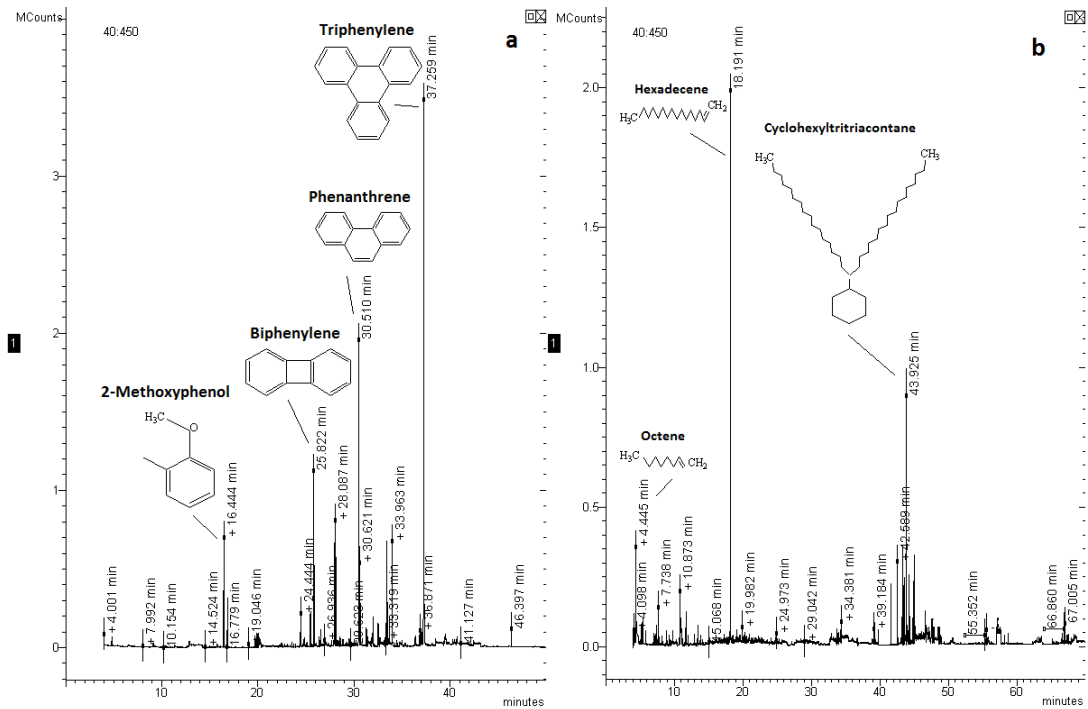


Figure 6-8 GCMS chromatograph of the oil from the processing of Offensive clinical waste; (a) Showing oxygenates and aromatics (b) Showing aliphatics.

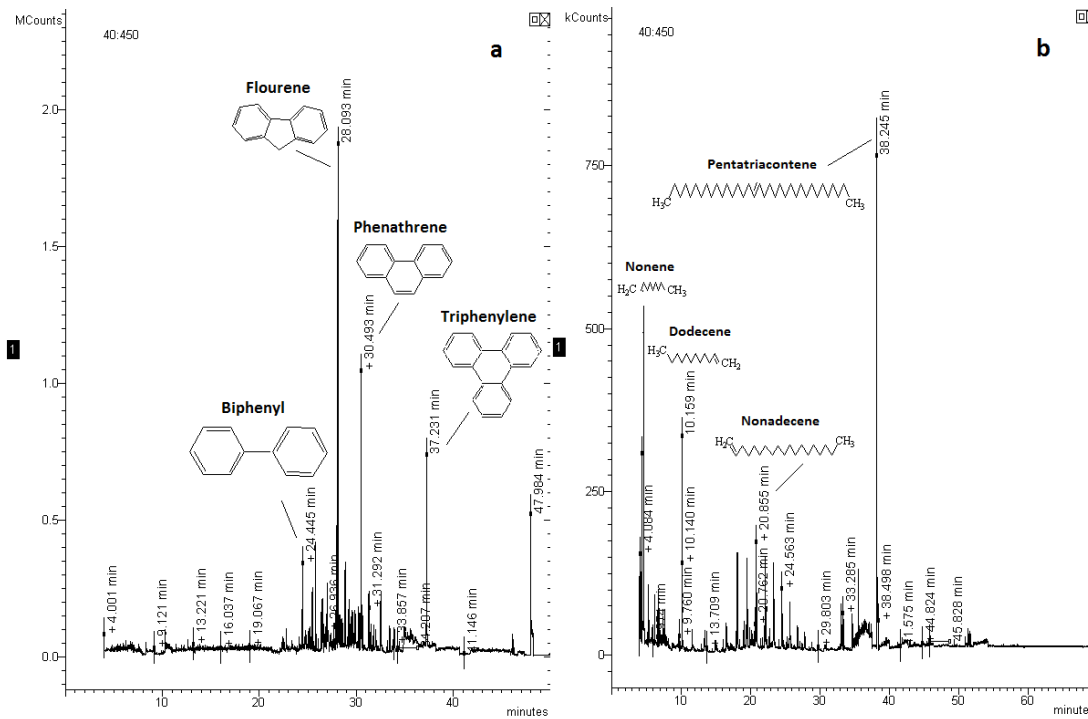


Figure 6-9 GCMS chromatograph of the oil from the processing of SAW; (a) Showing oxygenates and aromatics (b) Showing aliphatics.

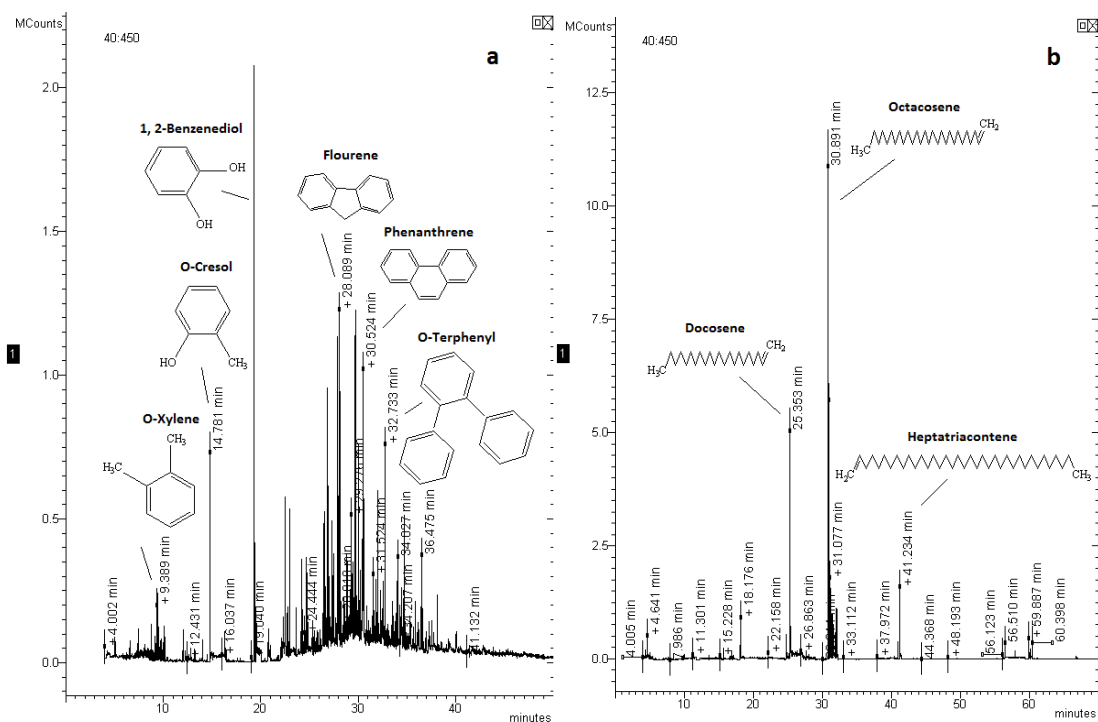


Figure 6-10 GCMS chromatograph of the oil from the processing of Wood; (a) Showing oxygenates and aromatics (b) Showing aliphatics.

6.2.5 Solid product characteristics

Samples of solid products from processing the different wastes were collected from the ash collector, and the results of the characterization of the samples by TGA, elemental analyser and bomb calorimeter are shown in Table 6-4. As expected the proximate analysis shows that the most abundant content of all the waste chars is ash, due to the thermal degradation of most of the other fractions. The TGA also revealed that the waste chars still contained some volatiles, up to 25 and 33 wt% for the MSW and wood waste respectively. This indicates that the selected solids residence time was insufficient for complete devolatilization of the wastes by pyrolysis and partial oxidation.

The CV of the chars were between 2.5 and 9 Mj Kg⁻¹ for the MSW+plastic and waste wood (respectively) mostly due to their residual volatile content.

Table 6-4

Characteristics of the solid char products

Properties of solid residue (wt%)	Waste wood	MSW + WSF	MSW + Plastic	MSW	Non-hazardous Clinical Waste	Waste plastics
Moisture	2.0	2.0	2.0	2.0	2.0	1.0
Volatile	33.0	20.0	14.0	25.0	13.0	15.0
Fixed carbon	6.0	4.0	3.0	9.0	11.5	11.0
Ash content	59.0	74.0	81.0	64.0	73.5	73.0
N content	1.0	0.7	0.5	0.8	0.8	
C content	26.5	15.1	8.7	16.0	28.4	
H content	2.5	1.3	0.4	1.1	0.5	
S content	0.5	0.3	0.5	0.8	1.5	
O content	10.5	8.7	8.9	17.3	0.0	
CV (MJ Kg ⁻¹)	9.0	6.0	2.5	8.0	5.4	3.6

6.3 Conclusions

The thermal conversion of different real life wastes were carried out on an industrial scale screw kiln pyrolysis and partial oxidation reactor, and samples of the products were taken and analysed, in order to investigate the effect of the process conditions on the product. The following main conclusions have been drawn:

- Due to process difference as a result of technical limitations of the ST-150 reactor, the results achieved from the pyrolysis of the materials in this commercial scale reactor were not comparable to the results achieved during pyrolysis using the laboratory scale continuous screw kiln reactor described in chapter five and the bench scale fixed bed reactor described in chapter four. This work therefore highlighted the practical challenges which were faced during the development of commercial scale waste and biomass pyrolysis and gasification processes. The ST-150 therefore required further development especially in ensuring an inert atmosphere during pyrolysis.

- The as-processed waste materials contained varying moisture contents and were very heterogeneous, making it very difficult to characterize a representative sample of processed wastes.
- The thermal processing of all the investigated materials yielded three major product fractions which were gas, liquid and solids.
- The energy content of the wastes was sufficient to sustain the process and provide heat for export to another process.
- Analysis of the gas products by GC TCD and FID showed that the major gas components were N₂ and CO₂, indicating that the thermal degradation of the wastes resulted from both pyrolysis and air partial oxidation within the pyrolysis reactor. The other major gases were H₂, CO and CH₄.
- Moisture was a major content of the liquid product, in addition to some brownish oil. GC/MS analysis of the oil indicated that they had a higher content of alkenes and aromatics, but also contained oxygenates and alkanes.
- The product gas was not appropriate for direct feed to a gas engine or turbine due to high contents of PAHs. The solid products contained volatile fractions indicating that a longer solids residence time was required for complete degradation.

References

1. Mohee, R., *Medical wastes characterisation in healthcare institutions in Mauritius*. Waste Management, 2005. **25**(6): p. 575-581.
2. Hossain, M.S., Santhanam, A., Nik Norulaini, N.A. and Omar, A.K.M., *Clinical solid waste management practices and its impact on human health and environment – A review*. Waste Management, 2011. **31**(4): p. 754-766.
3. Day, M., Shen, Z. and Cooney, J.D., *Pyrolysis of auto shredder residue: experiments with a laboratory screw kiln reactor*. Journal of Analytical and Applied Pyrolysis, 1999. **51**(1-2): p. 181-200.
4. Bridgwater, A.V., *Renewable fuels and chemicals by thermal processing of biomass*. Chemical Engineering Journal, 2003. **91**(2-3): p. 87-102.
5. Zhang, L., Xu, C. and Champagne, P., *Overview of recent advances in thermo-chemical conversion of biomass*. Energy Conversion and Management, 2010. **51**(5): p. 969-982.

6. Guo, X., Xiao, B., Liu, S., Hu, Z., Luo, S. and He, M., *An experimental study on air gasification of biomass micron fuel (BMF) in a cyclone gasifier*. International Journal of Hydrogen Energy, 2009. **34**(3): p. 1265-1269.
7. Sun, S., Zhao, Y., Ling, F. and Su, F., *Experimental research on air staged cyclone gasification of rice husk*. Fuel Processing Technology, 2009. **90**(4): p. 465-471.
8. Tinaut, F.V., Melgar, A., Pérez, J.F. and Horrillo, A., *Effect of biomass particle size and air superficial velocity on the gasification process in a downdraft fixed bed gasifier*. Fuel Processing Technology, 2008. **89**(11): p. 1076-1089.
9. Buragohain, B., Mahanta, P. and Moholkar, V.S., *Biomass gasification for decentralized power generation: The Indian perspective*. Renewable and Sustainable Energy Reviews, 2010. **14**(1): p. 73-92.
10. Boukis, I.P., Bezergianni, S., Grammelis, P. and Bridgwater, A.V., *CFB air-blown flash pyrolysis. Part II: Operation and experimental results*. Fuel, 2007. **86**(10-11): p. 1387-1395.
11. Gil, J., Corella, J., Aznar, M.P. and Caballero, M.A., *Biomass gasification in atmospheric and bubbling fluidized bed: Effect of the type of gasifying agent on the product distribution*. Biomass and Bioenergy, 1999. **17**(5): p. 389-403.
12. Ponzio, A., Kalisz, S. and Blasiak, W., *Effect of operating conditions on tar and gas composition in high temperature air/steam gasification (HTAG) of plastic containing waste*. Fuel Processing Technology, 2006. **87**(3): p. 223-233.
13. Thamavithya, M. and Dutta, A., *An investigation of MSW gasification in a spout-fluid bed reactor*. Fuel Processing Technology, 2008. **89**(10): p. 949-957.
14. Beaumont, O. and Schwob, Y., *Influence of physical and chemical parameters on wood pyrolysis*. Industrial & Engineering Chemistry Process Design and Development, 1984. **23**(4): p. 637-641.
15. Meesri, C. and Moghtaderi, B., *Lack of synergetic effects in the pyrolytic characteristics of woody biomass/coal blends under low and high heating rate regimes*. Biomass and Bioenergy, 2002. **23**(1): p. 55-66.
16. Kantarelis, E., Donaj, P., Yang, W. and Zabaniotou, A., *Sustainable valorization of plastic wastes for energy with environmental safety via High-Temperature Pyrolysis (HTP) and High-Temperature Steam Gasification (HTSG)*. Journal of Hazardous Materials, 2009. **167**(1-3): p. 675-684.
17. Streitwieser, A., Heathcock, C.H. and Kosower, E.M., *Introduction to organic chemistry*. 4th ed. 1992, USA: Macmillan Publishing Company. 1256.
18. Aznar, M.P., Caballero, M.A., Sancho, J.A. and Francés, E., *Plastic waste elimination by co-gasification with coal and biomass in fluidized bed with air in pilot plant*. Fuel Processing Technology, 2006. **87**(5): p. 409-420.
19. Guoxin, H., Hao, H. and Yanhong, L., *Hydrogen-Rich Gas Production from Pyrolysis of Biomass in an Autogenerated Steam Atmosphere*. Energy & Fuels, 2009. **23**(3): p. 1748-1753.
20. Williams, P.T. and Besler, S., *Polycyclic aromatic hydrocarbons in waste derived pyrolytic oils*. Journal of Analytical and Applied Pyrolysis, 1994. **30**(1): p. 17-33.
21. Piskorz, J., Radlein, D. and Scott, D.S., *On the mechanism of the rapid pyrolysis of cellulose*. Journal of Analytical and Applied Pyrolysis, 1986. **9**(2): p. 121-137.

22. Elbaba, I.F., Wu, C. and Williams, P.T., *Catalytic Pyrolysis-Gasification of Waste Tire and Tire Elastomers for Hydrogen Production*. Energy & Fuels, 2010. **24**(7): p. 3928-3935.
23. Mun, T.-Y., Seon, P.-G. and Kim, J.-S., *Production of a producer gas from woody waste via air gasification using activated carbon and a two-stage gasifier and characterization of tar*. Fuel, 2010. **89**(11): p. 3226-3234.
24. Cypres, R., *Aromatic-Hydrocarbons Formation during Coal Pyrolysis*. Fuel Processing Technology, 1987. **15**(0): p. 1-15.
25. Koo, J.-K., Kim, S.-W. and Seo, Y.-H., *Characterization of aromatic hydrocarbon formation from pyrolysis of polyethylene-polystyrene mixtures*. Resources, Conservation and Recycling, 1991. **5**(4): p. 365-382.
26. Milne, T.A. and Evans, R.J., *Biomass gasification "tars": their nature, formation and conversion*. 1998, NREL, Golden, CO, USA, Report no. NREL/TP-570-25357.
27. Phan, A.N., Ryu, C., Sharifi, V.N. and Swithenbank, J., *Characterisation of slow pyrolysis products from segregated wastes for energy production*. Journal of Analytical and Applied Pyrolysis, 2008. **81**(1): p. 65-71.
28. Ates, F. and Isikdag, M.A., *Influence of temperature and alumina catalyst on pyrolysis of corncob*. Fuel, 2009. **88**(10): p. 1991-1997.
29. Bui, T., Loof, R. and Bhattacharya, S.C., *Multi-stage reactor for thermal gasification of wood*. Energy, 1994. **19**(4): p. 397-404.

CHAPTER 7. CONCLUSIONS AND FUTURE WORK

7.1 Conclusions

This work investigated the production of gaseous products rich in hydrogen, from the pyrolysis and steam pyrolysis-gasification of solid wastes and biomass, using a laboratory scale fixed bed reactor, a continuous feed screw kiln reactor and a commercial scale pyrolysis/partial oxidation reactor. Solid wastes and waste wood as well as major singular components of municipal solid waste and waste wood were studied in order to investigate their contributions to the product gases. Process conditions such as pyrolysis temperature, heating rate, gasification temperature, steam to feedstock ratio and catalyst to feedstock ratio. Different nickel based catalysts were prepared in the university laboratory and their catalytic properties tested in terms of hydrogen production and the prevention of carbon deposition. The potential for CO₂ in-situ capture to improve hydrogen production from the steam pyrolysis-gasification of waste wood was also investigated. The main conclusions from this research are summarised in the following sections.

7.1.1 The pyrolysis of RDF and its single components in the fixed bed reactor

- TGA analysis of the RDF sample indicated that its major volatile degradation occurred at temperature zones which were characteristic of the volatile degradation of lignocellulosic and plastic materials.
- Increasing the heating rate from 5 to ≈ 350 °C min⁻¹ at 800 °C resulted in an increased gas yield, increased hydrogen yield, reduced liquid yield and reduced solids yield for the RDF, paper, cardboard and waste plastic samples as a result of promoted secondary decomposition of volatiles. The product gas was made up of mostly CO, CO₂, C₁ – C₄ hydrocarbons and H₂.

- It was found that at a heating rate of $\approx 350 \text{ }^\circ\text{C min}^{-1}$ and temperature of $800 \text{ }^\circ\text{C}$ the pyrolysis of the paper and cardboard samples resulted in a gas with the most abundant components as CO, while for the waste plastics the most abundant gas component were the hydrocarbon gases. It is suggested that during the fast pyrolysis of RDF at $800 \text{ }^\circ\text{C}$ the degradation of the plastics was a major contributor of the hydrocarbon gas products while the degradation of the lignocellulosic materials like paper and cardboard were the major contributors of the CO in the gas product.
- FTIR and GC/MS analysis suggested that the oil from the pyrolysis of the samples at $800 \text{ }^\circ\text{C}$ and at a heating rate of $\approx 350 \text{ }^\circ\text{C min}^{-1}$, contained a higher proportion of aromatic compounds as a result of Diels-Alder type reactions, compared to the oil from pyrolysis at $5 \text{ }^\circ\text{C min}^{-1}$, which was found to contain a higher proportion of alkanes, alkenes and oxygenates.
- Increasing the final temperature for RDF pyrolysis at slow ($90 \text{ }^\circ\text{C min}^{-1}$) and fast heating ($\approx 350 \text{ }^\circ\text{C min}^{-1}$) conditions resulted in an increased gas yield, reduced liquid yield and reduced solids yield.
- Pyrolysis of RDF at $\approx 350 \text{ }^\circ\text{C min}^{-1}$, and at $800 \text{ }^\circ\text{C}$ resulted in the production of the gas yield with highest calorific value. While pyrolysis of RDF at $900 \text{ }^\circ\text{C}$ resulted in the highest gas and hydrogen yield.
- Varying the particle sizes of RDF investigated in this work did not significantly impact its pyrolysis products

7.1.2 The pyrolysis of waste wood and its single components in the fixed bed reactor

- TGA analysis of the waste wood sample indicated its volatile degradation were characteristic of the combined volatile degradations of hemicellulose, cellulose and lignin.
- During the pyrolysis of the waste wood, cellulose, xylan and lignin samples at $800 \text{ }^\circ\text{C}$, increasing the heating rate from 5 to $\approx 350 \text{ }^\circ\text{C min}^{-1}$ resulted initially in an increased gas and oil yield, and a reduced solids

yield, followed finally by an increased gas and hydrogen yield, and reduced liquid and solid yields. The product gas was made up of mostly CO, CO₂, C₁ – C₄ hydrocarbons and H₂.

- During fast heating ($\approx 350 \text{ }^\circ\text{C min}^{-1}$) at 800 °C, the pyrolysis of the cellulose and lignin samples resulted in a gas product in which the most abundant components was CO, while for the xylan the most abundant gas component was CO₂. It is suggested that during the fast pyrolysis of waste wood at 800 °C the degradation of the hemicellulose content was a major contributor of the CO₂ content of the gas products while the degradation of the cellulose and lignin materials were the major contributors of the CO in the gas product.
- FTIR and GC/MS analysis suggested that the oil from pyrolysis of the samples at 800 °C and at a heating rate of $\approx 350 \text{ }^\circ\text{C min}^{-1}$, contained a higher proportion of aromatic compounds compared to the oil from pyrolysis at 800 °C and at $5 \text{ }^\circ\text{C min}^{-1}$, which was found to contain a higher proportion of alkanes, alkenes and oxygenates. The monocyclic aromatic compounds were formed via Dies-Alder reactions and finally converted to polycyclic aromatics.
- Increasing the final temperature from 700 to 900 °C for waste wood pyrolysis at slow ($90 \text{ }^\circ\text{C min}^{-1}$) and fast ($\approx 350 \text{ }^\circ\text{C min}^{-1}$) heating rates resulted in an increased gas yield, reduced liquid yield and reduced solids yield at the conditions investigated.
- Fast heating pyrolysis of the waste wood at 800 °C resulted in the production of a gas yield with the highest calorific value. While rapid pyrolysis of waste wood at 900 °C resulted in the highest gas and hydrogen yield.
- Varying the particle sizes of waste wood investigated in this work did not significantly impact its pyrolysis products

7.1.3 Two stage pyrolysis and steam pyrolysis-gasification of waste wood in the continuous screw kiln reactor

- Increasing the temperature of the first stage from 500 to 700 °C during two stage pyrolysis of waste wood resulted in increased gas and hydrogen yield while the oil and solid yields decreased. Increasing the temperature of the second stage from 700 to 900 °C during two stage pyrolysis of the waste wood had no significant yields on its product yields. The product gas was made up of mostly CO, CO₂, C₁ – C₄ hydrocarbons and H₂.
- Varying the steam to biomass ratio from 0.2 to 1 during the waste wood steam pyrolysis-gasification at first stage reactor temperature of 700 °C and second stage fixed bed reactor temperature of 900 °C did not have any notable impacts on the product yields and gas composition.
- Increasing the gasification temperature from 700 to 900 °C had no significant impacts on the product yields and gas composition from the steam pyrolysis gasification of waste wood.
- The solids for both two stage pyrolysis and steam pyrolysis-gasification in the screw kiln reactor were consistent due to the reactor design which was designed to prevent the gasification of solid char.

7.1.4 Steam pyrolysis-gasification of waste wood with nickel based catalysts

- Increasing the nickel loading from 5 to 20 wt% on the catalyst resulted in increased gas yield and reduced the tar yield by 75%, from the steam pyrolysis-gasification of waste wood due to increased catalytic activity. Increasing the nickel loading also resulted in increased hydrogen yield, as a result of the promotion of hydrocarbon cracking and steam reforming, and water-gas shift reactions.
- Increasing the catalyst to waste wood ratio from 0.5 to 2 resulted in increased gas yield and reduced the tar yield by 97%, as well as increased hydrogen yield. This was also as a result of the promotion of hydrocarbon cracking, steam reforming, and water-gas shift reactions,

due to increased availability of catalytically active sites as well as support on which organic activation and steam activation could take place respectively.

- Increasing the nickel loading and the catalyst to waste wood ratio during waste wood steam pyrolysis-gasification resulted in a decrease in the total detected tars, as well as a shift in the tar constituents to mostly aromatics. The aromatic compounds were products from the steam reforming of hydrocarbons, which was enhanced by the catalysts.
- The SEM analysis of the reacted Ni Al₂O₃ catalysts showed evidence of carbon deposits on the catalyst surface. It is suggested that these could lead to its deactivation.
- The promotion of the Ni Al₂O₃ catalyst with La, Co and Ce resulted in increased gas yields from steam pyrolysis gasification of waste wood in the order Ce > Co > La. The Ce promoted catalyst resulted in the production of the highest gas yield due to enhanced catalytic activity. The Cu, Mn and Mg promoted catalysts exhibited lower gas yield than the un-promoted catalyst in the order Cu > Mn > Mg. The Mg promoted catalyst produced the lowest gas yield due to a reduced catalytic activity.
- The promotion of the Ni Al₂O₃ catalyst with Ce resulted in a higher hydrogen yield due to its enhanced catalytic activity as well as enhanced carbon/coke gasification, while the La and Co promoted catalysts had similar hydrogen yields as the un-promoted catalyst. The Cu, Mn and Mg promoted catalysts resulted in reduced hydrogen yields in the same order noted for their gas yields.
- The Ce and La promoted catalysts resulted in a reduction in the total detected tar by 87 and 64% respectively as a result of their enhanced activity due to the interactions of Ce and La in the catalyst. The Mg promoted catalyst resulted in an increase in the total tar detected, compared to the un-promoted catalyst, for the steam pyrolysis-gasification of waste wood due to a reduction in catalyst activity.

- The Ni CeO₂ Al₂O₃ and Ni Al₂O₃ catalyst were both deactivated after 48 minutes of the life test, possibly as a result attrition and/or sintering. The Ni CeO₂ Al₂O₃ catalyst exhibited higher catalytic activity within the first 15 minutes of the life test, as well as after regeneration due to its enhanced activity and carbon/coking resistance. The regenerated catalysts showed signs of wear which were characteristic of attrition and/or sintering.
- TEM-EDXS mapping and TEM images showed carbon deposition concentrated around the nickel on the characterised reacted catalysts. CO₂ evolution peaks obtained by TPO-FTIR indicated the presence of peaks characteristic of the oxidation of amorphous and filamentous carbon on the promoted catalysts. The un-promoted catalyst exhibited the only detectable characteristic peak for graphitic carbon as well as the peak for amorphous carbon, indicating that it was prone to deactivation by carbon/coke encapsulation.
- The reacted Ce and La promoted catalysts exhibited negligible peaks for both amorphous and filamentous carbons, indicating higher resistance to carbon deposition as a result of enhanced steam gasification of carbon. The reacted Cu, Mn and Mg promoted catalysts exhibited in the evolution of the characteristic peak for amorphous carbon which could be converted to graphitic carbon and cause carbon/coke deactivation. The promoted catalysts indicated higher resistance to deactivation by carbon/coke deposition, however the presence of filamentous carbon on the catalysts indicated that they were prone to deactivation by attrition/crushing or pore plugging by the filamentous carbon growth.

7.1.5 Steam pyrolysis-gasification of waste wood with nickel based catalyst and CaO as a CO₂ sorbent

- The use of CaO as a CO₂ sorbent, integrated into a Ni Al₂O₃ catalyst both by co-impregnation of the CaO onto the catalyst, and by mixing of solid CaO powder with already prepared Ni Al₂O₃ catalyst, resulted in

the capture of CO₂ to form CaCO₃ during the steam pyrolysis-gasification of waste wood.

- The use of the catalyst-sorbent materials containing 5 wt% of CaO prepared by CaO integration into the catalyst and by mixing CaO powders with the catalyst, had no significant impacts on the gas and hydrogen yield compared to the use of just Ni Al₂O₃ catalyst during the steam pyrolysis-gasification of waste wood. Integrating the CaO by co-impregnation and by mixing of solid CaO with the catalyst had similar effects on gas yield, hydrogen yield and gas composition.
- Increasing the CaO quantity during the steam pyrolysis gasification waste wood resulted in a gradual reduction in the gas and hydrogen yield while the CO₂ yield increased, indicating a reduction in catalytic and CO₂ sorption activity of the catalyst-sorbents. It is suggested that this was linked to the deactivation of the CaO powders by tar and could be avoided by situating the CaO powder layer after the catalyst. It is also suggested having the CaO sorbent in a layer after the catalyst could reduce its deactivation by tar.
- Reducing the gasification temperature to 700 °C in the presence of the catalyst-sorbent resulted in reduced gas yield and hydrogen yield, compared to similar tests at 800 °C. Analysis of the product yields and gas composition indicated that this was mostly due to reduced thermal cracking of heavier hydrocarbons.

7.1.6 PYROLYSIS AND PARTIAL OXIDATION OF DIFFERENT REAL WORLD WASTES IN AN INDUSTRIAL SCALE SCREW KILN REACTOR

- Due to process difference as a result of technical limitations of the ST-150 reactor, the results achieved from the pyrolysis of the materials in this commercial scale reactor were not comparable to the results achieved during pyrolysis using the laboratory scale continuous screw kiln reactor described in chapter five and the bench scale fixed bed reactor described in chapter four. This work therefore highlighted the

practical challenges which were faced during the development of commercial scale waste and biomass pyrolysis and gasification processes. The ST-150 therefore required further development especially in ensuring an inert atmosphere during pyrolysis.

- The as-processed waste materials contained varying moisture contents and were very heterogeneous, making it very difficult to characterize a representative sample of processed wastes.
- The thermal processing of all the investigated materials yielded three major product fractions which were gas, liquid and solids.
- The energy content of the wastes were sufficient to sustain the process and provide heat for export another process.
- Analysis of the gas products by GC TCD and FID showed that the major gas components were N_2 and CO_2 , indicating that the thermal degradation of the wastes resulted from both pyrolysis and air partial oxidation within the pyrolysis. The other major gases were H_2 , CO and CH_4 .
- Moisture was a major content of the liquid product, in addition to some brownish oil. GC/MS analysis of the oil indicated that they had a higher content of alkenes and aromatics.
- The product gas was not appropriate for direct feed to a gas engine or turbine due to high contents of PAHs. The solid products contained volatile fractions indicating that a longer solids residence time was required.

7.2 Future work

- Further work could be carried out to investigate the effects of varying the weight space velocity over the catalyst by varying the biomass and steam feed rates in the continuous screw kiln reactor. This would provide information on the optimum weight space velocity for catalytic steam pyrolysis gasification for this reactor.
- During catalytic steam pyrolysis-gasification, the reaction kinetics differ from non-catalytic due to the presence of the catalyst and this could

have an impact on the optimum steam to biomass ratio. Work on varying the steam to waste wood ratio during catalytic pyrolysis-gasification could be carried out in order to determine the optimum steam to waste wood ratio in the presence of a catalyst.

- The rotary gravity feeder of the continuous screw kiln reactor could be modified in order for different types of waste and biomass (especially less dense materials) to be easily fed. This would enable investigations of the catalytic steam pyrolysis-gasification of different waste and biomass materials.
- The nickel based catalysts which were modified by Ce and La were shown to reduce coke deposition as well as increase gas yield and hydrogen yield (especially the Ce modified catalyst). However catalyst life and regeneration tests suggested catalytic activity loss on the tested catalysts due to attrition and sintering. Further work could be done on catalysts preparation in order to improve the catalyst strength. The influence of calcination temperature as well as the addition of other metals such Mg and Fe could be investigated. The effect of other preparation methods such as co-precipitation and sol-gel are also suggested.
- Analytical techniques such as SEM and TEM provide information of the surface of the fresh and reacted catalysts. However since the catalysts were porous spheres, reactions took place on both their surfaces and pores. Future work could be done in order to investigate below the catalyst surface. This could be done by adopting a non-destructive method to section the catalysts into 2 hemi-spheres after which SEM and or TEM could be used to analyse the sectioned sides of the hemi-sphere to provide information on activity, coke deposition as well as structural changes below the catalyst surface.
- Further work on improving hydrogen production via in-situ capture of CO₂ with CaO during catalytic steam pyrolysis-gasification of waste wood could be carried out. This work showed that mixing the CaO powders resulted in its easy deactivation therefore work could be done on investigating the effects of integrating separate CaO and catalyst

layers within the bed as shown in figure 7.1, with the CaO layer placed after the catalyst in order to reduce the tar concentration which the CaO is exposed to. The integration of Fe or Mg into the CaO powders or the use of dolomite as the CO₂ sorbent material could also be investigated.

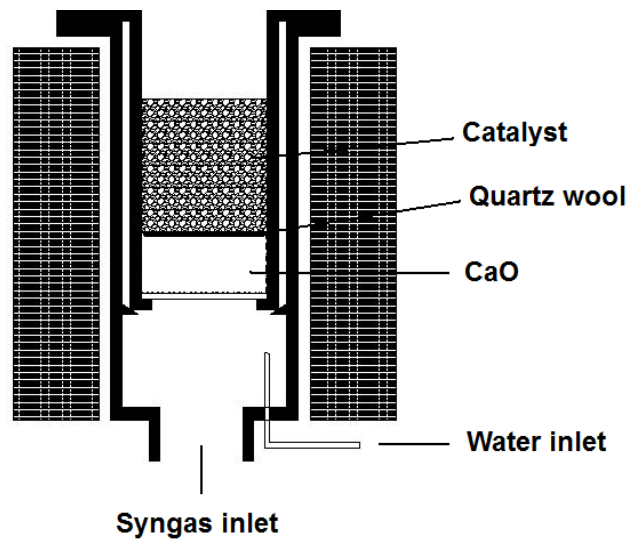
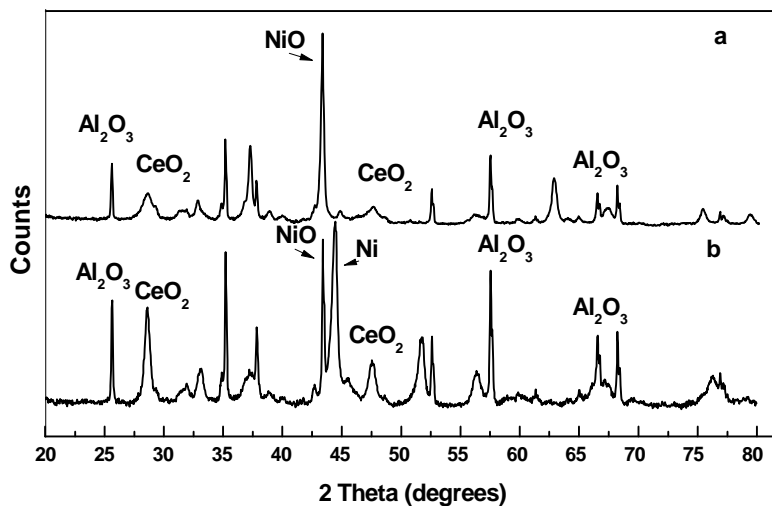
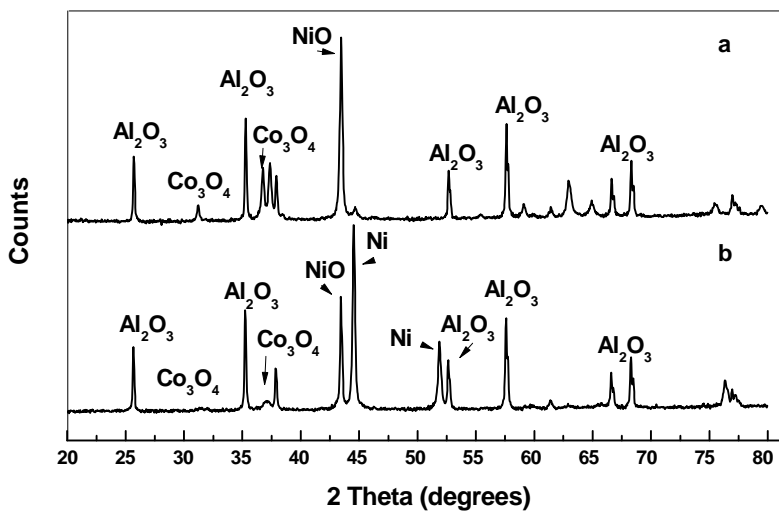


Figure 7-1 Schematic of fixed bed with suggested CaO and catalyst layer

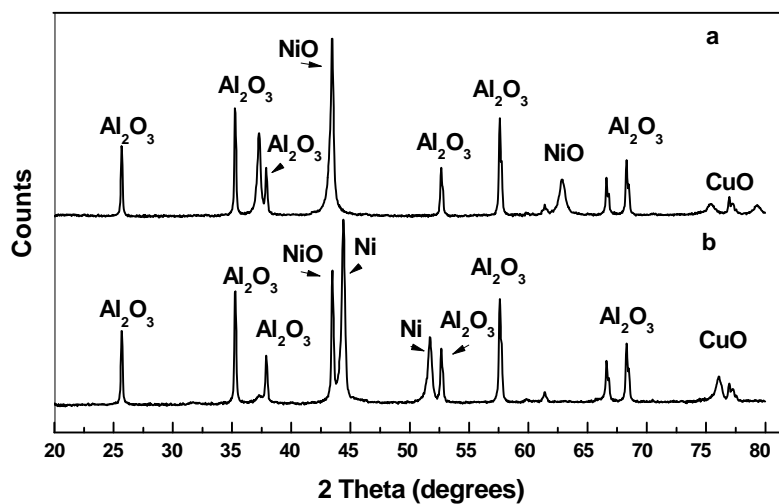
Appendix



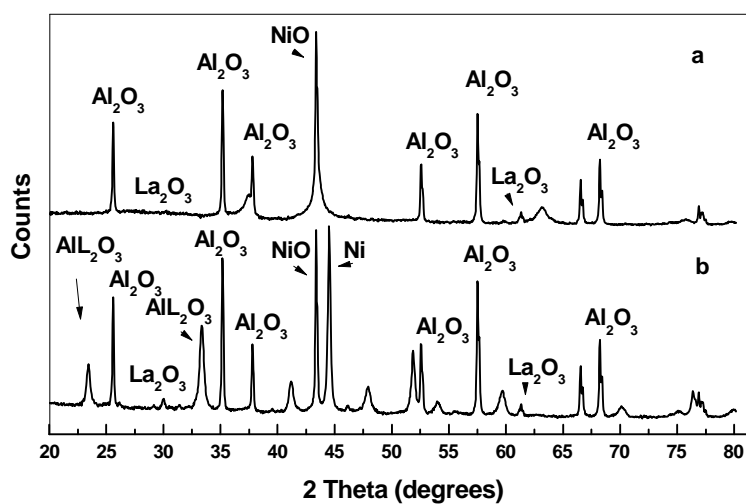
Appendix A- 1 XRD patterns of the Ni CeO_2 Al_2O_3 catalyst: (a) fresh, (b) reacted



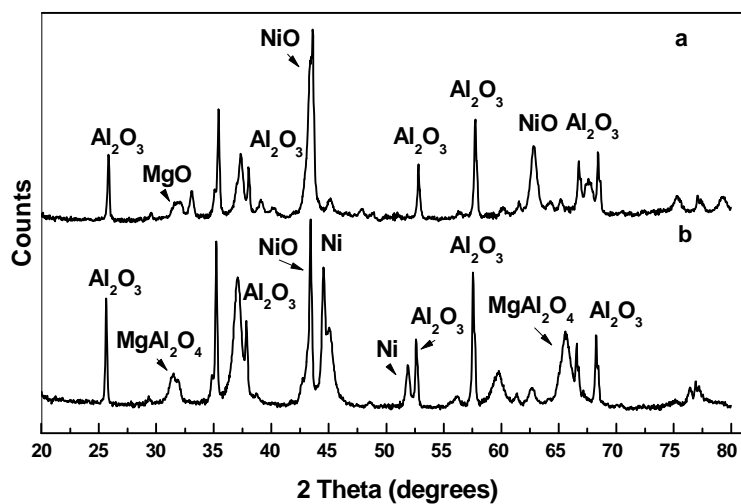
Appendix A- 2 XRD patterns of the Ni CoO Al_2O_3 catalyst: (a) fresh, (b) reacted



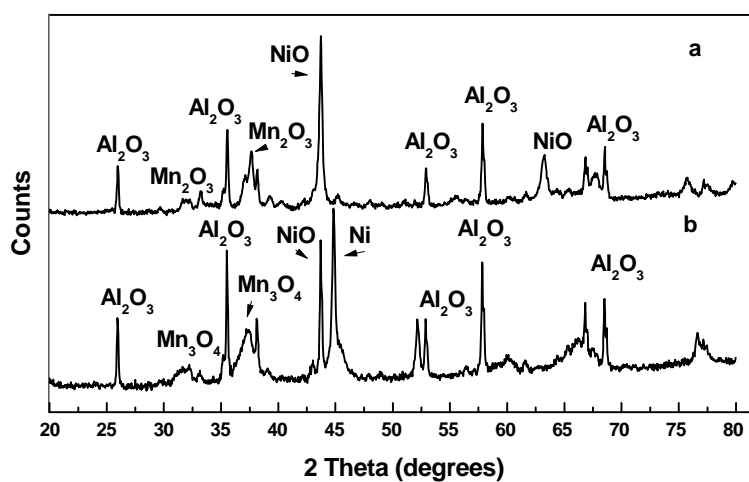
Appendix A- 3 XRD patterns of the Ni CuO Al₂O₃ catalyst: (a) fresh, (b) reacted



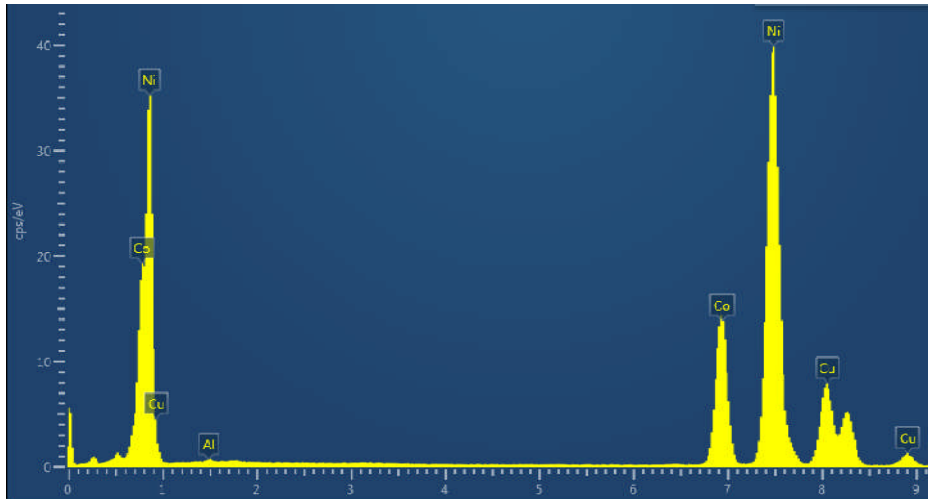
Appendix A- 4 XRD patterns of the Ni La₂O₃ Al₂O₃ catalyst: (a) fresh, (b) reacted



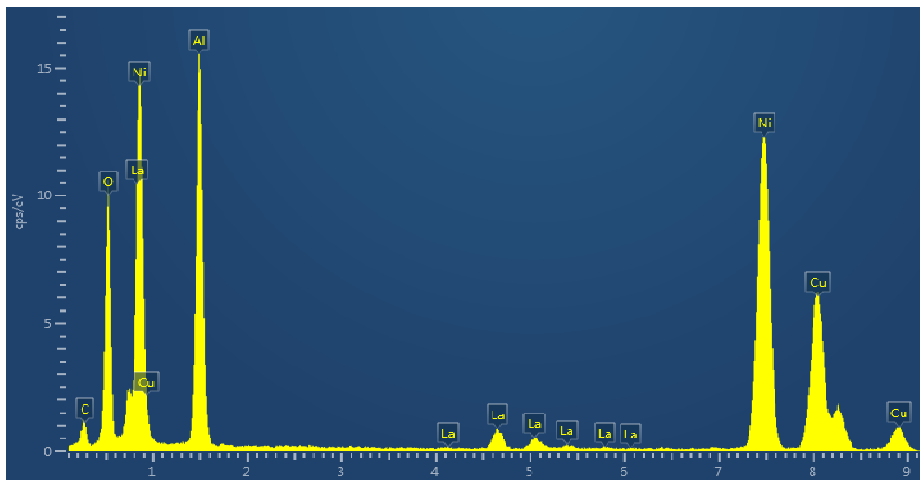
Appendix A- 5 XRD patterns of the Ni MgO Al₂O₃ catalyst: (a) fresh, (b) reacted



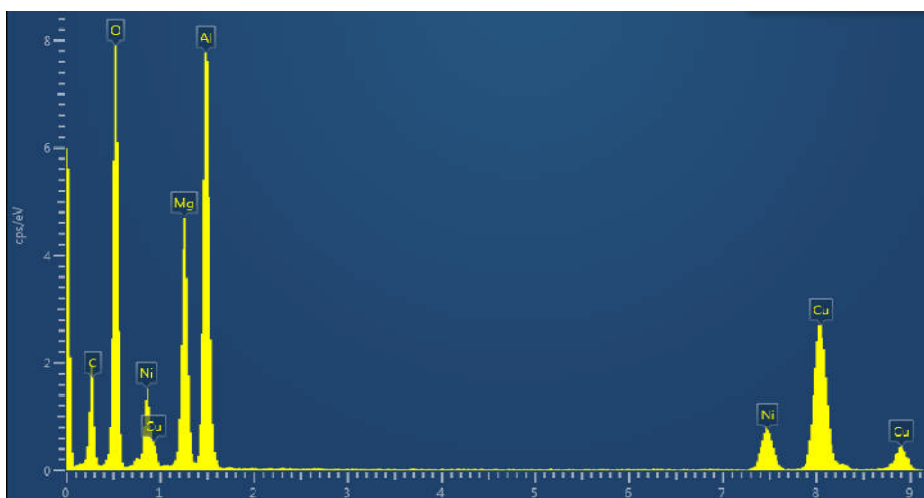
Appendix A- 6 XRD patterns of the Ni MnO Al₂O₃ catalyst: (a) fresh, (b) reacted



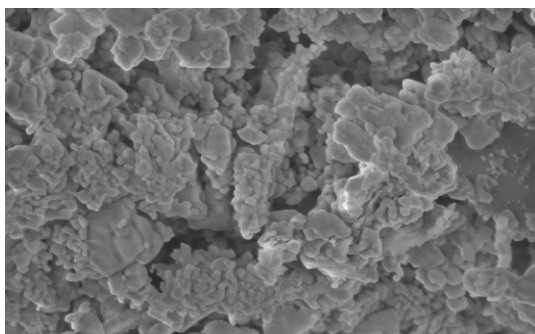
Appendix B- 1 TEM-EDXS spectra for Ni CoO Al₂O₃



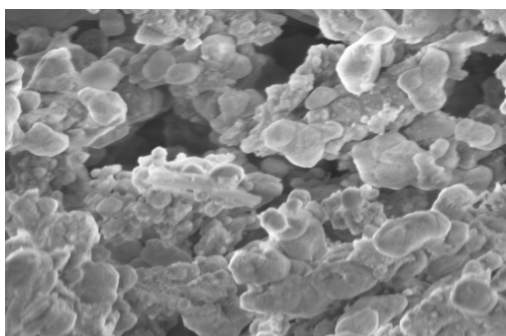
Appendix B- 2 TEM-EDXS spectra for Ni La₂O₃ Al₂O₃



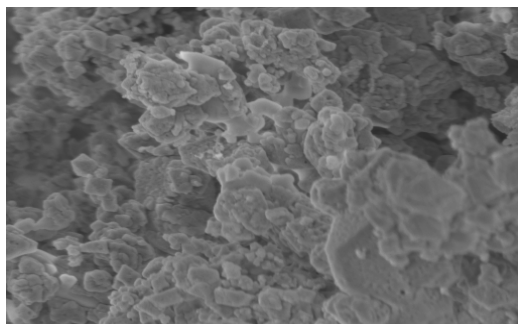
Appendix B- 3 TEM-EDXS spectra for Ni MgO Al₂O₃



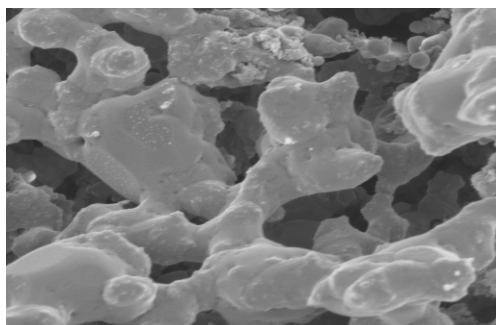
Appendix C- 1 SEM images of the fresh Ni CoO Al₂O₃



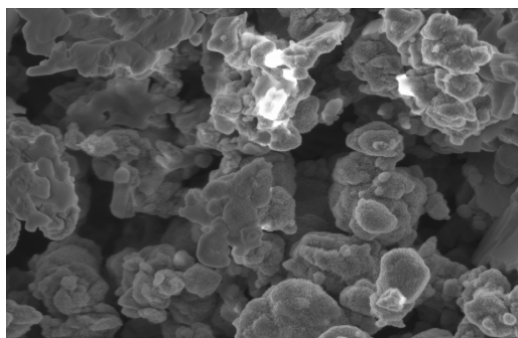
Appendix C- 2 SEM images of the reacted Ni CoO Al₂O₃



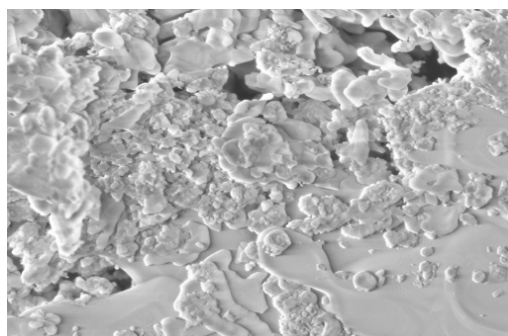
Appendix C- 3 SEM images of the fresh Ni CuO Al₂O₃



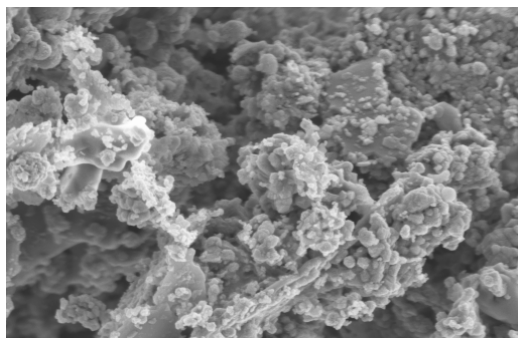
Appendix C- 4 SEM images of the reacted Ni CuO Al₂O₃



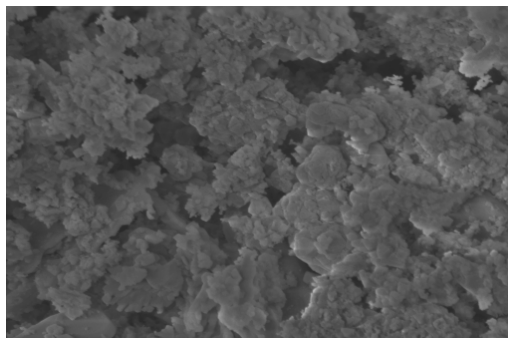
Appendix C- 5 SEM images of the fresh Ni La₂O₃ Al₂O₃



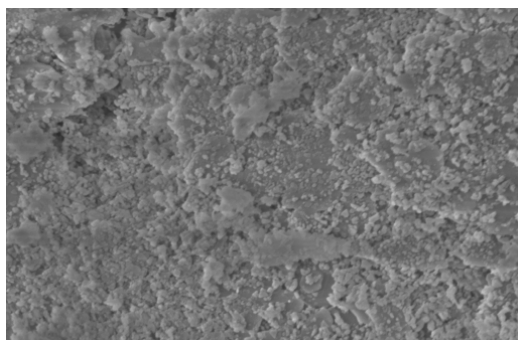
Appendix C- 6 SEM images of the reacted Ni La₂O₃ Al₂O₃



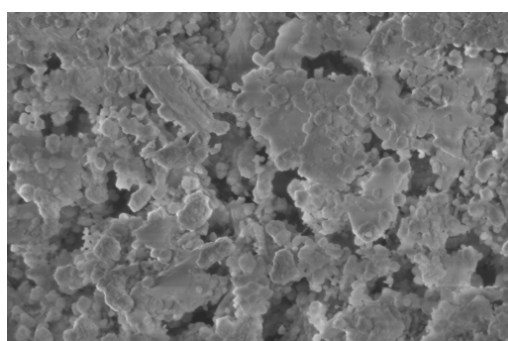
Appendix C- 7 SEM images of the fresh Ni MgO Al₂O₃



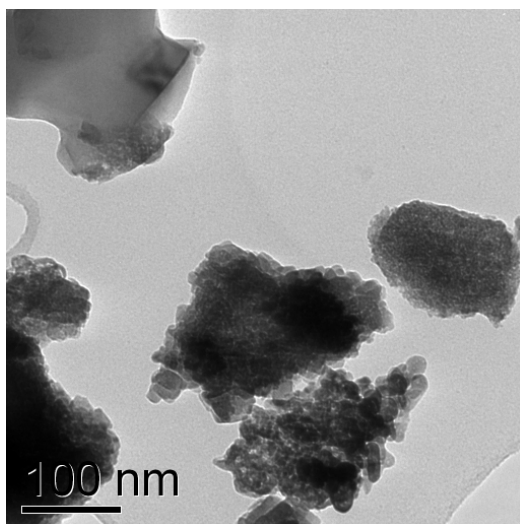
Appendix C- 8 SEM images of the reacted Ni MgO Al₂O₃



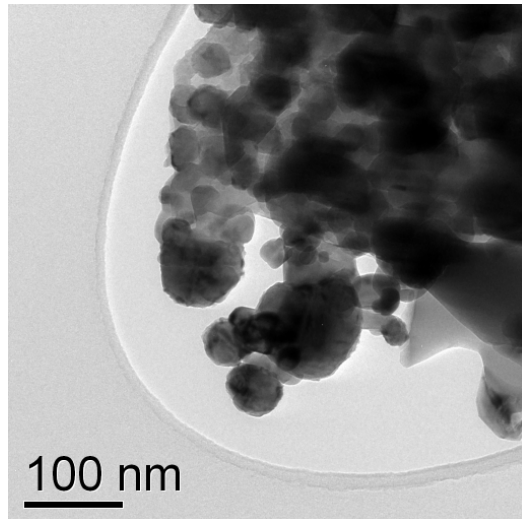
Appendix C- 9 SEM images of the Fresh Ni MnO Al₂O₃



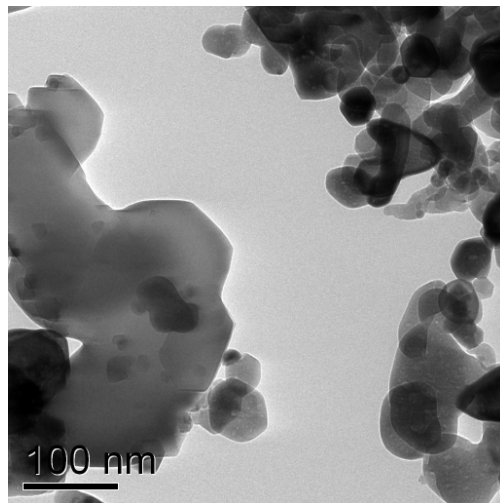
Appendix C- 10 SEM images of the reacted Ni MnO Al₂O₃



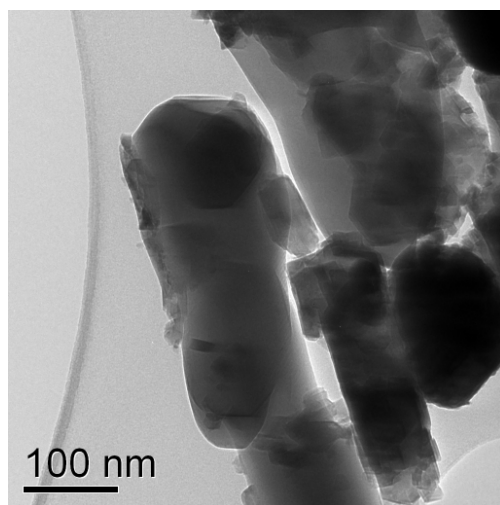
Appendix D- 1 TEM image of the fresh Ni La₂O₃ Al₂O₃



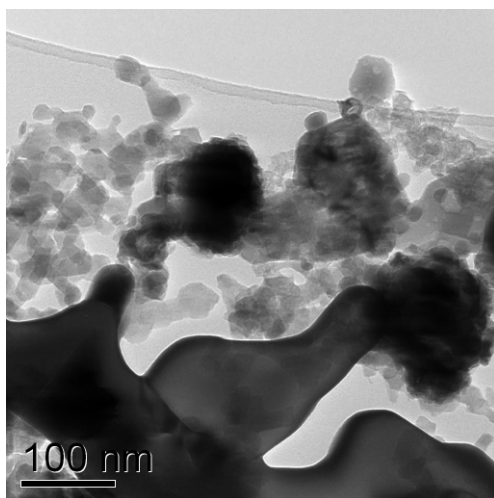
Appendix D- 2 TEM image of the reacted Ni La₂O₃ Al₂O₃



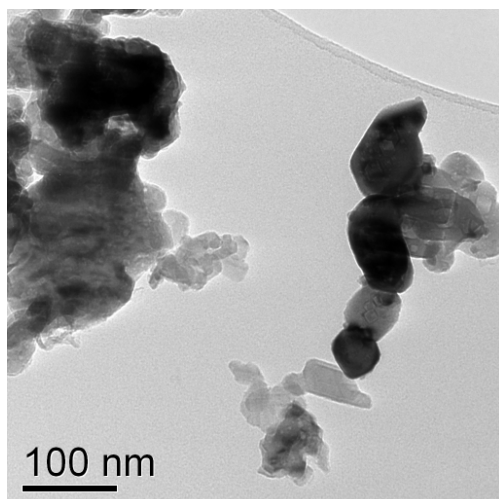
Appendix D- 3 TEM image of the fresh Ni CoO Al₂O₃



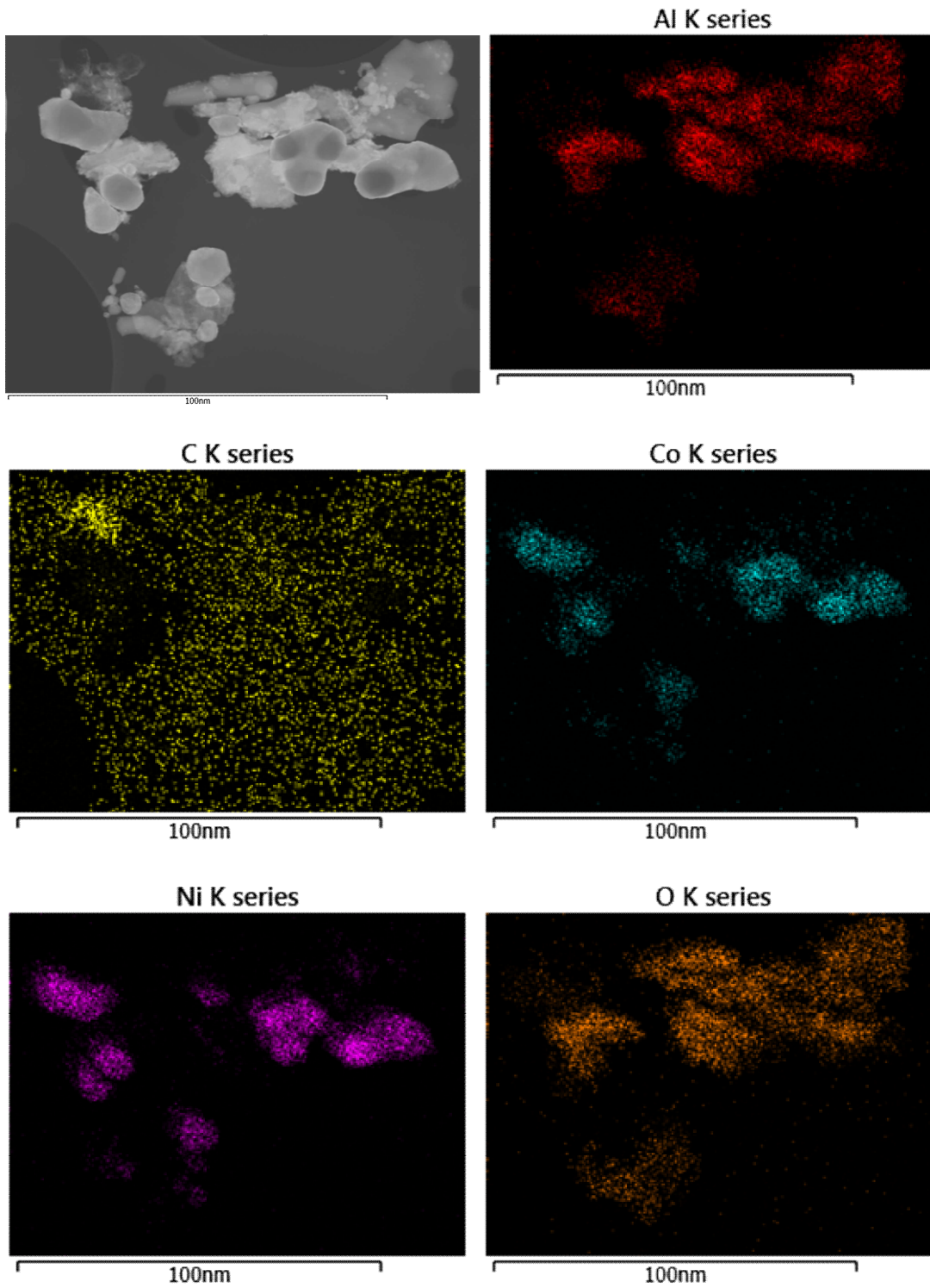
Appendix D- 4 TEM image of the reacted Ni CoO Al₂O₃



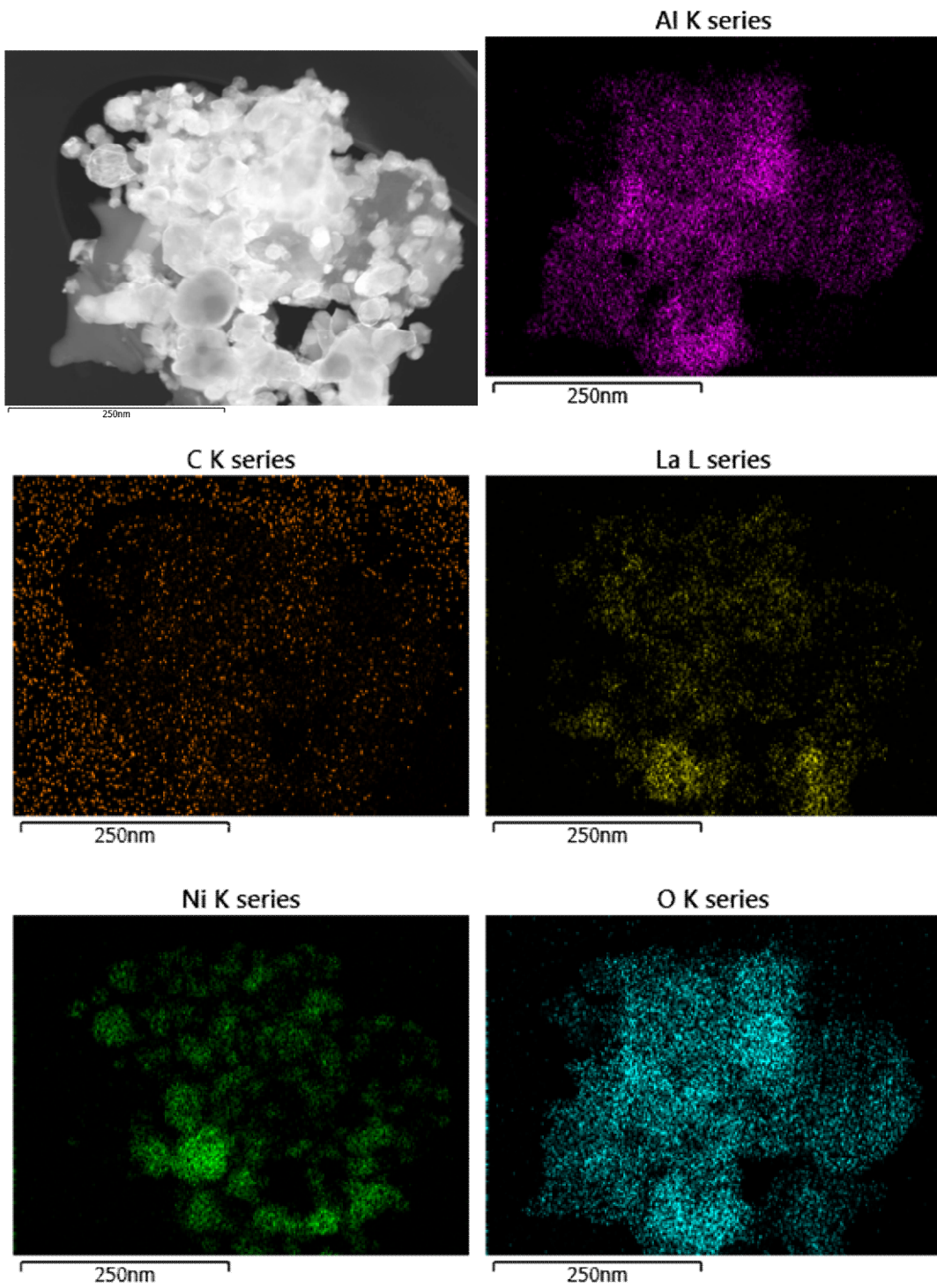
Appendix D- 5 TEM image of the fresh Ni MgO Al₂O₃



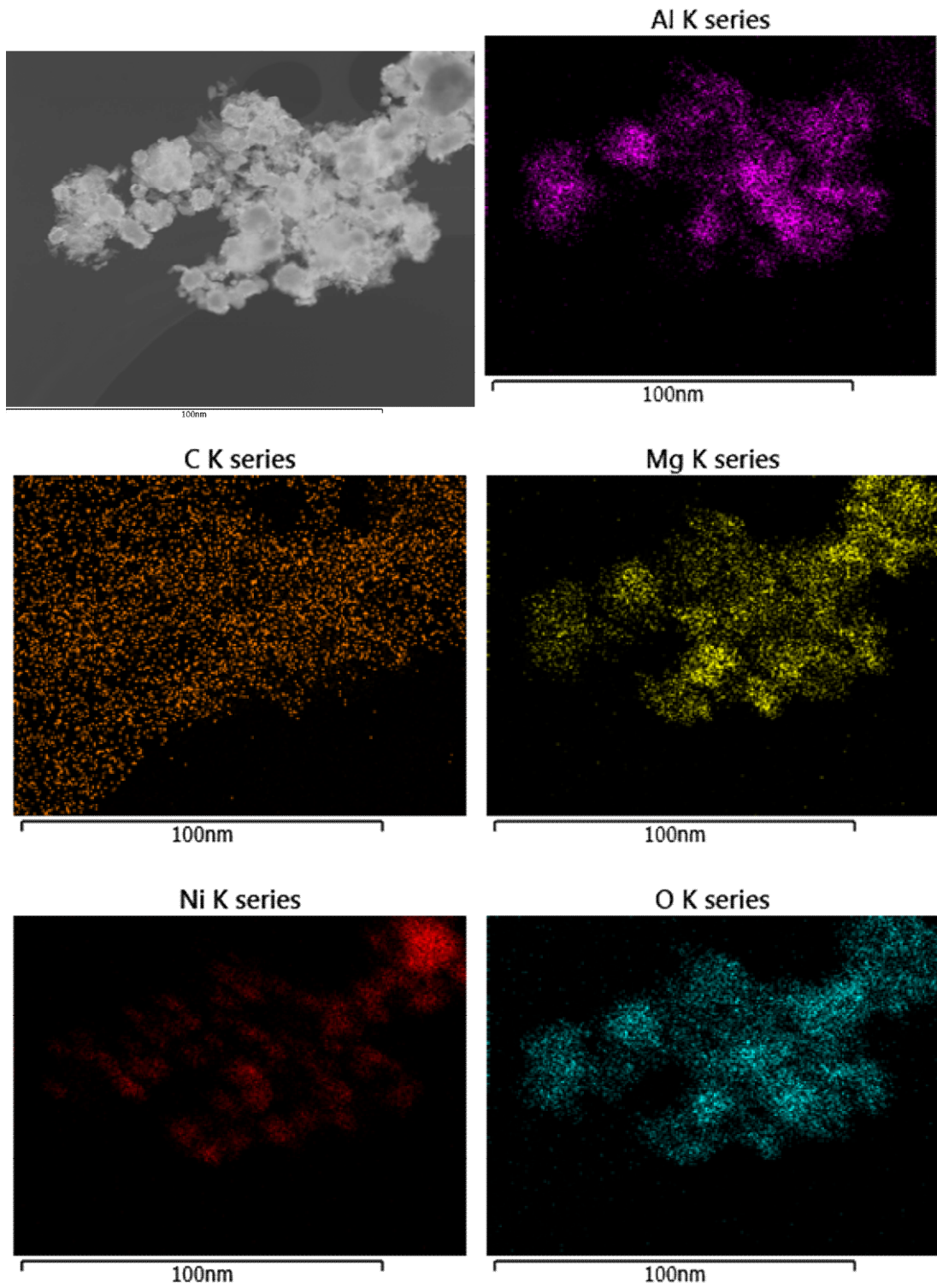
Appendix D- 6 TEM image of the reacted Ni MgO Al₂O₃



Appendix E-1 TEM-EDXS mapping of the reacted Ni CoO Al₂O₃



Appendix E- 2 TEM-EDXS mapping of the reacted Ni La₂O₃ Al₂O₃



Appendix E- 3 TEM-EDXS mapping of the reacted Ni MgO Al₂O₃